Numerical methods for multiphase mixture conservation laws with phase transition

Dissertation

zur Erlangung des akademischen Grades

doctor rerum naturalium
(Dr. rer. nat.)

von **Ali Zein, M.Sc.**
geb. am 12. Februar 1978 in Hebron, Palästina

genehmigt durch die Fakultät für Mathematik
der Otto-von-Guericke-Universität Magdeburg

Gutachter:
Prof. Dr. Gerald Warnecke
Prof. Dr. Philippe Helluy

Eingereicht am: 7. April 2010
Verteidigung am: 28. Juni 2010

Abstract

The seven-equation model for compressible two-phase flows is a full non-equilibrium model; each phase has its own pressure, velocity, temperature, etc. A single value for each property, an equilibrium value, can be achieved by relaxation methods. This model has better features than other reduced models of equilibrium pressure for the numerical approximations in the presence of non-conservative terms. In this thesis, we modify this model to include the heat and mass transfer. We insert the heat and mass transfer through temperature and Gibbs free energy relaxation effects. New relaxation terms are modeled and new numerical procedures for the instantaneous temperature and Gibbs free energy relaxation toward equilibrium are proposed. For modeling such relaxation terms, our idea is to make use of the assumptions that the mechanical properties, the pressure and the velocity, relax much faster than the temperature and the Gibbs free energy, and the ratio of the Gibbs free energy relaxation time to the temperature relaxation time is extremely high. By these assumptions we construct a new hierarchical model in which the relaxation steps are performed in the following order: first mechanical relaxation then temperature relaxation and at last Gibbs free energy relaxation. From one step to the other, what is relaxed stays relaxed. All relaxation processes are assumed to be instantaneous, i.e. the relaxation times are very close to zero. The temperature and the Gibbs free energy relaxation are used only at the interfaces.

We present a numerical validation of the new model on a number of test problems for metastable liquids. The model is able to deal with transition fronts, here evaporation fronts, where heat and mass transfer occurs. These fronts appear as extra waves in the system. Our results are in a good agreement with previously known results. In addition, computed front speeds of the evaporation waves are compared to the measured ones. A good agreement is achieved.

Further, we consider the six-equation model with a single velocity, which is obtained from the seven-equation model in the asymptotic limit of zero velocity relaxation time. The same procedure for the heat and mass transfer is used with the six-equation model and a numerical comparison is made between the results of this model with the results of the seven-equation model.

Then we present a numerical investigation for the collapse and rebound of a laser-induced cavitation bubble in liquid water. The main focus is devoted to the effects of phase transition and the existence of a non-condensable gas on the dynamics of the collapsing bubble. If the bubble contains vapor only we use our modified six-equation model for two-phase flows. To study the effect of the non-condensable gas inside the bubble a third phase is added to the original model. In this case the phase transition is considered only at the interface that separates the liquid and its vapor, while for the interface that separates the non-condensable gas and the liquid the condition of equal pressure only is imposed. The stiffened gas equations of state are used as closure relations. We use our own criteria to determine the parameters of them in order to obtain reasonable equations of state for a wide range of temperatures and make them suitable for the phase transition effects. We compare our results with experimental ones. Also our results confirm some expected physical phenomena.

Zusammenfassung

Das Modell mit sieben Gleichungen für die Zweiphasenströmung ist ein System im Nichtgleichgewicht. Dabei hat jede Phase einen eigenen Druck-, Geschwindigkeits- und Temperaturwert. Ein einziger Wert für jede dieser Eigenschaften - der Gleichgewichtswert - kann durch Relaxationsverfahren erreicht werden. Für die numerische Approximation bei Vorhandensein nicht-konservativer Terme hat dieses Modell bessere Eigenschaften, als die der bekannten reduzierten Druckgleichgewichtsmodelle. In dieser Dissertation modifizieren wir das Modell, um den Wärme- und Stoffaustausch mit zu berücksichtigen. Diese werden durch Relaxationseffekte der Temperatur und der Gibbsschen freien Energie hinzugefügt. Dabei werden neue Relaxationsterme modelliert und neue numerische Verfahren für die unmittelbare Relaxation der Temperatur und der Gibbsschen freien Energie in Richtung Gleichgewichtszustand vorgeschlagen. Unsere Idee zur Modellierung solcher Relaxationsterme ist es, von der Annahme Gebrauch zu machen, dass die mechanischen Eigenschaften, der Druck und die Geschwindigkeit, deutlich schneller in den Gleichgewichtszustand gehen, als die Temperatur und die Gibbssche freie Energie, und dass der Quotient der Relaxationszeit der Gibbsschen freien Energieüber der Relaxationszeit der Temperatur extrem hoch ist. Basierend auf dieser Annahme entwickeln wir ein hierarchisches Modell, in dem die Relaxationsschritte in dieser Reihenfolge durchgeführt werden: erst mechanische, dann Temperatur- und dann Gibbssche freie Energie-Relaxation. Was in einem Schritt relaxiert wird bleibt unverändert in den nächsten Schritten. Sämtliche Relaxationsprozesse sind als spontan vorausgesetzt, d.h. die Relaxationszeit ist nahe Null. Die Temperatur- und die Gibbssche freie Energie-Relaxation werden lediglich an den Phasengrenzflächen angesetzt.

Wir stellen eine numerische Validierung des neuen Modells anhand mehrerer Testfälle für metastabile Flüssigkeiten vor. Das Modell ist in der Lage Grenzflächen mit Phasenübergang zu behandeln, an denen Wärme- und Stoffaustausch vorkommen. Diese Fronten treten als zusätzliche Wellen im System auf. Unsere Ergebnisse stimmen gut mit vorher bekannten Ergebnissen überein. Darüber hinaus werden berechnete mit gemessenen Frontgeschwindigkeiten der Verdampfungswellen verglichen. Dabei wird auch eine gute Übereinstimmung erreicht.

Des Weiteren ziehen wir das Modell mit sechs Gleichungen, das aus dem Modell mit sieben Gleichungen im asymptotischen Limes der Geschwindigkeitsrelaxationszeit Null gewonnen wird, mit einer einzigen Geschwindigkeit in Betracht. Das oben beschriebene Verfahren für den Wärme- und Stoffaustausch wird auf das Modell mit sechs Gleichungen angesetzt. Ein numerischer Vergleich der Ergebnisse dieses Modells mit denen des Modells mit sieben Gleichungen wird durchgeführt.

Anschließend stellen wir eine numerische Untersuchung der Oszillation einer Laser-induzierten Kavitationsblase im flüssigen Wasser vor. Der Hauptfokus ist auf die Einflüsse des Phasenübergangs und der Existenz eines inerten Gases auf die Dynamik der kollabierenden Blase gerichtet. Sollte die Blase nur Wasserdampf enthalten, verwenden wir unser modifiziertes Sechsgleichungsmodel für Zweiphasenströmung. Um den Einfluss eines inerten Gases innerhalb der Blase zu untersuchen wird dem ursprünglichen Modell eine dritte

Phase zugefügt. In diesem Fall wird der Phasenübergang nur an der Grenzfläche zwischen der Flüssigkeit und deren Dampf betrachtet. Für die Grenzfläche zwischen dem Inertgas und der Flüssigkeit wird die Bedingung des Druckgleichgewichts eingeführt. Die “stiffend gas-”Zustandsgleichungen (eng. EOS) werden zum Abschluss des Systems verwendet. Wir setzen unsere eigenen Kriterien zur Bestimmung der Parameter dieser Gleichungen an, um angemessene Zustandsgleichungen für einen breiten Umfang von Temperaturenwerten zu erhalten, die damit für Phasenübergangseffekte geeignet sind. Wir vergleichen unsere Ergebnisse mit experimentellen Ergebnissen. Unsere Ergebnisse bestätigen einige erwartete physikalische Phänomene.

Acknowledgements

First of all, I would like to express my sincere and deep gratitude to my supervisor Prof. Dr. Gerald Warnecke for his constant help, inspiring guidance, invaluable advice, and continuous encouragement. The distinguished personality of Prof. Warnecke provides a wonderful atmosphere for his research group. I would also like to thank him for his generous support and encouragement to attend many scientific events in Germany and Europe.

I would like to express my sincere gratitude to my co-supervisor Dr. Maren Hantke for her help, encouragement, friendly direction and collaboration.

I am very grateful to Prof. Dr. Philippe Helluy (IRMA Strasbourg, France) for his interest in my thesis and his valuable remarks, and for hosting me in his department in Strasbourg. In addition, I highly appreciate his valuable suggestions for the future work.

I am also very grateful to the pioneering scientist Prof. Dr. Richard Saurel (Polytech'Marseille, France) for hosting me in his department in Marseille. The very useful and deep discussions with Prof. Saurel have strongly influenced my work in the field of multiphase flows. Also, many thanks go to his group members Dr. Olivier Le Metayer and Dr. Fabien Petitpas for their sharing of experience in the discussions.

My special thanks go to Prof. Dr. Shamsul Qamar (COMSATS Institute of Information Technology, Islamabad, Pakistan) for his valuable help and encouragement especially at the beginning of my work.

My special thanks go also to Prof. Dr. Naji Qatanani (Palestine) for his encouragement to pursue my doctoral studies in Germany, and establishing the first contact with my supervisor Prof. Warnecke.

Many thanks go to all members of the research group of Prof. Warnecke, with special thanks go to PD Dr. Matthias Kunik.

I am very grateful to the German Academic Exchange Service (DAAD) for granting me the scholarship to pursue my doctoral studies. For their help, I would like to thank Frau Karla Barth, Frau Andrea Gerecke, Dr. Helga Baumgarten, and Frau Eveline Muhareb.

I am overwhelmingly grateful to all my friends. Especially, I wish to express my deepest gratitude to my very special friend Dr. Zein I. Salah for his encouragement and support.

I am deeply indebted to my home university, the Palestine Polytechnic University. Especially, many thanks go to Ms. Khawla Al-Muhtaseb (Chairperson of Mathematics Department) for her continuous interest and encouragement.

Now, I would like to express my deep obligation to my father, mother, brother, sister, and friends in Palestine. Their consistent mental supports have always been the strong push for me during this period.

I should never forget to thank my wife Yasmeen and my son Mohammad. Without their love, patience, and understanding, this work would be unthinkable.

Contents

Chapter 1

Introduction

1.1 Overview

Multiphase mixtures appear everywhere in nature, from blood flow, to the formation and motion of rain droplets, sand storms, and volcanic clouds. Also the flow of compressible multiphase mixtures is of great importance in numerous industrial and technological applications. For example, in power plants, heat exchangers, as well as in chemical and nuclear reactors.

Due to the wide range of applications of the compressible multiphase flows considerable attention has been devoted to the modeling and simulation of these flows. Both the mathematical modeling and numerical computations have certain inherent difficulties. These difficulties originate from the existence of deformable and moving interfaces separating the phases or fluids. The modeling difficulties are concerned with the interaction between the fluids, which includes the transfer of mass, momentum and energy across the interfaces. While the discontinuities of the fluid properties at the interfaces are mainly responsible for difficulties in numerical methods. Therefore, the manner of treatment of the interfaces is the keypoint of each model.

Numerous models exist in the literature with different degrees of complexity and different ranges of applicability. In general, they are divided in two classes from the point view of interface treatment methods. The first class represents the models in which the interface is treated as a *sharp interface*, they are referred to as *sharp-interface models*. While the second class corresponds the models in which the interface is considered as a diffuse zone, they are called *diffuse-interface models*.

In the sharp interface methods special efforts are required to locate and treat the interfaces explicitly. These methods can be classified as Lagrangian methods, Eulerian methods, combined Euler-Lagrangian methods, and arbitrary Lagrangian-Eulerian methods. For reviews of these methods see Hu et al. [60], Saurel [119], Saurel and Abgrall [121], Saurel and Le Metayer [124], Scardovelli and Zaleski [128], as well as Tryggvason et al. [153]. Some details for these methods are given below.

Lagrangian methods: With these methods the mesh moves and is distorted with the material interface. But in real fluid flow the interface has large deformations. It follows that the mesh has large distortions. Also, these deformations frequently lead to changes in the flow pattern. Therefore a repetitive mesh adjustment is required. This makes the Lagrangian methods complex for implementations and expensive in CPU time, see Saurel and Le Metayer [124], Scheffler and Zukas [129].

Eulerian methods: A fixed mesh is used with some marker function to distinguish the interface. The most popular examples of such type of methods are the *volume-of-fluid* (VOF) and the *level set method*. In the VOF method the interface is reconstructed by calculating the volume fraction of each phase. This method was proposed by Hirt and Nichols [56] in the context of incompressible flows. Later it was used for compressible flows, see Miller and Puckett [90], Pilliod and Puckett [110]. In fact, the interface reconstruction consumes time. Moreover, still there are some questions related to the lack of the mathematical formalism of this method, see Saurel et al. [127], Rider and Kothe [116].

The second popular example of the Eulerian methods are the level set methods which were initially developed by Osher and Sethian [102] for calculating the interface in two or three dimensions. The interface is captured by a zero level set of some signed distance function. For a review of this method see Sethian [133], Osher and Fedkiw [101]. The main drawback of the level set methods is the non-conservation of the mass. Several attempts were made to circumvent this problem like the combination of this method with the VOF method or improving the used level set function, see Olsson and Kreiss [100].

Combined Euler-Lagrangian methods: With these methods the fluid flow is solved on an Eulerian fixed grid and the interfaces are tracked by using a set of markers. Usually these methods are referred to as *front tracking methods*. The major difficulty of these methods is their complexity. Indeed, it is very difficult to implement such methods, also a difficulty arises in coupling the interfaces with fixed Eulerian grids, see Unverdi and Tryggvason [154], Cocchi and Saurel [24].

Arbitrary Lagrangian-Eulerian (ALE) methods: This method allows for both types of strategies that are used by Lagrangian or Eulerian methods. The mesh may be moved in a Lagrangian fashion, or be held fixed in an Eulerian manner, or be moved in other ways to give a continuous rezoning capability [34]. This makes the method flexible and one can collect the benefits of both Lagrangian and Eulerian methods. But the difficulty of this method lies in the decision of which type of grid or strategy is used through the domain of computation and during the flow process. For more information see Doneal et al. [34], Hirt et al. [57] and Margolin [88].

All the above methods are still under improvement and extension to more applications, see Saurel and Le Metayer [124]. A general benefit of these sharp interface methods is that the interface does not diffuse. The general drawbacks of these methods are their complexity, cost in computation time and the most important point is that they are not

able to dynamically create emerging interfaces since they need the initial knowledge of the interfaces [127]. The last point, i.e. interface formation is a very important in *cavitating flows* [75, 124].

Let us now turn to the second class of the models, i.e. the diffuse-interface models. Here, the interface is solved as a numerical diffusion zone, like the capturing of contact discontinuities in gas dynamics [127]. Indeed, these diffusive interfaces are a type of artificial mixtures due to numerical computations.

Even though the diffusion is a drawback, these models posses several advantages over the previous class of models. One of the most important advantages is that they are solved on a fixed grid with the same type of numerical scheme for all computational cells, i.e. for all type of waves; *shocks*, *interfaces* and *rarefactions* [119]. These models are based either on the Euler equations or on the multiphase flow equations. Details for both groups are given below.

Models based on Euler equations: These models are used by several authors like Abgrall [1] and Shyue [134]. They are simple and efficient, but limited to simple physical models [119, 124], and they are limited regarding to the simplicity of *equations of state* used. In addition, they suffer from inaccuracy of the internal energies and temperatures at the interface.

Models based on multiphase flows equations: These models are based on the multifluid theory and so a larger number of equations is used. They are able to deal with a wide range of applications involving mixtures and interfaces. From the pioneering work of Saurel and Abgrall [120] in this direction, intensive research efforts have been devoted to these models, see [4, 7–10, 32, 72–75, 96, 106–108, 119, 123–127, 131, 161, 162]. The benefits of these models are summarized as

- Compared with the previous models, they have better flexibility regarding the equations of state, also they are conservative for the mixture; total energy, mass and momentum of the mixture. This leads to accurate computations for the internal energies and temperatures at the interfaces.

- These models are *unconditionally hyperbolic systems*. Therefore they utilize the facilities of the *Godunov-type schemes*. Indeed, the Godunov schemes with related *Riemann problems* were modified extensively in the last two decades, especially for the single-phase flows. Moreover, the Godunov schemes were extended to take into account the *non-conservative terms*. This has special importance for these models which are *non-conservative systems*. All concepts in this paragraph are explained in Chapter 2.

- These models are able to dynamically create interfaces. This feature is of great importance for some applications. For example, gas pockets can be formed during cavitating flows [107, 119, 124, 126].

The above benefits were introduced and detailed in several references, see [74, 75, 119, 124]. Moreover, these models were verified for a wide range of applications like: interface problems, solving strong shock waves in mixtures, and detonation waves in condensed materials, see the previous references.

Typically, the multiphase flow models of diffusive interfaces are derived by using *averaging procedures* [35–38, 61, 157]. Therefore these models are formulated in a macroscopic level. In other words, these models consider all phases as *continuum fluids*. Thus, they are called *homogenized* or *averaged mixture models*. In fact, with the macroscopic description we loose some microscopic details of the fluid motion which can be detected by the local instant formulations of the fluid. But the main advantage of averaging is to overcome the difficulties in coupling between the field equations of each phase and the *interfacial conditions*. Moreover, the microscopic details about the local instant motions and interfacial geometry usually are not needed for the applications and engineering problems. The macroscopic flow information is more important, see Drew[36] and Ishii and Hibiki [61].

Using averaging techniques of the single-phase equations results in additional terms, which describe the physical transfer processes taking place across the interface like mass, momentum and heat transfer. The exact expressions for these transfer terms are usually unknown. Also there appear differential terms that are extracted from the transfer terms that prevent the system from being in *divergence form* or *conservative form*. Therefore, they are referred to as the non-conservative terms and they are responsible for numerical difficulties.

In fact, there is a lack of the theory for numerical methods of non-conservative systems. This is related strongly to the lack of a theory of *multiplication of distributions*. However, the non-conservative terms always present in averaged mixture models, whatever the physical processes occurring at the interface [120]. For completeness, we refer to the attempt of building some conservative approximations to the non-conservative models, like the work of Deledicque and Papalexandris [33]. But these approximations are valid under certain conditions for the fluids properties.

The most general form of the multiphase flow models of diffusive interfaces is the *full non-equilibrium* one, i.e. each phase has its own pressure, velocity, temperature, etc. If we consider two phases only, then the most general model consists of seven partial differential equations as the model of Saurel and Abgrall [120]. This model consists of the evolution equation for the volume fraction of one of the phases together with balance equations for mass, momentum and energy for each phase. In this thesis frequently we will refer to this model as the *seven-equation model*.

The Saurel-Abgrall model [120] is derived by using the *ensemble averaging procedure* of Drew [36] and neglecting all dissipative terms everywhere except at the interfaces. This model is considered as a modified form of the Baer and Nunziato model [12] which was derived by applying the *continuum mixture theory* to describe the flame spread and

deflagration-to-detonation transition (DDT) in gas-permeable, reactive granular materials. The modifications of Saurel and Abgrall concern the interfacial variables as well as the modeling of *relaxation terms* for the velocity and the pressure.

By using instantaneous relaxation procedures equilibrium values for the velocity and the pressure can be achieved. Thus using relaxation techniques enlarges the capability of the model for application problems. Also, they are used to fulfill the conditions of equal velocities and pressures at the interface. Moreover, they are the keypoint of the reduced forms of the model.

Reduced models were derived from the general seven-equation model by the asymptotic analysis in the limit of zero relaxation time. A *six-equation model* which has a single velocity is deduced by assuming zero velocity relaxation time. This model was introduced by Kapila et al. [66], the first reduced model in [66]. Then it was validated for numerical computations by Saurel et al. [127]. This model consists of the volume fraction equation of one of the phases, two mass balance equations, a mixture momentum equation and two energy equations. In this thesis we will refer to this model by the six-equation model. It is important to note that this model differs from the classical six-equation model that appeared in the literature, like Stewart and Wendroff [143], Toumi and Raymond [151], Sainsaulieu [118], Tiselj and Petelin [145]. Indeed, the classical six-equation model consists of two mass equations, two momentum equations, and two energy equations. This model initially is *ill-posed*, i.e. it has complex eigenvalues, this is due to the assumption of single pressure in the model. Usually, extra terms are added to the model and some assumptions are made to remove the ill-posedness. Therefore, this model works under severe restrictions. See further details in Subsection 2.1.3. However, we will not use this classical model in this thesis.

Also a *five-equation model* with mechanical equilibrium, single velocity and single pressure, is deduced in the asymptotic limit of zero relaxation time for both the velocity and the pressure. Several authors considered this model, see Kapila et al. [66], the second reduced model in [66], Murrone and Guillard [96], Petitpas et al. [106] and Saurel et al. [126]. It is composed of two mass equations, a mixture momentum equation and a mixture energy equation. These equations are written in a conservative formulation, while the fifth equation of this model is a non-conservative equation for the volume fraction which contains a non-conservative term involving the divergence of the velocity. In this thesis we will refer to this model by the five-equation model.

Further reductions for the general seven-equation model are also possible, in particular, the *four-equation model* and the *three-equation model* [66]. The four-equation model has a single velocity, single pressure and also single temperature. Indeed this model consists of the *single-fluid reactive Euler equations*. While the three-equation model is the system of *Euler equations*. It has single velocity, pressure, temperature, and also single Gibbs free energy. This means that it is in full equilibrium. In fact, for two-phase flow there is no physical justification of imposing a single temperature and/or single Gibbs free energy in

the entire domain of the flow [66, 120].

It is worth to mention that the reduced models can be achieved by applying a reduction procedure in the presence of stiff relaxation terms, like the procedure of Chen et al. [22]. This procedure was used by Murrone and Guillard [96] to derive the five-equation model, also it was extensively used in the Ph.D. thesis of Labois [72]. In this thesis, we will apply this procedure to derive the six-equation model accompanied by heat and mass transfer from the full seven-equation model with heat and mass transfer, all details are given in Section 4.6.

Here we are interested in the *phase transition* for compressible two-phase flows with applications in cavitating flows. Thus the second class of models, i.e. multiphase diffusive interface models based on averaging procedures, are the best candidates for our purpose. This is due to their attractive properties for the numerical computations, dealing with interfaces formation and the ability of dealing with a wide range of problems as is explained above. In particular, we will focus on the seven-equation model and its first two reduced forms, i.e. the six-equation and the five-equation models. In fact, models with further reduction depend on unphysical assumptions and so are not suitable for the purpose of this thesis. Indeed, models with equilibrium temperature and pressure have severe modeling and numerical difficulties that make extending them to include the phase transition impossible or difficult and very limited, in Saurel et al. [126] you can find a good review of the difficulties in this type of models.

Recently, the five-equation model was modified by Saurel et al. [126] to take into account the phase transition by including temperature and chemical potential relaxation effects. Then it was extended to multiphase flows in Petitpas et al. [107]. Moreover, this model was used by Petitpas et al. [108] for modeling detonation waves in condensed energetic materials.

In comparison with the seven-equation and six-equation models: Even though the five-equation model is the most reduced it has severe numerical difficulties that are the results of the equilibrium of the pressure. These difficulties include:

- Shock computational difficulties due to the non-conservative character of the model.
- Maintaining volume fraction positivity due to the difficulties in the approximation of the non-conservative term involving the divergence of the velocity. This term appears in the volume fraction equation as a result of equilibrium pressure.
- Non-monotonic behavior of the *mixture sound speed*, that obeys the *Wood formula* [158], with respect to the volume fraction. This behavior may cause inaccurate wave transmission across diffuse interfaces.

The above difficulties were detailed in Saurel et al. [127] and Petitpas et al. [106], also more details are given in Section 2.4. In addition, it was noted that the conventional Godunov-type schemes are not suitable for the resolution of this model [106]. To circumvent these

difficulties, the Riemann problem is solved by the help of shock and Riemann invariant relations that were derived by Saurel et al. [125]. And a specific *relaxation projection method* is used instead of the conventional Godunov method, see Saurel et al. [122] and Petitpas et al. [106].

From the computational point of view both the seven-equation and six-equation models have several advantages over the five-equation model:

- Preserving the positivity of the volume fraction is easier.
- The mixture sound speed has a monotonic behavior with respect to the volume fraction, see Petitpas et al. [106].

See more details about these features in Subsection 2.4.

According to the attractive advantages of the seven-equation and six-equation models we aim in this thesis to modify them to include the heat and mass transfer and to present numerical investigations for the resulting models compared with some previously known results. In addition, we aim to validate the models against experimental data. Further, we aim to extend the new resultant models to deal with the existence of a *non-condensable gas*.

1.2 New Results

This thesis is mainly concerned with the modeling of phase transition for compressible two-phase flows. Thus, always we consider the flow of liquid and its vapor. A special attention is given to the equations of state. In particular, we are looking for equations of state that provide stability for the solution of the hyperbolic models as well as being appropriate for phase transitions. In addition, we aim to study the phase transition in the case of three-phase flows, where the third phase is assumed to be a non-condensable gas.

Initially, our attention is devoted to the evaporation that appears in cavitating flows. Thus we can compare our results with the results of Saurel et al. [126] for *metastable liquids*, i.e. liquids with a temperature higher than the saturation temperature. Then we apply our new model to a more general problem that includes evaporation and condensation, in specific, we consider the problem of collapse and rebound of a laser-induced cavitation bubble in liquid water.

We start with the seven-equation model of Saurel and Abgrall [120]. The numerical solution of this model is obtained by applying the *Strang splitting* [144] to take into account both parts of the model; the hyperbolic part and the non-differentiable source terms part. The last part consists of the relaxation terms of the velocity and the pressure. For the solution of the hyperbolic part of the model a modified Godunov-type scheme is used. For the mechanical relaxation, the instantaneous velocity and pressure relaxation procedures of Saurel and Abgrall [120] are taken.

We insert the heat and mass transfer through relaxation effects. New terms associated with the heat and mass transfer are modeled. These terms are given in terms of the temperature difference for the heat transfer and in terms of the Gibbs free energy difference for the mass transfer.

We propose new procedures for the instantaneous temperature and Gibbs free energy relaxation toward equilibrium. These procedures are used at each time step after the mechanical relaxations. They are used only at specific locations, i.e. at interfaces where the heat and mass transfer occur.

Since the exact expressions for the transfer terms are unknown, our idea to model them is to refer to some general physical observations besides *the second law of thermodynamics*. In particular we assume that the mechanical properties, the pressure and the velocity, relax much faster than the thermal properties, the temperature and Gibbs free energy. Also we assume that the relaxation time for the temperature is much smaller than that of the Gibbs free energy. In fact these assumptions agree with physical evidence in a large number of situations, see [16, 51, 66, 93]. In the book of Müller and Müller [93] some similar assumption is used in the analysis of the equilibrium conditions for droplets and bubbles, see Chapter 11 there. In Kapila et al. [66] there are some estimates given for the time scales of the relaxation of the velocity, pressure and temperature in granular materials. These estimations show that the relaxation time for the temperature is significantly larger than relaxation times for both the velocity and the pressure. Also other estimations for detonation applications show that the time scale of the velocity relaxation and pressure relaxation are of the same order of magnitude while the temperature relaxation time is much greater than that for the velocity and pressure, see [23, 108]. More discussion of this point is given in Subsection 3.3.4.

By the above assumptions with the seven-equation model we obtain a new hierarchical model in which the properties relax in the following order: first mechanical relaxation then temperature relaxation and at last Gibbs free energy relaxation. From one step to the other, what is relaxed is kept relaxed.

Our new model is able to deal with *transition fronts*, specifically in metastable liquids the evaporation fronts, where heat and mass transfer occur. These evaporation fronts appear as extra waves in the system, see Le Metayer et al. [81] and Saurel et al. [126].

Then we consider the six-equation model with a single velocity which is obtained from the seven-equation model in the asymptotic limit of zero velocity relaxation time. We model the heat and mass transfer for this model by using two methods. Both methods give the same resulting model. In the first method, we use our procedure that is proposed for the seven-equation model under the same assumptions. In the second method, the six-equation model with heat and mass transfer is obtained directly by applying the reduction method of Chen et al. [22] to the seven-equation model involving the heat and mass transfer and assuming stiff velocity relaxation.

We use the same test problems as Saurel et al. [126] for metastable liquids. We see in our results the extra waves that appear due to the phase transition. Also our results are in a good agreement with the results of Saurel et al. [126].

Computed results are compared to the experimental data of Simões-Moreira and Shepherd [136]. Indeed, the computed front speeds of the evaporation waves are compared to the measured ones at several initial temperatures. There is a good agreement with the experimental data. In addition, our results are significantly more close to the experimental values than those of Saurel et al. [126].

A comparison between the results of the seven-equation and six-equation models is made. In general, there is no significant difference between the results of both models under the same conditions, but there is a significant difference in the CPU time consumed by both models, this makes the six-equation model less expensive.

Then we turn to investigate the collapse and rebound of a laser-induced cavitation bubble in liquid water. This problem is the keypoint in the study of *cavitation erosion*, i.e. cavitation material damage, which may have destructive effects in many engineering problems of hydrodynamics, see Philipp and Lauterborn [109]. In the literature, numerous models were proposed to investigate this problem. But none of these models are free from drawbacks nor are able to take into account all physical effects, see a review in Subsection 5.1.1.

In this thesis we introduce a model which is able to consider the main physical effects. In particular, our model takes into account the compressibility of both phases, heat transfer, mass transfer and the existence of a non-condensable gas inside the bubble. Indeed, If the bubble contains vapor only we use our modified six-equation model in spherical coordinates assuming rotational symmetry. We choose to use the six-equation model since it is less expensive than the seven-equation model and is easier to be modified for multiphase flows.

To study the effect of the non-condensable gas inside the bubble a third phase is added to the original six-equation model. Thus the whole model consists of nine equations. In this situation the phase transition is considered only at the interface between the liquid and its vapor. But if the interface separates the liquid and the non-condensable gas the pressure relaxation is only used to fulfill the condition of the equilibrium of the pressure.

In the problem of the bubble collapse it is expected that the temperature in the bubble will exceed the *critical point*. Thus the temperature range is very wide, i.e. it starts from low temperatures like the room temperature and exceeds the critical temperature. This makes the choice of the equations of state a difficult task. Moreover, including the phase transition requires further attention. In this work we use the *stiffened gas equations of state* which are the simplest formulation that contains the main physical properties of the pure fluid. We use our own method to estimate the parameters of the equations of state. These estimations respect the saturation curve. This idea was used by Barberon and Helluy [13, 14] as well as Le Metayer et al. [80]. This makes the equations of state

appropriate if the phase transition is included in the model.

To verify our results we compare the computed radius-time curve to the experimental one that used in Müller et al. [94]. Also we confirm some known and expected physical behaviors. Our results show that the pressure and the temperature at the center of the bubble increase to very high values at the collapse time. Also the velocity at the interface of the bubble goes to a high value at the collapse instant.

When the phase transition is considered the results show that there is no rebound if the bubble contains vapor only. And inserting a non-condensable gas is responsible for the rebound. This result confirms the idea of Dreyer et al. [40] that inserting an inert gas is essential for the rebound. Moreover, we see that the temperature and the pressure inside the bubble before the collapse point decrease if the mass transfer is included. This is due to the loss of energy by the mass transfer process.

In summary, the main results of the thesis are

- Modeling heat and mass transfer for the seven-equation and six-equation models.
- Proposing procedures for the temperature and Gibbs free energy relaxation that are used in the numerical solution of the models.
- Validating the new models numerically through comparison with other computations and experiment. And comparing the results of the models to each other.
- Extending the six-equation model to include a non-condensable gas.
- Proposing new estimations of the parameters of the stiffened gas equations of state to be suitable for the problem of a laser-induced cavitation bubble.
- Investigating the collapse and rebound of a laser-induced cavitation bubble with the new models and new equations of state.

The results in the first three points were published as

- A. Zein, M. Hantke, and G. Warnecke. Modeling phase transition for compressible two-phase flows applied to metastable liquids. *J. Comput. Phys.*, 229(8):2964-2998, 2010.

The rest of the results have been submitted for publication as

- A. Zein, M. Hantke, and G. Warnecke. On the modeling and simulation of a laser-induced cavitation bubble, 2010.

1.3 Outline

This thesis is organized as follows:

Chapter 2 is intended to be an introduction of the basic concepts and facts of multiphase

flow modeling as well as the related mathematical theory. Special attention is devoted to the three models that are in the center of the interest of this thesis, i.e. the seven-equation, six-equation and five-equation models. The chapter starts with the derivation of the averaged two-phase flow model. Firstly, the single-phase flow equations with interfacial conditions are presented. Then the basic facts of the ensemble averaging procedure are recalled. This procedure is applied to the single-phase equations leading to the averaged model. A classical problem of this model is that the number of variables is larger than the number of equations, thus closure assumptions or relations are required. We discuss the most common closure procedures used in the literature. By using a volume fraction equation as a closure relation and with some simplifications we get the seven-equation model of Saurel and Abgrall [120]. Since the resulting model is hyperbolic we present the basic facts of the mathematical theory for hyperbolic systems of balance laws. We consider both the conservative and non-conservative systems. A special attention is devoted to the Riemann problem. Then we present the idea of the most important numerical scheme for conservation laws, namely, the Godunov scheme. This scheme will be used in later chapters in modified forms to take into account the non-conservative terms. In the last section of this chapter, we study the mathematical properties of the seven-equation model. A review for the recent developments in the Riemann problem and the treatment of non-conservative terms is introduced. Then, we present the six-equation and five-equation reduced models. The main features, benefits and difficulties of these models are addressed in details.

Chapter 3 is devoted to the modeling of heat and mass transfer for compressible flows by using the seven-equation model. Firstly, we consider the hyperbolic part of the seven-equation model. We give a brief on the required equations of state, phasic entropy equations and Godunov-type schemes. In addition, we construct an HLLC-type Riemann solver for the seven-equation model, some approximation is used for the volume fraction. This type of solvers is described in Toro [148] in the context of Euler equations. Then we turn our attention to the non-differentiable source part of the model which consists of the relaxation terms. We address in details the physical background to our assumptions for the differences in relaxation rates. By using these assumptions and the second law of thermodynamics we model the heat transfer through the temperature relaxation terms and the mass transfer through the Gibbs free energy relaxation terms. Then we introduce mathematical procedures for the temperature relaxation and Gibbs free energy relaxation with infinite parameters. Finally, we validate the new model numerically. A physical explanation for the results is given as well as validation against experimental data is made.

In Chapter 4 we model the heat and mass transfer for the six-equation model. The previous assumptions are used. In the first part of the chapter, we address some issues related to the numerical method of the hyperbolic part of the model. In particular, we recall some previous results of Saurel et al. [125, 127], like the non-conventional shock relations for multiphase mixtures with stiff mechanical properties, the HLLC-type Riemann solver and the correction criterion by using the mixture energy equation. These results are used for the solution of the model. In addition, we construct a VFRoe-type solver for the model based on Gallouët and Masella [46]. In the second part of the chapter, we use

our previous procedure which was introduced for the seven-equation model to insert the heat and mass transfer directly into the six-equation model. Then we use the reduction method of Chen et al. [22] to derive the modified six-equation model directly from the modified seven-equation model. After that we investigate the numerical results of the model. Detailed comparisons with the results of the seven-equation model are shown.

Chapter 5 is concerned with the problem of a laser-induced cavitation bubble in liquid water. An overview of the problem and previous work is given. Then we proceed to investigate the problem by using the modified models. First, we assume that the bubble contains vapor only, i.e. there are two phases. For this case we use the six-equation model that is modified in Chapter 4. Spherical coordinates are used in the radial direction with an assumption of rotational symmetry. Then we extend the model to take into account the existence of a non-condensable gas inside the bubble. Thus a nine-equation model is proposed. Next we introduce our method for determining the parameters of the stiffened gas equations of state. Then we present a numerical investigation of the problem. A comparison with experimental data is made. In addition, a physical explanation is given where our results cover some general physical behaviors.

Chapter 6 presents a summary to the results and some general conclusions. Some suggestions for future work is also given.

Most material of Chapters 3 and 4 has been published in the Journal of Computational Physics [162]. Chapter 5 has been submitted for publication [161].

Chapter 2

Mathematical formulation

The aim of this chapter is to study the main features of the seven-equation, six-equation and five-equation models. To give a complete picture, some review for the modeling procedure is given. Also some mathematical theory for the balance laws is presented.

At the beginning we consider the derivation of the general averaged model by applying an ensemble averaging procedure on the single-phase equations. Then, the simplification of the resulting model is introduced. This leads to the seven-equation model of Saurel and Abgrall [120]. Then a short review of mathematical concepts and theory is presented. Also, a short review of the Godunov scheme is given. After that, the mathematical properties of the seven-equation model are studied. In addition, the reduced forms of the model are introduced and studied.

2.1 Averaged two-phase flow model

Averaging procedures are the direct mathematical way to construct macroscopic equations from the microscopic ones. In the literature, there are several types of averaging, including time averaging [61], volume averaging [142, 157], combinations of time and volume averaging [35] and ensemble averaging [36–38]. The volume and time averages are the most commonly used due to their direct physical interpretation. But they are applied under certain restrictions and they may be inappropriate for some situations, see [37, 38] for examples. Moreover, it can be shown that the volume and time averages, in appropriate situations, are special cases of the ensemble average [38]. However, all averaging procedures lead to averaged equations which essentially have the same structure. They may differ in the interpretations of the variables and in the calculations regarding the interfacial source terms [36]. In this section, our attention is devoted to the ensemble averaging for its generality.

2.1.1 Single-phase flow

The flow of a compressible single-phase fluid is described by the following system of balance equations

Mass balance (continuity equation)

$$\frac{\partial \rho}{\partial t} + \nabla \cdot (\rho \mathbf{u}) = 0, \tag{2.1}$$

Momentum balance (Newton's second law)

$$\frac{\partial \rho \mathbf{u}}{\partial t} + \nabla \cdot (\rho \mathbf{u}\mathbf{u}) = \nabla \cdot \mathbb{T} + \rho \mathbf{g}, \tag{2.2}$$

Energy balance

$$\frac{\partial \rho (e + \frac{1}{2}\mathbf{u}^2)}{\partial t} + \nabla \cdot \left(\rho \left(e + \frac{1}{2}\mathbf{u}^2 \right) \mathbf{u} \right) = -\nabla \cdot \mathbf{q} + \nabla \cdot (\mathbb{T} \cdot \mathbf{u}) + \rho \mathbf{g} \cdot \mathbf{u} + q_s. \tag{2.3}$$

Where ρ is the *density*, $\mathbf{u}$ the *velocity*, $\mathbf{g}$ the *gravity acceleration*, e the *internal energy*, $\mathbf{q}$ the *heat flux*, q_s the body heating source, and $\mathbb{T} = -p\mathbb{I} + \boldsymbol{\tau}$ the *stress tensor*, where p is the *pressure*, $\mathbb{I}$ a *unit vector tensor* and $\boldsymbol{\tau}$ the *shear stress tensor* (*viscous stress tensor*).

Equations (2.1)-(2.3) are well known and have direct physical interpretations, so we will not show their derivation here. For that we refer to Kleinstreuer [69], Müller [92], Ishii and Hibiki [61].

If the viscosity is neglected, i.e. $\boldsymbol{\tau} = \mathbf{0}$, the heat effects and the body forces are omitted then the equations (2.1)-(2.3) reduces to the usual form of the Euler equations.

The system (2.1)-(2.3) is augmented by several constitutive equations that connect between the variables in order to obtain a closed system, .i.e the number of variables equal the number of equations. These closure relations include a constitutive equation for the viscous stress tensor like the *Newton's law of viscosity*, a constitutive equation for the heat flux like the *Fourier's law of heat conduction*, and constitutive equations between the thermodynamics variables. See a detailed description of such closure equations in Ishii and Hibiki [61].

Later in this thesis we will neglect the viscosity and the heat flux. Thus we will focus on the last group of the constitutive equations, i.e. the thermodynamics closure equations which are called the *equations of state*. For a single phase substance, two basic properties such as the pressure and the density are sufficient to determine all other thermodynamics variables, such as the temperature and the internal energy

$$T = T(p, \rho), \tag{2.4a}$$

$$e = e(p, \rho). \tag{2.4b}$$

Here T is the *temperature*.

For two-phase flow, equations (2.1)-(2.3) are applied to each phase separately up to the interface, but not across it. At the interface, a special treatment is used to take into account

the discontinuities in various variables. In particlar, a specific form of balance equation is derived for the interface in limit sense, from which jump conditions are specified. These conditions express the exchange of mass, momentum and energy through the interface. These jump conditions across the interface are given as

Mass jump

$$[\![\rho(\mathbf{u}-\mathbf{u}_i)]\!]\cdot\mathbf{n}=0 \tag{2.5}$$

Momentum jump

$$[\![\rho\mathbf{u}(\mathbf{u}-\mathbf{u}_i)+\mathbb{T}]\!]\cdot\mathbf{n}=m_i^{\xi} \tag{2.6}$$

Energy jump

$$[\![\rho\left(e+\frac{1}{2}\mathbf{u}^2\right)(\mathbf{u}-\mathbf{u}_i)+\mathbb{T}\cdot\mathbf{u}-\mathbf{q}]\!]\cdot\mathbf{n}=e_i^{\xi}. \tag{2.7}$$

For the derivation of these conditions, see Müller [92], Slattery et al. [137], Ishii and Hibiki [61]. Here, $[\![f]\!]=f^+-f^-$ is the jump in the variable f at the both sides of the interface, $\mathbf{u}_i$ is the velocity of the interface, $\mathbf{n}$ the *unit normal vector* to the interface, m_i^{ξ} the resultant interfacial force due to the *surface tension* ξ, and e_i^{ξ} is the surface energy associated with the interface. For specific expressions of m_i^{ξ} and e_i^{ξ} see Aris [11], Müller [92], Ishii and Hibiki [61].

The conditions (2.5)-(2.7) do not identify the solution to the problem uniquely. Thus they are supplemented by some boundary conditions. Usually, the boundary conditions are obtained by assuming the entropy production at the interface to be zero, see Dreyer [39]. Since the resulting conditions are complex and depend on many parameters several simplifications are used, see Ishii and Hibiki [61].

More details about the interfacial conditions, boundary conditions at the interfaces and their simplifications require a knowledge of surface geometry. Since going more in this direction is out of scope of this thesis, we just show the simplification of condition (2.6). Neglecting the viscosity, i.e. $\boldsymbol{\tau}=\mathbf{0}$, assuming the normal velocity to the interface to be continuous, and assuming the surface tension is constant, then the condition (2.6) reduces to

$$[\![p]\!]=2\mathcal{H}\xi, \tag{2.8}$$

where $\mathcal{H}$ is the *mean curvature*. For a spherical bubble or droplet $\mathcal{H}=\dfrac{1}{R}$, R is the *radius*. Then (2.8) can be written as

$$p^+-p^-=\frac{2\xi}{R}. \tag{2.9}$$

This equation is the well known *Young-Laplace equation*, see Wörner [159].

At this step it clear that the modeling of a two-phase flow by using single-phase equations (2.1)-(2.3) augmented by the interfacial conditions (2.5)-(2.7) is impractical. This is due to the complexity of coupling between the field equations and the jump conditions in the presence of moving and deformable interfaces. This shows the importance of the averaging

procedures.

For the next section, it is easy to use generic forms for the balance equations and the interfacial conditions. For the balance equations (2.1)-(2.3), the generic equation can be written as

$$\frac{\partial \rho\Psi}{\partial t} + \nabla \cdot (\rho\Psi\mathbf{u}) = \nabla \cdot \mathbf{J} + \rho\Upsilon. \tag{2.10}$$

For the interfacial conditions (2.5)-(2.7), the generic form is expressed as

$$[\![\rho\Psi(\mathbf{u} - \mathbf{u}_i) + \mathbf{J}]\!] \cdot \mathbf{n} = M_i \tag{2.11}$$

The values for Ψ, $\mathbf{J}$, Υ, and M_i are shown in Table 2.1.

	Ψ	$\mathbf{J}$	Υ	M_i
Mass	1	0	0	0
Momentum	$\mathbf{u}$	$\mathbb{T}$	$\mathbf{g}$	m_i^ξ
Energy	$e + \frac{1}{2}\mathbf{u}^2$	$\mathbb{T} \cdot \mathbf{u} - \mathbf{q}$	$\mathbf{g} \cdot \mathbf{u} + \frac{q_s}{\rho}$	e_i^ξ

Table 2.1: The variables in the generic equations (2.10) and (2.11).

2.1.2 Ensemble averaging

An ensemble is considered as a set of large number of two-phase flow experiments with the same initial conditions, boundary conditions, and properties. Over this set the averaging is performed by 'adding' the values of the variable for each realization and dividing by the number of observations. Here a realization refers to a possible motion that could have happened [38]. Thus, the ensemble averaging is some generalization to the elementary averaging in which the observed values are added and divided by the number of observations. For more details about the concept of the ensemble averaging see [37, 38].

In general, we expect an infinite number of realizations. Thus, the ensemble averaging is given by the following definition, see Drew and Lahey [37].

Definition 2.1. The ensemble average for a field f on $\mathbf{x} \in \mathbb{R}^3$, $t \in [0, \infty)$ is given by

$$\overline{f}(\mathbf{x}, t) = \int_{\mathcal{E}} f(\mathbf{x}, t; \mu) dm(\mu), \tag{2.12}$$

where $dm(\mu)$ is the *measure*, i.e. probability, of *observing process* μ and $\mathcal{E}$ is the set of all processes, i.e. the *ensemble set*.

To apply the averaging procedure some mathematical results are needed. They are given hereafter.

Remark 2.1. To identify each phase separately, we use a *phase indicator function* or *characteristic function* $\chi_k(\mathbf{x},t)$ which is unity if the *position vector* $\mathbf{x}$ is in *phase* k at time t and zero otherwise, i.e.

$$\chi_k(\mathbf{x},t) = \begin{cases} 1, & \text{if phase } k \text{ presents at } (\mathbf{x},t), \\ 0, & \text{otherwise.} \end{cases}$$

We consider only two phases, i.e. $k = 1, 2$.

The two phase indicator functions are related by

$$\chi_1 + \chi_2 = 1 \tag{2.13}$$

The quantities $\dfrac{\partial \chi_k}{dt}$ and $\nabla\chi_k$ play an important role later. Since χ_k is a discontinuous function, then its derivatives will be found in the generalized sense. Such derivatives are introduced in the following definition, see e.g Hörmander [58] and Warnecke [156].

Definition 2.2. Assume Φ is a *set of test functions* on $\mathbb{R}^3 \times [0,\infty)$, that is, $\phi(\mathbf{x},t) \in \Phi$ if it has compact support and derivatives to all orders. Then if $f(\mathbf{x},t)$ is a generalized function, its derivatives are defined as

$$\int_\Omega \phi(\mathbf{x},t)\frac{\partial f(\mathbf{x},t)}{\partial t} dV dt = -\int_\Omega \frac{\partial \phi(\mathbf{x},t)}{\partial t} f(\mathbf{x},t) dV dt, \tag{2.14}$$

and

$$\int_\Omega \phi(\mathbf{x},t)\nabla f(\mathbf{x},t) dV dt = -\int_\Omega \nabla\phi(\mathbf{x},t) f(\mathbf{x},t) dV dt, \tag{2.15}$$

for any $\phi \in \Phi$. The integration domain Ω is a compact set in space and time that contains the support of ϕ.

To find $\nabla\chi_k$ use (2.15)

$$\begin{aligned} \int_\Omega \phi(\mathbf{x},t)\nabla\chi_k dV dt &= -\int_\Omega \nabla\phi(\mathbf{x},t)\chi_k dV dt, \\ &= -\int_{\Omega_k} \nabla\phi(\mathbf{x},t) dV dt. \end{aligned} \tag{2.16}$$

By using the divergence theorem, we get

$$\begin{aligned} \int_{\Omega_k} \nabla\phi(\mathbf{x},t) dV dt &= \int_{\partial\Omega_k} \mathbf{n}_k \phi(\mathbf{x},t) dV dt, \\ &= \int_\Omega \mathbf{n}_k \delta(\mathbf{x}-\mathbf{x}_i,t)\phi(\mathbf{x},t) dV dt. \end{aligned} \tag{2.17}$$

Note that Ω_k is the domain of phase k, $\partial\Omega_k$ the interface between phases, $\mathbf{n}_k$ is the unit normal vector to the interface in the direction outward of phase k, and $\delta(\mathbf{x}-\mathbf{x}_i,t)$ is the *Dirac delta generalized function*, where $\mathbf{x}_i$ is a point on the interface.

From (2.16) and (2.17) we have

$$\nabla\chi_k = \mathbf{n}_k\delta(\mathbf{x}-\mathbf{x}_i,t). \tag{2.18}$$

Using the generalized derivatives (2.14) and (2.15) for χ_k with the help of the *Reynolds transport theorem* [11], one can show that

$$\frac{\partial\chi_k}{\partial t} + \mathbf{u}_i\cdot\nabla\chi_k = 0. \tag{2.19}$$

All details are given in Drew and Passman [38]. Equation (2.19) is called the *topological equation*. And it means that the material derivative of χ_k is zero.

The ensemble average satisfies the linearity property; if a_1 and a_2 are constants, f_1 and f_2 are fields, then

$$\overline{a_1f_1 + a_2f_2} = a_1\overline{f_1} + a_2\overline{f_2}.$$

This relation is directly derived from the definition of the ensemble average (2.12). In addition, it is easy to show that

$$\overline{\overline{f_1}f_2} = \overline{f_1}\;\overline{f_2}.$$

Also, the ensemble averaging is assumed to satisfy

$$\overline{\frac{\partial f}{\partial t}} = \frac{\partial\overline{f}}{\partial t},$$

$$\overline{\nabla f} = \nabla\overline{f}.$$

Using these relations we obtain

$$\overline{\chi_k\nabla f} = \nabla\overline{\chi_k f} - \overline{f\nabla\chi_k}, \tag{2.20}$$

and

$$\overline{\chi_k\frac{\partial f}{\partial t}} = \frac{\partial\overline{\chi_k f}}{\partial t} - \overline{f\frac{\partial\chi_k}{\partial t}}. \tag{2.21}$$

Equation (2.20) is called *Gauss rule*, and equation (2.21) is called *Leibniz rule*, see Drew and Passman [38].

Two types of averaged variables are commonly used for two-phase flow. They are given in the following definitions, see Drew [36].

Definition 2.3. The *phasic average*, or χ_k-*weighted average* of the variable f is given by

$$\tilde{f}_k = \frac{\overline{\chi_k f}}{\alpha_k}, \tag{2.22}$$

where $\alpha_k = \overline{\chi_k}$ is conventionally called the *volume fraction.*

Definition 2.4. The *mass-weighted average* of the variable f is given by

$$\hat{f}_k = \frac{\overline{\chi_k \rho f}}{\overline{\chi_k \rho}} = \frac{\overline{\chi_k \rho f}}{\alpha_k \tilde{\rho}_k}. \tag{2.23}$$

The averaging procedure

By multiplying each side of the generic equation (2.10) by χ_k, then performing the ensemble averaging, we obtain

$$\overline{\chi_k \frac{\partial \rho\Psi}{\partial t}} + \overline{\chi_k \nabla \cdot (\rho\Psi\mathbf{u})} = \overline{\chi_k \nabla \cdot \mathbf{J}} + \overline{\chi_k \rho \Upsilon} \tag{2.24}$$

Using (2.20) and (2.21) in (2.24), we get

$$\frac{\partial \overline{\chi_k \rho\Psi}}{\partial t} + \nabla \cdot \overline{(\chi_k \rho\Psi\mathbf{u})} - \nabla \cdot \overline{\chi_k \mathbf{J}} - \overline{\chi_k \rho \Upsilon} = \overline{\rho\Psi(\frac{\partial \chi_k}{\partial t} + \mathbf{u} \cdot \nabla\chi_k) - \mathbf{J} \cdot \nabla\chi_k} \tag{2.25}$$

From the topological equation (2.19), $\dfrac{\partial \chi_k}{\partial t} = -\mathbf{u}_i \cdot \nabla\chi_k$. Using this in (2.25), we have

$$\frac{\partial \overline{\chi_k \rho\Psi}}{\partial t} + \nabla \cdot \overline{(\chi_k \rho\Psi\mathbf{u})} - \nabla \cdot \overline{\chi_k \mathbf{J}} - \overline{\chi_k \rho \Upsilon} = \overline{\rho\Psi(\mathbf{u} - \mathbf{u}_i) \cdot \nabla\chi_k - \mathbf{J} \cdot \nabla\chi_k} \tag{2.26}$$

This is the generic averaged equation, from which we derive the averaged equations for mass, momentum, and energy by using the values in Table 2.1. These averaged equations are shown below.

Averaged mass equation

The averaged mass equation is

$$\frac{\partial \overline{\chi_k \rho}}{\partial t} + \nabla \cdot \overline{(\chi_k \rho\mathbf{u})} = \overline{\rho(\mathbf{u} - \mathbf{u}_i) \cdot \nabla\chi_k} \tag{2.27}$$

Using $\tilde{\rho}_k = \dfrac{\overline{\chi_k \rho}}{\alpha_k}$, and $\hat{\mathbf{u}}_k = \dfrac{\overline{\chi_k \rho \mathbf{u}}}{\alpha_k \tilde{\rho}_k}$, then equation (2.27) will be

$$\frac{\partial \alpha_k \tilde{\rho}_k}{\partial t} + \nabla \cdot (\alpha_k \tilde{\rho}_k \hat{\mathbf{u}}_k) = \overline{\rho(\mathbf{u} - \mathbf{u}_i) \cdot \nabla\chi_k} = \Lambda_k. \tag{2.28}$$

From (2.18) $\nabla\chi_k$ is a Dirac delta function centered at the interface. Thus Λ_k is an interfacial term, indeed it represents a mass transfer. For the two phases, the unit normal

vectors at the interface are in opposite directions, i.e. $\mathbf{n}_1 = -\mathbf{n}_2$. Using this with the interfacial condition (2.5), we get

$$\sum_{k=1}^{2} \Lambda_k = 0.$$

Alternatively, this result is achieved by averaging the jump condition (2.5), i.e. multiply the jump condition (2.5) by $\mathbf{n} \cdot \nabla \chi_k$ and take the average.

Averaged momentum equation

The averaged momentum equation is

$$\frac{\partial \overline{\chi_k \rho \mathbf{u}}}{\partial t} + \nabla \cdot \overline{(\chi_k \rho \mathbf{u}\mathbf{u})} = \nabla \cdot \overline{\chi_k \mathbb{T}} + \overline{\chi_k \rho \mathbf{g}} + \overline{\rho \mathbf{u}(\mathbf{u} - \mathbf{u}_i) \cdot \nabla \chi_k - \mathbb{T} \cdot \nabla \chi_k}. \tag{2.29}$$

A typical approach is to assume that the velocity $\mathbf{u}$ can be decomposed as

$$\mathbf{u} = \hat{\mathbf{u}} + \grave{\mathbf{u}}, \tag{2.30}$$

where $\grave{\mathbf{u}}$ expresses the *velocity fluctuations* which may due to the turbulence, see Drew and Passman [38]. Also they consider $\overline{\chi_k \rho \grave{\mathbf{u}}} = 0$.

Now, we treat with the term $\overline{\chi_k \rho \mathbf{u}\mathbf{u}}$, by using (2.30), where

$$\begin{aligned} \overline{\chi_k \rho \mathbf{u}\mathbf{u}} &= \overline{\chi_k \rho (\hat{\mathbf{u}}_k + \grave{\mathbf{u}}_k)(\hat{\mathbf{u}}_k + \grave{\mathbf{u}}_k)}, \\ &= \alpha_k \tilde{\rho}_k \hat{\mathbf{u}}_k \ \hat{\mathbf{u}}_k - \alpha_k \mathcal{T}_k^{Re}, \end{aligned}$$

where

$$\mathcal{T}_k^{Re} = -\frac{\overline{\chi_k \rho \grave{\mathbf{u}}_k \grave{\mathbf{u}}_k}}{\alpha_k}, \tag{2.31}$$

is called the *Reynolds stress*.

By Definitions 2.3 and 2.4, we have

$$\tilde{\mathbb{T}}_k = \frac{\overline{\chi_k \mathbb{T}}}{\alpha_k},$$

$$\hat{\mathbf{g}}_k = \frac{\overline{\chi_k \rho \mathbf{g}}}{\alpha_k \tilde{\rho}_k}.$$

Then equation (2.29) will become

$$\begin{aligned} \frac{\partial \alpha_k \tilde{\rho}_k \hat{\mathbf{u}}_k}{\partial t} + \nabla \cdot (\alpha_k \tilde{\rho}_k \hat{\mathbf{u}}_k \ \hat{\mathbf{u}}_k) = \nabla \cdot \alpha_k (\tilde{\mathbb{T}}_k + \mathcal{T}_k^{Re}) + \alpha_k \tilde{\rho}_k \hat{\mathbf{g}}_k \\ + \overline{\rho \mathbf{u}(\mathbf{u} - \mathbf{u}_i) \cdot \nabla \chi_k - \mathbb{T}_k \cdot \nabla \chi_k}. \end{aligned} \tag{2.32}$$

The interfacial momentum term is separated into several parts. The first part of this term is expressed as

$$\overline{\rho\mathbf{u}(\mathbf{u}-\mathbf{u}_i)\cdot\nabla\chi_k} = \mathbf{u}_{ki}\Lambda_k, \tag{2.33}$$

where $\mathbf{u}_{ki}$ is defined as an interfacial velocity of phase k.

Using $\mathbb{T} = -p\mathbb{I} + \boldsymbol{\tau}$, then the second part of the interfacial momentum term is denoted by $\mathbf{M}_k$ and separated as

$$\begin{aligned}\mathbf{M}_k = -\overline{\mathbb{T}_k\cdot\nabla\chi_k} &= \overline{p\nabla\chi_k} - \overline{\boldsymbol{\tau}\nabla\chi_k},\\ &= p_{ki}\overline{\nabla\chi_k} - \boldsymbol{\tau}_{ki}\cdot\overline{\nabla\chi_k} + \overline{(\grave{p}_{ki}\mathbb{I} - \grave{\boldsymbol{\tau}}_{ki})\cdot\nabla\chi_k},\\ &= p_{ki}\nabla\alpha_k - \boldsymbol{\tau}_{ki}\cdot\nabla\alpha_k + \grave{M}_k. \end{aligned}\tag{2.34}$$

Here, p_{ki} and $\boldsymbol{\tau}_{ki}$ are the averaged interfacial values in phase k, with fluctuations $\grave{p}_{ki}$ and $\grave{\boldsymbol{\tau}}_{ki}$ respectively. The term $\overline{(\grave{p}_{ki}\mathbb{I} - \grave{\boldsymbol{\tau}}_{ki})\cdot\nabla\chi_k}$ is denoted by $\grave{M}_k$. Then the averaged momentum equation (2.32) can be written as

$$\begin{aligned}\frac{\partial\alpha_k\tilde{\rho}_k\hat{\mathbf{u}}_k}{\partial t} + \nabla\cdot(\alpha_k\tilde{\rho}_k\hat{\mathbf{u}}_k\,\hat{\mathbf{u}}_k) = \nabla\cdot\alpha_k(\tilde{\mathbb{T}}_k + \mathcal{T}_k^{Re}) + \alpha_k\tilde{\rho}_k\hat{\mathbf{g}}_k + \mathbf{u}_{ki}\Lambda_k\\ + p_{ki}\nabla\alpha_k - \boldsymbol{\tau}_{ki}\cdot\nabla\alpha_k + \grave{M}_k.\end{aligned}\tag{2.35}$$

Note that the averaging of the momentum jump condition (2.6) yields

$$\sum_{k=1}^{2}(\mathbf{u}_{ki}\Lambda_k + p_{ki}\nabla\alpha_k - \boldsymbol{\tau}_{ki}\cdot\nabla\alpha_k + \grave{M}_k) = \overline{m_i^{\xi}}.$$

Averaged energy equation

The averaged energy equation is

$$\begin{aligned}\overline{\frac{\partial\chi_k\rho(e+\frac{1}{2}\mathbf{u}^2)}{\partial t}} + \nabla\cdot\overline{(\chi_k\rho(e+\frac{1}{2}\mathbf{u}^2)\mathbf{u})} = \nabla\cdot\overline{\chi_k(\mathbb{T}\cdot\mathbf{u}-\mathbf{q})}\\ + \overline{\chi_k(\rho\mathbf{g}\cdot\mathbf{u}+q_s)} + \overline{\rho(e+\frac{1}{2}\mathbf{u}^2)(\mathbf{u}-\mathbf{u}_i)\cdot\nabla\chi_k - (\mathbb{T}\cdot\mathbf{u}-\mathbf{q})\cdot\nabla\chi_k}.\end{aligned}\tag{2.36}$$

If we proceed similarly as in the case of the momentum equation using the decomposition of variables as in (2.30), then the energy equation (2.36) will become

$$\begin{aligned}\frac{\partial\alpha_k\tilde{\rho}_k(\hat{e}_k+\frac{1}{2}\hat{\mathbf{u}}_k^2+\mathcal{U}_k^{Re})}{\partial t} + \nabla\cdot\alpha_k\tilde{\rho}_k\hat{\mathbf{u}}_k(\hat{e}_k+\frac{1}{2}\hat{\mathbf{u}}_k^2+\mathcal{U}_k^{Re}) =\\ \nabla\cdot\alpha_k((\tilde{\mathbb{T}}_k+\mathcal{T}_k^{Re})\cdot\hat{\mathbf{u}}_k - \tilde{\mathbf{q}}_k - \mathcal{L}_k^{Re}) + \alpha_k\tilde{\rho}_k\hat{\mathbf{g}}_k\cdot\hat{\mathbf{u}}_k + \alpha_k\tilde{q}_{s,k}\\ + \overline{\rho(e+\frac{1}{2}\mathbf{u}^2)(\mathbf{u}-\mathbf{u}_i)\cdot\nabla\chi_k - (\mathbb{T}\cdot\mathbf{u}-\mathbf{q})\cdot\nabla\chi_k},\end{aligned}\tag{2.37}$$

where $\mathcal{T}_k^{Re}$ is specified by (2.31). The term $\mathcal{U}_k^{Re}$ is called the *fluctuation Reynolds kinetic energy* and given as

$$\mathcal{U}_k^{Re} = \overline{\frac{\chi_k \rho \grave{\mathbf{u}}_k^2}{2\alpha_k \tilde{\rho}_k}},$$

and $\mathcal{L}_k^{Re}$ is called the *fluctuation Reynolds energy flux*, it is expressed as

$$\mathcal{L}_k^{Re} = \overline{\frac{\chi_k \rho \grave{e}_k \grave{\mathbf{u}}_k}{\alpha_k}} + \overline{\frac{\chi_k \rho \grave{\mathbf{u}}_k \grave{\mathbf{u}}_k^2}{2\alpha_k}} - \overline{\frac{\chi_k \mathbb{T} \cdot \grave{\mathbf{u}}_k}{\alpha_k}}.$$

The interfacial energy term is separated in the same way as was done for the interfacial momentum term. Assume that

$$(e_{ki} + \frac{1}{2}\mathbf{u}_{ki}^2)\Lambda_k = \overline{\rho(e + \frac{1}{2}\mathbf{u}^2)(\mathbf{u} - \mathbf{u}_i) \cdot \nabla \chi_k}, \tag{2.38}$$

here the left hand side is considered as the interfacial total energy where e_{ki} is assumed to be an interfacial internal energy.

Also assume that

$$\begin{aligned} \mathcal{W}_k &= -\overline{\mathbb{T} \cdot \mathbf{u} \cdot \nabla \chi_k}, \\ \mathcal{Q}_k &= \overline{\mathbf{q} \cdot \nabla \chi_k} \end{aligned} \tag{2.39}$$

where $\mathcal{W}_k$ is the *interfacial work*, and $\mathcal{Q}_k$ is the *interfacial heat source*.

Use the assumption (2.30) in (2.39), with the help of (2.34), we obtain

$$\begin{aligned} \mathcal{W}_k = -\overline{\mathbb{T} \cdot \mathbf{u} \cdot \nabla \chi_k} &= -\overline{\mathbb{T} \cdot \hat{\mathbf{u}}_k \cdot \nabla \chi_k} - \overline{\mathbb{T} \cdot \grave{\mathbf{u}}_k \cdot \nabla \chi_k}, \\ &= \mathbf{u}_{ki} \cdot \mathbf{M}_k + \grave{\mathcal{W}}_k, \end{aligned}$$

where $\grave{\mathcal{W}}_k$ is called the *interfacial extra work* [37].

Using the above separated terms for the interfacial energy, then the averaged energy equation (2.37) is written as

$$\begin{aligned} \frac{\partial \alpha_k \tilde{\rho}_k (\hat{e}_k + \frac{1}{2}\hat{\mathbf{u}}_k^2 + \mathcal{U}_k^{Re})}{\partial t} + \nabla \cdot \alpha_k \tilde{\rho}_k \hat{\mathbf{u}}_k (\hat{e}_k + \frac{1}{2}\hat{\mathbf{u}}_k^2 + \mathcal{U}_k^{Re}) = \\ \nabla \cdot \alpha_k ((\tilde{\mathbb{T}}_k + \mathcal{T}_k^{Re}) \cdot \hat{\mathbf{u}}_k - \tilde{\mathbf{q}}_k - \mathcal{L}_k^{Re}) + \alpha_k \tilde{\rho}_k \hat{\mathbf{g}}_k \cdot \hat{\mathbf{u}}_k + \alpha_k \tilde{q}_{s,k} \\ + (e_{ki} + \frac{1}{2}\mathbf{u}_{ki}^2)\Lambda_k + \mathbf{u}_{ki} \cdot \mathbf{M}_k + \grave{\mathcal{W}}_k + \mathcal{Q}_k. \end{aligned} \tag{2.40}$$

Again, by averaging the boundary condition (2.7), we obtain

$$\sum_{k=1}^{2} \left((e_{ki} + \frac{1}{2}\mathbf{u}_{ki}^2)\Lambda_k + \mathbf{u}_{ki} \cdot \mathbf{M}_k + \grave{\mathcal{W}}_k + \mathcal{Q}_k \right) = \overline{e_i^{\xi}}.$$

2.1.3 Closure problem

The resultant averaged model consists of six equations, two mass equations (2.28), two momentum equations (2.35), and two energy equations (2.40). It is obvious that extra terms appear in the model, which express the interfacial transfer processes across the interface. In fact, the exact expressions for these interfacial terms are unknown. Thus extra issues are considered. Usually, some simplifications are assumed and coupled with some experimental data and observations.

Moreover, a new variable appears in the model called the volume fraction and characterize the existence of each phase. Thus the number of the variables is larger than the number of equations. This occurs even if we use thermodynamic closure relations like (2.4). Thus the averaged model is not closed.

One of the most common approaches to close the averaged model is the assumption of equal pressure for both phases. This approach has been used for a long time and the resulting model is known in the literature as the classical six-equation model [118, 143, 145, 151]. It is well known that this model is ill-posed, i.e. it has complex characteristics, where this leads to numerical instabilities, see Stewart and Wendroff [143]. This problem has been studied extensively, and several procedures were proposed to avoid the numerical instabilities. In general, this includes adding numerical viscosity to dampen out the instabilities or by adding some correction terms to remove the complex character of the eigenvalues, see Toro [149], Kumbaro et al. [71], Toumi and Raymond [151], Sainsaulieu [118], Tiselj and Petelin [145]. So the model is well-posed under certain assumptions which may restrict its validity for the problems. Moreover, adding numerical viscosity may lead to unphysical solutions, see Saurel and Le Metayer [124].

Another approach to close the averaged model is by adding an extra equation for the volume fraction. This leads to the full non-equilibrium seven-equation models. To be more specific, this approach was initially introduced to close the multiphase models which were derived by applying the continuum mixture theory, like the Baer and Nunziato model [12]. Before the work of Baer and Nunziato [12] there were some trials to close these models by using an extra equation for the volume fraction, like the work of Passman et al. [104], see some review of these efforts in Berry [15]. In Baer and Nunziato [12] the entropy inequality for the two-phase mixture was used to establish the volume fraction equation. This model is unconditionally hyperbolic, i.e. well posed. See its mathematical structure in Embid and Baer [42].

Saurel and Abgrall [120] closed the model by using a volume fraction equation which is achieved by the averaging of the topological equation (2.19). This makes the model hyperbolic as we will see in Section 2.4.1.

Following [15, 47], applying averaging operator to the topological equation (2.19), and

using $\alpha_k = \overline{\chi_k}$, we get

$$\begin{aligned}\overline{\frac{\partial \chi_k}{\partial t}} + \overline{\mathbf{u}_i \cdot \nabla \chi_k} &= \frac{\partial \overline{\chi_k}}{\partial t} + \overline{\mathbf{u}_i \cdot \nabla \chi_k}, \\ &= \frac{\partial \alpha_k}{\partial t} + \overline{\mathbf{u}_i \cdot \nabla \chi_k}, \\ &= \frac{\partial \alpha_k}{\partial t} + \mathbf{u}_{ki} \cdot \overline{\nabla \chi_k} + \overline{\grave{\mathbf{u}}_i \cdot \nabla \chi_k}, \\ &= \frac{\partial \alpha_k}{\partial t} + \mathbf{u}_{ki} \cdot \nabla \alpha_k + \overline{\grave{\mathbf{u}}_i \cdot \nabla \chi_k} = 0. \end{aligned} \tag{2.41}$$

Here, $\grave{\mathbf{u}}_i$ represents the fluctuations in the interfacial velocity.

Assume $S_I = -\overline{\grave{\mathbf{u}}_i \cdot \nabla \chi_k}$, then the equation (2.41) is written as

$$\frac{\partial \alpha_k}{\partial t} + \mathbf{u}_{ki} \cdot \nabla \alpha_k = S_I. \tag{2.42}$$

This equation is the volume fraction equation that used by Saurel and Abgrall [120] to close the averaged model.

2.1.4 The Saurel-Abgrall model

The Saurel-Abgrall model [120] is the most promising model of two-phase flows. This model essentially consists of the averaged equations (2.28), (2.35), (2.40), complemented with the volume fraction equation (2.42). Neglecting all turbulent terms, the viscosity, the surface tension, the surface energy, the heat terms and mass transfer. Moreover, relaxation terms associated with the velocity and the pressure are inserted in the model. Dropping the averaging notations for simplicity, then the Saurel and Abgrall model is written as

$$\frac{\partial \alpha_1}{\partial t} + \mathbf{u}_I \cdot \nabla \alpha_1 = \mu(p_1 - p_2), \tag{2.43a}$$

$$\frac{\partial \alpha_1 \rho_1}{\partial t} + \nabla \cdot (\alpha_1 \rho_1 \mathbf{u}_1) = 0, \tag{2.43b}$$

$$\frac{\partial \alpha_1 \rho_1 \mathbf{u}_1}{\partial t} + \nabla \cdot (\alpha_1 \rho_1 \mathbf{u}_1 \mathbf{u}_1) + \nabla(\alpha_1 p_1) = p_I \nabla \alpha_1 + \lambda(\mathbf{u}_2 - \mathbf{u}_1), \tag{2.43c}$$

$$\begin{aligned}\frac{\partial \alpha_1 \rho_1 E_1}{\partial t} + \nabla \cdot ((\alpha_1 \rho_1 E_1 + \alpha_1 p_1)\mathbf{u}_1) = p_I \mathbf{u}_I \cdot \nabla \alpha_1 + \mu p_I (p_2 - p_1) \\ + \lambda \mathbf{u}_I \cdot (\mathbf{u}_2 - \mathbf{u}_1),\end{aligned} \tag{2.43d}$$

$$\frac{\partial \alpha_2 \rho_2}{\partial t} + \nabla \cdot (\alpha_2 \rho_2 \mathbf{u}_2) = 0, \tag{2.43e}$$

$$\frac{\partial \alpha_2 \rho_2 \mathbf{u}_2}{\partial t} + \nabla \cdot (\alpha_2 \rho_2 \mathbf{u}_2 \mathbf{u}_2) + \nabla(\alpha_2 p_2) = -p_I \nabla \alpha_1 - \lambda(\mathbf{u}_2 - \mathbf{u}_1) \tag{2.43f}$$

$$\begin{aligned}\frac{\partial \alpha_2 \rho_2 E_2}{\partial t} + \nabla \cdot ((\alpha_2 \rho_2 E_2 + \alpha_2 p_2)\mathbf{u}_2) = -p_I \mathbf{u}_I \cdot \nabla \alpha_1 - \mu p_I (p_2 - p_1) \\ - \lambda \mathbf{u}_I \cdot (\mathbf{u}_2 - \mathbf{u}_1).\end{aligned} \tag{2.43g}$$

Here $E_k = e_k + \frac{1}{2}\mathbf{u}_k^2$, $k = 1, 2$, is the *total energy*.

The volume fractions of both phases are related by the *saturation constraint* $\alpha_1 + \alpha_2 = 1$. This constraint is deduced directly by the averaging of equation (2.13).

The terms $p_I \nabla\alpha_1$ and $p_I \mathbf{u}_I \cdot \nabla\alpha_1$ prevent the system of equations (2.43b)-(2.43g) from being in conservative form, i.e. divergence form. Thus, they are called non-conservative terms and the system (2.43) is a non-conservative system. These terms are also called *nozzling terms*, this is due to the analogy with the duct variation cross-section terms that appear in the Euler equations averaged over a duct of variable cross-section.

The terms $\mathbf{u}_I$ and p_I are used to represent the *interfacial velocity* and the *interfacial pressure* respectively. As in [120], the interfacial pressure is defined as the mixture pressure, while the interfacial velocity is defined as the velocity of the center of mass

$$p_I = \alpha_1 p_1 + \alpha_2 p_2, \qquad \mathbf{u}_I = \frac{\alpha_1\rho_1\mathbf{u}_1 + \alpha_2\rho_2\mathbf{u}_2}{\alpha_1\rho_1 + \alpha_2\rho_2}. \tag{2.44}$$

Other closure relations for the interfacial terms are possible. One other choice is defined by Baer and Nunziato [12] as

$$p_I = p_1, \qquad \mathbf{u}_I = \mathbf{u}_2, \tag{2.45}$$

where the interfacial velocity is assumed equal to the velocity of the less compressible phase and the interfacial pressure is assumed equal to pressure of the most compressible phase.

Further closure relations were derived by Saurel et al. [123] and written as follows

$$p_I = \frac{Z_1 p_2 + Z_2 p_1}{Z_1 + Z_2} + \frac{Z_1 Z_2}{Z_1 + Z_2}\frac{\nabla\alpha_1}{|\nabla\alpha_1|} \cdot (\mathbf{u}_2 - \mathbf{u}_1), \tag{2.46}$$

$$\mathbf{u}_I = \frac{Z_1\mathbf{u}_1 + Z_2\mathbf{u}_2}{Z_1 + Z_2} + \frac{\nabla\alpha_1}{|\nabla\alpha_1|}\frac{p_2 - p_1}{Z_1 + Z_2}, \tag{2.47}$$

where Z_k represents the *acoustic impedance*

$$Z_k = \rho_k c_k, \quad k = 1, 2. \tag{2.48}$$

Here c_k is the *speed of sound*,

$$c_k^2 = \frac{\dfrac{p_k}{\rho_k^2} - \left(\dfrac{\partial e_k}{\partial \rho_k}\right)_{p_k}}{\left(\dfrac{\partial e_k}{\partial p_k}\right)_{\rho_k}}, \quad k = 1, 2. \tag{2.49}$$

There are more closure relations for the interfacial variables in the literature. Some of these relations are derived to satisfy an entropy inequality, see Coquel et al. [26], Guillard

and Labois [51].

The choice of the interfacial closure relations has an important effect on the structure of the waves present in the models, see Andrianov [8]. In the case of stiff mechanical relaxation, i.e. infinite relaxation parameters, all choices play similar roles. Indeed, you can see in Murrone and Guillard [96] that the choice of these interfacial variables has no effect on the derivation of the five-equation model of single pressure and single velocity from the seven-equation model (2.43) assuming stiff mechanical relaxation.

An interaction between the fluids is inserted through relaxation terms for the pressure and the velocity. These terms are detailed below.

Pressure relaxation terms

These terms are $\mu(p_1 - p_2)$ in the volume fraction equation, and $\pm\mu p_I(p_2 - p_1)$ terms in the energy equations. Here $\mu > 0$ is the relaxation parameter which determines the rate at which the pressures relax to a common value. The existence of such parameter was verified by Baer and Nunziato [12].

The pressure relaxation terms are used to take into account the relaxation phenomena behind shock and pressure waves in two-phase mixture, this is detailed in [120]. Also, these terms are of special importance to fulfill the interfacial pressure condition between fluids. This condition expresses the equality of the pressures at the interface which is given by (2.8) in the absence of the surface tension. To satisfy this condition the relaxation procedure is assumed to be instantaneous, i.e. the parameter μ is assumed to be infinite.

Velocity relaxation terms

These terms are $\pm\lambda(\mathbf{u}_2 - \mathbf{u}_1)$ in the momentum equations and $\pm\lambda\mathbf{u}_I \cdot (\mathbf{u}_2 - \mathbf{u}_1)$ in the energy equations, where $\lambda > 0$ is the velocity relaxation parameter which determine the rate at which the velocities relax to a common value. The velocity relaxation terms are used to model the *drag force*, which is due to the imbalance of the pressure and due to the viscous stresses on the surface of an elementary particle, i.e. solid particle, bubble or droplet. It depends on the nature of the particle itself as well as on the nature of the fluid [62, 63, 124]. Based on an empirical relation deduced from experiments, the drag force is modeled as

$$\mathbf{F}_d = \lambda(\mathbf{u}_2 - \mathbf{u}_1).$$

The parameter λ is a function of the geometric parameters of the particle and the *Reynolds number* which characterize the nature of the flow. See the details in Saurel and Le Metayer [124].

By assuming that the parameter λ tends to infinity an instantaneous equilibrium velocity is achieved. And this can be used to satisfy the interface condition for the velocity between pure fluids. This condition imposes an equal normal velocity at the interface.

This can be seen from the jump condition (2.5) if there is no mass transfer.

Using instantaneous relaxation procedures for the pressure and the velocity extends the validity of the Saurel-Abgrall model to a wider range of applications, like interfaces, detonation, cavitation, etc., see details in Saurel and Le Metayer [124].

2.2 Mathematical theory of the hyperbolic balance laws

In this section we will certainly not attempt to cover all aspects of the theory of balance laws. Rather, we present a brief review for the basic concepts and facts related to the work in this thesis. First, we present a short summary to the main concepts of hyperbolic conservation laws theory. For a comprehensive study for the theory of the conservation laws, we refer to Dafermos [29], Godlewski and Raviart [49], Kröner [70], LeVeque [84, 85], Serre [132], or Smoller [138].

After a brief review of conservation laws, we introduce a brief discussion on the theory developed for the non-conservative systems. Then, special attention is devoted to the concept and theory of the Riemann problem.

2.2.1 Hyperbolic systems of conservation laws

Consider the Cauchy problem for a system of conservation laws in one dimension

$$\mathbf{u}_t + \mathbf{f}(\mathbf{u})_x = \mathbf{0}, \tag{2.50}$$

$$\mathbf{u}(x,0) = \mathbf{u}_0(x). \tag{2.51}$$

Here $(x,t) \in \mathbb{R} \times [0,\infty)$, $\mathbf{u} \in \Omega$, where Ω is an open subset of $\mathbb{R}^n$ and $\mathbf{f} : \Omega \to \mathbb{R}^n$ is a smooth function.

Let $\mathbf{A}(\mathbf{u}) = \mathbf{f}'(\mathbf{u})$ be the $n \times n$ *Jacobian matrix* of the flux function $\mathbf{f}(\mathbf{u})$, the system (2.50) can be written in the quasilinear form

$$\mathbf{u}_t + \mathbf{A}(\mathbf{u})\mathbf{u}_x = \mathbf{0}. \tag{2.52}$$

Definition 2.5. The system (2.50) is called *hyperbolic* if the matrix $\mathbf{A}(\mathbf{u})$ has n real eigenvalues

$$\lambda_1(\mathbf{u}) \le \lambda_2(\mathbf{u}) \le \cdots \le \lambda_n(\mathbf{u}),$$

and a complete set of eigenvectors, i.e. n linearly independent corresponding right eigenvectors

$$\mathbf{r}_1(\mathbf{u}),\ \mathbf{r}_2(\mathbf{u}), \cdots,\ \mathbf{r}_n(\mathbf{u}).$$

In addition, the system (2.50) is called *strictly hyperbolic* if the eigenvalues are all distinct

$$\lambda_1(\mathbf{u}) < \lambda_2(\mathbf{u}) < \cdots < \lambda_n(\mathbf{u}).$$

On the other hand, the system (2.50) is called *parabolic degenerate* if some eigenvectors become linearly dependent.

It is well known that smooth solutions for the problem (2.50), (2.51) may do not exist beyond some finite time interval, even if the initial data $\mathbf{u}_0$ are smooth, see examples in LeVeque [84, 85], and Smoller [138]. Thus, solutions globally in time are defined in a generalized sense. This leads us to introduce the following definition for the generalized solution which is called *weak solution* or *integral solution*.

Definition 2.6. A function $\mathbf{u} \in L^\infty_{loc}(\mathbb{R} \times [0,\infty))^n$ is called a weak solution of the Cauchy problem (2.50), (2.51) if for any test function $\boldsymbol{\phi} \in C^1_0(\mathbb{R} \times [0,\infty))^n$, it holds

$$\int\int_{\mathbb{R}\times[0,\infty)} [\boldsymbol{\phi}_t \cdot \mathbf{u} + \boldsymbol{\phi}_x \cdot \mathbf{f}(\mathbf{u})] dxdt + \int_{\mathbb{R}} \boldsymbol{\phi}(x,0) \cdot \mathbf{u}(x,0) dx = 0. \tag{2.53}$$

Here L^∞_{loc} is the *space of locally bounded measurable functions*, and $C^1_0(\mathbb{R} \times [0,\infty))$ the space of C^1 functions with compact support in $\mathbb{R} \times [0,\infty)$.

The integral formulation (2.53) allows for discontinuous solutions. These solutions often consist of piecewise smooth parts connected by discontinuities. Indeed, not every discontinuity is permissible, where some jump conditions across the curve of discontinuity should be satisfied. These conditions are called the *Rankine-Hugoniot conditions* and given as

$$[\![\mathbf{f}(\mathbf{u})]\!] = \sigma [\![\mathbf{u}]\!], \tag{2.54}$$

where σ is the *speed of the discontinuity*. The conditions (2.54) are a direct result of the integral (2.53) across the discontinuity curve, see e.g. Kröner [70], and Smoller [138].

Another difficulty for the solution of the problem (2.50), (2.51) is that the weak solution is not unique. Hence, additional admissibility conditions are required to pick out the physical relevant solution. In fact, this solution is the limiting solution of the viscous system

$$\mathbf{u}_t + \mathbf{f}(\mathbf{u})_x = \epsilon \mathbf{B} \mathbf{u}_{xx}, \quad \epsilon > 0, \tag{2.55}$$

as $\epsilon \to 0$. Here, $\mathbf{B}$ is a viscous matrix, i.e. it is a constant matrix of the viscosity coefficients, see specific cases in Smoller [138].

The system (2.55) is considered as the true physical form of the system (2.50). Thus the physical solution of the system (2.50) is called the *vanishing viscosity solution*. But finding solutions in the vanishing viscosity sense is very difficult. Thus, simpler conditions were deduced to pick out the physical solution. These admissibility conditions are called *entropy conditions*. This terminology comes from the gas dynamics in conjuction with the second law of thermodynamics, see Lax [79]. In addition, a discontinuity satisfying the Rankine-Hugoniot conditions (2.54) and an entropy condition is called a *shock*.

There are several admissibility criteria, like the conditions of Dafermos [28], Liu [86, 87], and Lax [78], see a review in Dafermos [29]. The classical criterion used in the literature

is the Lax condition [78]. This condition states that an $i-$shock wave, $1 \leq i \leq n$, of speed σ is admissible if the inequalities

$$\lambda_{i-1}(\mathbf{u}_L) < \sigma < \lambda_i(\mathbf{u}_L),$$
$$\lambda_i(\mathbf{u}_R) < \sigma < \lambda_{i+1}(\mathbf{u}_R)$$

hold. Here $\mathbf{u}_L$ and $\mathbf{u}_R$ are the states to the left and the right of the shock respectively. In addition, if the equality

$$\lambda_i(\mathbf{u}_L) = \sigma = \lambda_i(\mathbf{u}_R),$$

holds, then the admissible $i-$wave is called an $i-$contact discontinuity.

2.2.2 Hyperbolic systems in the presence of non-conservative terms

Consider the general quasilinear hyperbolic system

$$\mathbf{u}_t + \mathbf{A}(\mathbf{u})\mathbf{u}_x = \mathbf{0}, \tag{2.56}$$

where $\mathbf{u} \in \Omega \subset \mathbb{R}^n$. Since the system (2.56) is hyperbolic, the matrix $\mathbf{A}(\mathbf{u})$ has n real eigenvalues $\lambda_1,\ \lambda_2, \cdots,\ \lambda_n$ with n linearly independent right eigenvectors $\mathbf{r}_1,\ \mathbf{r}_2, \cdots,\ \mathbf{r}_n$.

As in the previous section, $\mathbf{A}(\mathbf{u})$ is the Jacobian of flux function $\mathbf{f}(\mathbf{u})$, so the system (2.56) is conservative. But if there is no a such flux function the system (2.56) is non-conservative.

It is clear that the Definition 2.6 of the weak solution, and the classical Rankine-Hugoniot conditions (2.54) of the conservative systems cannot be used for non-conservative systems. This is a source of the main difficulties for the theory and numerics of the non-conservative systems. However, in this thesis we are interested in the non-conservative systems, since all models used in this thesis contain non-conservative terms, see Section 2.4.

In recent years, several authors have focused on the theory of non-conservative systems, see Crasta and LeFloch [27], Dal Maso et al. [30] as well as LeFloch [82]. Most developments in the theory and later in numerical schemes for these systems were based on the so-called *DLM theory* of Dal Maso, LeFloch and Murat [30] where across a discontinuity the non-conservative product is defined along paths connecting the left and right states.

Following [30], we consider family of paths in $\Omega \subset \mathbb{R}^n$ which is a locally Lipschitz map

$$\Phi : [0,1] \times \Omega \times \Omega \to \Omega$$

and it is assumed to satisfy the following properties:

- $\Phi(0, \mathbf{u}_L, \mathbf{u}_R) = \mathbf{u}_L,$ and $\Phi(1, \mathbf{u}_L, \mathbf{u}_R) = \mathbf{u}_R$, for any $\mathbf{u}_L,\ \mathbf{u}_R \in \Omega$;
- $\Phi(\varsigma, \mathbf{u}, \mathbf{u}) = \mathbf{u}$, for any $\mathbf{u} \in \Omega$ and $\varsigma \in [0,1]$;

- for every bounded set $\mathscr{U} \subset \Omega$, there exists $K \geqslant 1$ such that

$$\left| \frac{\partial \Phi(\varsigma, \mathbf{u}_L, \mathbf{u}_R)}{\partial \varsigma} - \frac{\partial \Phi(\varsigma, \mathbf{w}_L, \mathbf{w}_R)}{\partial \varsigma} \right| \leqslant K|(\mathbf{u}_L - \mathbf{w}_L) - (\mathbf{u}_R - \mathbf{w}_R)|,$$

  for every $\mathbf{u}_L,\ \mathbf{u}_R,\ \mathbf{w}_L,\ \mathbf{w}_R \in \mathscr{U}$ and almost every $\varsigma \in [0,1]$.

Using the above notation, the *generalized Rankine-Hugoniot* conditions across a discontinuity of speed σ is defined as

$$\int_0^1 \left(\sigma \mathbf{I} - \mathbf{A}(\Phi(\varsigma, \mathbf{u}_L, \mathbf{u}_R))\right) \frac{\partial \Phi(\varsigma, \mathbf{u}_L, \mathbf{u}_R)}{\partial \varsigma} d\varsigma = 0, \tag{2.57}$$

where $\mathbf{I}$ is the identity matrix.

The relation (2.57) shows that the weak solution for the non-conservative system depends on the choice of the path Φ. In the particular case that the matrix $\mathbf{A}(\mathbf{u})$ is a Jacobian matrix of some flux function $\mathbf{f}(\mathbf{u})$, the integral (2.57) is independent of paths and reduces to the classical Rankine-Hugoniot conditions (2.54).

2.2.3 Riemann problem

The initial value problem for the system (2.56) with the piecewise constant initial condition

$$\mathbf{u}(x,0) = \mathbf{u}_0(x) = \begin{cases} \mathbf{u}_L, & x \leq 0 \\ \mathbf{u}_R, & x > 0 \end{cases} \tag{2.58}$$

is known as the *Riemann problem*.

The Riemann problem is the simplest initial value problem for hyperbolic systems. It is used, as a basic problem, to study the main features of the hyperbolic problems. In addition, it is the basic building block for an important class of numerical methods, namely the Godunov-type schemes. Moreover, due to their simplicity they are also used as test cases for numerical schemes.

In fact, the general solution of the Riemann problem is difficult to obtain. Moreover, the Riemann problem may have no weak solution when the difference $\|\mathbf{u}_L - \mathbf{u}_R\|$ is sufficiently large. Just for specific systems of conservation laws one can show that the solution to the Riemann problem exists globally, see Godlewski and Raviart [49] as well as Smoller [138] for details and examples.

According to great difficulties with a general solution for the Riemann problem, we consider only the structure of elementary wave solutions corresponding to an eigenvalue. Indeed, the $i-th$ eigenvalue λ_i determines a characteristic field, called the *i-field* and the corresponding solution is referred to as the *i-wave*. The characterstic fields are classified in two types, they are given in the following definition

Definition 2.7. For each $i = 1, \cdots, n$, the i-characteristic field of (2.56) is said to be *genuinely nonlinear* if

$$\nabla_{\mathbf{u}} \lambda_i(\mathbf{u}) \cdot \mathbf{r}_i(\mathbf{u}) \neq 0, \quad \text{for all } \mathbf{u} \in \Omega, \tag{2.59}$$

and *linearly degenerate* if

$$\nabla_{\mathbf{u}} \lambda_i(\mathbf{u}) \cdot \mathbf{r}_i(\mathbf{u}) = 0, \quad \text{for all } \mathbf{u} \in \Omega, \tag{2.60}$$

where $\nabla_{\mathbf{u}} = \left(\dfrac{\partial}{\partial u_1}, \dfrac{\partial}{\partial u_2}, ..., \dfrac{\partial}{\partial u_n} \right)$.

The elementary i-wave solutions include the shock wave, contact discontinuity and the so-called rarefaction wave. The shocks and contact discontinuities satisfy the jump conditions (2.54). While, the rarefaction waves are continuous solutions, also called expansion waves. Moreover, if the i-characteristic field is genuinely nonlinear then the i-wave is either a shock or a rarefaction, while the linearly degenerate i-characteristic field results in a contact discontinuity, see Smoller [138].

Combining shock, contact discontinuity and rarefaction waves we are able to solve the Riemann problem (2.56), (2.58). Indeed, the solution consists of at most $(n+1)$ constant states separated by shocks, rarefaction waves, or contact discontinuities.

Remark 2.2. We are interested only in the case when each characteristic field is either genuinely nonlinear or linearly degenerate. In the case when the characteristic fields are not globally non-linear the situation is more complicated and one classical entropy condition, like conditions mentioned in Subsection 2.2.1, is not enough to single out the unique solution. For this case the so-called *non-classical entropy conditions* are used, see the book of LeFloch [83].

To construct the solution of the Riemann problem, it is useful to define the concept of the Riemann invariant.

Definition 2.8. A smooth function $\vartheta : \Omega \to \mathbb{R}$ is called an i-Riemann invariant if

$$\nabla_{\mathbf{u}} \vartheta(\mathbf{u}) \cdot \mathbf{r}_i(\mathbf{u}) = 0, \qquad \text{for all } \ \mathbf{u} \in \Omega. \tag{2.61}$$

The next theorems state some facts related to the Riemann invariants and play an important role in constructing a solution for the Riemann problem.

Theorem 2.1. *On an i-rarefaction wave, all i-Riemann invariants are constant..*

Proof. See the proof in Godlewski and Raviart [49]. □

Theorem 2.2. *Consider the hyperbolic system* (2.56)*, if some eigenvalue λ_i has constant multiplicity m, then there exist locally $(n-m)$ i-Riemann invariants $\vartheta_1, ..., \vartheta_{n-m}$ such that the gradients $\nabla\vartheta_1, ..., \nabla\vartheta_{n-m}$ are linearly independent.*

Proof. See Serre [132]. In particular if λ_i is distinct, i.e. $m = 1$, you can find the proof for this case in Godlewski and Raviart [49]. □

2.3 Godunov method

Here we present a short review of the Godunov method which is one of the most powerful numerical methods for the conservation systems. This method in its basic form is a first order upwind-type scheme. For more details of this method we refer to Guinot [52], LeVeque [84] and Toro [148].

Recall the hyperbolic system of conservation laws (2.50)

$$\mathbf{u}_t + \mathbf{f}(\mathbf{u})_x = \mathbf{0}, \tag{2.62}$$

with the initial data

$$\mathbf{u}(x,0) = \mathbf{u}_0(x). \tag{2.63}$$

Assume that the $x-t$ plane is discretized uniformly with time step Δt and spatial grid size Δx. The discrete grid points $(x_j,\ t^n)$ are chosen as

$$x_j = j\Delta x, \quad j \in \mathbb{Z},$$
$$t^n = n\Delta t, \quad n \in \mathbb{N}_0.$$

Let $x_{j+\frac{1}{2}} = (j+\frac{1}{2})\Delta x$. In addition, define an approximation $\mathbf{u}_j^n \in \Omega$ to the solution $\mathbf{u}(x_j,\ t^n)$.

Let us use the approximation $\mathbf{u}_j^n$ to define a piecewise constant function $\check{\mathbf{u}}(x,t_n)$ as

$$\check{\mathbf{u}}(x,t_n) = \mathbf{u}_j^n, \quad x_{j-\frac{1}{2}} \le x \le x_{j+\frac{1}{2}}.$$

Now, consider the following Cauchy problem

$$\begin{aligned} &\check{\mathbf{u}}_t + \mathbf{f}(\check{\mathbf{u}})_x = \mathbf{0}, \qquad x \in \mathbb{R},\ t \ge t^n, \\ &\check{\mathbf{u}}(x,t_n) = \mathbf{u}_j^n, \qquad x_{j-\frac{1}{2}} \le x \le x_{j+\frac{1}{2}}, \qquad j \in \mathbb{Z}. \end{aligned} \tag{2.64}$$

Integrating (2.64) over $[x_{j-\frac{1}{2}}, x_{j+\frac{1}{2}}] \times [t^n, t^{n+1}]$, we have

$$\begin{aligned} \int_{x_{j-\frac{1}{2}}}^{x_{j+\frac{1}{2}}} \check{\mathbf{u}}(x,t^{n+1})dx = &\int_{x_{j-\frac{1}{2}}}^{x_{j+\frac{1}{2}}} \check{\mathbf{u}}(x,t^n)dx \\ &- \left[\int_{t^n}^{t^{n+1}} \mathbf{f}(\check{\mathbf{u}}(x_{j+\frac{1}{2}},t))dt - \int_{t^n}^{t^{n+1}} \mathbf{f}(\check{\mathbf{u}}(x_{j-\frac{1}{2}},t))dt \right]. \end{aligned} \tag{2.65}$$

We set

$$\mathbf{u}_j^{n+1} = \frac{1}{\Delta x} \int_{x_{j-\frac{1}{2}}}^{x_{j+\frac{1}{2}}} \check{\mathbf{u}}(x,t^{n+1})dx,$$

and define the *numerical flux* $\mathbf{F}(\mathbf{u}_j^n, \mathbf{u}_{j+1}^n)$ as

$$\mathbf{F}(\mathbf{u}_j^n, \mathbf{u}_{j+1}^n) = \frac{1}{\Delta t} \int_{t^n}^{t^{n+1}} \mathbf{f}(\check{\mathbf{u}}(x_{j+\frac{1}{2}},t))dt. \tag{2.66}$$

Then from (2.65) we obtain the following scheme

$$\mathbf{u}_j^{n+1} = \mathbf{u}_j^n - \frac{\Delta t}{\Delta x}[\mathbf{F}(\mathbf{u}_j^n, \mathbf{u}_{j+1}^n) - \mathbf{F}(\mathbf{u}_{j-1}^n, \mathbf{u}_j^n)]. \tag{2.67}$$

To compute the numerical flux $\mathbf{F}(\mathbf{u}_j^n, \mathbf{u}_{j+1}^n)$ we solve the Riemann problem at the cell edge $x_{j+\frac{1}{2}}$, which consists of the system (2.64) and the initial data

$$\check{\mathbf{u}}(x, t^n) = \begin{cases} \mathbf{u}_j^n, & x < x_{j+\frac{1}{2}} \\ \mathbf{u}_{j+1}^n, & x > x_{j+\frac{1}{2}} \end{cases} \tag{2.68}$$

Now, it is obvious that the integral (2.66) is trivial since the Riemann problem along the line $x = x_{j+\frac{1}{2}}$ is constant and depends only on the states $\mathbf{u}_j^n$ and $\mathbf{u}_{j+1}^n$. Denote this value by $\mathbf{u}^*(\mathbf{u}_j^n, \mathbf{u}_{j+1}^n)$, then the integral (2.66) reduces to

$$\mathbf{F}(\mathbf{u}_j^n, \mathbf{u}_{j+1}^n) = \mathbf{f}(\mathbf{u}^*(\mathbf{u}_j^n, \mathbf{u}_{j+1}^n)) \tag{2.69}$$

This leads to the Godunov scheme

$$\mathbf{u}_j^{n+1} = \mathbf{u}_j^n - \frac{\Delta t}{\Delta x}[\mathbf{f}(\mathbf{u}^*(\mathbf{u}_j^n, \mathbf{u}_{j+1}^n)) - \mathbf{f}(\mathbf{u}^*(\mathbf{u}_{j-1}^n, \mathbf{u}_j^n))]. \tag{2.70}$$

This scheme is written in the standard form of the so-called conservative schemes which has the general form

$$\mathbf{u}_j^{n+1} = \mathbf{u}_j^n - \frac{\Delta t}{\Delta x}[\mathbf{F}_{j+\frac{1}{2}}^n - \mathbf{F}_{j-\frac{1}{2}}^n].$$

This type of schemes has the ability to capture shock discontinuities correctly, whereas the non-conservative schemes are not able to capture the exact location of the discontinuity, see LeVeque [84], Hou and LeFloch [59].

Remark 2.3. In the above derivation it is assumed that the Riemann solution at the edge $x_{j+\frac{1}{2}}$ is not influenced by adjacent Riemann problems. To ensure this condition we require the following restriction on the time step

$$\left| \frac{\Delta t}{\Delta x} \lambda_i(\mathbf{u}_j^n) \right| \leq 1 \tag{2.71}$$

for all λ_i at $\mathbf{u}_j^n$. Here, λ_i are the eigenvalues of the Jacobian matrix $\mathbf{f}'(\mathbf{u})$.

The maximum value of the quantity in the left hand side of (2.71) is called the *Courant number* or *CFL number*.

Remark 2.4. If we use the entropy-satisfying Riemann solutions, then the weak solutions obtained by Godunov's method satisfy the entropy condition.

Proof. See LeVeque [84]. □

2.4 Mathematical analysis of the current models

In this section we investigate the mathematical properties of the three models lying in the center of interest of this thesis, i.e. the seven-equation, the six-equation and the five-equation models. The aim of this study is to highlight either the benefits or the difficulties related to each model for the numerical approximations. This study is used in later chapters when the numerical methods will be introduced. In addition, some notes are also given related to the main issues of the treatment of non-conservative terms and the Riemann problem.

Throughout the thesis we restrict ourselves to one-dimensional flows, then the seven-equation model of Saurel and Abgrall (2.43) without heat and mass transfer is written in one-dimension as

$$\frac{\partial \alpha_1}{\partial t} + u_I \frac{\partial \alpha_1}{\partial x} = \mu(p_1 - p_2), \tag{2.72a}$$

$$\frac{\partial \alpha_1\rho_1}{\partial t} + \frac{\partial (\alpha_1\rho_1 u_1)}{\partial x} = 0, \tag{2.72b}$$

$$\frac{\partial \alpha_1\rho_1 u_1}{\partial t} + \frac{\partial (\alpha_1\rho_1 u_1^2 + \alpha_1 p_1)}{\partial x} = p_I \frac{\partial \alpha_1}{\partial x} + \lambda(u_2 - u_1), \tag{2.72c}$$

$$\frac{\partial \alpha_1\rho_1 E_1}{\partial t} + \frac{\partial (\alpha_1(\rho_1 E_1 + p_1)u_1)}{\partial x} = p_I u_I \frac{\partial \alpha_1}{\partial x} + \mu p_I(p_2 - p_1) + \lambda u_I(u_2 - u_1), \tag{2.72d}$$

$$\frac{\partial \alpha_2\rho_2}{\partial t} + \frac{\partial (\alpha_2\rho_2 u_2)}{\partial x} = 0, \tag{2.72e}$$

$$\frac{\partial \alpha_2\rho_2 u_2}{\partial t} + \frac{\partial (\alpha_2\rho_2 u_2^2 + \alpha_2 p_2)}{\partial x} = -p_I \frac{\partial \alpha_1}{\partial x} - \lambda(u_2 - u_1), \tag{2.72f}$$

$$\frac{\partial \alpha_2\rho_2 E_2}{\partial t} + \frac{\partial (\alpha_2(\rho_2 E_2 + p_2)u_2)}{\partial x} = -p_I u_I \frac{\partial \alpha_1}{\partial x} - \mu p_I(p_2 - p_1) - \lambda u_I(u_2 - u_1). \tag{2.72g}$$

2.4.1 Mathematical properties of the seven-equation model

In order to investigate the mathematical properties of the model (2.72), we rewrite it in terms of primitive variables as

$$\frac{\partial \mathbf{W}}{\partial t} + \mathbf{A}\frac{\partial \mathbf{W}}{\partial x} = 0 \tag{2.73}$$

where

$$\mathbf{W} = (\alpha_1, \rho_1, u_1, p_1, \rho_2, u_2, p_2)^T.$$

The non-differential source terms are omitted in the system (2.73) since they have no effect on the type of the model, i.e. the hyperbolicity.

The matrix $\mathbf{A}$ is given as

$$\mathbf{A} = \begin{bmatrix} u_I & 0 & 0 & 0 & 0 & 0 & 0 \\ \frac{\rho_1}{\alpha_1}(u_1 - u_I) & u_1 & \rho_1 & 0 & 0 & 0 & 0 \\ \frac{p_1 - p_I}{\alpha_1 \rho_1} & 0 & u_1 & \frac{1}{\rho_1} & 0 & 0 & 0 \\ \frac{\rho_1 c_{I,1}^2}{\alpha_1}(u_1 - u_I) & 0 & \rho_1 c_1^2 & u_1 & 0 & 0 & 0 \\ -\frac{\rho_2}{\alpha_2}(u_2 - u_I) & 0 & 0 & 0 & u_2 & \rho_2 & 0 \\ -\frac{p_2 - p_I}{\alpha_2 \rho_2} & 0 & 0 & 0 & 0 & u_2 & \frac{1}{\rho_2} \\ -\frac{\rho_2 c_{I,2}^2}{\alpha_2}(u_2 - u_I) & 0 & 0 & 0 & 0 & \rho_2 c_2^2 & u_2 \end{bmatrix}.$$

Where the speed of sound c_k is given in (2.49) and $c_{I,k}$, *the speed of sound at interface*, is determined by

$$c_{I,k}^2 = \frac{\frac{p_I}{\rho_k^2} - \left(\frac{\partial e_k}{\partial \rho_k}\right)_{p_k}}{\left(\frac{\partial e_k}{\partial p_k}\right)_{\rho_k}}, \quad k = 1, 2. \tag{2.74}$$

The matrix $\mathbf{A}$ has real eigenvalues that are given by the following expressions

$$\begin{aligned} &\lambda_1 = u_I, \\ &\lambda_2 = u_1 - c_1, \qquad \lambda_3 = u_1, \qquad \lambda_4 = u_1 + c_1, \\ &\lambda_5 = u_2 - c_2, \qquad \lambda_6 = u_2, \qquad \lambda_7 = u_2 + c_2. \end{aligned}$$

The corresponding right eigenvectors are

$$\mathbf{r}_1 = \begin{bmatrix} \alpha_1 \alpha_2 \zeta_1 \zeta_2 \\ -\alpha_2 \zeta_2 (\rho_1 (\zeta_1 - c_{I,1}^2) + p_1 - p_I) \\ \alpha_2 \zeta_2 (u_1 - u_I)(p_1 - p_I - \rho_1 c_{I,1}^2)/\rho_1 \\ \alpha_2 \zeta_2 (\rho_1 c_{I,1}^2 (u_1 - u_I)^2 - c_1^2 (p_1 - p_I)) \\ -\alpha_1 \zeta_1 (\rho_2 (c_{I,2}^2 - \zeta_2) - p_2 + p_I) \\ \alpha_1 \zeta_1 (u_2 - u_I)(-p_2 + p_I + \rho_2 c_{I,2}^2)/\rho_2 \\ \alpha_1 \zeta_1 (-\rho_2 c_{I,2}^2 (u_2 - u_I)^2 + c_2^2 (p_2 - p_I)) \end{bmatrix}, \tag{2.75}$$

$$\mathbf{r}_2 = \begin{bmatrix} 0 \\ \rho_1 \\ -c_1 \\ \rho_1 c_1^2 \\ 0 \\ 0 \\ 0 \end{bmatrix}, \qquad \mathbf{r}_3 = \begin{bmatrix} 0 \\ 1 \\ 0 \\ 0 \\ 0 \\ 0 \\ 0 \end{bmatrix}, \qquad \mathbf{r}_4 = \begin{bmatrix} 0 \\ \rho_1 \\ c_1 \\ \rho_1 c_1^2 \\ 0 \\ 0 \\ 0 \end{bmatrix} \tag{2.76}$$

$$\mathbf{r}_5 = \begin{bmatrix} 0 \\ 0 \\ 0 \\ 0 \\ \rho_2 \\ -c_2 \\ \rho_2 c_2^2 \end{bmatrix}, \qquad \mathbf{r}_6 = \begin{bmatrix} 0 \\ 0 \\ 0 \\ 0 \\ 1 \\ 0 \\ 0 \end{bmatrix}, \qquad \mathbf{r}_7 = \begin{bmatrix} 0 \\ 0 \\ 0 \\ 0 \\ \rho_2 \\ c_2 \\ \rho_2 c_2^2 \end{bmatrix}, \tag{2.77}$$

where

$$\zeta_1 = c_1^2 - (u_1 - u_I)^2,$$
$$\zeta_2 = c_2^2 - (u_2 - u_I)^2.$$

Thus, the system (2.72) is strictly hyperbolic except when some of the eigenvalues coincide. Indeed the eigenvectors (2.75)-(2.77) become linearly dependent if any one of the conditions

$$\alpha_1 = 0, \qquad \alpha_2 = 0, \qquad \zeta_1 = 0, \qquad \zeta_2 = 0$$

holds. For more details see Andrianov [8].

Consider the Riemann problem for the system (2.73) which is the initial-value problem with initial data of the form

$$\mathbf{W}(x,0) = \begin{cases} \mathbf{W}_L, & x < 0 \\ \\ \mathbf{W}_R, & x > 0. \end{cases}$$

One can show that the characteristic fields associated with λ_1, λ_3 and λ_6 are linearly degenerate, and the 2-, 4-, 5- and 7- fields are genuinely nonlinear, for a proof see Gallouët et al. [45].

In particular, if the interfacial variables p_I and u_I are defined by (2.45), then the model (2.72) is equivalent to the Baer-Nunziato model [12], and two of the eigenvalues of the

model will coincide, see full details in [8, 42]. We emphasize again the fact that the choice of the interfacial variables plays an important role in the wave structure of the model and so in the solution of the Riemann problem.

On the Riemann problem

Several authors have considered the exact solution of the Riemann problem of the model (2.72). A first step in this direction was made by Andrianov and Warnecke [10]. They constructed exact solutions, by an indirect way, to the Riemann problem of the Baer-Nunziato model, i.e. the model (2.72) with the interfacial closure expressions (2.45). Indeed, this approach uses a given intermediate state and the configuration of the Riemann problem to find the end left and right states that can be connected to the intermediate state by admissible waves. This procedure was implemented by Andrianov in a software package CONSTRUCT [7]. The constructed exact solutions were used later as test cases by several researchers, like Schwendeman et al. [131], Deledicque and Papalexandris [32], as well as Tokareva and Toro [146].

Schwendeman et al. [131] proposed a new direct method to find an exact solution to the Riemann problem of the Baer-Nunziato model. This method is a two-stage iterative procedure. The first stage involves two independent Newton iterations to obtain intermediate pressures of both phases. Then the second stage involves a Newton iteration to find the complete intermediate states by solving the contact jump conditions that used in [10] following the work of [42].

In a very recent paper, Tokareva and Toro [146] proposed an HLLC-type Riemann solver for the Baer-Nunziato model. In fact this method depends strongly on the previous one of Schwendeman et al. [131]. Approximations in sense of an HLLC solver are used with one stage of Newton iterations.

Deledicque and Papalexandris [32] proposed another method for the exact solution of the Riemann problem of the Baer-Nunziato model. This method investigates the possible Riemann configurations until the admissible one is calculated. This method uses the ideas of Andrianov and Warnecke [10].

Castro and Toro [19] proposed a four-rarefaction approximate solver to the Riemann problem of the model (2.72) with the interfacial expressions (2.44), their approach is applied only for the isentropic flow. To my knowledge, until now the exact Riemann solver for the full model model (2.72) with the interfacial expressions (2.44) is unavailable. In fact, this is a very difficult task due to the existence of seven waves in the Riemann structure and this leads to many possible configurations.

In result the exact Riemann solution for the model (2.72) with general interfacial expressions like (2.44) is still unknown. Moreover, all exact solvers utilize Newton iterations and this is very expensive in numerical computations where the Riemann problem is solved

at every cell boundary in each time step. Thus as usually used for numerical computations we will use in this thesis approximate Riemann solvers, like the HLL-type and HLLC-type solvers [148] as well as a VFRoe-type solver [46].

On the treatment of non-conservative terms

The system (2.72) is non-conservative which adds extra difficulties for the numerical computations even if the exact Riemann solution is known. Indeed, the numerical approximation of non-conservative terms is still unclear, see Hou and LeFloch [59]. However, several procedures were developed to deal with this difficulty, some details are given below regarding the non-conservative systems in general with more attention to the model (2.72).

In a particular case, Gonthier and Powers [50] considered the Baer-Nunziato model and neglected the non-conservative terms. They introduced some justifications for this choice, specially for applications in deflagration-to-detonation in granular materials. However, this is not a general case and neglecting non-conservative terms may be justified for only a few applications. Thus, we will not accept this approach in this work.

Based on the DLM theory of Dal Maso et al. [30] a new numerical scheme has been modified for the non-conservative systems, called *path-conservative* scheme. Indeed, this scheme uses the generalized Rankine-Hugoniot conditions (2.57) that were defined by the DLM theory, see Subsection 2.2.2. The first step in this direction was made by Toumi [150] who generalized the Roe approximate Riemann solver [117] to the non-conservative systems. Then, Parés [103] extended this idea and introduced the so-called path conservative scheme. In the last four years this scheme has received further attention, see e.g. Castro et al. [20, 21], Dumbser et al. [41], Tokareva and Toro [146].

In a very recent paper, Abgrall and Karni [2] showed by using a simple example that the path-conservative schemes are not able to compute correctly the solution of non-conservative hyperbolic systems. Initially, it is difficult to determine the correct path. But even if the correct path is known, the numerical solution does not, in general, converge to this path. In result, we believe that a comprehensive theory for the non-conservative hyperbolic systems is still very far from completeness. In addition, there is still a gap between the current known theory and the numerical methods. However, in this thesis we will not consider such type of schemes.

In this thesis, following Saurel and Abgrall [120], we use a modified Godunov-type method to take into account the discretization of the non-conservative terms. The discretization based on the idea of Abgrall [1], that a numerical approximation with uniform velocity and pressure should maintain uniform velocity and pressure during the time evolution. This method is simple, efficient and appropriate for a wide range of problems. In addition, it was verified numerically in several papers, see [9, 74, 75, 124].

It is worth to mention that Abgrall and Saurel [4] modified a new method to solve the

seven-equation model with non-conservative terms by a 'non-classical philosophy'. This method is referred to as *discrete equations method* (DEM). Unlike the classical methods which solve the model in macroscopic form, this method starts from the microscopic level. Where the pure phase Euler equations are discretized by the Godunov method then these numerical approximations are averaged in sense of the ensemble averaging of Drew and Passman [38] generating a numerical scheme for the multiphase flow. This method is efficient and gives the correct wave dynamics of the solutions. In addition, Saurel and collaborators [23, 123] used the continuous limit of this discrete equations to obtain the seven-equation model (2.72). Moreover, symmetric closure relations for p_I (2.46) and u_I (2.47) were obtained.

The DEM method as proposed by Abgrall and Saurel [4] can be considered more general than the method in [120]. We can see in the numerical tests in [4] a good agreement between the results of both methods. The method in [120] is simpler and sufficient for all test problems in this thesis. Moreover, in our results we will see a good agreement between the results of this method with results obtained with different models and different methods.

2.4.2 Mathematical properties of the six-equation model

The six-equation model is derived from the seven-equation model (2.72) in the asymptotic limit of stiff velocity relaxation, see Kapila et al. [66]. This model without heat and mass transfer can be written as

$$\frac{\partial \alpha_1}{\partial t} + u\frac{\partial \alpha_1}{\partial x} = \mu(p_1 - p_2), \tag{2.78a}$$

$$\frac{\partial \alpha_1\rho_1}{\partial t} + \frac{\partial(\alpha_1\rho_1 u)}{\partial x} = 0, \tag{2.78b}$$

$$\frac{\partial \alpha_2\rho_2}{\partial t} + \frac{\partial(\alpha_2\rho_2 u)}{\partial x} = 0, \tag{2.78c}$$

$$\frac{\partial \rho u}{\partial t} + \frac{\partial(\rho u^2 + \alpha_1 p_1 + \alpha_2 p_2)}{\partial x} = 0, \tag{2.78d}$$

$$\frac{\partial \alpha_1\rho_1 e_1}{\partial t} + \frac{\partial \alpha_1\rho_1 e_1 u}{\partial x} + \alpha_1 p_1\frac{\partial u}{\partial x} = \mu p_I(p_2 - p_1), \tag{2.78e}$$

$$\frac{\partial \alpha_2\rho_2 e_2}{\partial t} + \frac{\partial \alpha_2\rho_2 e_2 u}{\partial x} + \alpha_2 p_2\frac{\partial u}{\partial x} = -\mu p_I(p_2 - p_1). \tag{2.78f}$$

In terms of the primitive variables, the homogenous part of the model (2.78) can be expressed as

$$\frac{\partial \mathbf{W}}{\partial t} + \mathbf{A}\frac{\partial \mathbf{W}}{\partial x} = \mathbf{0}, \tag{2.79}$$

where

$$\mathbf{W} = (\alpha_1, \rho_1, \rho_2, u, p_1, p_2), \tag{2.80}$$

and the matrix $\mathbf{A}$ is given as

$$\mathbf{A} = \begin{bmatrix} u & 0 & 0 & 0 & 0 & 0 \\ 0 & u & 0 & \rho_1 & 0 & 0 \\ 0 & 0 & u & \rho_2 & 0 & 0 \\ \dfrac{p_1 - p_2}{\rho} & 0 & 0 & u & \dfrac{\alpha_1}{\rho} & \dfrac{1-\alpha_1}{\rho} \\ 0 & 0 & 0 & \rho_1 c_1^2 & u & 0 \\ 0 & 0 & 0 & \rho_2 c_2^2 & 0 & u \end{bmatrix}, \tag{2.81}$$

where $\rho = \alpha_1\rho_1 + \alpha_2\rho_2$.

The matrix $\mathbf{A}$ has six eigenvalues, only three of them are distinct

$$\begin{aligned} &\lambda_1 = \lambda_2 = \lambda_3 = \lambda_4 = u, \\ &\lambda_5 = u + c, \\ &\lambda_6 = u - c. \end{aligned} \tag{2.82}$$

Here c is the *mixture sound speed* for the six-equation model and is expressed as

$$c^2 = \frac{\alpha_1\rho_1}{\rho}c_1^2 + \frac{\alpha_2\rho_2}{\rho}c_2^2. \tag{2.83}$$

The sound speeds c_k, $k = 1, 2$, are defined by (2.49).

The corresponding right eigenvectors are

$$\mathbf{r}_1 = \begin{bmatrix} 0 \\ 0 \\ 0 \\ 0 \\ -\dfrac{\alpha_2}{\alpha_1} \\ 1 \end{bmatrix}, \quad \mathbf{r}_2 = \begin{bmatrix} 0 \\ 0 \\ 1 \\ 0 \\ 0 \\ 0 \end{bmatrix}, \quad \mathbf{r}_3 = \begin{bmatrix} 0 \\ 1 \\ 0 \\ 0 \\ 0 \\ 0 \end{bmatrix}, \quad \mathbf{r}_4 = \begin{bmatrix} 1 \\ 0 \\ 0 \\ 0 \\ \dfrac{p_2 - p_1}{\alpha_1} \\ 0 \end{bmatrix}, \quad \mathbf{r}_5 = \begin{bmatrix} 0 \\ 1 \\ \dfrac{\rho_2}{\rho_1} \\ \dfrac{c}{\rho_1} \\ c_1^2 \\ \dfrac{\rho_2}{\rho_1}c_2^2 \end{bmatrix}, \quad \mathbf{r}_6 = \begin{bmatrix} 0 \\ 1 \\ \dfrac{\rho_2}{\rho_1} \\ -\dfrac{c}{\rho_1} \\ c_1^2 \\ \dfrac{\rho_2}{\rho_1}c_2^2 \end{bmatrix}, \tag{2.84}$$

Therefore, the system (2.78) is hyperbolic, but not strictly hyperbolic.

Remark 2.5. The characteristic fields associated to the waves $\lambda_5 = u + c$ and $\lambda_6 = u - c$ are genuinely nonlinear, while the characteristic field associated with the wave $\lambda_1 = \lambda_2 = \lambda_3 = \lambda_4 = u$ is linearly degenerate.

A Godunov-type scheme that satisfies the Abgrall principle [1] for uniformity of velocity and pressure is used. In addition, during the numerical computations, the model (2.78) is augmented by the mixture energy equations to correct the inaccuracies in the approximations of the non-conservative internal energy equations, see details in Subsection 4.4.5.

The mixture sound speed of this model (2.83) has a monotonic behavior with respect to the volume fraction. This feature is nice in the numerical computations regarding the diffuse interfaces and wave transmission, see Saurel et al. [127]. Another nice feature for computations is that the volume fraction, in absence of relaxation effects, is constant along fluid trajectories.

2.4.3 Mathematical properties of the five-equation model

The five-equation model is derived from the seven-equation model (2.72) in the asymptotic limit of zero velocity and pressure relaxation times, see Kapila et al. [66], Murrone and Guillard [96]. Or simply, it is derived from the six-equation model (2.78) by assuming zero pressure relaxation time, see Saurel et al. [127].

The five-equation model without heat and mass transfer reads

$$\frac{\partial \alpha_1}{\partial t} + u\frac{\partial \alpha_1}{\partial x} = \eta(p, \rho_1, \rho_2, \alpha_1)\frac{\partial u}{\partial x}, \tag{2.85a}$$

$$\frac{\partial \alpha_1\rho_1}{\partial t} + \frac{\partial (\alpha_1\rho_1 u)}{\partial x} = 0, \tag{2.85b}$$

$$\frac{\partial \alpha_2\rho_2}{\partial t} + \frac{\partial (\alpha_2\rho_2 u)}{\partial x} = 0, \tag{2.85c}$$

$$\frac{\partial \rho u}{\partial t} + \frac{\partial (\rho u^2 + p)}{\partial x} = 0, \tag{2.85d}$$

$$\frac{\partial \rho E}{\partial t} + \frac{\partial (\rho E u + p u)}{\partial x} = 0, \tag{2.85e}$$

where $\rho = \alpha_1\rho_1 + \alpha_2\rho_2$, $\rho E = \alpha_1\rho_1 e_1 + \alpha_2\rho_2 e_2 + \frac{1}{2}\rho u^2$ and $\eta(p, \rho_1, \rho_2, \alpha_1)$ is expressed as

$$\eta(p, \rho_1, \rho_2, \alpha_1) = \alpha_1\alpha_2 \frac{\rho_2 c_2^2 - \rho_1 c_1^2}{\alpha_1\rho_2 c_2^2 + \alpha_2\rho_1 c_1^2}.$$

The sound speeds c_k, $k = 1, 2$, are defined by (2.49).

Let s_k be the phasic *specific entropy*, then the entropy equations of the model (2.85) reads

$$\frac{\partial s_k}{\partial t} + u\frac{\partial s_k}{\partial x} = 0, \qquad k = 1, 2. \tag{2.86}$$

The derivation of these equations is quite technical, see e.g. Murrone and Guillard [96].

Also, it is straightforward to obtain the mass fraction equations from the mass equations (2.85b) and (2.85c). Let $Y_k = \dfrac{\alpha_k \rho_k}{\rho}$ to be the *mass fraction*, then we get

$$\frac{\partial Y_k}{\partial t} + u \frac{\partial Y_k}{\partial x} = 0, \qquad k = 1, 2. \tag{2.87}$$

To study the properties of the model (2.85), we choose the following set of primitive variables $\mathbf{W} = (Y_1, s_1, s_2, u, p)$, then the model (2.85) is written as

$$\frac{\partial \mathbf{W}}{\partial t} + \mathbf{A} \frac{\partial \mathbf{W}}{\partial x} = \mathbf{0}, \tag{2.88}$$

with

$$\mathbf{A} = \begin{bmatrix} u & 0 & 0 & 0 & 0 \\ 0 & u & 0 & 0 & 0 \\ 0 & 0 & u & 0 & 0 \\ 0 & 0 & 0 & u & \dfrac{1}{\rho} \\ 0 & 0 & 0 & \dfrac{\rho_1 \rho_2 c_1^2 c_2^2}{\alpha_1 \rho_2 c_2^2 + \alpha_2 \rho_1 c_1^2} & u \end{bmatrix}.$$

The matrix $\mathbf{A}$ has five eigenvalues, only three of them are distinct

$$\begin{aligned} \lambda_1 &= \lambda_2 = \lambda_3 = u, \\ \lambda_4 &= u + c_w, \\ \lambda_5 &= u - c_w. \end{aligned} \tag{2.89}$$

Here c_w is the mixture sound speed for the five-equation model and is given by

$$\frac{1}{\rho c_w^2} = \frac{\alpha_1}{\rho_1 c_1^2} + \frac{\alpha_2}{\rho_2 c_2^2}. \tag{2.90}$$

This relation is known as *Wood equation* [158] and c_w is the *Wood speed of sound*.

The corresponding right eigenvectors are

$$\mathbf{r}_1 = \begin{bmatrix} 1 \\ 0 \\ 0 \\ 0 \\ 0 \end{bmatrix}, \quad \mathbf{r}_2 = \begin{bmatrix} 0 \\ 1 \\ 0 \\ 0 \\ 0 \end{bmatrix}, \quad \mathbf{r}_3 = \begin{bmatrix} 0 \\ 0 \\ 1 \\ 0 \\ 0 \end{bmatrix}, \quad \mathbf{r}_4 = \begin{bmatrix} 0 \\ 0 \\ 0 \\ 1 \\ \rho c_w \end{bmatrix}, \quad \mathbf{r}_5 = \begin{bmatrix} 0 \\ 0 \\ 0 \\ 1 \\ -\rho c_w \end{bmatrix}. \tag{2.91}$$

Thus the system (2.85) is hyperbolic.

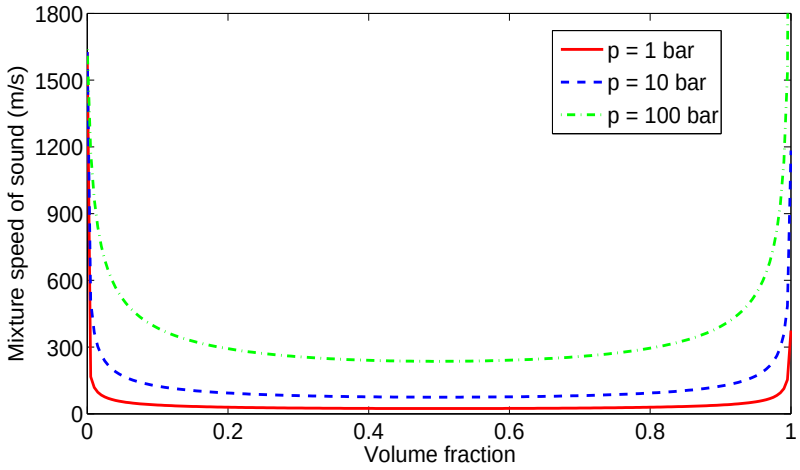

Figure 2.1: Sound speed of an air-water mixture for the five-equation model. A stiffened gas equation of state (3.2a) is used with parameters: $\gamma_{air} = 1.4$, $\pi_{air} = 0$, $q_{air} = 0$, $\gamma_{water} = 4.4$, $\pi_{water} = 6 \times 10^8$ Pa, $q_{water} = 0$. Densities are $\rho_{air} = 1$ kg/m^3 and $\rho_{water} = 1000$ kg/m^3.

The characteristic fields associated to the waves $\lambda_4 = u + c_w$ and $\lambda_5 = u - c_w$ are genuinely nonlinear, while the characteristic field associated with the wave $\lambda_1 = \lambda_2 = \lambda_3 = u$ is linearly degenerate, see a proof in Murrone and Guillard [96].

As mentioned in the introductory chapter several difficulties are encountered in using the five-equation model. One difficulty comes from the fact that the Wood speed of sound c_w (2.90) has a nonmonotonic behavior with respect to the volume fraction, see Figure 2.1. This behavior has bad consequences on the accuracy of wave transmission across diffuse interfaces, this problem is explained in details in Saurel et al. [127].

Another difficulty comes from the non-conservative character of the model. This is due to the non-conservative product that appears in the volume fraction equation, i.e. the term $\eta \dfrac{\partial u}{\partial x}$. This term is still a real challenge to the numerical schemes, some details are given below.

Some authors neglected the term $\eta \dfrac{\partial u}{\partial x}$ for certain applications, like Perigaud and Saurel [105]. In this case, the model is similar to the one considered by Allaire et al. [6]. However, the resulting model is simpler, but it works only for specific problems. In fact, the term $\eta \dfrac{\partial u}{\partial x}$ is important to predict correct thermodynamic behavior for the pure phases and mixtures, see the discussion in Saurel et al. [125].

Deledicque and Papalexandris [32] proposed a conservative approximation for the model (2.85). This method requires that certain material properties of one phase are considerably different from those in the other phase. This method is appropriate for gas-solid particles

mixtures, where the density and the sound speed of solid phase are consideably higher than those of the gaseous phase. In result, this approximation is valid under certain constraints.

Murrone and Guillard [96] added $\alpha_1 \dfrac{\partial u}{\partial x}$ to both sides of the volume fraction equation (2.85a), this leads to

$$\frac{\partial \alpha_1}{\partial t} + \frac{\partial \alpha_1 u}{\partial x} = (\eta + \alpha_1)\frac{\partial u}{\partial x}.$$

Then, they integrated the whole model assuming that the term $(\eta+\alpha_1)$ is constant during the time step. Some similar thing is done in Labois et al. [73], where a splitting method is used, the conservative part of the model is solved by Godunov method and the non-conservative part is solved by a semi-implicit scheme. In the term $(\eta + \alpha_1)$, they assumed that α_k is variable and other properties are constant. Both methods use roughly approximations and this leads to serious complications regarding the positivity of the volume fraction in the presence of shock or strong rarefaction waves.

Abgrall and Perrier [3] proposed a discretization to the model (2.85) by using the DEM method that was explained in Subsection 2.4.1. The scheme here is deduced by a reduction to the discrete equations for the seven-equation model. This keeps the philosophy of the DEM method and provides an indirect discretization to the five-equation model (2.85). Again, note that this method is not a direct treatment to the averaged model. Rather, it is an averaging to the numerical scheme itself.

Saurel and collaborators in a series of papers [106, 108, 122, 125, 127] considered the five-equation model (2.85). A new method and a new philosophy were developed to circumvent the above difficulties. In [125] shock relations for the model (2.85) were proposed. For sure, since the model is non-conservative, these relations are non-classical, i.e. they were not derived in a classical way as relations (2.54). Instead, these relations were derived to satisfy some admissibility conditions and they were tested successfully for a large number of experiments, see some details in Section 4.3. With the help of these shock relations the Riemann problem of the five-equation model is solved, see [106]. Then a special relaxation projection method was modified in [106] to solve the model (2.85), this method is an extension to the relaxation projection method that was proposed for Euler equations in [122]. This projection method provides an indirect way to discretize the volume fraction equation (2.85a). This method is efficient and more satisfying than previous methods. But it is more difficult to be implemented and difficult to extend to unstructured grids. This last point motivated Saurel et al. [127] to solve the five-equation model by another philosophy. Indeed, since the six-equation model (2.78) is equivalent to the five-equation if the pressure relaxation is stiff, the six-equation model is used assuming instantaneous pressure relaxation. Then one can use a Godunov-type method for the hyperbolic part, and a simple instantaneous pressure relaxation procedure is applied at each time step as the method of Saurel and Abgrall [120]. Thus, the method of [127] is simple and efficient to solve the system (2.85). But this method does not use the five-equation model directly, instead it uses the six-equation model.

Chapter 3

Modeling phase transition for the seven-equation model

3.1 Introduction

In the previous chapters we presented the seven-equation model and studied its main features. As mentioned, this model has better properties for numerical computations over the single pressure models. In addition, this model with its relaxation terms is applicable for a wide range of applications, besides its ability to deal with interface formation in cavitating flows.

In this chapter, we modify this model to include the heat and mass transfer. Our considerations are based on the second law of thermodynamics and some other general physical observations. We validate the model numerically with applications in metastable liquids. The results are compared with previous results of Saurel et al. [126]. A physical explanation of the results is given as well as a validation against experimental data is made.

This chapter is organized as follows: In Section 3.2 we recall the seven-equation model that was presented in Section 2.4. Then we present the required equations of state to close the model. Also we deduce phasic entropy equations that will be used in later sections. Section 3.3 is devoted to the numerical method, in particular, we present a modified Godunov-type scheme with an HLLC-type Riemann solver. In addition, we recall the instantaneous velocity and pressure relaxation procedures of Saurel and Abgrall [120]. In Section 3.4 we start to introduce our procedure for the modeling of heat and mass transfer. In particular, this section gives some prerequisites that are the manner of location of the interface and the computation of the saturation curve. In Sections 3.5 and 3.6 we model the heat and mass transfer through the temperature and the Gibbs free energy relaxation effects. Our modeled terms keep the mechanical equilibrium during the temperature relaxation, also they keep the mechanical equilibrium and the temperature equilibrium during the Gibbs free energy relaxation. Mathematical procedures are introduced for the instantaneous relaxation of the temperature and the Gibbs free energy. These procedures are used at each

time step after the velocity and the pressure relaxation procedures. The final form of the model with heat and mass transfer is summarized in Section 3.7. Finally, in Section 3.8 we present some numerical results. A comparison with experimental data is also made.

3.2 Mathematical model

Recall the two-phase flow model of Saurel and Abgrall [120] without heat and mass transfer in one dimension that was presented in Section 2.4

$$\frac{\partial \alpha_1}{\partial t} + u_I \frac{\partial \alpha_1}{\partial x} = \mu(p_1 - p_2), \tag{3.1a}$$

$$\frac{\partial \alpha_1 \rho_1}{\partial t} + \frac{\partial (\alpha_1 \rho_1 u_1)}{\partial x} = 0, \tag{3.1b}$$

$$\frac{\partial \alpha_1 \rho_1 u_1}{\partial t} + \frac{\partial (\alpha_1 \rho_1 u_1^2 + \alpha_1 p_1)}{\partial x} = p_I \frac{\partial \alpha_1}{\partial x} + \lambda(u_2 - u_1), \tag{3.1c}$$

$$\frac{\partial \alpha_1 \rho_1 E_1}{\partial t} + \frac{\partial (\alpha_1 (\rho_1 E_1 + p_1) u_1)}{\partial x} = p_I u_I \frac{\partial \alpha_1}{\partial x} + \mu p_I (p_2 - p_1) + \lambda u_I (u_2 - u_1), \tag{3.1d}$$

$$\frac{\partial \alpha_2 \rho_2}{\partial t} + \frac{\partial (\alpha_2 \rho_2 u_2)}{\partial x} = 0, \tag{3.1e}$$

$$\frac{\partial \alpha_2 \rho_2 u_2}{\partial t} + \frac{\partial (\alpha_2 \rho_2 u_2^2 + \alpha_2 p_2)}{\partial x} = -p_I \frac{\partial \alpha_1}{\partial x} - \lambda(u_2 - u_1), \tag{3.1f}$$

$$\frac{\partial \alpha_2 \rho_2 E_2}{\partial t} + \frac{\partial (\alpha_2 (\rho_2 E_2 + p_2) u_2)}{\partial x} = -p_I u_I \frac{\partial \alpha_1}{\partial x} - \mu p_I (p_2 - p_1) - \lambda u_I (u_2 - u_1). \tag{3.1g}$$

In this chapter we use the relations that are given in (2.44) as closure relations for the interfacial pressure p_I and the interfacial velocity u_I. The relaxation parameters λ and μ are assumed to be infinite; since we are interested in the instantaneous equilibrium for both the velocity and the pressure.

3.2.1 Equations of state (EOS)

Equations of state are used to close the system of equations (3.1). Since this model will be modified to include the heat and mass transfer, appropriate EOS are required.

Most phase transition models use a cubic EOS, like the Van der Waals EOS. But using such an EOS produces negative squared sound speed in a certain zone of the two phase flow, the *spinodal zone*. This causes a loss of hyperbolicity and leads to computational failure [107, 126]. To overcome this problem each fluid obeys its own EOS as a pure material, also these EOS should satisfy certain convexity constraints [89, 107, 126].

Indeed, in van der Waals modeling the mass transfer is a thermodynamic path, while in the present model an equilibrium is achieved by relaxation processes where this preserves the hyperbolicity of the model.

In this chapter we will use a modified form of the stiffened gas EOS (SG-EOS) with the same parameters for the dodecane and the water as in Saurel et al. [126] and Le Métayer et al. [80]. An essential issue is that the various parameters are linked to each other to fulfill some constraints to recover the phase diagram. This makes such a choice of EOS suitable for phase transitions [80, 126], see more details in Section 5.3. For $k = 1, 2$, these SG-EOS are expressed as

$$e_k(p_k, \rho_k) = \frac{p_k + \gamma_k \pi_k}{\rho_k(\gamma_k - 1)} + q_k, \tag{3.2a}$$

$$T_k(p_k, \rho_k) = \frac{p_k + \pi_k}{C_{vk}\rho_k(\gamma_k - 1)}, \tag{3.2b}$$

$$s(p_k, T_k) = C_{vk} \ln \frac{T_k^{\gamma_k}}{(p_k + \pi_k)^{(\gamma_k - 1)}} + q'_k, \tag{3.2c}$$

where C_{vk} is the *specific heat capacity at constant volume*. The parameters γ_k, π_k, q_k and q'_k are characteristic constants of the thermodynamic behavior of the fluid. All parameters of the SG-EOS are given in Table 3.1 for the water and in Table 3.2 for the dodecane. Note that the *specific heat capacity at constant pressure* C_{pk} is also given in the tables. This quantity is expressed as $C_{pk} = \gamma_k C_{vk}$.

Phase	γ	$\pi(Pa)$	$C_v(J/kg/K)$	$C_p(J/kg/K)$	$q(J/kg)$	$q'(J/kg/K)$
vapor	1.43	0	1.04×10^3	1.487×10^3	2030×10^3	-23×10^3
liquid	2.35	10^9	1.816×10^3	4.267×10^3	-1167×10^3	0

Table 3.1: EOS parameters for vapor and liquid water

Phase	γ	$\pi(Pa)$	$C_v(J/kg/K)$	$C_p(J/kg/K)$	$q(J/kg)$	$q'(J/kg/K)$
vapor	1.025	0	1.956×10^3	2.005×10^3	-237×10^3	-24×10^3
liquid	2.35	4×10^8	1.077×10^3	2.534×10^3	-755×10^3	0

Table 3.2: EOS parameters for vapor and liquid dodecane

3.2.2 Entropy equations

In this part we deduce the entropy equation for each phase. These equations will be used later. Denote the material derivative as

$$\frac{D_k(.)}{Dt} = \frac{\partial(.)}{\partial t} + u_k \frac{\partial(.)}{\partial x}, \quad k = 1, 2.$$

Using the continuity equation (3.1b) with the momentum equation (3.1c), we have

$$\alpha_1\rho_1\frac{D_1u_1}{Dt}+\frac{\partial\alpha_1p_1}{\partial x}=p_I\frac{\partial\alpha_1}{\partial x}+\lambda(u_2-u_1).$$

Multiplying this equation by u_1, we get the following equation for the *kinetic energy*

$$\alpha_1\rho_1\frac{D_1(\frac{u_1^2}{2})}{Dt}+u_1\frac{\partial\alpha_1p_1}{\partial x}=u_1p_I\frac{\partial\alpha_1}{\partial x}+\lambda u_1(u_2-u_1).$$

Subtracting this equation from the total energy equation (3.1d), we obtain the *internal energy equation*

$$\alpha_1\rho_1\frac{D_1e_1}{Dt}+\alpha_1p_1\frac{\partial u_1}{\partial x}=p_I(u_I-u_1)\frac{\partial\alpha_1}{\partial x}+\mu p_I(p_2-p_1)+\lambda(u_I-u_1)(u_2-u_1). \quad (3.3)$$

From the volume fraction equation (3.1a) with the continuity equation (3.1b) we have

$$\alpha_1\frac{D_1\rho_1}{Dt}+\alpha_1\rho_1\frac{\partial u_1}{\partial x}=\rho_1(u_I-u_1)\frac{\partial\alpha_1}{\partial x}+\mu\rho_1(p_2-p_1). \quad (3.4)$$

To get an equation for the entropy we use the Gibbs relation

$$T_1ds_1=de_1-\frac{p_1}{\rho_1^2}d\rho_1.$$

By taking the material derivative for this relation and multiplying by $\alpha_1\rho_1$, we obtain

$$\alpha_1\rho_1T_1\frac{D_1s_1}{Dt}=\alpha_1\rho_1\frac{D_1e_1}{Dt}-\frac{\alpha_1p_1}{\rho_1}\frac{D_1\rho_1}{Dt}. \quad (3.5)$$

Using (3.3) and (3.4) in (3.5), we have

$$\alpha_1\rho_1T_1\frac{D_1s_1}{Dt}=(p_I-p_1)(u_I-u_1)\frac{\partial\alpha_1}{\partial x}+\mu(p_I-p_1)(p_2-p_1)+\lambda(u_I-u_1)(u_2-u_1).$$

In a similar way we deduce the entropy equation for phase "2" which is given as

$$\alpha_2\rho_2T_2\frac{D_2s_2}{Dt}=(p_I-p_2)(u_I-u_2)\frac{\partial\alpha_2}{\partial x}-\mu(p_I-p_2)(p_2-p_1)-\lambda(u_I-u_2)(u_2-u_1).$$

3.3 Numerical method

The source terms of the system (3.1) consist of differential part and non-differential part. As in Saurel and Abgrall [120] to account for both parts we use the Strang splitting approach [144]. Let $L_h^{\Delta t}$ be the operator of numerical solution of the hyperbolic part of the system (3.1) over Δt and $L_s^{\frac{\Delta t}{2}}$ the operator of integration of the source and relaxation terms over half of the time interval, i.e. $\dfrac{\Delta t}{2}$. Thus the solution is obtained by the succession of operators.

$$\mathbf{U}_j^{n+1}=L_s^{\frac{\Delta t}{2}}L_h^{\Delta t}L_s^{\frac{\Delta t}{2}}\mathbf{U}_j^n, \quad (3.6)$$

where

$$\mathbf{U}=(\alpha_1,\alpha_1\rho_1,\alpha_1\rho_1u_1,\alpha_1\rho_1E_1,\alpha_2\rho_2,\alpha_2\rho_2u_2,\alpha_2\rho_2E_2)^T.$$

3.3.1 Hyperbolic operator

Consider the hyperbolic part of the system (3.1)

$$\frac{\partial \alpha_1}{\partial t} + u_I \frac{\partial \alpha_1}{\partial x} = 0, \tag{3.7a}$$

$$\frac{\partial \mathbf{u}}{\partial t} + \frac{\partial \mathbf{f}(\mathbf{u}, \alpha_1)}{\partial x} = \mathbf{h}(\mathbf{u}, \alpha_1) \frac{\partial \alpha_1}{\partial x}, \tag{3.7b}$$

where

$$\mathbf{u} = \begin{bmatrix} \alpha_1\rho_1 \\ \alpha_1\rho_1 u_1 \\ \alpha_1\rho_1 E_1 \\ \alpha_2\rho_2 \\ \alpha_2\rho_2 u_2 \\ \alpha_2\rho_2 E_2 \end{bmatrix}, \quad \mathbf{f}(\mathbf{u}, \alpha_1) = \begin{bmatrix} \alpha_1\rho_1 u_1 \\ \alpha_1\rho_1 u_1^2 + \alpha_1 p_1 \\ \alpha_1(\rho_1 E_1 + p_1)u_1 \\ \alpha_2\rho_2 u_2 \\ \alpha_2\rho_2 u_2^2 + \alpha_2 p_2 \\ \alpha_2(\rho_2 E_2 + p_2)u_2 \end{bmatrix}, \quad \mathbf{h}(\mathbf{u}, \alpha_1) = \begin{bmatrix} 0 \\ p_I \\ p_I u_I \\ 0 \\ -p_I \\ -p_I u_I \end{bmatrix}.$$

Following [120] a modified Godunov scheme is used to take into account the discretization of the non-conservative part of the system (3.7). Assume that we have some Godunov-type discretization for the system (3.7b) of the following form, see Section 2.3

$$\mathbf{u}_j^{n+1} = \mathbf{u}_j^n - \frac{\Delta t}{\Delta x}[\mathbf{f}(\mathbf{u}^*(\mathbf{u}_j^n, \mathbf{u}_{j+1}^n)) - \mathbf{f}(\mathbf{u}^*(\mathbf{u}_{j-1}^n, \mathbf{u}_j^n))] + \Delta t \mathbf{h}_j \Delta_j, \tag{3.8}$$

where Δ_j is the discrete form of the term $\dfrac{\partial \alpha_1}{\partial x}$, which has to be determined, and $\mathbf{u}^*(\mathbf{u}_j^n, \mathbf{u}_{j+1}^n)$ is the value of $\mathbf{u}$ along the line $x = x_{j+\frac{1}{2}}$ for the Riemann problem with the states $\mathbf{u}_j^n, \mathbf{u}_{j+1}^n$.

The components of the system (3.8) for phase "1" can be written as

$$(\alpha\rho)_j^{n+1} = (\alpha\rho)_j^n - \frac{\Delta t}{\Delta x}[(\alpha\rho u)^*_{j+\frac{1}{2}} - (\alpha\rho u)^*_{j-\frac{1}{2}}], \tag{3.9a}$$

$$(\alpha\rho u)_j^{n+1} = (\alpha\rho u)_j^n - \frac{\Delta t}{\Delta x}[(\alpha\rho u^2 + \alpha p)^*_{j+\frac{1}{2}} - (\alpha\rho u^2 + \alpha p)^*_{j-\frac{1}{2}}] + \Delta t (p_I)_j^n \Delta_j, \tag{3.9b}$$

$$(\alpha\rho E)_j^{n+1} = (\alpha\rho E)_j^n - \frac{\Delta t}{\Delta x}[(\alpha\rho u E + \alpha p u)^*_{j+\frac{1}{2}} - (\alpha\rho u E + \alpha p u)^*_{j-\frac{1}{2}}] + \Delta t (p_I)_j^n (u_I)_j^n \Delta_j. \tag{3.9c}$$

The index "1" is omitted for simplicity.

In order to find an expression for Δ_j, the idea of Abgrall [1] is used, that a uniform pressure and velocity must remain uniform during time evolution, for more discussion about this idea see [121]. Assume p and u are a constant pressure and velocity everywhere at time t^n. Then according to the Abgrall principle we have

$$p_j^n = p_j^{n+1} = (p_I)_j^n = p^*_{j\pm\frac{1}{2}} = p, \tag{3.10}$$

$$u_j^n = u_j^{n+1} = (u_I)_j^n = u^*_{j\pm\frac{1}{2}} = u. \tag{3.11}$$

Multiplying (3.9a) by u and subtracting the result from (3.9b), we obtain

$$\Delta_j = \frac{1}{\Delta x}(\alpha^*_{j+\frac{1}{2}} - \alpha^*_{j-\frac{1}{2}}). \tag{3.12}$$

Using the definition of E and (3.12) in (3.9c), and using (3.9a), we have the following equation for internal energy

$$(\alpha\rho e)_j^{n+1} = (\alpha\rho e)_j^n - \frac{\Delta t}{\Delta x}u[(\alpha\rho e)^*_{j+\frac{1}{2}} - (\alpha\rho e)^*_{j-\frac{1}{2}}]. \tag{3.13}$$

Multiplying (3.9a) by the parameter q in the EOS (3.2a) and subtracting the result from (3.13), we obtain

$$(\alpha\rho(e-q))_j^{n+1} = (\alpha\rho(e-q))_j^n - \frac{\Delta t}{\Delta x}u[(\alpha\rho(e-q))^*_{j+\frac{1}{2}} - (\alpha\rho(e-q))^*_{j-\frac{1}{2}}]. \tag{3.14}$$

From the EOS (3.2a) and uniformity of pressure (3.10), we see that

$$\rho(e-q) = \frac{p+\gamma\pi}{\gamma-1} = const. \tag{3.15}$$

Thus from (3.14) with (3.15), we get by taking out the constant and using (3.11)

$$\alpha_j^{n+1} = \alpha_j^n - (u_I)_j^n\frac{\Delta t}{\Delta x}(\alpha^*_{j+\frac{1}{2}} - \alpha^*_{j-\frac{1}{2}}). \tag{3.16}$$

This equation provides a discretization for the volume fraction equation.

For the Riemann values the approximate solvers HLL, HLLC [148] and VFRoe [46] are used. For the seven-equation model (3.1) the HLL solver is introduced in [120] and the VFRoe solver is considered in [9]. In the following section we introduce an HLLC-type Riemann solver for the system (3.1).

3.3.2 HLLC-type solver

The intercell flux of the HLLC Riemann solver is given by, see Toro [148]

$$\mathbf{F}^{HLLC}_{j+\frac{1}{2}} = \begin{cases} \mathbf{f}(\mathbf{u}_L), & 0 \le S_L \\ \mathbf{f}(\mathbf{u}_{*L}) = \mathbf{f}(\mathbf{u}_L) + S_L(\mathbf{u}_{*L} - \mathbf{u}_L), & S_L \le 0 \le S_* \\ \mathbf{f}(\mathbf{u}_{*R}) = \mathbf{f}(\mathbf{u}_R) + S_R(\mathbf{u}_{*R} - \mathbf{u}_R), & S_* \le 0 \le S_R \\ \mathbf{f}(\mathbf{u}_R), & 0 \ge S_R. \end{cases}$$

Where 'L' and 'R' refer to the left and right states of a cell boundary respectively.

Following the Davis estimates [31] the wave speeds can be taken as

$$S_L = \min\{u_{1L} - c_{1L}, u_{2L} - c_{2L}, u_{1R} - c_{1R}, u_{2R} - c_{2R}\},$$
$$S_R = \max\{u_{1L} + c_{1L}, u_{2L} + c_{2L}, u_{1R} + c_{1R}, u_{2R} + c_{2R}\}.$$

Following Toro [148] for a single phase, the vectors $\mathbf{u}_{*L}$ and $\mathbf{u}_{*R}$ can be given as

$$\mathbf{u}_{*K} = \begin{bmatrix} \alpha_{1K}\rho_{1K}\dfrac{S_K - u_{1K}}{S_K - S_*} \\ \alpha_{1K}\rho_{1K}\dfrac{S_K - u_{1K}}{S_K - S_*}S_* \\ \alpha_{1K}\rho_{1K}\dfrac{S_K - u_{1K}}{S_K - S_*}\left(E_{1K} + (S_* - u_{1K})(S_* + \dfrac{p_{1K}}{\rho_{1K}(S_K - u_{1K})})\right) \\ \alpha_{2K}\rho_{2K}\dfrac{S_K - u_{2K}}{S_K - S_*} \\ \alpha_{2K}\rho_{2K}\dfrac{S_K - u_{2K}}{S_K - S_*}S_* \\ \alpha_{2K}\rho_{2K}\dfrac{S_K - u_{2K}}{S_K - S_*}\left(E_{2K} + (S_* - u_{2K})(S_* + \dfrac{p_{2K}}{\rho_{2K}(S_K - u_{2K})})\right) \end{bmatrix}, \qquad K = L, R.$$

We take the speed S_* as in [148] but with mixture values for pressure, velocity and density, i.e

$$S_* = \frac{p_R - p_L + \rho_L u_L(S_L - u_L) - \rho_R u_R(S_R - u_R)}{\rho_L(S_L - u_L) - \rho_R(S_R - u_R)},$$

where $\rho = \alpha_1\rho_1 + \alpha_2\rho_2$, $p = \alpha_1 p_1 + \alpha_2 p_2$ and $u = \dfrac{\alpha_1\rho_1 u_1 + \alpha_2\rho_2 u_2}{\rho}$.

We refer to the mathematical properties of the model (3.1) in Subsection 2.4.1. Consider the eigenvectors (2.76) and (2.77) for the 2- to 7- fields. It is clear that the function $\vartheta(\mathbf{W}) = \alpha_1$ is a Riemann invariant for all 2- to 7- characteristic fields. This means that α_1 is constant across all rarefaction waves of the 2- to 7- fields. Also note that the action of the non-conservative terms is reflected in the 1-field which corresponds to the eigenvalue $\lambda_1 = u_I$. Moreover, this eigenvalue comes from the evolutionary equation for α_1. Considering these observations we will assume that α_1 changes only across S_*, this means that

$$\alpha_{1*K} = \alpha_{1K}, \qquad K = L,\ R.$$

In Qiang et al. [114] one can see another approximation for the discretization of the volume fraction.

3.3.3 Extension to the second order

To achieve second order accuracy we use the MUSCL method, where MUSCL stands for Monotone Upstream-centered Scheme for Conservation Laws. In the following we will give a summary of this method, and for details we refer to Toro [148]. This method has three steps, they are

- *Data reconstruction:* The primitive variables on the cell boundary are extrapolated as
$$\mathbf{W}^{-}_{j+\frac{1}{2}} = \mathbf{W}^{n}_{j} + \frac{1}{2}\delta_j, \qquad \mathbf{W}^{+}_{j-\frac{1}{2}} = \mathbf{W}^{n}_{j} - \frac{1}{2}\delta_j.$$
Performing this step in primitive variables ensures the preservation of uniformity of pressure and velocity, which is an essential issue in the discretization of the model.

  The limited slope δ_j is taken as
$$\delta_j = \begin{cases} \max\{0, \min(\beta d_{j-\frac{1}{2}}, d_{j+\frac{1}{2}}), \min(d_{j-\frac{1}{2}}, \beta d_{j+\frac{1}{2}})\}, & d_{j+\frac{1}{2}} > 0 \\ \min\{0, \max(\beta d_{j-\frac{1}{2}}, d_{j+\frac{1}{2}}), \max(d_{j-\frac{1}{2}}, \beta d_{j+\frac{1}{2}})\}, & d_{j+\frac{1}{2}} < 0 \end{cases}$$
where
$$d_{j-\frac{1}{2}} = \mathbf{W}^{n}_{j} - \mathbf{W}^{n}_{j-1}, \qquad d_{j+\frac{1}{2}} = \mathbf{W}^{n}_{j+1} - \mathbf{W}^{n}_{j}.$$
For particular values of β, the value $\beta = 1$ corresponds to the minmod limiter and $\beta = 2$ corresponds to the superbee limiter.

- *Evolution*: Using (2.73) the values $\mathbf{W}^{\pm}_{j\mp\frac{1}{2}}$ are evolved by a time $\dfrac{\Delta t}{2}$ as
$$\widehat{\mathbf{W}}^{+}_{j-\frac{1}{2}} = \mathbf{W}^{+}_{j-\frac{1}{2}} - \frac{\Delta t}{2\Delta x}\mathbf{A}(\mathbf{W}_j)(\mathbf{W}^{-}_{j+\frac{1}{2}} - \mathbf{W}^{+}_{j-\frac{1}{2}}),$$
$$\widehat{\mathbf{W}}^{-}_{j+\frac{1}{2}} = \mathbf{W}^{-}_{j+\frac{1}{2}} - \frac{\Delta t}{2\Delta x}\mathbf{A}(\mathbf{W}_j)(\mathbf{W}^{-}_{j+\frac{1}{2}} - \mathbf{W}^{+}_{j-\frac{1}{2}}).$$

- *Solution of the Riemann problem:* We rewrite $\widehat{\mathbf{W}}^{\pm}_{j\pm\frac{1}{2}}$ in conservative form, and solve the Riemann problem with the piecewise constant data $(\widehat{\mathbf{U}}^{-}_{j+\frac{1}{2}}, \widehat{\mathbf{U}}^{+}_{j+\frac{1}{2}})$.

3.3.4 Source and relaxation operators

According to the Strang splitting (3.6), to take into account for source and relaxation terms we have to solve the following system of ordinary differential equations (ODE).

$$\frac{d\mathbf{U}}{dt} = \mathbf{S} \tag{3.17}$$

where

$$\mathbf{U} = (\alpha_1, \alpha_1\rho_1, \alpha_1\rho_1 u_1, \alpha_1\rho_1 E_1, \alpha_2\rho_2, \alpha_2\rho_2 u_2, \alpha_2\rho_2 E_2)^T.$$

The source vector $\mathbf{S}$ can be decomposed as the sum

$$\mathbf{S} = \mathbf{S}_V + \mathbf{S}_P + \mathbf{S}_{Thermal},$$

where $\mathbf{S}_V$ and $\mathbf{S}_P$ are associated with the velocity and pressure relaxation terms respectively. The vector $\mathbf{S}_{Thermal}$ represents the thermal relaxation terms that include the temperature and Gibbs free energy relaxation terms that have to be modeled. The mechanical relaxation terms $\mathbf{S}_V$ and $\mathbf{S}_P$ are given by

$$\mathbf{S}_V = \begin{bmatrix} 0 \\ 0 \\ \lambda(u_2 - u_1) \\ \lambda u_I(u_2 - u_1) \\ 0 \\ -\lambda(u_2 - u_1) \\ -\lambda u_I(u_2 - u_1) \end{bmatrix}, \quad \text{and} \quad \mathbf{S}_P = \begin{bmatrix} \mu(p_1 - p_2) \\ 0 \\ 0 \\ \mu p_I(p_2 - p_1) \\ 0 \\ 0 \\ -\mu p_I(p_2 - p_1) \end{bmatrix}.$$

The system (3.17) is solved by successive integrations considering each one of the source vectors alone.

Relaxation rates

The relaxation time scales depend on many parameters of the fluids and also possibly on the process, i.e. evaporation, condensation, combustion, etc. For example the rate of the pressure relaxation μ depends on the compressibility of each fluid besides the nature of each fluid and the two phase mixture topology [120, 124]. The velocity relaxation time may be greater than that required for the pressure relaxation, since the velocity relaxation depends on the fluid viscosity which has slow effects compared to others, also it depends on the pressure relaxation which is in general fast compared to the longitudinal wave propagation [120, 124]. The interface conditions, for the interface that separates two pure fluids, impose an equality for pressure and velocity, see Subsection 2.1.4. In many physical situations it is reasonable to assume that the pressure and velocity relax instantaneously. Such an assumption also fulfills the interface conditions. Some estimations in certain situations show that the time scale of the velocity relaxation and pressure relaxation are of the same order of magnitude [23, 108].

The temperature relaxation depends on the thermal conductivity of the fluids. Where this conduction occurs due to the collisions of the molecules of the fluids. To reach temperature equilibrium a large number of collisions is required. This in general has long characteristic time compared to the pressure and velocity relaxation.

The Gibbs free energy relaxation parameter depends on local chemical relaxation [126]. And this is a slow process compared with other processes that related to the pressure,

velocity and temperature relaxation at the interfaces. Therefore the relaxation time of the Gibbs free energy relaxation is the longest compared to other relaxation times.

In this thesis we assume that the relaxation times are very close to zero i.e. instantaneous relaxations. This assumption is justified for the pressure and the velocity in the entire flow field. For the temperature and the Gibbs free energy this assumption is considered only at the interface where the heat and mass transfer occur, indeed this assumption is standard at equilibrium interfaces when mass transfer occurs, see Saurel et al. [126]. The assumption of instantaneous relaxations means that all relaxation parameters are taken to be infinite and this makes the model free of parameters.

Moreover we assume that the relaxation time of the mechanical variables is much smaller than that of the thermal variables. We assume that the mechanical variables relax very fast to equilibrium values, and they will stay in equilibrium during the thermal relaxation. Also we assume that the temperature relaxes much faster than the Gibbs free energy.

For the velocity and pressure relaxation we use the same procedures as Saurel and Abgrall [120], other procedures for pressure relaxation also are possible, see [74, 75, 124]. For the thermal relaxation terms we modeled them depending on the observation of the differences between relaxation times for various variables, they are the subject of the next sections.

Velocity relaxation

Following [120], to achieve an instantaneous velocity relaxation, we solve the following system of ODE

$$\frac{d\mathbf{U}}{dt} = \mathbf{S}_V$$

with $\lambda \to \infty$.

Assume that '0' and '$\star$' refer to the states before and after the relaxation process respectively. Then, the result of the velocity relaxation is

$$u_1^\star = u_2^\star = u_I^\star = \frac{\alpha_1^0\rho_1^0u_1^0 + \alpha_2^0\rho_2^0u_2^0}{\alpha_1^0\rho_1^0 + \alpha_2^0\rho_2^0},$$

$$e_1^\star = e_1^0 + \frac{1}{2}(u_1^\star - u_1^0)^2,$$

$$e_2^\star = e_2^0 + \frac{1}{2}(u_2^\star - u_2^0)^2.$$

The volume fraction and density stay constant. All details are given in [120].

Pressure relaxation

For instantaneous pressure relaxation we have to solve the following system of ODE

$$\frac{d\mathbf{U}}{dt} = \mathbf{S}_P \tag{3.19}$$

with $\mu \to \infty$.

The components of the system (3.19) for phase '1' are

$$\frac{\partial \alpha_1}{\partial t} = \mu(p_1 - p_2), \tag{3.20a}$$

$$\frac{\partial \alpha_1 \rho_1}{\partial t} = 0, \tag{3.20b}$$

$$\frac{\partial \alpha_1 \rho_1 u_1}{\partial t} = 0, \tag{3.20c}$$

$$\frac{\partial \alpha_1 \rho_1 E_1}{\partial t} = \mu p_I(p_2 - p_1). \tag{3.20d}$$

From the first and last equations we obtain

$$\frac{\partial \alpha_1 \rho_1 E_1}{\partial t} = -p_I \frac{\partial \alpha_1}{\partial t}. \tag{3.21}$$

Using (3.20b) and (3.20c) with (3.21) we have

$$\frac{\partial e_1}{\partial t} = -\frac{p_I}{\alpha_1 \rho_1} \frac{\partial \alpha_1}{\partial t}. \tag{3.22}$$

Note that (3.20b) implies that $\alpha_1 \rho_1$ is constant through the relaxation process. By integrating of (3.22) we get the following approximated relation

$$e_1^\star = e_1^0 - \frac{\bar{p}_I}{\alpha_1^0 \rho_1^0}(\alpha_1^\star - \alpha_1^0) \tag{3.23}$$

where $\bar{p}_I$ is the mean interfacial pressure between the states $(\alpha_1^0, \rho_1^0, e_1^0)$ and $(\alpha_1^\star, \rho_1^\star, e_1^\star)$. A similar result can be attained for phase '2'.

We consider (3.23) as an equation for e_1 as a function of α_1, i.e. $e_1 = e_1^0 - \frac{\bar{p}_I}{\alpha_1^0 \rho_1^0}(\alpha_1 - \alpha_1^0)$, and from (3.20b) $\rho_1 = \frac{const}{\alpha_1}$. And analogously for the other phase, since $\alpha_2 = 1 - \alpha_1$ we have only one variable α_1 in the relation

$$f_p(\alpha_1) = p_2(e_2, \rho_2) - p_1(e_1, \rho_1) = 0. \tag{3.24}$$

Our aim now is to find an α_1 that satisfies the equilibrium condition (3.24). The pressure $\bar{p}_I$ can be approximated as $\bar{p}_I = \frac{\tilde{p}_I + p_I^0}{2}$, where $\tilde{p}_I$ is estimated at the new state resulting from iterative procedure for solving $f_p(\alpha_1) = 0$.

3.4 Thermal relaxation, modeling of heat and mass transfer

At each time step after the procedures for the velocity and pressure relaxations we have a two-phase mixture in mechanical equilibrium, but each phase has its own temperature

and its own Gibbs free energy. In this section we will insert the effect of heat and mass transfer that take place at the interface.

To locate the interface we use the ideas of [126], that the cell is filled with pure fluid when its volume fraction is close to 1, say $(1-\varepsilon)$, with $\varepsilon = 10^{-6}$. The interface corresponds to mixture cells when the volume fraction ranges between $\bar{\varepsilon}$ and $1-\bar{\varepsilon}$, with $\bar{\varepsilon} = 10^{-4}$. The value of $\bar{\varepsilon}$ has to be chosen larger than the value of ε to ensure that phase transitions occur only in the interfacial zone, see Figure 3.1 for illustration.

The choice of epsilons is not unique, you can for example take $\varepsilon = 10^{-8}$ and $\bar{\varepsilon} = 10^{-6}$ or 10^{-5}. We checked several choices with no changes in the results. But there is a problem if we choose both values very close to each other. This leads to starting the phase transition in the pure fluids and not only at the interfaces, see also a discussion on this point in Saurel et al. [126].

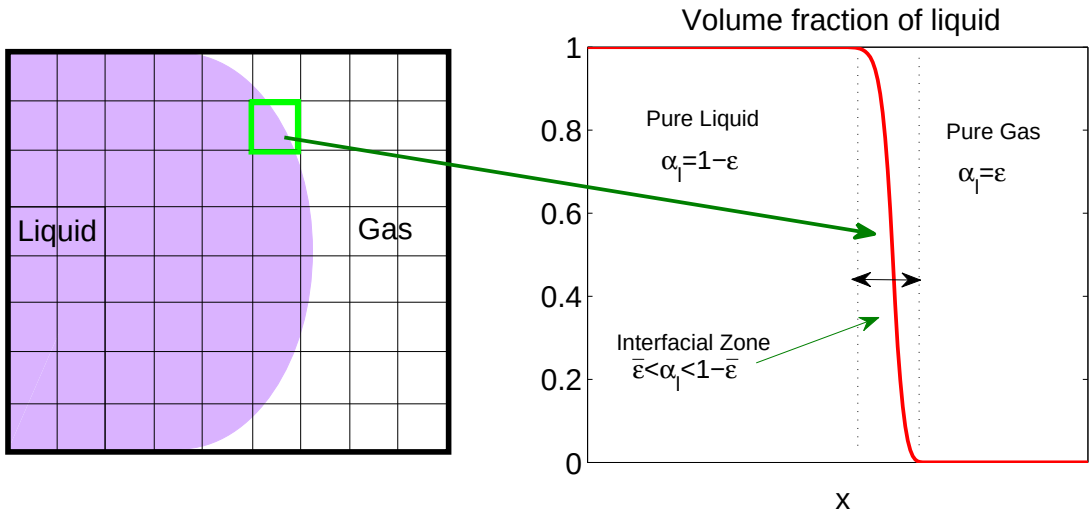

Figure 3.1: An interface location as a diffuse zone.

Mass transfer is allowed if the liquid is metastable, i.e. $T_l > T_{sat}(p_{equi})$. Thus it is necessary to compute the curve $T = T_{sat}(p_{equi})$. For this we use the same idea of [81, 126], that at thermodynamic equilibrium the Gibbs free energies are equal, and this equality provides a direct relation between the saturation pressure and temperature. Let g_k denotes the *Gibbs free energy* which is expressed as

$$g_k = e_k + \frac{p_k}{\rho_k} - T_k s_k. \tag{3.25}$$

Using the SG-EOS (3.2) g_k can be written as

$$g_k = (\gamma_k C_{vk} - q'_k)T_k - T_k C_{vk} \ln \frac{T_k^{\gamma_k}}{(p_k + \pi_k)^{(\gamma_k - 1)}} + q_k.$$

At the saturation curve we have an equilibrium pressure p, an equilibrium temperature T and by the equality of the two Gibbs free energies g_1 and g_2 we have

$$(\gamma_1 C_{v1} - q_1')T - TC_{v1}\ln\frac{T^{\gamma_1}}{(p+\pi_1)^{(\gamma_1-1)}} + q_1 = (\gamma_2 C_{v2} - q_2')T - TC_{v2}\ln\frac{T^{\gamma_2}}{(p+\pi_2)^{(\gamma_2-1)}} + q_2. \tag{3.26}$$

This equation is nonlinear and can be solved by any iterative technique to find the saturation temperature in terms of the saturation pressure.

Now we turn to model the heat and mass transfer through relaxation effects. According to our assumption that the mechanical relaxation time is very small compared with the thermal relaxation time we may also assume that the mechanical quantities will stay in equilibrium during the thermal relaxation. Therefore, our modeled terms will keep this assumption.

Also we assume that the temperature relaxes much faster than the Gibbs free energy. So we will split the thermal terms into two parts. One is related to the heat transfer $\mathbf{S}_Q$ and the other is related to the mass transfer $\mathbf{S}_m$, i.e.

$$\mathbf{S}_{Thermal} = \mathbf{S}_Q + \mathbf{S}_m.$$

The system of ODE (3.17) is solved for the temperature relaxation then for the Gibbs free energy relaxation. During the Gibbs free energy relaxation we assume that the temperature will stay in equilibrium, and our modeled terms will keep this condition.

3.5 Heat transfer and temperature relaxation

The heat transfer is added through the temperature relaxation terms. In the model (3.1) the heat transfer term Q initially appears in the energy equations, see the averaged energy equation (2.40). As the pressure equilibrium is maintained through the temperature relaxation we will modify the volume fraction equation to include the effect of the heat transfer in a way to be able to keep an equilibrium pressure during the temperature relaxation process. Therefore the heat source vector $\mathbf{S}_Q$ is modeled as

$$\mathbf{S}_Q = (\frac{Q}{\kappa}, 0, 0, Q, 0, 0, -Q)^T, \tag{3.27}$$

where the new variable κ has to be determined.

Then to take into account for the heat transfer we have to solve the following system of ODE

$$\frac{d\mathbf{U}}{dt} = \mathbf{S}_Q. \tag{3.28}$$

To find the expression for κ we will use the assumption that the pressure will stay in equilibrium, and to do that we assume

$$\frac{\partial p_1}{\partial t} = \frac{\partial p_2}{\partial t}. \tag{3.29}$$

3.5.1 Determination of κ

Consider the components of the system (3.28) for phase "1"

$$\frac{\partial \alpha_1}{\partial t} = \frac{Q}{\kappa}, \tag{3.30a}$$

$$\frac{\partial \alpha_1 \rho_1}{\partial t} = 0, \tag{3.30b}$$

$$\frac{\partial \alpha_1 \rho_1 u_1}{\partial t} = 0, \tag{3.30c}$$

$$\frac{\partial \alpha_1 \rho_1 E_1}{\partial t} = Q. \tag{3.30d}$$

From (3.30a) and (3.30d) we obtain

$$\frac{\partial \alpha_1 \rho_1 E_1}{\partial t} = \kappa \frac{\partial \alpha_1}{\partial t}. \tag{3.31}$$

Using the definition of E_1, (3.30b) and (3.30c) with (3.31) we have

$$\alpha_1 \rho_1 \frac{\partial e_1}{\partial t} = \kappa \frac{\partial \alpha_1}{\partial t}. \tag{3.32}$$

The internal energy e_1 is expressed in terms of p_1 and ρ_1, i.e. $e_1 = e_1(p_1, \rho_1)$. Differentiating it with respect to t and substituting the result in (3.32), we obtain

$$\alpha_1 \rho_1 \left(\frac{\partial e_1}{\partial p_1}\right)_{\rho_1} \frac{\partial p_1}{\partial t} + \alpha_1 \rho_1 \left(\frac{\partial e_1}{\partial \rho_1}\right)_{p_1} \frac{\partial \rho_1}{\partial t} = \kappa \frac{\partial \alpha_1}{\partial t}. \tag{3.33}$$

From (3.30b) we have $\alpha_1 \dfrac{\partial \rho_1}{\partial t} = -\rho_1 \dfrac{\partial \alpha_1}{\partial t}$. Using this in (3.33) we get

$$\alpha_1 \rho_1 \left(\frac{\partial e_1}{\partial p_1}\right)_{\rho_1} \frac{\partial p_1}{\partial t} - \rho_1^2 \left(\frac{\partial e_1}{\partial \rho_1}\right)_{p_1} \frac{\partial \alpha_1}{\partial t} = \kappa \frac{\partial \alpha_1}{\partial t},$$

or

$$\frac{\partial p_1}{\partial t} = \frac{\kappa + \rho_1^2 \left(\dfrac{\partial e_1}{\partial \rho_1}\right)_{p_1}}{\alpha_1 \rho_1 \left(\dfrac{\partial e_1}{\partial p_1}\right)_{\rho_1}} \frac{\partial \alpha_1}{\partial t}. \tag{3.34}$$

A similar equation can be attained for p_2

$$\frac{\partial p_2}{\partial t} = -\frac{\kappa + \rho_2^2 \left(\dfrac{\partial e_2}{\partial \rho_2}\right)_{p_2}}{\alpha_2 \rho_2 \left(\dfrac{\partial e_2}{\partial p_2}\right)_{\rho_2}} \frac{\partial \alpha_1}{\partial t}. \tag{3.35}$$

Using (3.34) and (3.35) in the condition (3.29) and after some manipulations we have the following expression for κ

$$\kappa = \frac{\dfrac{\rho_1 c_1^2}{\alpha_1} + \dfrac{\rho_2 c_2^2}{\alpha_2}}{\dfrac{\Gamma_1}{\alpha_1} + \dfrac{\Gamma_2}{\alpha_2}} - \frac{\dfrac{\Gamma_1}{\alpha_1} p_1 + \dfrac{\Gamma_2}{\alpha_2} p_2}{\dfrac{\Gamma_1}{\alpha_1} + \dfrac{\Gamma_2}{\alpha_2}}. \tag{3.36}$$

Here Γ_k denotes the *Grüneisen coefficient* of phase k which is given as

$$\Gamma_k = \frac{1}{\rho_k} \left(\frac{\partial p_k}{\partial e_k} \right)_{\rho_k}, \quad k = 1, 2. \tag{3.37}$$

Since the heat transfer relaxation is considered when pressure equilibrium is maintained, i.e. $p_1 = p_2 = p_{eq}$, the second term in the right hand side of (3.36) is equivalent to the equilibrium pressure. Thus we have

$$\kappa = \frac{\dfrac{\rho_1 c_1^2}{\alpha_1} + \dfrac{\rho_2 c_2^2}{\alpha_2}}{\dfrac{\Gamma_1}{\alpha_1} + \dfrac{\Gamma_2}{\alpha_2}} - p_{eq}. \tag{3.38}$$

It is interesting to note that the first term on the right hand side of (3.38) is exactly the same term that appears in a similar manner with heat transfer that is given in the model of Saurel et al. [126].

In the context of the SG-EOS (3.2), we have the following expression for κ

$$\kappa = \frac{\dfrac{p_1 + \gamma_1 \pi_1}{\alpha_1} + \dfrac{p_2 + \gamma_2 \pi_2}{\alpha_2}}{\dfrac{\gamma_1 - 1}{\alpha_1} + \dfrac{\gamma_2 - 1}{\alpha_2}}.$$

3.5.2 Mixture entropy

Now let us consider the equation of the mixture entropy. If we follow the same method in Section 3.2.2 for the model with new modifications, we have

$$\alpha_1 \rho_1 T_1 \frac{Ds_1}{Dt} = (1 + \frac{p_1}{\kappa}) Q, \tag{3.39a}$$

$$\alpha_2 \rho_2 T_2 \frac{Ds_2}{Dt} = -(1 + \frac{p_2}{\kappa}) Q. \tag{3.39b}$$

After the mechanical relaxation p_1 and p_2 are in equilibrium, so $p_1 = p_2 = p_{eq}$.

Combining the two equations in (3.39) we get the following equation for the mixture entropy

$$\frac{\partial \rho s}{\partial t} + \frac{\partial \rho s u}{\partial x} = (1 + \frac{p_{eq}}{\kappa}) Q \left(\frac{T_2 - T_1}{T_1 T_2} \right),$$

where $\rho s = \alpha_1\rho_1 s_1 + \alpha_2\rho_2 s_2$ and $u = u_1 = u_2$ is the equilibrium velocity.

The heat transfer Q is modeled as $Q = \theta(T_2 - T_1)$, where $\theta > 0$ is the temperature relaxation parameter. Since κ is always positive the mixture entropy satisfies the second law of thermodynamics, i.e.

$$\frac{\partial \rho s}{\partial t} + \frac{\partial \rho s u}{\partial x} = \theta(1 + \frac{p_{eq}}{\kappa})\frac{(T_2 - T_1)^2}{T_1 T_2} \geq 0.$$

In this thesis the parameter θ is assumed to tend to infinity, i.e. the temperature relaxes to a common value instantaneously at any time. This assumption is considered at the interface only.

3.5.3 Temperature relaxation

Now to solve the system (3.30) with $\theta \to \infty$, we proceed as for the pressure relaxation in Subsection 3.3.4. It is clear from (3.30) that $\alpha_1\rho_1$ and $\alpha_1\rho_1 u_1$, therefore also u_1 stay constant through the relaxation process.

From the system (3.30) we obtain (3.32) for the internal energy, which can be rewritten as

$$\frac{\partial e_1}{\partial t} = \frac{\kappa}{\alpha_1\rho_1}\frac{\partial \alpha_1}{\partial t}.$$

Integrating this equation, we obtain the following approximation

$$e_1^\star = e_1^0 + \frac{\bar{\kappa}}{\alpha_1^0\rho_1^0}(\alpha_1^\star - \alpha_1^0) \tag{3.40}$$

where $\bar{\kappa}$ is the mean value between the states $(\alpha_1^0, \rho_1^0, e_1^0)$ and $(\alpha_1^\star, \rho_1^\star, e_1^\star)$. Also, we can proceed in the same way to get a similar result for phase '2'.

Now, we aim to find α_1 that satisfies the equilibrium condition

$$f_T(\alpha_1) = T_2(e_2, \rho_2) - T_1(e_1, \rho_1) = 0.$$

An iterative procedure is used to solve this equation. The variable $\bar{\kappa}$ can be approximated as $\bar{\kappa} = \dfrac{\tilde{\kappa} + \kappa^0}{2}$, where $\tilde{\kappa}$ is estimated at the new state resulting from iterative procedure for solving $f_T(\alpha_1) = 0$.

In this way we get the temperature equilibrium, while keeping the mechanical equilibrium.

3.6 Mass transfer and Gibbs free energy relaxation

Analogous to the heat transfer, the mass transfer is also modeled through relaxation terms. As mentioned we assume that the temperature relaxation time is very small compared with

the Gibbs free energy relaxation time, and so we will consider that the mechanical equilibrium and the equilibrium of temperature will be satisfied through the Gibbs free energy relaxation.

To take into account the mass transfer we have to solve the following system of ODE

$$\frac{d\mathbf{U}}{dt} = \mathbf{S}_m. \tag{3.41}$$

Our aim now is to model the mass transfer source vector $\mathbf{S}_m$.

The averaging techniques show that the mass transfer appears in the homogenized model as a mass rate in the interfacial momentum and in the interfacial energy. This is clear in the averaged model presented in Subsection 2.1.2 . In particular, see the relation (2.33) for an interfacial momentum term and the relation (2.38) for an interfacial energy term. But the exact expressions for these terms are unknown. Here we will insert these terms into the model as they appear by averaging, but we will use some assumptions to find appropriate expressions for these terms.

Let us assume that $\mathbf{S}_m$ is given in the model as

$$\frac{\partial \alpha_1}{\partial t} = \frac{\dot{m}}{\varrho}, \tag{3.42a}$$

$$\frac{\partial \alpha_1 \rho_1}{\partial t} = \dot{m}, \tag{3.42b}$$

$$\frac{\partial \alpha_1 \rho_1 u_1}{\partial t} = u_I \dot{m}, \tag{3.42c}$$

$$\frac{\partial \alpha_1 \rho_1 E_1}{\partial t} = (e_i + \frac{u_I^2}{2})\dot{m}, \tag{3.42d}$$

$$\frac{\partial \alpha_2 \rho_2}{\partial t} = -\dot{m}, \tag{3.42e}$$

$$\frac{\partial \alpha_2 \rho_2 u_2}{\partial t} = -u_I \dot{m}, \tag{3.42f}$$

$$\frac{\partial \alpha_2 \rho_2 E_2}{\partial t} = -(e_i + \frac{u_I^2}{2})\dot{m}. \tag{3.42g}$$

The new variables ϱ and e_i have to be determined.

According to our assumption the relaxation time of the Gibbs free energy is much larger than other relaxation times, so during the Gibbs free energy relaxation process we will assume that the pressure and temperature stay in equilibrium. Thus to find the new variables we use the following assumptions

$$\frac{\partial p_1}{\partial t} = \frac{\partial p_2}{\partial t}, \tag{3.43a}$$

$$\frac{\partial T_1}{\partial t} = \frac{\partial T_2}{\partial t}. \tag{3.43b}$$

3.6.1 Determination of e_i and ϱ

Since the model (3.42) is solved after the mechanical relaxation we have $u_1 = u_2 = u_I$. From (3.42b) and (3.42c) the velocity u_1 is constant through the relaxation procedure, also from (3.42e) and (3.42f) the velocity u_2 is constant.

Using the equations (3.42a) - (3.42d) and the definition of E_1, we get

$$\alpha_1\rho_1\frac{\partial e_1}{\partial t} = (e_i - e_1)\dot{m}. \tag{3.44}$$

Differentiate $e_1(p_1, \rho_1)$ with respect to t and substitute the result in (3.44). We obtain

$$\alpha_1\rho_1\left(\frac{\partial e_1}{\partial p_1}\right)_{\rho_1}\frac{\partial p_1}{\partial t} + \alpha_1\rho_1\left(\frac{\partial e_1}{\partial \rho_1}\right)_{p_1}\frac{\partial \rho_1}{\partial t} = \varrho(e_i - e_1)\frac{\partial \alpha_1}{\partial t}. \tag{3.45}$$

From (3.42a) and (3.42b), we get

$$\alpha_1\frac{\partial \rho_1}{\partial t} = (\varrho - \rho_1)\frac{\partial \alpha_1}{\partial t}. \tag{3.46}$$

Using this in (3.45), we have

$$\alpha_1\rho_1\left(\frac{\partial e_1}{\partial p_1}\right)_{\rho_1}\frac{\partial p_1}{\partial t} + \rho_1(\varrho - \rho_1)\left(\frac{\partial e_1}{\partial \rho_1}\right)_{p_1}\frac{\partial \alpha_1}{\partial t} = \varrho(e_i - e_1)\frac{\partial \alpha_1}{\partial t}. \tag{3.47}$$

This leads to

$$\frac{\partial p_1}{\partial t} = \frac{\Gamma_1}{\alpha_1}\left(-\rho_1(\varrho - \rho_1)\left(\frac{\partial e_1}{\partial \rho_1}\right)_{p_1} + \varrho(e_i - e_1)\right)\frac{\partial \alpha_1}{\partial t}. \tag{3.48}$$

In a similar way we have an equation for p_2

$$\frac{\partial p_2}{\partial t} = -\frac{\Gamma_2}{\alpha_2}\left(-\rho_2(\varrho - \rho_2)\left(\frac{\partial e_2}{\partial \rho_2}\right)_{p_2} + \varrho(e_i - e_2)\right)\frac{\partial \alpha_1}{\partial t}. \tag{3.49}$$

By the condition (3.43a) with (3.48) and (3.49), we obtain

$$\begin{aligned}\frac{\Gamma_1}{\alpha_1}\left(-\rho_1(\varrho - \rho_1)\left(\frac{\partial e_1}{\partial \rho_1}\right)_{p_1} + \varrho(e_i - e_1)\right) = \\ -\frac{\Gamma_2}{\alpha_2}\left(-\rho_2(\varrho - \rho_2)\left(\frac{\partial e_2}{\partial \rho_2}\right)_{p_2} + \varrho(e_i - e_2)\right).\end{aligned} \tag{3.50}$$

On the other hand, e_1 can be written in terms of T_1 and ρ_1, i.e. $e_1 = e_1(T_1, \rho_1)$. Differentiating it with respect to t, substituting the result in (3.44) and using (3.46), we get

$$\frac{\partial T_1}{\partial t} = \frac{1}{\alpha_1\rho_1\left(\frac{\partial e_1}{\partial T_1}\right)_{\rho_1}}\left(-\rho_1(\varrho - \rho_1)\left(\frac{\partial e_1}{\partial \rho_1}\right)_{T_1} + \varrho(e_i - e_1)\right)\frac{\partial \alpha_1}{\partial t}.$$

But $\left(\frac{\partial e_1}{\partial T_1}\right)_{\rho_1} = C_{v1}$, the specific heat at constant volume. Thus

$$\frac{\partial T_1}{\partial t} = \frac{1}{\alpha_1\rho_1 C_{v1}}\left(-\rho_1(\varrho-\rho_1)\left(\frac{\partial e_1}{\partial \rho_1}\right)_{T_1} + \varrho(e_i - e_1)\right)\frac{\partial \alpha_1}{\partial t}. \tag{3.51}$$

A similar equation can be attained for T_2

$$\frac{\partial T_2}{\partial t} = \frac{-1}{\alpha_2\rho_2 C_{v2}}\left(-\rho_2(\varrho-\rho_2)\left(\frac{\partial e_2}{\partial \rho_2}\right)_{T_2} + \varrho(e_i - e_2)\right)\frac{\partial \alpha_1}{\partial t}. \tag{3.52}$$

By the condition (3.43b) with (3.51) and (3.52), we get

$$\frac{1}{\alpha_1\rho_1 C_{v1}}\left(-\rho_1(\varrho-\rho_1)\left(\frac{\partial e_1}{\partial \rho_1}\right)_{T_1} + \varrho(e_i - e_1)\right) = \frac{-1}{\alpha_2\rho_2 C_{v2}}\left(-\rho_2(\varrho-\rho_2)\left(\frac{\partial e_2}{\partial \rho_2}\right)_{T_2} + \varrho(e_i - e_2)\right). \tag{3.53}$$

It is clear now that (3.50) and (3.53) are two equations for the two unknowns e_i and ϱ. After some manipulations, we get from these equations

$$\varrho = \frac{\varphi\left(\frac{\rho_1 c_1^2}{\alpha_1} + \frac{\rho_2 c_2^2}{\alpha_2}\right) - \varphi\left(\frac{\Gamma_1}{\alpha_1}p_1 + \frac{\Gamma_2}{\alpha_2}p_2\right) + \psi\left(\frac{\rho_1^2\left(\frac{\partial e_1}{\partial \rho_1}\right)_{T_1}}{\alpha_1\rho_1 C_{v1}} + \frac{\rho_2^2\left(\frac{\partial e_2}{\partial \rho_2}\right)_{T_2}}{\alpha_2\rho_2 C_{v2}}\right)}{\varphi\left(\frac{c_1^2}{\alpha_1} + \frac{c_2^2}{\alpha_2}\right) - \varphi\left(\frac{\Gamma_1}{\alpha_1}h_1 + \frac{\Gamma_2}{\alpha_2}h_2\right) + \psi\left(\frac{e_1 + \rho_1\left(\frac{\partial e_1}{\partial \rho_1}\right)_{T_1}}{\alpha_1\rho_1 C_{v1}} + \frac{e_2 + \rho_2\left(\frac{\partial e_2}{\partial \rho_2}\right)_{T_2}}{\alpha_2\rho_2 C_{v2}}\right)}, \tag{3.54a}$$

$$e_i = \frac{\frac{e_1 + \rho_1\left(\frac{\partial e_1}{\partial \rho_1}\right)_{T_1}}{\alpha_1\rho_1 C_{v1}} + \frac{e_2 + \rho_2\left(\frac{\partial e_2}{\partial \rho_2}\right)_{T_2}}{\alpha_2\rho_2 C_{v2}}}{\varphi} - \frac{\frac{\rho_1^2\left(\frac{\partial e_1}{\partial \rho_1}\right)_{T_1}}{\alpha_1\rho_1 C_{v1}} + \frac{\rho_2^2\left(\frac{\partial e_2}{\partial \rho_2}\right)_{T_2}}{\alpha_2\rho_2 C_{v2}}}{\varrho\varphi} \tag{3.54b}$$

where $\varphi = \frac{1}{\alpha_1\rho_1 C_{v1}} + \frac{1}{\alpha_2\rho_2 C_{v2}}$, $\psi = \frac{\Gamma_1}{\alpha_1} + \frac{\Gamma_2}{\alpha_2}$ and $h_k = e_k + \frac{p_k}{\rho_k}$ is the *specific enthalpy* for phase k.

Consider the expression of ϱ given by (3.54a), the terms that are multiplied by ψ come from the temperature equilibrium condition. While the terms that are multiplied by φ come from the pressure equilibrium condition. It is interesting to see that a similar expression is given in the Saurel et al. [126] by

$$\rho_I = \frac{\frac{\rho_1 c_1^2}{\alpha_1} + \frac{\rho_2 c_2^2}{\alpha_2}}{\frac{c_1^2}{\alpha_1} + \frac{c_2^2}{\alpha_2}},$$

see relation (5.9) in [126]. The term ρ_I in [126] appears with the volume fraction equation in the same way as our variable ϱ, see volume fraction equation (3.42a). It is obvious that all terms of ρ_I appear in the expression of ϱ. Note also that the terms are related to the equilibrium of the temperature in the variable ϱ do not appear in the variable ρ_I, this is due to the fact that ρ_I uses the pressure equilibrium with other assumptions, but it does not use the temperature equilibrium condition.

In the context of the SG-EOS we have the following expressions for ϱ and e_i,

$$\varrho = \frac{\varphi\left(\frac{p_1+\gamma_1\pi_1}{\alpha_1}+\frac{p_2+\gamma_2\pi_2}{\alpha_2}\right)-\psi\left(\frac{\pi_1}{\alpha_1\rho_1C_{v1}}+\frac{\pi_2}{\alpha_2\rho_2C_{v2}}\right)}{-\varphi\left(\frac{(\gamma_1-1)q_1}{\alpha_1}+\frac{(\gamma_2-1)q_2}{\alpha_2}\right)+\psi\left(\frac{e_1-\frac{\pi_1}{\rho_1}}{\alpha_1\rho_1C_{v1}}+\frac{e_2-\frac{\pi_2}{\rho_2}}{\alpha_2\rho_2C_{v2}}\right)},$$

$$e_i = \frac{\left(\frac{e_1-\frac{\pi_1}{\rho_1}}{\alpha_1\rho_1C_{v1}}+\frac{e_2-\frac{\pi_2}{\rho_2}}{\alpha_2\rho_2C_{v2}}\right)}{\varphi}+\frac{\left(\frac{\pi_1}{\alpha_1\rho_1C_{v1}}+\frac{\pi_2}{\alpha_2\rho_2C_{v2}}\right)}{\varrho\varphi}.$$

Note that $\Gamma_k = \gamma_k - 1$, $k = 1, 2$, for the SG-EOS.

3.6.2 Mixture entropy

Now we consider the equation of mixture entropy. If we follow the same argument as in Section 3.2.2, under the mechanical equilibrium and temperature equilibrium, we have

$$\alpha_1\rho_1T_1\frac{Ds_1}{Dt} = (e_i+\frac{p_1}{\varrho})\dot{m}-(e_1+\frac{p_{eq}}{\rho_1})\dot{m}, \tag{3.56a}$$

$$\alpha_2\rho_2T_2\frac{Ds_2}{Dt} = -(e_i+\frac{p_2}{\varrho})\dot{m}+(e_2+\frac{p_{eq}}{\rho_2})\dot{m}. \tag{3.56b}$$

Using the mass equations (3.42b) and (3.42e) with system (3.56), we have

$$T_1(\frac{\partial\alpha_1\rho_1s_1}{\partial t}+\frac{\partial\alpha_1\rho_1s_1u_1}{\partial x}) = (e_i+\frac{p_{eq}}{\varrho})\dot{m}-(e_1+\frac{p_1}{\rho_1}-T_1s_1)\dot{m}, \tag{3.57a}$$

$$T_2(\frac{\partial\alpha_2\rho_2s_2}{\partial t}+\frac{\partial\alpha_2\rho_2s_2u_2}{\partial x}) = -(e_i+\frac{p_{eq}}{\varrho})\dot{m}+(e_2+\frac{p_2}{\rho_2}-T_2s_2)\dot{m}. \tag{3.57b}$$

Note that the quantity $e_k+\frac{p_k}{\rho_k}-T_ks_k$, $k=1,2$ is the Gibbs free energy, i.e. $g_k = e_k+\frac{p_k}{\rho_k}-T_ks_k$.

Add the two entropy equations in (3.57) after division by temperatures, we obtain

$$\frac{\partial\rho s}{\partial t}+\frac{\partial\rho su}{\partial x} = (e_i+\frac{p_{eq}}{\varrho})\dot{m}\left(\frac{T_2-T_1}{T_1T_2}\right)+\dot{m}\left(\frac{g_2}{T_2}-\frac{g_1}{T_1}\right). \tag{3.58}$$

Since the temperatures are in equilibrium by the temperature relaxation the first term in the right hand side of (3.58) vanishes and the mass transfer is modeled as $\dot{m} = \nu(g_2 - g_1)$,

where $\nu > 0$ is the relaxation parameter of the Gibbs free energy. Thus the mixture entropy satisfies the second law of thermodynamics, i.e.

$$\frac{\partial \rho s}{\partial t} + \frac{\partial \rho s u}{\partial x} = \nu \frac{(g_2 - g_1)^2}{T_{eq}} \geq 0, \tag{3.59}$$

where T_{eq} is the equilibrium temperature, $T_1 = T_2 = T_{eq}$.

In this thesis we assume that the parameter ν tends to infinity. This means that the Gibbs free energy relaxes instantaneously to equilibrium. This is considered at the interface only.

3.6.3 Gibbs free energy relaxation, procedure I

Now, we will solve the system (3.42) when $\nu \to \infty$, this means that the mass transfer occurs until the Gibbs free energies reach equilibrium. Thus we have to find the value of $\dot{m}$ that makes the difference of the Gibbs free energies at the end of the time step is zero. To do that we use the equations for the rate of change of Gibbs free energies in terms of $\dot{m}$. Assume that

$$\frac{\partial g_1}{\partial t} = A\dot{m}, \quad \text{and} \quad \frac{\partial g_2}{\partial t} = B\dot{m}. \tag{3.60}$$

Using the SG-EOS, A and B can be given as

$$\begin{aligned} A = \frac{\gamma_1 C_{v1} - C_{v1} - s_1}{\alpha_1 \rho_1 \varrho C_{v1}} \left[(e_1 - q_1)(\varrho - \rho_1) + \varrho(e_i - e_1)\right] \\ + \left[T_1(s_1 + \gamma_1 C_{v1}) - \frac{p_1}{\rho_1} - (e_1 - q_1)\right] \frac{(\varrho - \rho_1)}{\alpha_1 \rho_1 \varrho}, \end{aligned}$$

$$\begin{aligned} B = -\frac{\gamma_2 C_{v2} - C_{v2} - s_2}{\alpha_2 \rho_2 \varrho C_{v2}} \left[(e_2 - q_2)(\varrho - \rho_2) + \varrho(e_i - e_2)\right] \\ - \left[T_2(s_2 + \gamma_2 C_{v2}) - \frac{p_2}{\rho_2} - (e_2 - q_2)\right] \frac{(\varrho - \rho_2)}{\alpha_2 \rho_2 \varrho}. \end{aligned}$$

From (3.60) we get

$$\frac{\partial \Delta g}{\partial t} = \frac{\partial (g_1 - g_2)}{\partial t} = (A - B)\dot{m}.$$

The simplest numerical approximation of this equation is

$$\frac{(\Delta g)^{n+1} - (\Delta g)^n}{\Delta t} = (A - B)^n (\dot{m})^n.$$

To satisfy the equilibrium condition for the Gibbs free energies we require $(\Delta g)^{n+1} = 0$. Thus the mass transfer can be approximated as

$$(\dot{m})^n = \frac{-(\Delta g)^n}{\Delta t (A - B)^n}.$$

Using this approximation for $(\dot{m})^n$ we can integrate the system (3.42). But we may face the problem of loosing the positivity of the volume fraction. Therefore a limitation on the

value $\dot{m}/\varrho$ must be used. We take the following procedure from [126] which we cite for the sake of completeness. Assume that $S_{\alpha_1} = \dot{m}/\varrho$. Then the maximum admissible source term for the volume fraction evolution in order to presereve the positivity is given as

$$S_{\max,\ \alpha_1} = \begin{cases} \dfrac{1-\alpha_1}{\Delta t}, & S_{\alpha_1} > 0 \\ \\ -\dfrac{\alpha_1}{\Delta t}, & \text{otherwise.} \end{cases} \tag{3.61}$$

Then, if $|S_{\max,\ \alpha_1}| > |S_{\alpha_1}|$, the numerical integration for the system (3.42) can be done with the hydrodynamics time step which is restricted by the CFL number. Otherwise, the integration time step has to be reduced. The ratio $R_{\alpha_1} = S_{\max,\ \alpha_1}/S_{\alpha_1}$ is computed and the system (3.42) is integrated over a fraction of the time step, typically $\Delta t_m = R_{\alpha_1}\Delta t/2$. Successive point integrations are done to cover the complete hydrodynamic step.

The above procedure is cheap, fast and easy to implement. But this procedure is not an instantaneous one. This means that the equilibrium of the Gibbs free energy is reached very fast after a very short time but not instantaneously. Hereafter we propose another method for the Gibbs free energy relaxation which is an instantaneous relaxation procedure.

3.6.4 Gibbs free energy relaxation, procedure II

By considering (3.42b) and (3.42c) with the fact that the velocities are in equilibrium we get $\dfrac{\partial u_1}{\partial t} = 0$. Using this with (3.42c) and (3.42d) we get

$$\frac{\partial \alpha_1\rho_1 e_1}{\partial t} = e_i \dot{m}. \tag{3.62}$$

From (3.62) with (3.42a) we have

$$\frac{\partial \alpha_1\rho_1 e_1}{\partial t} = \varrho e_i \frac{\partial \alpha_1}{\partial t}. \tag{3.63}$$

Integrating (3.63) we get the following approximation

$$(\alpha_1\rho_1 e_1)^\star = (\alpha_1\rho_1 e_1)^0 + \overline{\varrho e}_i(\alpha_1^\star - \alpha_1^0), \tag{3.64}$$

where $\overline{\varrho e}_i$ is the mean value between the states $(\alpha_1^0, \rho_1^0, e_1^0)$ and $(\alpha_1^\star, \rho_1^\star, e_1^\star)$.

From (3.42a) and (3.42b) we have

$$\frac{\partial \alpha_1\rho_1}{\partial t} = \varrho \frac{\partial \alpha_1}{\partial t}.$$

Integrating this equation we get

$$(\alpha_1\rho_1)^\star = (\alpha_1\rho_1)^0 + \bar{\varrho}(\alpha_1^\star - \alpha_1^0), \tag{3.65}$$

where $\bar{\varrho}$ is the mean value between the states $(\alpha_1^0, \rho_1^0, e_1^0)$ and $(\alpha_1^\star, \rho_1^\star, e_1^\star)$.

In the same way we have the following equations for phase '2'

$$(\alpha_2\rho_2 e_2)^\star = (\alpha_2\rho_2 e_2)^0 - \overline{\varrho e}_i(\alpha_1^\star - \alpha_1^0), \tag{3.66}$$

$$(\alpha_2\rho_2)^\star = (\alpha_2\rho_2)^0 - \bar{\varrho}(\alpha_1^\star - \alpha_1^0). \tag{3.67}$$

Equation (3.65) shows that the density ρ_1 is a function of α_1. Using this fact with (3.64) we conclude that e_1 is also a function of α_1. Analogously ρ_2 and e_2 are functions of α_1, $\alpha_1 = 1 - \alpha_2$.

We aim now to find the α_1 which satisfies the equilibrium condition

$$f_g(\alpha_1) = g_2(e_2, \rho_2) - g_1(e_1, \rho_1) = 0. \tag{3.68}$$

The equation (3.68) can be solved by any iterative procedure. In this way the Gibbs free energy equilibrium is reached instantaneously.

This procedure for the Gibbs free energy relaxation is more expensive since an iterative method is used, but this method has a better resolution than the previous procedure.

3.7 The final model

In result of the previous sections, the full model with heat and mass transfer is given as

$$\frac{\partial \alpha_1}{\partial t} + u_I \frac{\partial \alpha_1}{\partial x} = \mu(p_1 - p_2) + \frac{Q}{\kappa} + \frac{\dot{m}}{\varrho}, \tag{3.69a}$$

$$\frac{\partial \alpha_1\rho_1}{\partial t} + \frac{\partial(\alpha_1\rho_1 u_1)}{\partial x} = \dot{m}, \tag{3.69b}$$

$$\frac{\partial \alpha_1\rho_1 u_1}{\partial t} + \frac{\partial(\alpha_1\rho_1 u_1^2 + \alpha_1 p_1)}{\partial x} = p_I \frac{\partial \alpha_1}{\partial x} + \lambda(u_2 - u_1) + u_I\dot{m}, \tag{3.69c}$$

$$\frac{\partial \alpha_1\rho_1 E_1}{\partial t} + \frac{\partial(\alpha_1(\rho_1 E_1 + p_1)u_1)}{\partial x} = p_I u_I \frac{\partial \alpha_1}{\partial x} + \mu p_I(p_2 - p_1) + \lambda u_I(u_2 - u_1) + Q + (e_i + \frac{u_I^2}{2})\dot{m}, \tag{3.69d}$$

$$\frac{\partial \alpha_2\rho_2}{\partial t} + \frac{\partial(\alpha_2\rho_2 u_2)}{\partial x} = -\dot{m}, \tag{3.69e}$$

$$\frac{\partial \alpha_2\rho_2 u_2}{\partial t} + \frac{\partial(\alpha_2\rho_2 u_2^2 + \alpha_2 p_2)}{\partial x} = -p_I \frac{\partial \alpha_1}{\partial x} - \lambda(u_2 - u_1) - u_I\dot{m}, \tag{3.69f}$$

$$\frac{\partial \alpha_2\rho_2 E_2}{\partial t} + \frac{\partial(\alpha_2(\rho_2 E_2 + p_2)u_2)}{\partial x} = -p_I u_I \frac{\partial \alpha_1}{\partial x} - \mu p_I(p_2 - p_1) - \lambda u_I(u_2 - u_1) - Q - (e_i + \frac{u_I^2}{2})\dot{m}, \tag{3.69g}$$

where

$$Q = \theta(T_2 - T_1),$$

$$\dot{m} = \nu(g_2 - g_1).$$

The variables κ, ϱ and e_i are given in (3.36), (3.54a) and (3.54b) respectively. All relaxation parameters λ, μ, θ and ν are assumed to be infinite.

The model (3.69) is solved by the Strang splitting (3.6). The operator L_s approximates the solution of the ordinary differential system (3.17). This system is solved by successive integrations considering separately each one of the source vectors that are related to the relaxation of the velocity, pressure, temperature and Gibbs free energy. The order of the successive integrations are essential for this model. They are done firstly for the velocity relaxation, then for the pressure relaxation, after for the temperature relaxation and finally for the Gibbs free energy relaxation. The velocity and the pressure relaxation are performed for the entire flow field while the temperature and the Gibbs free energy relaxation are used at the interface only. For the hyperbolic operator L_h a Godunov-type scheme is used.

3.8 Numerical results

The tests for metastable liquids in Saurel et al. [126] are used.

3.8.1 Two-phase shock tube

Consider a 1 m shock tube filled with liquid dodecane under high pressure at the left, and with the vapor dodecane at atmospheric pressure at the right. The initial discontinuity is set at 0.75 m, and the initial data are

Left	Right
$p_l = 10^8$ Pa	$p_v = 10^5$ Pa
$\rho_l = 500$ kg/m^3	$\rho_v = 2$ kg/m^3
$u_l = 0$ m/s	$u_v = 0$ m/s

For numerical reasons, in each side of the shock tube we allow the presence of a small volume fraction of the other fluid, typically 10^{-6}.

All computations for this example were done with a CFL number of 0.6. They used the first Gibbs free energy relaxation procedure with a limitation on the source terms given by (3.61). The time step for the fluid motion is restricted by the CFL number, but we observed that the Gibbs free energy relaxation procedure may require smaller time to ensure the positivity of the volume fraction. This means that sometimes the equations (3.42) are stiff. Thus by using the limitation (3.61) a smaller time step is used for the Gibbs free energy relaxation procedure and successive point integrations are done to cover

the complete hydrodynamic step that is restricted by the CFL number. In the presence of stiffness from the Gibbs free energy relaxation, the first Gibbs free energy relaxation procedure is more appropriate than the second relaxation procedure, this is due to the easy of impostion the limitation (3.61) on the source terms.

By using the above seven-equation model the results are shown at time $t = 473\mu$s. Figure 3.2 gives the results without phase transition, while in Figure 3.3 we see the case when the phase transition is included.

In comparison between the two figures, an extra wave appears between the rarefaction wave and the contact discontinuity which corresponds the evaporation front. Indeed, a rarefaction wave propagates through the liquid producing a superheated liquid and evaporation has occurred. An extra wave representing the evaporation front propagates through the superheated liquid and produces a liquid-vapor mixture at thermodynamic equilibrium with a high velocity, see the graphs of the velocity in Figures 3.2 and 3.3, where the velocity jumps from 141 m/s up to about 371 m/s. For more physical explanations see Saurel et al. [126].

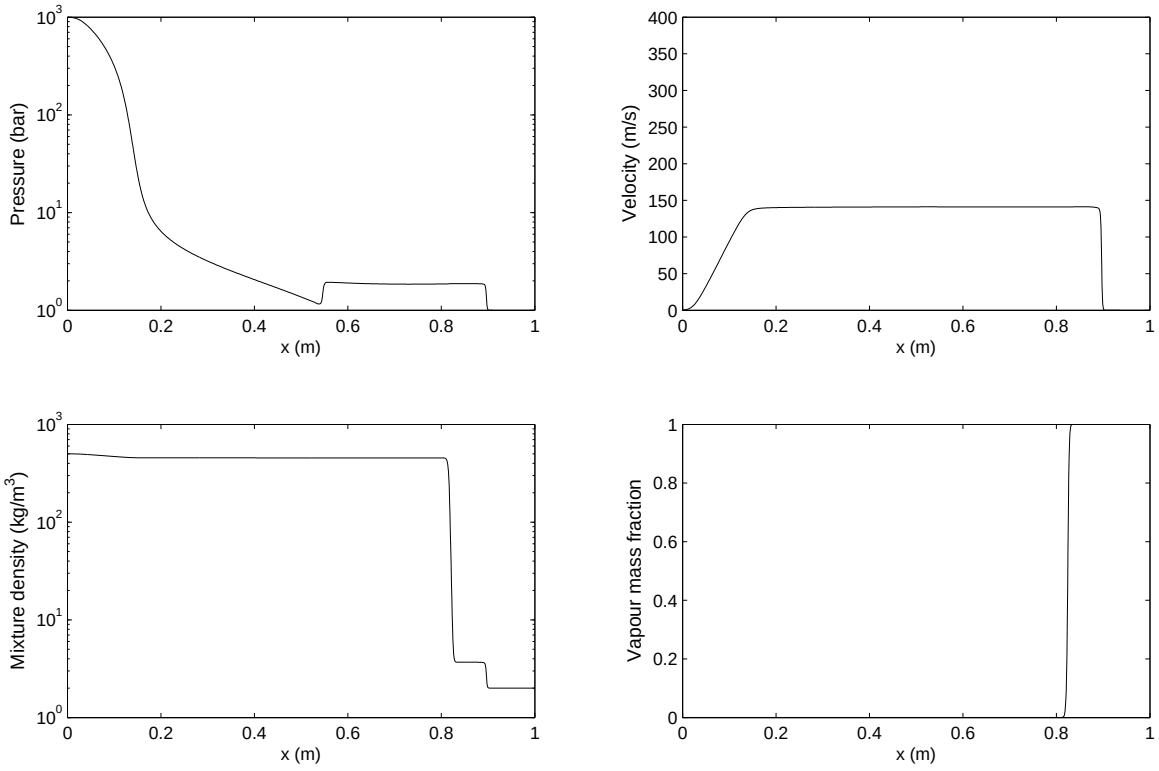

Figure 3.2: Dodecane liquid-vapor shock tube without phase transition, by using the seven-equation model. The mesh involves 1250 cells, the CPU time is 100.65 seconds and the number of time steps is 7197. The scale for the velocity graph is chosen in this way for a direct comparison with the velocity graph in Figure 3.3.

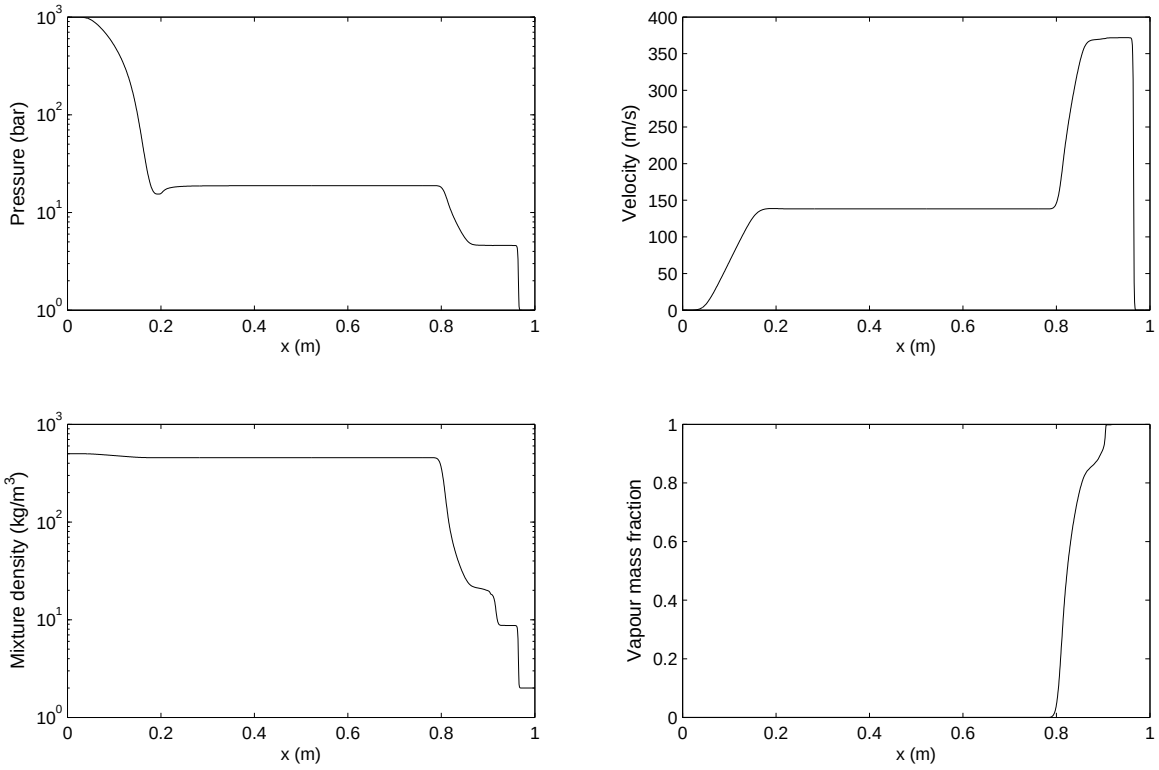

Figure 3.3: Dodecane liquid-vapor shock tube with phase transition, by using the seven-equation model. The mesh involves 1250 cells, the CPU time is 151.98 seconds and the number of time steps is 8828.

Figure 3.4 shows different waves that are formed in the tube by using the mixture density graph where all states are visible. It is clear that the evaporation front looks like an expansion wave.

The results in Figure 3.3 are almost similar to the results of Saurel et al. [126]. But at the right end of the left rarefaction wave in the pressure profile in this figure we see a small distortion which does not appear in the results of Saurel et al. [126] by using the five-equation model. We reran this test for a higher number of cells, but observed no change. In fact we see the same feature on the curve of the pressure without heat and mass transfer, see Figure 3.2 where the computations used 1250 cells. In Figure 3.5 the pressure curve is shown on a logarithmic scale, 10000 cells were used in the computations but this distortion still appears. Thus we conclude that this is not related to our new modifications for heat and mass transfer. This may come from the nature of the initial seven-equation model or from the numerical method for the model without phase transition. Moreover, such differences between the results of the seven-equation model and the five-equation model without phase transition appear also in the results of Murrone and Guillard [96]. This requires further investigation.

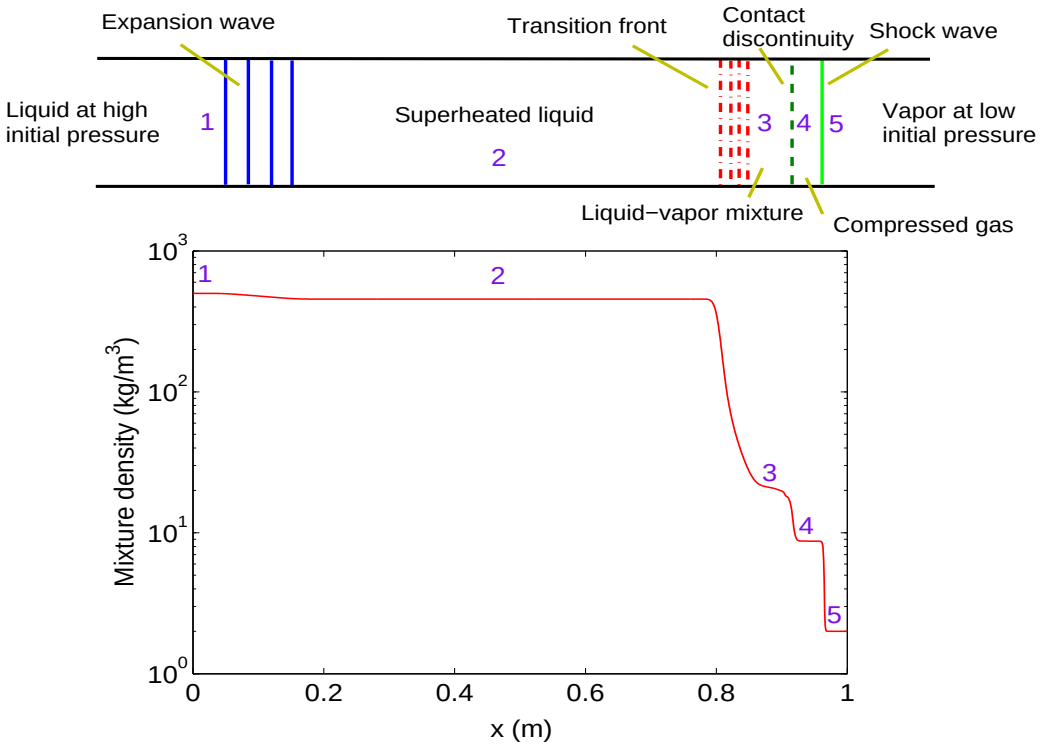

Figure 3.4: Dodecane liquid-vapor shock tube with phase transition. Different waves which are formed in the tube are shown with a correspondence to the graph of the mixture density where all states are visible.

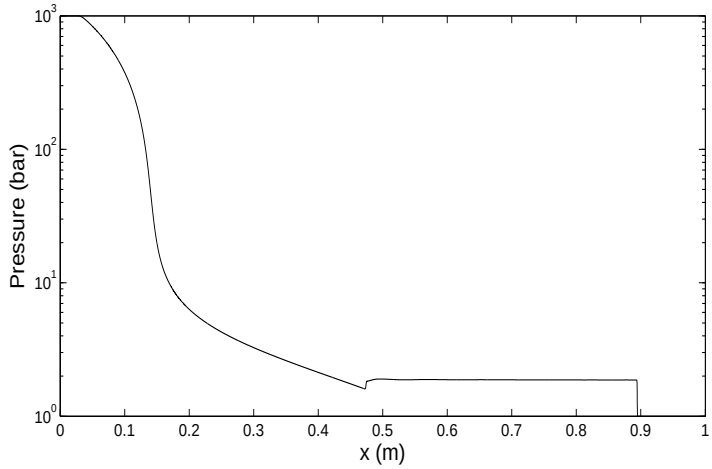

Figure 3.5: Dodecane liquid-vapor shock tube without phase transition. The pressure profile over (10000) cells, by the seven-equation model. The CPU time is 8145.17 seconds taking 56749 time steps.

3.8.2 Validation against shock tube experiments

Experimental results were obtained by Simões-Moreira and Shepherd [136]. Liquid dodecane in a tube, with a certain initial temperature, was suddenly expanded into a low pressure chamber (1 mbar). An evaporation front or wave propagated into metastable liquid with a steady mean velocity. This velocity was measured for different initial temperatures of liquid dodecane. Also pressure data were obtained during the evaporation event before and after the evaporation wave, see [136] and for full details see the Ph.D. thesis of Simões-Moreira [135].

At each temperature we compute the front velocity under conditions which are close to the experimental conditions with help of Le Metayer [81]. We consider a low pressure chamber (1 mbar) filled with gaseous dodecane at right side of the shock tube with density 10^{-4}kg/m^3. While a liquid dodecane is considered initially at the left side of the shock tube with a higher pressure. We adjust the initial pressure of the left hand side, so that the pressure in the state before the evaporation front is equal to the measured value. The density of the liquid is calculated from the equation of state (3.2b), as the initial temperature is known.

Table 3.3 shows the estimated initial pressure that we use for each temperature in the left hand side of the tube, see column two. The columns three and four represent the experimental data for the pressure before the evaporation wave and the front velocity respectively [136]. The fifth column shows the computed values for the front velocity by the present model.

As in [126] the front velocity is computed as a local wave speed, i.e.

$$U_F = \frac{(\rho u)_i - (\rho u)_{i-1}}{\rho_i - \rho_{i-1}},$$

where U_F is the front velocity, i refers to the state after the evaporation wave, ρ is the mixture density and u the equilibrium velocity, see Figure 3.4.

The computed values for the front velocity are calculated at several time points in the range between $200\mu s$ and $500\mu s$. Then an averaged value is taken. We see that for each case the computed values at different times are very close.

A comparison between our results with the experimental results and the results of Saurel et al. [126] is shown in Figure 3.6. It is clear that our results are more close to the experimental results. There is still not perfect agreement with the experimental data. This is related to several sources, like how realistic the equations of state we used are and how close we are to the real initial conditions of the experiments. However we have a reasonable agreement with the experimental data also in the tendency of the relation between the front velocity and the initial temperature, i.e. the front velocity increases if the temperature increases.

T_l (K)	p_l (bar)	p_B (bar)	U_F (m/s)(measured)	U_F (m/s)(computed)
453	1.5	0.24	0.253	0.147
473	2.2	0.33	0.309	0.240
489	3.0	0.44	0.390	0.328
503	3.9	0.59	0.472	0.441
523	5.0	0.83	0.648	0.576
543	7.5	1.19	0.837	0.888
563	11.0	1.91	1.381	1.337
573	13.0	2.12	1.578	1.620

Table 3.3: Estimated initial pressure (column two), experimental results (columns three and four) and the computed front velocity (column five) at several initial temperatures (column one).

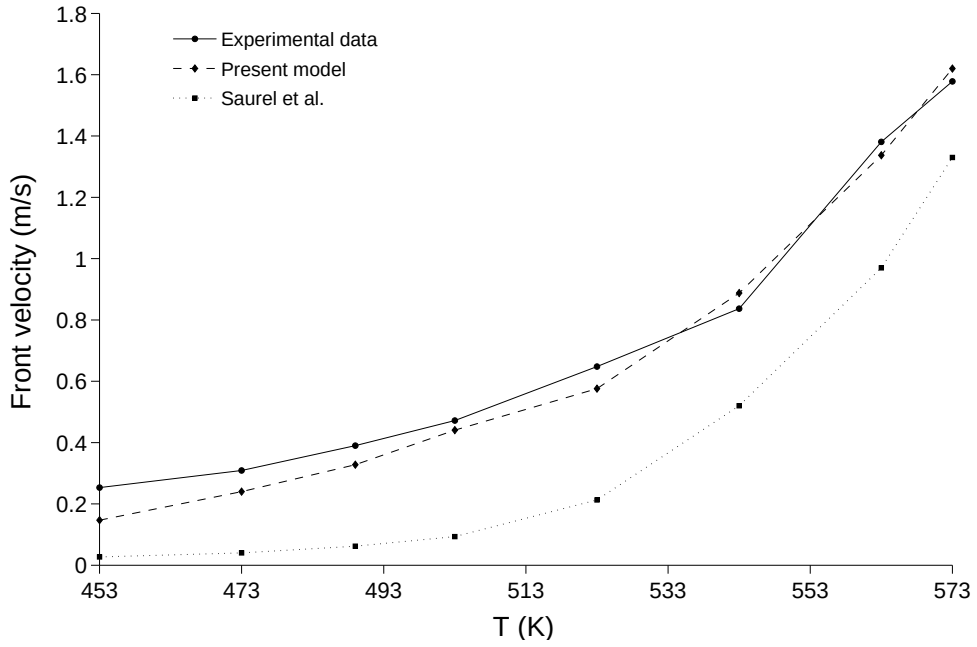

Figure 3.6: Evaporation front velocity in superheated dodecane versus initial temperature of liquid dodecane. Comparison between results of the present model with the experimental results of Simões-Moreira and Shepherd [136] and the computed results of Saurel et al. [126].

3.8.3 Two-phase expansion tube

This test consists of a 1 m long tube filled with liquid water at atmospheric pressure and with density $\rho_l = 1150$ kg/m^3. A weak volume fraction of vapor ($\alpha_v = 0.01$) is initially added to the liquid. The initial discontinuity is set at 0.5 m, the left velocity is -2 m/s and the right velocity is 2 m/s.

In this test the water can not be treated as pure, and only the metastability condition is used to activate the phase transition, i.e. phase transition occurs if the liquid is metastable, i.e. if $T_l > T_{sat}(p_{equi})$.

For the computation of $T_{sat}(p_{equi})$ we solve equation (3.26) by the Newton iterative method at each point in the domain during the time evolution.

This test case requires a small time step to obtain a stable solution (CFL ≈ 0.15). When the strong rarefaction are considered a smaller time step is required (CFL ≈ 0.03). Here for the sake of comparison we choose to do all computations with CFL $= 0.03$. The small time here indicates that there is a stiffness coming from the relaxation procedures.

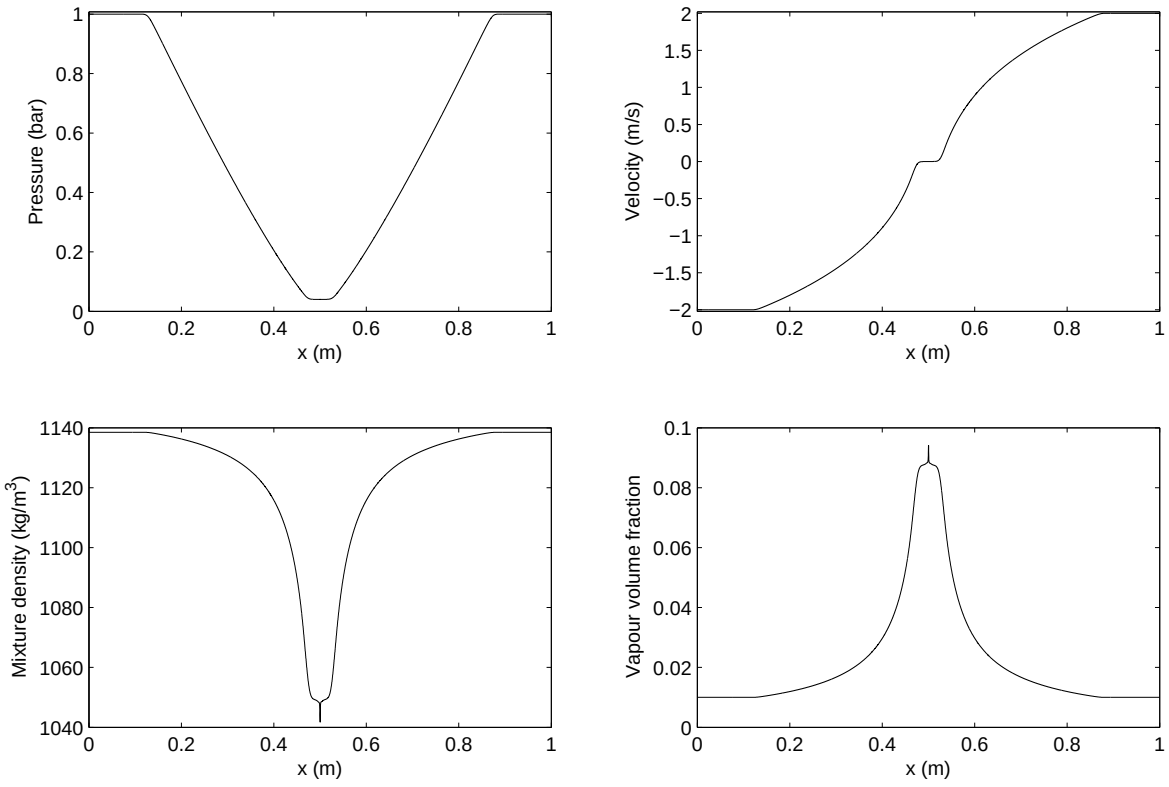

Figure 3.7: Water liquid-vapor expansion tube without phase transition, by using the seven-equation model. The computations were done with 5000 cells. The CPU time is 14.772 hours with 763,550 time steps.

Both procedures of the Gibbs free energy relaxation give almost the same results, but we consider that the second procedure has a better resolution, thus it is adopted for this test case.

In Figure 3.7, we see the solution of this problem without phase transition at $t = 3.2$ ms. The solution involves two expansion waves. The vapor volume fraction increases at the center of the domain due to the mechanical expansion of the gas present in small proportions [126].

The rarefaction waves make the liquid metastable and phase transition has to be added. Figure 3.8 presents the solution when the phase transition is included and is compared with the solution without phase transition at $t = 3.2$ ms. Liquid water is expanded until the saturation pressure is reached (see the pressure graph) then evaporation appears and quite small of vapor is created, for details see [126].

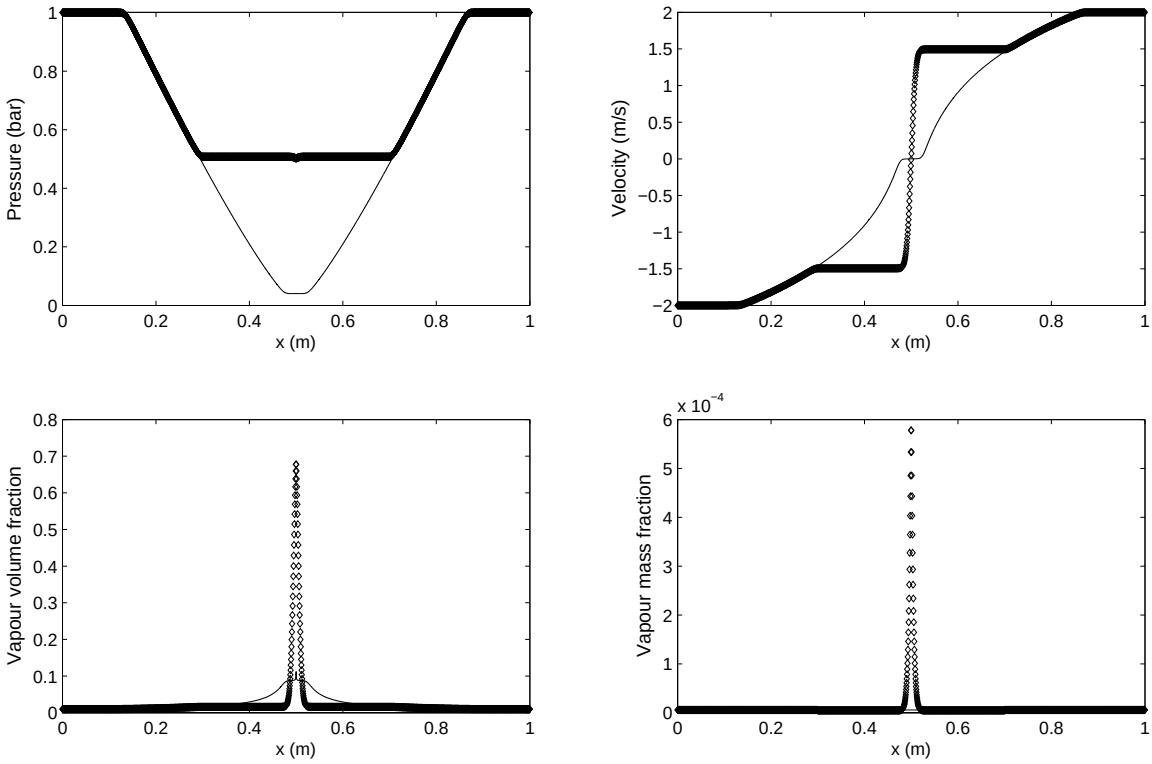

Figure 3.8: Water liquid-vapor expansion tube results at $t = 3.2$ ms, the computed results by the seven-equation model with phase transition (symbols) are compared with the results of the same model without phase transition (lines). The computations were done with 5000 cells. For the model without phase transition: The CPU time is 14.772 hours with 763,550 time steps. when the phase transition is included: The CPU time is 18.838 hours with 763,550 time steps.

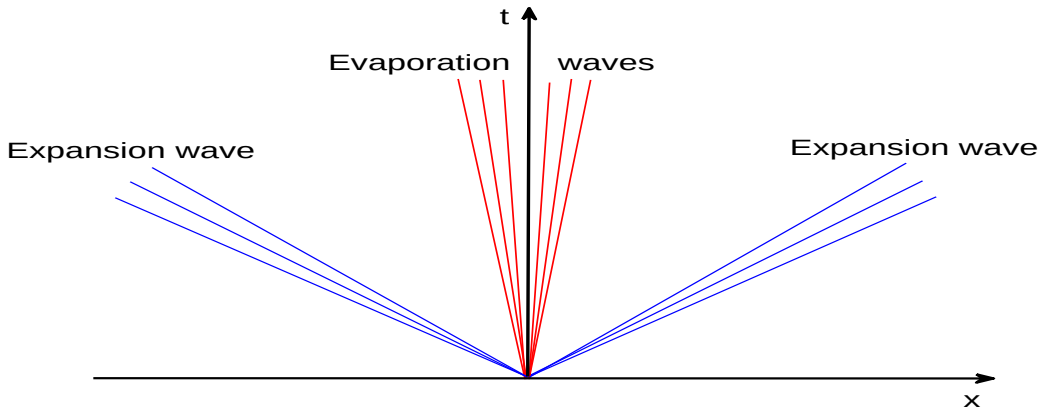

Figure 3.9: The waves pattern that correspond to the solution in Figure 3.8, with phase transition. As shown the evaporation waves are expansion waves.

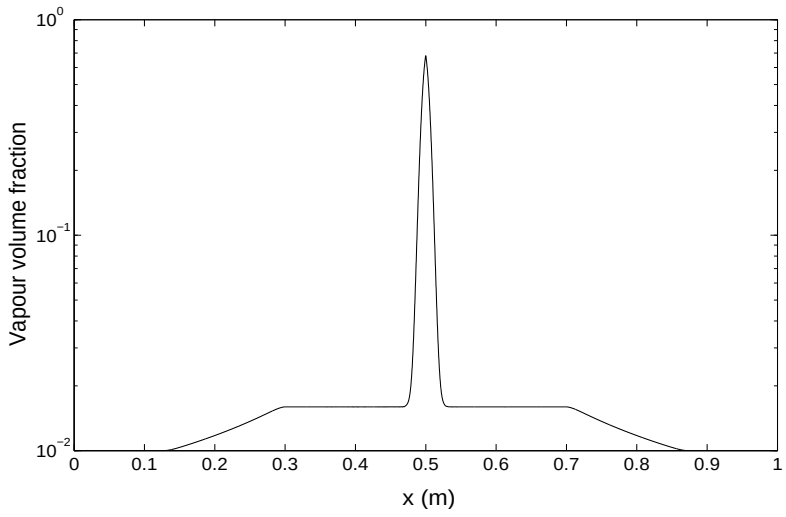

Figure 3.10: Water liquid-vapor expansion tube with phase transition at $t = 3.2$ ms, the vapor volume fraction profile on a logarithmic scale. The seven-equation model is used.

The solution with phase transition, Figure 3.8, is composed of four expansion waves. This is clear if we consider the vapor volume fraction profile on a logarithmic scale as in Figure 3.10. Thus the wave pattern is as drawn in Figure 3.9. The extra two expansion waves correspond to the evaporation fronts.

If we consider the solution at later time, when $t = 59$ ms as in Figure 3.11, the two leading fast expansion waves leave the tube and the two slow evaporation waves are clearly visible. It is clear that these evaporation waves look like expansion waves.

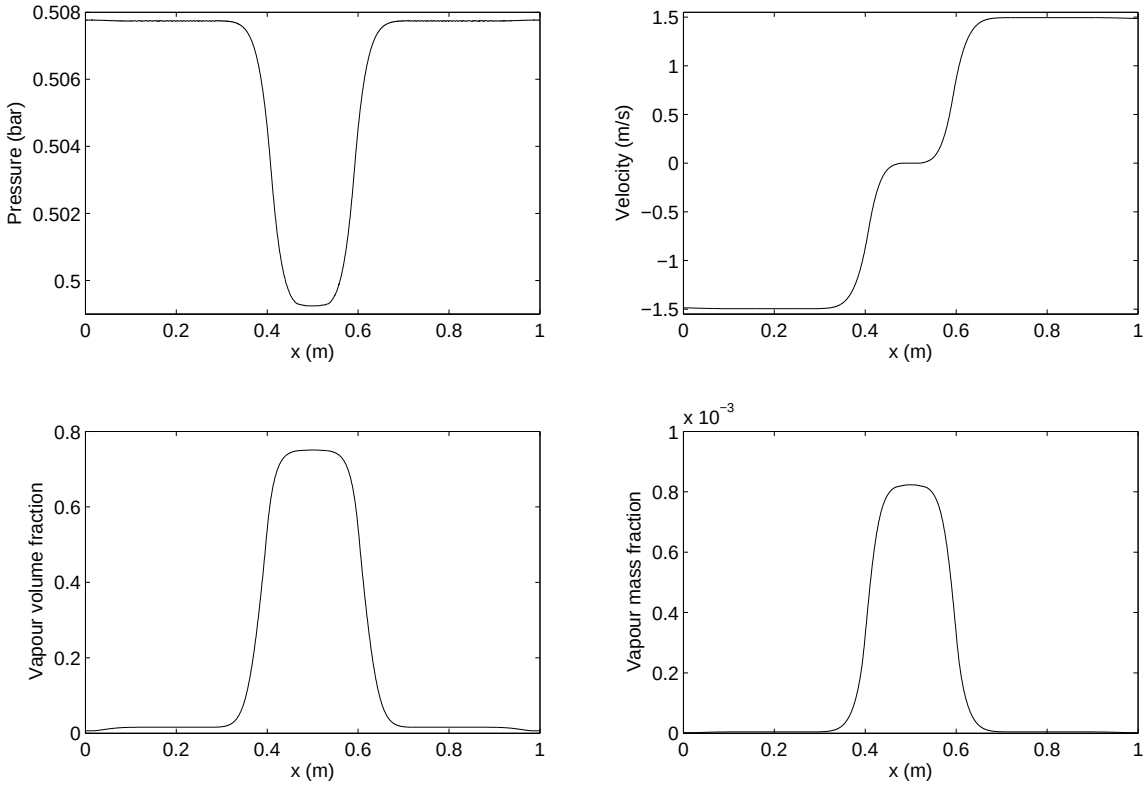

Figure 3.11: Water liquid-vapor expansion tube with phase transition at time $t = 59$ ms, by using the seven-equation model. The two slow evaporation waves are visible. The computations were done with 3200 cells. The CPU time is 116.078 hours with 8,217,444 time steps.

To see the four expansion waves in one single graph we increase the value of the velocity which means an increase in the rarefaction effects. Under the same conditions except with a velocity -100 m/s on the left and 100 m/s on the right, the four waves are clearly visible as shown in Figure 3.12 at time $t = 1.5$ ms. Figure 3.13 shows the wave pattern of the solution. In this case the evaporation waves are faster compared to the previous case shown in Figure 3.9.

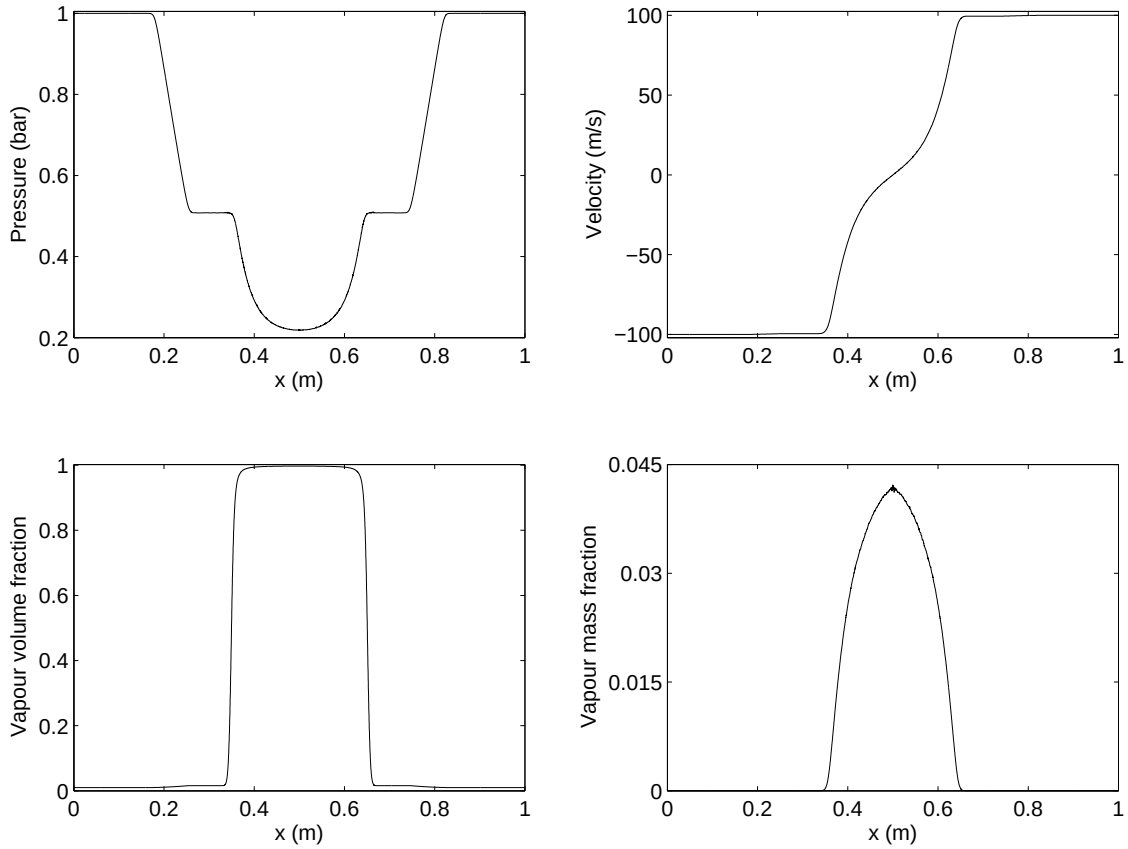

Figure 3.12: Water liquid-vapor expansion tube with phase transition and strong rarefaction effects (initial $|u| = 100$ m/s) at time $t = 1.5$ ms. The computations are done with 5000 cells by the seven-equation model. The CPU time is 8.537 hours with 449,836 time steps.

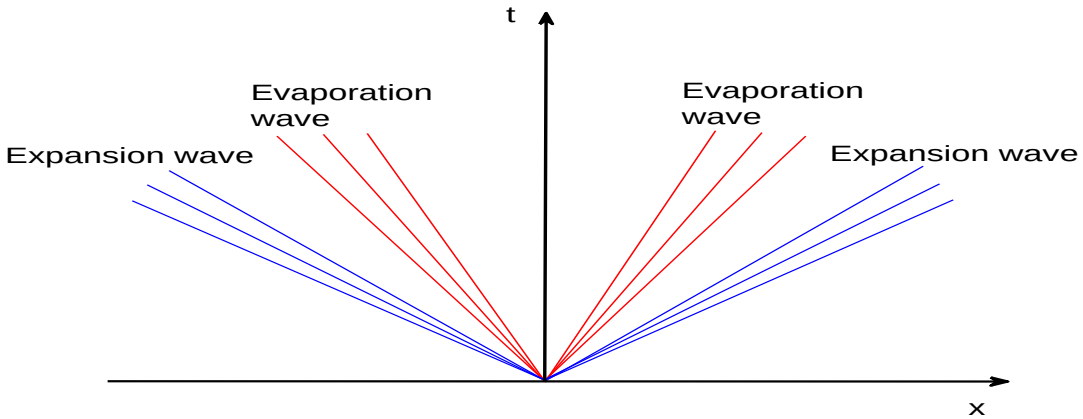

Figure 3.13: The waves pattern that correspond to the solution in Figure 3.12.

Chapter 4

Modeling phase transition for the six-equation model

4.1 Introduction

The six-equation model with a single velocity is obtained from the seven-equation model in the asymptotic limit of zero velocity relaxation time, see Kapila et al. [66]. This model, as the seven-equation model, has attractive advantages over the five-equation model for the numerical computations, see Chapters 1 and 2. Also this model is less expensive than the seven-equation model.

In this chapter, we insert the heat and mass transfer in the six-equation model by the relaxation effects. The previous assumptions and ideas for the seven-equation model are used, i.e. we assume that the pressure relaxes much faster than the thermal properties and the temperature relaxation time is much smaller than that of the Gibbs free energy. By using these assumptions we proceed in the same way as in the case of the seven-equation model to insert the heat and mass transfer in the six-equation model. On the other hand we will show the derivation of the six-equation model with heat and mass transfer directly from the full seven-equation model (3.69) by applying the reduction method of Chen et al. [22] assuming stiff velocity relaxation.

We consider the same numerical tests that were used in Chapter 3. Mainly we focus on the comparisons between the results of both models, i.e. the seven-equation and the six-equation model. In general both models almost give the same results. We observe differences in the results for both models under strong rarefaction in mixtures. This point receives special attention.

This chapter is organized as follows: In Section 4.2 we recall the six-equation model that was studied in Subsection 2.4.2. In Section 4.3 we present the non-conventional shock relations which were derived in Saurel et al. [125] for multiphase mixtures with stiff mechanical properties. Section 4.4 is devoted to the numerical method. A Godunov-type scheme is

presented with two Riemann solvers, namely, VFRoe-type solver and HLLC-type solver. In addition the pressure relaxation procedure and correction criterion of Saurel et al. [127] are recalled. In Section 4.5 we model the heat and mass transfer for the six-equation model directly by using the same procedure for the seven-equation model that was proposed in Chapter 3. While Section 4.6 shows the derivation of the six-equation model with heat and mass transfer from the seven-equation model accompanied with heat and mass transfer by using the reduction method of Chen et al. [22]. Finally, in Section 4.7 we validate the modified model numerically. Comparisons with the results of the seven-equation model are made.

4.2 Mathematical model

The six-equation model without heat and mass transfer can be written as, see Subsection 2.4.2

$$\frac{\partial \alpha_1}{\partial t} + u\frac{\partial \alpha_1}{\partial x} = \mu(p_1 - p_2), \tag{4.1a}$$

$$\frac{\partial \alpha_1\rho_1}{\partial t} + \frac{\partial(\alpha_1\rho_1 u)}{\partial x} = 0, \tag{4.1b}$$

$$\frac{\partial \alpha_2\rho_2}{\partial t} + \frac{\partial(\alpha_2\rho_2 u)}{\partial x} = 0, \tag{4.1c}$$

$$\frac{\partial \rho u}{\partial t} + \frac{\partial(\rho u^2 + \alpha_1 p_1 + \alpha_2 p_2)}{\partial x} = 0, \tag{4.1d}$$

$$\frac{\partial \alpha_1\rho_1 e_1}{\partial t} + \frac{\partial \alpha_1\rho_1 e_1 u}{\partial x} + \alpha_1 p_1\frac{\partial u}{\partial x} = \mu p_I(p_2 - p_1), \tag{4.1e}$$

$$\frac{\partial \alpha_2\rho_2 e_2}{\partial t} + \frac{\partial \alpha_2\rho_2 e_2 u}{\partial x} + \alpha_2 p_2\frac{\partial u}{\partial x} = -\mu p_I(p_2 - p_1). \tag{4.1f}$$

In this chapter we use the relation (2.46) for the interfacial pressure p_I, i.e.

$$p_I = \frac{Z_2 p_1 + Z_1 p_2}{Z_1 + Z_2}. \tag{4.2}$$

The acoustic impedance Z_k, $k = 1, 2$, is defined by (2.48).

The choice (4.2) for the interfacial pressure fulfills the second law of thermodynamics [127]. Indeed, by using the Gibbs relation (3.5) and the closure expression (4.2) with the system (4.1) we get the following phasic entropy equations

$$\alpha_1\rho_1 T_1\frac{Ds_1}{Dt} = \mu(p_2 - p_1)^2\frac{Z_1}{Z_1 + Z_2}, \tag{4.3a}$$

$$\alpha_2\rho_2 T_2\frac{Ds_2}{Dt} = \mu(p_2 - p_1)^2\frac{Z_2}{Z_1 + Z_2}. \tag{4.3b}$$

Combining the two equations in (4.3) we get the following relation for the mixture entropy, which agrees with the second law of thermodynamics

$$\frac{\partial \rho s}{\partial t} + \frac{\partial \rho s u}{\partial x} = \frac{\mu (p_2 - p_1)^2}{Z_1 + Z_2} \left(\frac{Z_1}{T_1} + \frac{Z_2}{T_2} \right) \geq 0,$$

where $\rho s = \alpha_1 \rho_1 s_1 + \alpha_2 \rho_2 s_2$.

We apply the idea of Saurel et al. [127] that during the numerical computations we use the mixture energy equation to correct the thermodynamic state predicted by the two non-conservative internal energy equations. By summing the two internal energy equations and using the mass and momentum equations we obtain the mixture energy equation

$$\frac{\partial (\rho e + \frac{1}{2}\rho u^2)}{\partial t} + \frac{\partial u(\rho e + \frac{1}{2}\rho u^2 + \alpha_1 p_1 + \alpha_2 p_2)}{\partial x} = 0, \tag{4.4}$$

where $\rho = \alpha_1 \rho_1 + \alpha_2 \rho_2$ and $\rho e = \alpha_1 \rho_1 e_1 + \alpha_2 \rho_2 e_2$

4.3 Shock relations

The model (4.1) is non-conservative and there is no way to determine its conventional Rankine-Hugoniot conditions which satisfy (2.54). Instead of that, non-conventional jump conditions are used.

In this thesis we are interested in a single pressure for both phases in the whole domain. For that an instantanous pressure relaxation is used. This makes the six-equation model (4.1) equivalent to the five-equation model (2.85) that is derived from the six-equation model in the limit of zero time for the pressure relaxation [127]. Therfore, as in Saurel et al. [127], for the six-equation model we use the non-conventional shock relations that were derived in Saurel et al. [125] for the five equation model. Indeed, the shock relations are used to build an HLLC-type Riemann solver. Thus there is no need to determine precise shock relations. In addition, the system (4.1) is non-conservative, so it is difficult to make the numerical solution converge to the end shock state solution even if the exact shock relations are given, see Saurel et al. [127].

However, these shock relations for the model (4.1) are written as

$$\alpha_1 = \alpha_1^0, \tag{4.5a}$$

$$\alpha_1 \rho_1 (u - \sigma) = \alpha_1^0 \rho_1^0 (u^0 - \sigma) = m_1, \tag{4.5b}$$

$$\alpha_2 \rho_2 (u - \sigma) = \alpha_2^0 \rho_2^0 (u^0 - \sigma) = m_2, \tag{4.5c}$$

$$p - p^0 + m^2 (v - v^0) = 0, \tag{4.5d}$$

$$e_k - e_k^0 + \frac{p_k + p_k^0}{2}(v_k - v_k^0) = 0, \qquad k = 1, 2. \tag{4.5e}$$

Where σ denotes the shock speed, $m = m_1 + m_2$, $p = \alpha_1 p_1 + \alpha_2 p_2$ and $v = Y_1 v_1 + Y_2 v_2$, where $v_k = \dfrac{1}{\rho_k}$ is the *specific volume*. The mass fraction $Y_k = \dfrac{\alpha_k \rho_k}{\rho}$, $k = 1, 2$.

It is worth mentioning that the above shock relations satisfy some general admissibility conditions that are

- Preserving the conservation of the total energy.
- In agreement with the single phase limit.
- Symmetry
- The mixture Hugoniot is tangent to the mixture isentrope.
- Entropy production.

Moreover, these relations were validated against experiments for both weak and strong shocks. For all details see [125, 127].

4.4 Numerical method

To take into account the non-differential source terms the Strang splitting (3.6) is used. In this case the vector of conservative variables $\mathbf{U}$ is given as

$$\mathbf{U} = (\alpha_1, \alpha_1\rho_1, \alpha_2\rho_2, \rho u, \alpha_1\rho_1 e_1, \alpha_2\rho_2 e_2, \rho e + \frac{1}{2}\rho u^2)^T.$$

The last element in $\mathbf{U}$ corresponds to the redundant equation (4.4).

For the hyperbolic part of the system a Godunov-type scheme is used that takes into account the discretization of the non-conservative terms.

The source vector $\mathbf{S}$ is associated with the relaxation terms and is decomposed as

$$\mathbf{S} = \mathbf{S}_P + \mathbf{S}_Q + \mathbf{S}_m,$$

where $\mathbf{S}_P = (\mu(p_1 - p_2), 0, 0, 0, \mu p_I(p_2 - p_1), -\mu p_I(p_2 - p_1), 0)^T$ represents the pressure relaxation terms. In this section we will present the instantaneous pressure relaxation procedure which was recently proposed by Saurel et al. [127]. This procedure can be easily extended to multiphase flows. So it has a special importance in the next chapter.

The vectors $\mathbf{S}_Q$ and $\mathbf{S}_m$ are associated with the heat and mass transfer relaxation terms respectively, they will be considered in the next section.

4.4.1 Godunov-type method

The equations in systems (4.1) that are written in a conservative form are discretized by the conventional Godunov scheme, see Section 2.3

$$\mathbf{u}_j^{n+1} = \mathbf{u}_j^n - \frac{\Delta t}{\Delta x}[\mathbf{f}(\mathbf{u}^*(\mathbf{u}_j^n, \mathbf{u}_{j+1}^n)) - \mathbf{f}(\mathbf{u}^*(\mathbf{u}_{j-1}^n, \mathbf{u}_j^n))],$$

where

$$\mathbf{u} = (\alpha_1\rho_1,\ \alpha_2\rho_2,\ \rho u,\ \rho e + \frac{1}{2}\rho u^2)^T$$

and

$$\mathbf{f(u)} = \left(\alpha_1\rho_1 u,\ \alpha_2\rho_2 u,\ \rho u^2 + \alpha_1 p_1 + \alpha_2 p_2,\ u(\rho e + \frac{1}{2}\rho u^2 + \alpha_1 p_1 + \alpha_2 p_2)\right)^T.$$

The volume fraction equation and the internal energy equations are discretized as, see [127],

$$\alpha_{1j}^{n+1} = \alpha_{1j}^n - \frac{\Delta t}{\Delta x}((u\alpha_1)^*_{j+\frac{1}{2}} - (u\alpha_1)^*_{j-\frac{1}{2}} - \alpha_{1j}^n(u^*_{j+\frac{1}{2}} - u^*_{j-\frac{1}{2}})),$$

$$(\alpha\rho e)_{kj}^{n+1} = (\alpha\rho e)_{kj}^n - \frac{\Delta t}{\Delta x}((\alpha\rho eu)^*_{k,j+\frac{1}{2}} - (\alpha\rho eu)^*_{k,j-\frac{1}{2}} + (\alpha p)_{kj}^n(u^*_{j+\frac{1}{2}} - u^*_{j-\frac{1}{2}})).$$

The above approximations satisfy the uniform flow test of Abgrall [1], see the details in Saurel et al. [127].

To achieve a second order accuracy we use the MUSCL method detailed in Section 3.3.3.

For the solution of the Riemann problem, the HLL, HLLC and VFRoe Riemann solvers can be used. For the HLL solver we refer to the book of Toro [148], it is explained in the context of Euler equations there but it is easily modified to the six-equation model. The HLLC solver was introduced in Section 3.3.2 for the seven-equation model and is detailed in [127] for the six-equation model. The VFRoe solver [46] is explained hereafter in the context of the six-equation model. In addition, we recall the HLLC-type solver of Saurel et al. [127] which can be easily extended to multiphase flows. This will be useful for the problems in the next chapter.

4.4.2 VFRoe-type solver

Consider the Riemann problem consists of the homogenous part of the system (4.1) written in primitive variables

$$\frac{\partial \mathbf{W}}{\partial t} + \mathbf{A}\frac{\partial \mathbf{W}}{\partial x} = 0,$$

with the initial condition

$$\mathbf{W}(x,0) = \begin{cases} \mathbf{W}_L, & x < 0 \\ \\ \mathbf{W}_R, & x > 0. \end{cases}$$

Where $\mathbf{W}$ and $A(\mathbf{W})$ are given by (2.80) and (2.81) respectively. The indeces 'L' and 'R' refer to the left and right states of a cell boundary respectively.

Following Gallouët and Masella [46], the Jacobian matrix $A(\overline{\mathbf{W}})$ is calculated in the average state

$$\overline{\mathbf{W}} = \frac{\mathbf{W}_L + \mathbf{W}_R}{2}.$$

The intermediate state in the solution of the Riemann problem is

$$\mathbf{W}^* = \mathbf{W}_L + \sum_{\lambda_i<0} a_i \mathbf{r}_i,$$

where the eigenvalues λ_i and the corresponding eigenvectors $\mathbf{r}_i$ are given by (2.82) and (2.91).

The coefficients a_i are determined by

$$\mathbf{W}_R - \mathbf{W}_L = \sum_{i=1}^{6} a_i \mathbf{r}_i,$$

Indeed, they are given by the following expressions

$$\begin{aligned}
a_4 &= \Delta_1, \\
a_1 &= -\frac{\frac{\rho_2}{\rho_1} c_2^2 \Delta_5 - c_1^2 \Delta_6 - \frac{\rho_2 c_2^2 a_4 (p_2 - p_1)}{\alpha_1 \rho_1}}{\frac{\alpha_2 \rho_2}{\alpha_1 \rho_1} c_2^2 + c_1^2}, \\
a_5 &= \frac{\rho_1 \rho_2 c_2^2 \Delta_4 + \rho_1 c \Delta_6 - \rho_1 c a_1}{2 \rho_2 c c_2^2}, \\
a_6 &= a_5 - \frac{\rho_1}{c} \Delta_4, \\
a_2 &= \Delta_3 - \frac{\rho_2}{\rho_1}(a_5 + a_6), \\
a_3 &= \Delta_2 - a_5 - a_6,
\end{aligned}$$

where Δ_k is the *k-th* component of $\mathbf{W}_R - \mathbf{W}_L = (\Delta_1, ..., \Delta_6)^T$.

4.4.3 HLLC-type solver

The intercell flux of the HLLC Riemann solver is given by, see Toro [148]

$$\mathbf{F}_{j+\frac{1}{2}}^{HLLC} = \begin{cases} \mathbf{f}(\mathbf{u}_L), & 0 \le S_L \\ \mathbf{f}(\mathbf{u}_{*L}) = \mathbf{f}(\mathbf{u}_L) + S_L(\mathbf{u}_{*L} - \mathbf{u}_L), & S_L \le 0 \le S_* \\ \mathbf{f}(\mathbf{u}_{*R}) = \mathbf{f}(\mathbf{u}_R) + S_R(\mathbf{u}_{*R} - \mathbf{u}_R), & S_* \le 0 \le S_R \\ \mathbf{f}(\mathbf{u}_R), & 0 \ge S_R. \end{cases}$$

Following the Davis estimates [31] the wave speeds can be taken as

$$S_L = \min\{u_L - c_L, u_R - c_R\},$$

$$S_R = \max\{u_L + c_L, u_R + c_R\}.$$

The speed of the intermediate wave is determined as in Toro [148] but instead of single values the mixture density and pressure are used. Thus we have

$$S_* = \frac{p_R - p_L + \rho_L u_L(S_L - u_L) - \rho_R u_R(S_R - u_R)}{\rho_L(S_L - u_L) - \rho_R(S_R - u_R)}$$

where $\rho = \alpha_1\rho_1 + \alpha_2\rho_2$ and $p = \alpha_1 p_1 + \alpha_2 p_2$.

Following Saurel et al. [127], the intermediate state is determined by the help of the shock relations (4.5). From (4.5b) and (4.5c) we have

$$(\alpha_k\rho_k)^*_L = (\alpha_k\rho_k)_L \frac{S_L - u_L}{S_L - S_*}, \tag{4.6}$$

$$(\alpha_k\rho_k)^*_R = (\alpha_k\rho_k)_R \frac{S_R - u_R}{S_R - S_*}. \tag{4.7}$$

The volume fraction is constant across the fluid trajectories, thus it changes only across S_*, i.e.

$$\alpha^*_{1L} = \alpha_{1L},$$
$$\alpha^*_{1R} = \alpha_{1R}.$$

By using (4.5e) with the SG-EOS (3.2a), the phasic pressure is given as

$$p^*_k = (p_k + \pi_k)\frac{(\gamma_k - 1)\rho_k - (\gamma_k + 1)\rho^*_k}{(\gamma_k - 1)\rho^*_k - (\gamma_k + 1)\rho_k} - \pi_k.$$

All other variables now are determined from the known ones. That are:

$$\rho^*_L = \sum_k (\alpha_k\rho_k)^*_L,$$

$$\rho^*_R = \sum_k (\alpha_k\rho_k)^*_R,$$

$$\rho^*_{kL} = \rho_{kL}\frac{S_L - u_L}{S_L - S_*},$$

$$\rho^*_{kR} = \rho_{kR}\frac{S_R - u_R}{S_R - S_*}.$$

The phasic internal energy is determined by using the SG-EOS (3.2a), i.e.

$$e^*_{kL} = e^*_{kL}(p^*_{kL}, \rho^*_{kL}),$$
$$e^*_{kR} = e^*_{kR}(p^*_{kR}, \rho^*_{kR}).$$

4.4.4 Pressure relaxation

For the instantaneous pressure relaxation of the system (4.1) we have to solve the following system of differential equations

$$\frac{\partial \alpha_1}{\partial t} = \mu(p_1 - p_2),$$

$$\frac{\partial \alpha_1 \rho_1}{\partial t} = 0,$$

$$\frac{\partial \alpha_2 \rho_2}{\partial t} = 0,$$

$$\frac{\partial \rho u}{\partial t} = 0,$$

$$\frac{\partial \alpha_1 \rho_1 e_1}{\partial t} = \mu p_I(p_2 - p_1),$$

$$\frac{\partial \alpha_2 \rho_2 e_2}{\partial t} = -\mu p_I(p_2 - p_1),$$

$$\frac{\partial (\rho e + \frac{1}{2}\rho u^2)}{\partial t} = 0,$$

with $\mu \to \infty$.

Using the volume fraction equation with mass equations we can reformulate the internal energy equations as

$$\frac{\partial e_k}{\partial t} + p_I \frac{\partial v_k}{\partial t} = 0, \qquad k = 1, 2.$$

Integrating these equations, we obtain the following approximations

$$e_k^\star(p^\star, v_k^\star) - e_k^0(p_k^0, v_k^0) + \bar{p}_I(v_k^\star - v_k^0) = 0, \qquad k = 1, 2, \tag{4.8}$$

where '0' and '$\star$' refer to the states before and after relaxation process respectively. The average of the interface pressure can be approximated as $\bar{p}_I = p_I^0$ or $\bar{p}_I = p^\star$, where $p^\star$ is the relaxed pressure. This approximation has no significant effects on the computations, see also [127].

Equations (4.8) form a system of two equations with three unknowns; $p^\star$, $v_1^\star$, and $v_2^\star$. A closure relation is given by the saturation constraint

$$\sum_k \alpha_k^\star = 1,$$

or

$$\sum_k (\alpha\rho)_k^\star v_k^\star = 1. \tag{4.9}$$

But

$$(\alpha\rho)_k^\star = (\alpha\rho)_k^0.$$

Thus (4.9) is rewritten as

$$\sum_k (\alpha\rho)_k^0 v_k^\star = 1 \tag{4.10}$$

Using the SG-EOS (3.2a) with (4.8), the specific volume can be written as

$$v_k^\star(p^\star) = v_k^0 \frac{p_k^0 + \gamma_k\pi_k + (\gamma_k - 1)\bar{p}_I}{p^\star + \gamma_k\pi_k + (\gamma_k - 1)\bar{p}_I}. \tag{4.11}$$

Substituting (4.11) in (4.10), we obtain a single equation with a single unknown $p^\star$

$$\sum_k (\alpha\rho)_k^0 v_k^\star(p^\star) = 1.$$

This equation is solved by Newton iteration technique to obtain the relaxed pressure. Then the volume fraction and the specific volumes can be determined.

Remark 4.1. The pressure relaxation procedure for the seven-equation model that was explained in Subsection 3.3.4 can easily be used for the six-equation model. But the current procedure is easier for implementation and can be directly extended to multiphase flows. However, we see that there is no significant difference between the results of the two procedures in our computations.

4.4.5 Correction criterion

To make the relaxed pressure in agreement with the mixture EOS a correction criterion of [127] is used. From the SG-EOS (3.2a) for each phase with the pressure equilibrium we obtain the following expression for the mixture EOS, see [126, 127]

$$p(\rho_1, \rho_2, e, \alpha_1) = \frac{\rho e - \alpha_1\rho_1 q_1 - \alpha_2\rho_2 q_2 - \left(\dfrac{\alpha_1\gamma_1\pi_1}{\gamma_1 - 1} + \dfrac{\alpha_2\gamma_2\pi_2}{\gamma_2 - 1}\right)}{\dfrac{\alpha_1}{\gamma_1 - 1} + \dfrac{\alpha_2}{\gamma_2 - 1}}. \tag{4.12}$$

The mixture pressure (4.12) is obtained from the evolution of the mixture total energy (4.4). This is expected to be accurate in the entire field flow since the equation (4.4) is written in the conservative formulation.

By using evolution of the mixture total energy (4.4) we can find the value of ρe. Using this value in (4.12) we can find the value of the mixture pressure. Other variables in the relation (4.12) are estimated by the relaxation step. In this way we determine the value of the mixture pressure that agrees with the mixture EOS, then we use this value with the SG-EOS for each phase to reset the values of the internal energies.

4.5 Modeling of the heat and mass transfer directly

To take into account the heat and mass transfer we have to solve the following system of ODE at each time step after the pressure relaxation step

$$\frac{d\mathbf{U}}{dt} = \mathbf{S}_Q + \mathbf{S}_m. \tag{4.13}$$

The system (4.13) is solved by considering each one of the source vectors alone. First it is solved with the temperature relaxation terms, then with the Gibbs free energy relaxation terms.

According to our assumptions during the temperature relaxation the pressures will stay in equilibrium, i.e. the condition (3.29) holds. And during the Gibbs free energy relaxation the pressures and the temperatures will stay in equilibrium, i.e. the conditions (3.43) hold.

The heat source vector is modeled as

$$\mathbf{S}_Q = \left(\frac{Q}{\kappa}, 0, 0, 0, Q, -Q, 0\right)^T,$$

where $Q = \theta(T_2 - T_1)$. Note that the last element of $\mathbf{S}_Q$ corresponds to the redundant equation (4.4).

It is clear that the value of κ (3.36) for the seven-equation model works also for the six-equation model and satisfies the condition (3.29). Also it is easy to see that the same method of temperature relaxation for the seven-equation model, which is introduced in Subsection 3.5.3, can be used for the six-equation model. In addition, it is straightforward to check that with these new additions for the heat transfer the model satisfies the second law of thermodynamics. This is shown in the context of the seven-equation model in Subsection 3.5.2.

The vector $\mathbf{S}_m$ is modeled as

$$\mathbf{S}_m = \left(\frac{\dot{m}}{\varrho}, \dot{m}, -\dot{m}, 0, e_i\dot{m}, -e_i\dot{m}, 0\right)^T,$$

where $\dot{m} = \nu(g_2 - g_1)$.

The values of ϱ and e_i that satisfy the conditions (3.43) are given in (3.54). Also the Gibbs free energy relaxation procedures for the seven-equation model, that are introduced in Subsections 3.6.3 and 3.6.4, can be used directly here. Moreover, it is easy to check that the model with new modifications for the mass transfer satisfies the second laws of thermodynamics.

Thus the final six-equation model with heat and mass transfer is written as

$$\frac{\partial \alpha_1}{\partial t} + u\frac{\partial \alpha_1}{\partial x} = \mu(p_1 - p_2) + \frac{1}{\kappa}Q + \frac{1}{\varrho}\dot{m}, \tag{4.14a}$$

$$\frac{\partial \alpha_1\rho_1}{\partial t} + \frac{\partial(\alpha_1\rho_1 u)}{\partial x} = \dot{m}, \tag{4.14b}$$

$$\frac{\partial \alpha_2\rho_2}{\partial t} + \frac{\partial(\alpha_2\rho_2 u)}{\partial x} = -\dot{m}, \tag{4.14c}$$

$$\frac{\partial \rho u}{\partial t} + \frac{\partial(\rho u^2 + \alpha_1 p_1 + \alpha_2 p_2)}{\partial x} = 0, \tag{4.14d}$$

$$\frac{\partial \alpha_1\rho_1 e_1}{\partial t} + \frac{\partial \alpha_1\rho_1 e_1 u}{\partial x} + \alpha_1 p_1\frac{\partial u}{\partial x} = \mu p_I(p_2 - p_1) + Q + e_i\dot{m}, \tag{4.14e}$$

$$\frac{\partial \alpha_2\rho_2 e_2}{\partial t} + \frac{\partial \alpha_2\rho_2 e_2 u}{\partial x} + \alpha_2 p_2\frac{\partial u}{\partial x} = -\mu p_I(p_2 - p_1) - Q - e_i\dot{m}, \tag{4.14f}$$

where

$$Q = \theta(T_2 - T_1),$$
$$\dot{m} = \nu(g_2 - g_1).$$

The variables κ, ϱ and e_i are given in (3.36), (3.54a) and (3.54b) respectively. All relaxation parameters μ, θ and ν are assumed to be infinite. The relaxation procedures are performed in the following order: first pressure relaxation then temperature relaxation and at last Gibbs free energy relaxation.

4.6 Derivation of the six-equation model from the seven-equation model

This section is devoted to the derivation of the six-equation model with heat and mass transfer from the full seven-equation model with heat and mass transfer (3.69) by the asymptotic limit considering stiff velocity relaxation. We follow the reduction method of Chen et al. [22]. This method was used by Murrone and Guillard [96] in the derivation of the five-equation model from the seven-equation model.

Firstly, we introduce briefly the method of reduction for a system of hyperbolic conservation laws in the presence of stiff relaxation terms using the notations of Murrone and Guillard [96] .

Consider a hyperbolic system with stiff source relaxation terms, i.e. consider the following system

$$\frac{\partial \mathbf{W}}{\partial t} + \mathbf{A}(\mathbf{W})\frac{\partial \mathbf{W}}{\partial x} = \frac{\mathbf{R}(\mathbf{W})}{\epsilon} + \mathbf{S}(\mathbf{W}) \tag{4.15}$$

with $\epsilon \to 0^+$. The vector $\mathbf{W}$ belongs to Ω, some open subset of $\mathbb{R}^N$.

As $\epsilon \to 0^+$, the solution of the system (4.15) is expected to be close to the set $\Im \subset \mathbb{R}^N$, where

$$\Im = \{\mathbf{W} \in \mathbb{R}^N; \mathbf{R}(\mathbf{W}) = \mathbf{0}\}.$$

We make use of the following assumption, Murrone and Guillard [96]:

Assumption 4.1. *The set of equations $\boldsymbol{R}(\boldsymbol{W}) = 0$ defines a smooth manifold of dimension n, where $0 < n < N$. Moreover, for any $\boldsymbol{W} \in \Im$ we explicitly know the parameterization M from ω an open subset of $\mathbb{R}^n$ onto V a neighborhood of $\boldsymbol{W}$ in $\Im$, i.e.*

$$\begin{aligned} M : \omega \subset \mathbb{R}^n &\to V \subset \Im \subset \mathbb{R}^N, \\ \boldsymbol{w} &\to \boldsymbol{W} = M(\boldsymbol{w}). \end{aligned}$$

Under Assumption 4.1 the following hold

- For any $\mathbf{w} \in \omega$ the Jacobian matrix $dM_{\mathbf{w}}$ is a full rank matrix.
- The column vectors of $dM_{\mathbf{w}}$ form a basis of $\ker(\mathbf{R}'(M(\mathbf{w})))$.

For the proof see [96].

Let

$$\mathbf{C} = [dM^1_{\mathbf{w}}, ..., dM^n_{\mathbf{w}}, I^1, ..., I^{N-n}], \tag{4.16}$$

where $dM^1_{\mathbf{w}}, ..., dM^n_{\mathbf{w}}$ are the column vectors of $dM_{\mathbf{w}}$ and $I^1, ..., I^{N-n}$ are a basis of the range $\mathrm{rng}(\mathbf{R}'(M(\mathbf{w})))$ of $\mathbf{R}'(M(\mathbf{w}))$. The matrix (4.16) is invertible, let $\mathbf{B}$ be the matrix composed of the first n rows of the inverse of the matrix $\mathbf{C}$. Then we have the following results:

$$\mathbf{B} \cdot dM_{\mathbf{w}} = \mathbf{I}_{n\times n}, \text{ the identity matrix} \tag{4.17a}$$

$$\mathbf{B} \cdot \mathbf{R}'(M(\mathbf{w})) = 0. \tag{4.17b}$$

For proof see the same reference [96].

Decompose the state vector $\mathbf{W}$ as

$$\mathbf{W} = M(\mathbf{w}) + \epsilon \mathbf{V}, \tag{4.18}$$

where $\mathbf{V}$ is a small perturbation around the state vector $M(\mathbf{w})$.

To obtain the reduced model we use the expression (4.18) in the system (4.15) and get

$$\frac{\partial M(\mathbf{w})}{\partial t} + \mathbf{A}(M(\mathbf{w}))\frac{\partial M(\mathbf{w})}{\partial x} - \mathbf{R}'(M(\mathbf{w})) \cdot \mathbf{V} = \mathbf{S}(M(\mathbf{w})) + O(\epsilon). \tag{4.19}$$

Multiplying (4.19) by $\mathbf{B}$, using (4.17) and neglecting the terms of order ϵ, we obtain the reduced model of the system (4.15)

$$\frac{\partial \mathbf{w}}{\partial t} + \mathbf{B} \cdot \mathbf{A}(M(\mathbf{w})) \cdot dM_{\mathbf{w}} \frac{\partial \mathbf{w}}{\partial x} = \mathbf{B} \cdot \mathbf{S}(M(\mathbf{w})). \tag{4.20}$$

Now, we apply the above method for the reduction by using the asymptotic limit on the seven-equation model assuming a stiff velocity relaxation.

Take the vector of primitive variables as

$$\mathbf{W} = (\alpha_1, \rho_1, \rho_2, u_1, u_2, p_1, p_2)^T.$$

Write the seven-equation model (3.69) accompanied with all relaxation terms in the form (4.15). In this case, the source vector $\dfrac{\mathbf{R}(\mathbf{W})}{\epsilon}$ consists of the velocity relaxation terms which is stiff, i.e. $\lambda = \dfrac{1}{\epsilon}$, where $\epsilon \to 0^+$. While the source vector $\mathbf{S(W)}$ is decomposed as

$$\mathbf{S}(\mathbf{W}) = \mathbf{S}_P(\mathbf{W}) + \mathbf{S}_Q(\mathbf{W}) + \mathbf{S}_m(\mathbf{W}).$$

The matrix $\mathbf{A}(\mathbf{W})$ and the source vectors can be given as

$$\mathbf{A}(\mathbf{W}) = \begin{bmatrix} u_I & 0 & 0 & 0 & 0 & 0 & 0 \\ -\dfrac{\rho_1}{\alpha_1}(u_I - u_1) & u_1 & 0 & \rho_1 & 0 & 0 & 0 \\ \dfrac{\rho_2}{\alpha_2}(u_I - u_2) & 0 & u_2 & 0 & \rho_2 & 0 & 0 \\ -\dfrac{p_I - p_1}{\alpha_1\rho_1} & 0 & 0 & u_1 & 0 & \dfrac{1}{\rho_1} & 0 \\ \dfrac{p_I - p_2}{\alpha_2\rho_2} & 0 & 0 & 0 & u_2 & 0 & \dfrac{1}{\rho_2} \\ -\dfrac{\Gamma_1}{\alpha_1}\left[p_I - \rho_1^2\left(\dfrac{\partial e_1}{\partial \rho_1}\right)_{p_1}\right](u_I - u_1) & 0 & 0 & \rho_1 c_1^2 & 0 & u_1 & 0 \\ \dfrac{\Gamma_2}{\alpha_2}\left[p_I - \rho_2^2\left(\dfrac{\partial e_2}{\partial \rho_2}\right)_{p_2}\right](u_I - u_2) & 0 & 0 & 0 & \rho_2 c_2^2 & 0 & u_2 \end{bmatrix},$$

$$\frac{\mathbf{R}(\mathbf{W})}{\epsilon} = \begin{bmatrix} 0 \\ 0 \\ 0 \\ \dfrac{\lambda}{\alpha_1\rho_1}(u_2 - u_1) \\ -\dfrac{\lambda}{\alpha_2\rho_2}(u_2 - u_1) \\ \lambda\dfrac{\Gamma_1}{\alpha_1}(u_I - u_1)(u_2 - u_1) \\ -\lambda\dfrac{\Gamma_2}{\alpha_2}(u_I - u_2)(u_2 - u_1) \end{bmatrix},$$

$$\mathbf{S}_P(\mathbf{W}) = \begin{bmatrix} \mu(p_1 - p_2) \\ \mu\dfrac{\rho_1}{\alpha_1}(p_2 - p_1) \\ -\mu\dfrac{\rho_2}{\alpha_2}(p_2 - p_1) \\ 0 \\ 0 \\ \mu\dfrac{\Gamma_1}{\alpha_1}\left[p_I - \rho_1^2\left(\dfrac{\partial e_1}{\partial \rho_1}\right)_{p_1}\right](p_2 - p_1) \\ -\mu\dfrac{\Gamma_2}{\alpha_2}\left[p_I - \rho_2^2\left(\dfrac{\partial e_2}{\partial \rho_2}\right)_{p_2}\right](p_2 - p_1) \end{bmatrix}, \qquad \mathbf{S}_Q(\mathbf{W}) = \begin{bmatrix} \dfrac{1}{\kappa}Q \\ -\dfrac{\rho_1}{\alpha_1\kappa}Q \\ \dfrac{\rho_2}{\alpha_2\kappa}Q \\ 0 \\ 0 \\ -\dfrac{\rho_1 c_1^2}{\alpha_1\kappa}Q + \dfrac{\Gamma_1}{\alpha_1}(1 + \dfrac{p_1}{\kappa})Q \\ \dfrac{\rho_2 c_2^2}{\alpha_2\kappa}Q - \dfrac{\Gamma_2}{\alpha_2}(1 + \dfrac{p_2}{\kappa})Q \end{bmatrix},$$

$$\mathbf{S}_m(\mathbf{W}) = \begin{bmatrix} \dfrac{1}{\varrho}\dot{m} \\ \dfrac{1}{\alpha_1}(1 - \dfrac{\rho_1}{\varrho})\dot{m} \\ -\dfrac{1}{\alpha_2}(1 - \dfrac{\rho_2}{\varrho})\dot{m} \\ \dfrac{1}{\alpha_1\rho_1}(u_I - u_1)\dot{m} \\ -\dfrac{1}{\alpha_2\rho_2}(u_I - u_2)\dot{m} \\ \dfrac{c_1^2}{\alpha_1}(1 - \dfrac{\rho_1}{\varrho})\dot{m} + \dfrac{\Gamma_1}{\alpha_1}\left[(e_i - e_1) + \dfrac{(u_I - u_1)^2}{2} - \dfrac{p_1}{\rho_1}(1 - \dfrac{\rho_1}{\varrho})\right]\dot{m} \\ -\dfrac{c_2^2}{\alpha_2}(1 - \dfrac{\rho_2}{\varrho})\dot{m} - \dfrac{\Gamma_2}{\alpha_2}\left[(e_i - e_2) + \dfrac{(u_I - u_2)^2}{2} - \dfrac{p_2}{\rho_2}(1 - \dfrac{\rho_2}{\varrho})\right]\dot{m} \end{bmatrix},$$

where the Grüneisen coefficient Γ_k is given in (3.37).

The limit of zero velocity relaxation time gives a single velocity, i.e. $u_1 = u_2 = u$. Thus the vector of the primitive variables for the reduced model is

$$\mathbf{w} = (\alpha_1, \rho_1, \rho_2, u, p_1, p_2)^T.$$

So $M(\mathbf{w})$ is defined as

$$M : \mathbf{w} \rightarrow M(\mathbf{w}) = (\alpha_1, \rho_1, \rho_2, u, u, p_1, p_2)^T. \tag{4.21}$$

Then the Jacobian matrix of the transformation (4.21) is given as

$$dM_{\mathbf{w}} = \begin{bmatrix} 1 & 0 & 0 & 0 & 0 & 0 \\ 0 & 1 & 0 & 0 & 0 & 0 \\ 0 & 0 & 1 & 0 & 0 & 0 \\ 0 & 0 & 0 & 1 & 0 & 0 \\ 0 & 0 & 0 & 1 & 0 & 0 \\ 0 & 0 & 0 & 0 & 1 & 0 \\ 0 & 0 & 0 & 0 & 0 & 1 \end{bmatrix}. \tag{4.22}$$

It is easy to see that the Jacobian matrix $\mathbf{R}'$ evaluated on the transformation is given as

$$\mathbf{R}'(M(\mathbf{w})) = \begin{bmatrix} 0 & 0 & 0 & 0 & 0 & 0 & 0 \\ 0 & 0 & 0 & 0 & 0 & 0 & 0 \\ 0 & 0 & 0 & 0 & 0 & 0 & 0 \\ 0 & 0 & 0 & -\dfrac{1}{\alpha_1\rho_1} & \dfrac{1}{\alpha_1\rho_1} & 0 & 0 \\ 0 & 0 & 0 & \dfrac{1}{\alpha_2\rho_2} & -\dfrac{1}{\alpha_2\rho_2} & 0 & 0 \\ 0 & 0 & 0 & 0 & 0 & 0 & 0 \\ 0 & 0 & 0 & 0 & 0 & 0 & 0 \end{bmatrix}.$$

Obviously, the basis of $\mathrm{rng}(\mathbf{R}'(M(\mathbf{w})))$ is

$$I^1 = \begin{bmatrix} 0 \\ 0 \\ 0 \\ -\dfrac{1}{\alpha_1\rho_1} \\ \dfrac{1}{\alpha_2\rho_2} \\ 0 \\ 0 \end{bmatrix}. \tag{4.23}$$

From (4.22) and (4.23) we can find the matrix $\mathbf{C}$, then we can find the matrix $\mathbf{B}$

$$\mathbf{B} = \begin{bmatrix} 1 & 0 & 0 & 0 & 0 & 0 & 0 \\ 0 & 1 & 0 & 0 & 0 & 0 & 0 \\ 0 & 0 & 1 & 0 & 0 & 0 & 0 \\ 0 & 0 & 0 & \frac{\alpha_1\rho_1}{\rho} & \frac{\alpha_2\rho_2}{\rho} & 0 & 0 \\ 0 & 0 & 0 & 0 & 0 & 1 & 0 \\ 0 & 0 & 0 & 0 & 0 & 0 & 1 \end{bmatrix}.$$

where $\rho = \alpha_1\rho_1 + \alpha_2\rho_2$.

By using the matrix $\mathbf{B}$ together with the above matrices we can find the reduced model as in (4.20). Thus the reduced model in primitive variables is given as

$$\frac{\partial \alpha_1}{\partial t} + u\frac{\partial \alpha_1}{\partial x} = \mu(p_1 - p_2) + \frac{1}{\kappa}Q + \frac{1}{\varrho}\dot{m}, \tag{4.24a}$$

$$\frac{\partial \rho_1}{\partial t} + u\frac{\partial \rho_1}{\partial x} + \rho_1\frac{\partial u}{\partial x} = \mu\frac{\rho_1}{\alpha_1}(p_2 - p_1) - \frac{\rho_1}{\alpha_1\kappa}Q + \frac{1}{\alpha_1}(1 - \frac{\rho_1}{\varrho})\dot{m}, \tag{4.24b}$$

$$\frac{\partial \rho_2}{\partial t} + u\frac{\partial \rho_2}{\partial x} + \rho_2\frac{\partial u}{\partial x} = -\mu\frac{\rho_2}{\alpha_2}(p_2 - p_1) + \frac{\rho_2}{\alpha_2\kappa}Q - \frac{1}{\alpha_2}(1 - \frac{\rho_2}{\varrho})\dot{m}, \tag{4.24c}$$

$$\frac{\partial u}{\partial t} + u\frac{\partial u}{\partial x} + \frac{(p_1 - p_2)}{\rho}\frac{\partial \alpha_1}{\partial x} + \frac{\alpha_1}{\rho}\frac{\partial p_1}{\partial x} + \frac{\alpha_2}{\rho}\frac{\partial p_2}{\partial x} = 0, \tag{4.24d}$$

$$\begin{aligned}\frac{\partial p_1}{\partial t} + u\frac{\partial p_1}{\partial x} + \rho_1 c_1^2\frac{\partial u}{\partial x} &= \mu\frac{\Gamma_1}{\alpha_1}\left[p_I - \rho_1^2\left(\frac{\partial e_1}{\partial \rho_1}\right)_{p_1}\right](p_2 - p_1) - \frac{\rho_1 c_1^2}{\alpha_1\kappa}Q \\ &+ \frac{\Gamma_1}{\alpha_1}(1 + \frac{p_1}{\kappa})Q + \frac{c_1^2}{\alpha_1}(1 - \frac{\rho_1}{\varrho})\dot{m} + \frac{\Gamma_1}{\alpha_1}\left[(e_i - e_1) - \frac{p_1}{\rho_1}(1 - \frac{\rho_1}{\varrho})\right]\dot{m},\end{aligned} \tag{4.24e}$$

$$\begin{aligned}\frac{\partial p_2}{\partial t} + u\frac{\partial p_2}{\partial x} + \rho_2 c_2^2\frac{\partial u}{\partial x} &= -\mu\frac{\Gamma_2}{\alpha_2}\left[p_I - \rho_2^2\left(\frac{\partial e_2}{\partial \rho_2}\right)_{p_2}\right](p_2 - p_1) + \frac{\rho_2 c_2^2}{\alpha_2\kappa}Q \\ &- \frac{\Gamma_2}{\alpha_2}(1 + \frac{p_2}{\kappa})Q - \frac{c_2^2}{\alpha_2}(1 - \frac{\rho_2}{\varrho})\dot{m} - \frac{\Gamma_2}{\alpha_2}\left[(e_i - e_2) - \frac{p_2}{\rho_2}(1 - \frac{\rho_2}{\varrho})\right]\dot{m},\end{aligned} \tag{4.24f}$$

Now we proceed to write this model in terms of conservative variables,

$$\mathbf{U} = (\alpha_1, \alpha_1\rho_1, \alpha_2\rho_2, \rho u, \alpha_1\rho_1 e_1, \alpha_2\rho_2 e_2)^T.$$

Using equations (4.24b) and (4.24c) with (4.24a), we obtain

$$\frac{\partial \alpha_1\rho_1}{\partial t} + \frac{\partial(\alpha_1\rho_1 u)}{\partial x} = \dot{m},$$
$$\frac{\partial \alpha_2\rho_2}{\partial t} + \frac{\partial(\alpha_2\rho_2 u)}{\partial x} = -\dot{m}.$$

Using these equations with (4.24d), we get

$$\frac{\partial \rho u}{\partial t} + \frac{\partial(\rho u^2 + \alpha_1 p_1 + \alpha_2 p_2)}{\partial x} = 0.$$

The internal energy of each phase can be written as a function of the phase density and pressure, i.e.

$$e_k = e_k(\rho_k, p_k), \quad k = 1, 2.$$

Then we obtain the following expression for the differential de_k

$$de_k = \left(\frac{\partial e_k}{\partial \rho_k}\right)_{p_k} d\rho_k + \left(\frac{\partial e_k}{\partial p_k}\right)_{\rho_k} dp_k.$$

With the help of this equation and with the equations of the system (4.24), we obtain the following equations for the internal energies

$$\frac{\partial \alpha_1\rho_1 e_1}{\partial t} + \frac{\partial \alpha_1\rho_1 e_1 u}{\partial x} + \alpha_1 p_1 \frac{\partial u}{\partial x} = \mu p_I(p_2 - p_1) + Q + e_i\dot{m},$$
$$\frac{\partial \alpha_2\rho_2 e_2}{\partial t} + \frac{\partial \alpha_2\rho_2 e_2 u}{\partial x} + \alpha_2 p_2 \frac{\partial u}{\partial x} = -\mu p_I(p_2 - p_1) - Q - e_i\dot{m}.$$

Thus the whole model can be written as in (4.14).

4.7 Numerical results

In this section we again reconsider the tests for metastable liquids of Saurel et al. [126]. These tests were used in Subsections 3.8.1 and 3.8.3 for the seven-equation model. The main focus now is devoted to the comparisons between the results of the six-equation and the seven-equation models.

The comparisons are made by using the same CFL number, the same number of cells, the same type of Riemann solver and the same Gibbs free energy relaxation procedure.

For all computations we give the following: the number of cells, the number of time steps, and the CPU time. These discretization and computation parameters are shown below each figure for both models for the sake of comparisons.

4.7.1 Two-phase shock tube

Consider again the same test problem as in Subsection 3.8.1 for the dodecane shock tube. We use CFL number of 0.6 with the first Gibbs free energy relaxation procedure, see the discussion in Subsection 3.8.1.

A comparison between the results of the six-equation model and the seven-equation model is shown in Figures 4.1 - 4.4. It is clear that for both cases, with or without the phase transition, the results almost coincide. Just a very small difference appears at the left rarefaction in the curves of the pressure. Such a small difference has no significant numerical meaning. This small difference appears in both cases i.e. with or without the phase transition in the same manner, see the pressure profiles on logarithmic scales, Figures 4.1 and 4.3, the pressure profile of the results with phase transition is drawn separately to be able to see the differences. Thus this small difference is not related to the treatment of the phase transition. In addition, this difference still appears under grid refinement, see Figure 4.2 where 10000 cells were used in the computations.

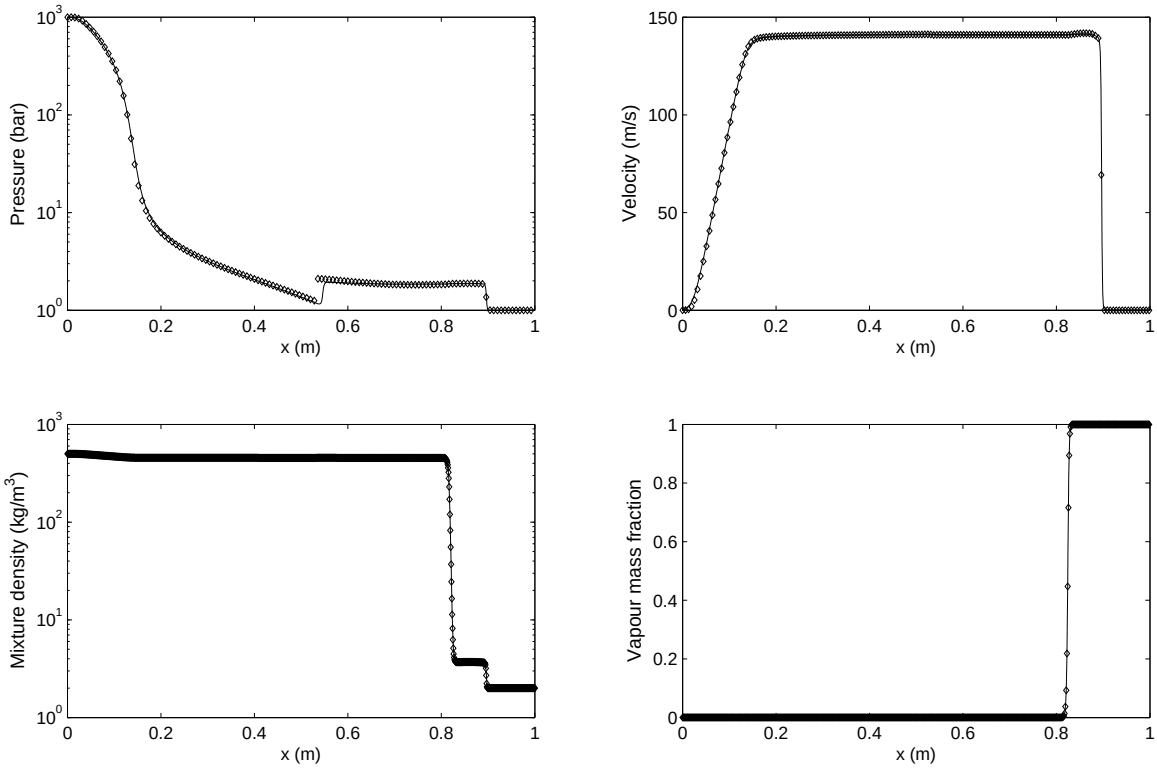

Figure 4.1: Dodecane liquid-vapor shock tube without phase transition, a comparison between the results of the seven-equation model (lines) and the six-equation model results (symbols). The computations used 1250 cells. For the seven-equation model results: The CPU time is 100.65 seconds with 7197 time steps. For the six-equation model results: The CPU time is 14.46 seconds with 1557 time steps.

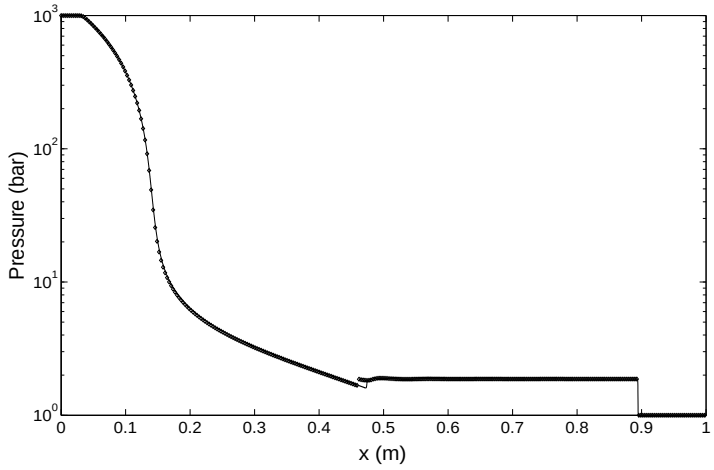

Figure 4.2: Dodecane liquid-vapor shock tube without phase transition. The pressure profile over (10000) cells, by the seven-equation model (lines) and the six-equation model (symbols). For the seven-equation model: The CPU time is 8145.17 seconds taking 56749 time steps. For the six-equation model: The CPU time is 1035.01 seconds with 12452 time steps.

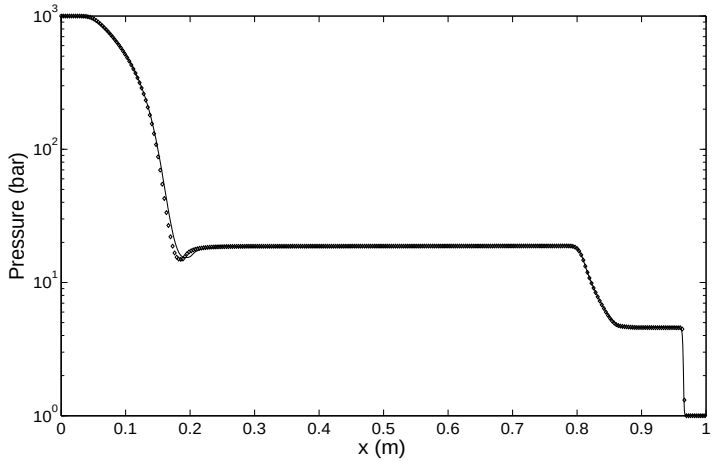

Figure 4.3: Dodecane liquid-vapor shock tube with phase transition. The pressure profile, a comparison between the results of the seven-equation model (lines) and the six-equation model results (symbols). The computations were done with 1250 cells. For the seven-equation model: The CPU time is 151.98 seconds with 8828 time steps. For the six-equation model: The CPU time is 19.87 seconds with 1556 time steps.

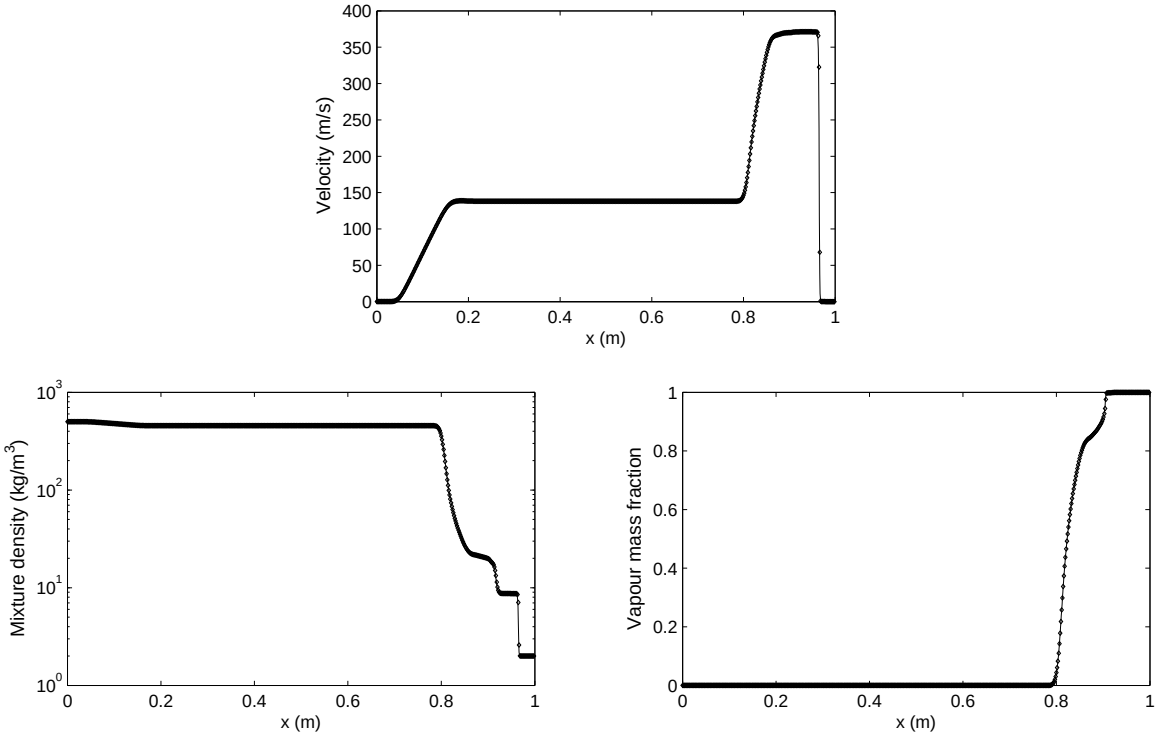

Figure 4.4: Dodecane liquid-vapor shock tube with phase transition, a comparison between the results of the seven-equation model (lines) and the six-equation model results (symbols). The computations used 1250 cells. For the seven-equation model: The CPU time is 151.98 seconds with 8828 time steps. For the six-equation model: The CPU time is 19.87 seconds with 1556 time steps.

As discussed in Subsection 3.8.1, at the right end of the left rarefaction in the pressure profiles, there is a small distortion. This distortion appears also here in the results of the six-equation model either with or without the phase transition, see Figures 4.1 - 4.3. Besides the previous discussion in Subsection 3.8.1, this feature may comes from the pressure relaxation procedure, since it appears in both the six-equation and the seven-equation models but not in the results of five-equation model as in Saurel et al. [126]. However, this still an open issue.

# of Figure	4.1	4.2	4.3 & 4.4
The ratio	0.144	0.127	0.131

Table 4.1: The ratio of the CPU time for the six-equation model to the seven-equation model.

In result, for this example, we see that there is no significant difference between the results using both models. But there is a significant difference in the required CPU time. The required time for the six-equation model is much smaller ($\approx 13\%$) than that required for the seven-equation model, see Table 4.1.

4.7.2 Two-phase expansion tube

Consider again the water liquid-vapor expansion tube that is given in Subsection 3.8.3. The CFL number is taken 0.03 with the second Gibbs free energy relaxation procedure, see the discussion in Subsection 3.8.3.

In Figure 4.5, we see the solution of this problem without phase transition at $t = 3.2$ ms. The results are obtained by the six-equation model and are compared with those of the seven-equation model, they are completely coinciding. Figure 4.6 presents a comparison between the results of the two models when the phase transition is involved, the curves are completely coinciding.

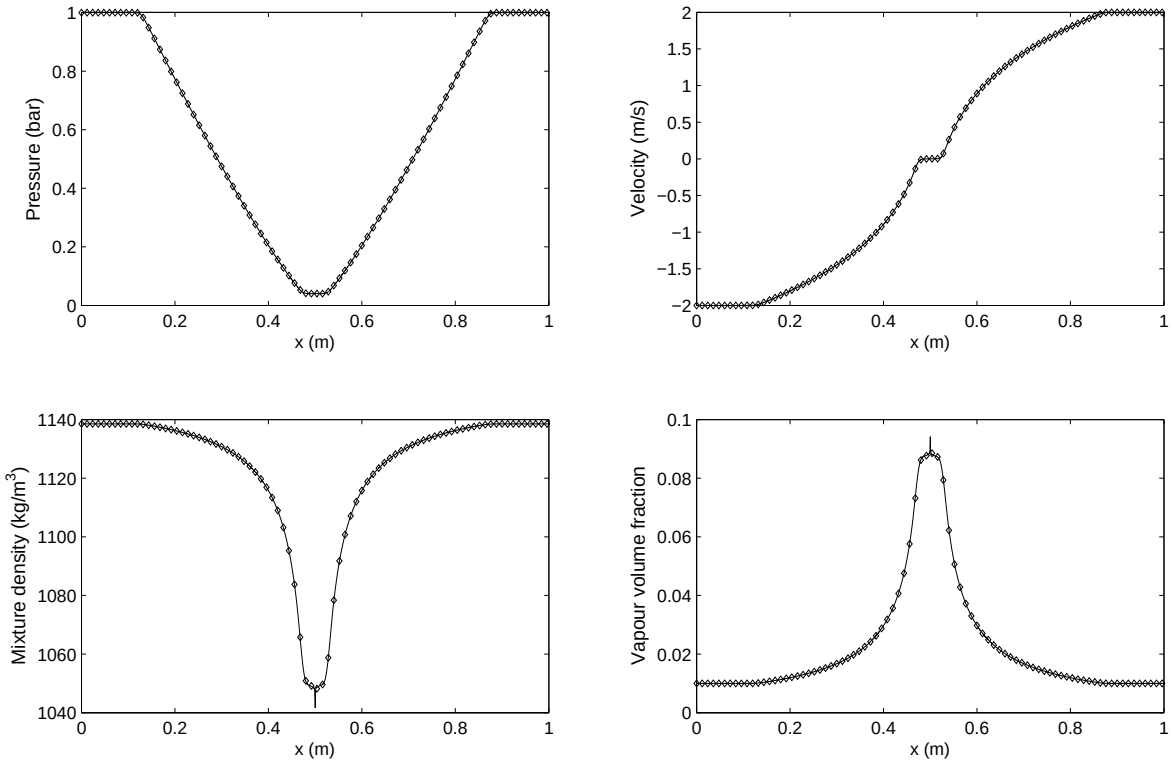

Figure 4.5: Water liquid-vapor expansion tube without phase transition, by using the seven-equation model (lines) and six-equation model (symbols). The computations were done with 5000 cells. For the seven-equation model: The CPU time is 14.772 hours with 763,550 time steps. For the six-equation model: The CPU time is 7.305 hours with 763,726 time steps.

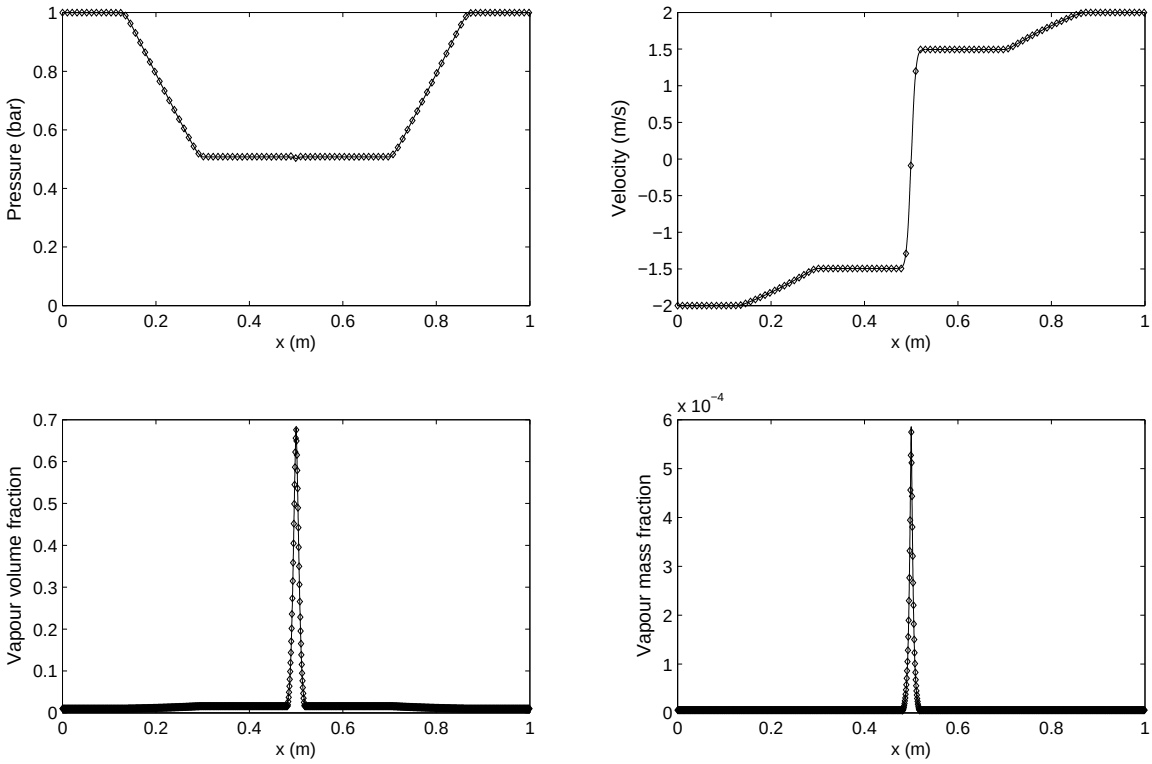

Figure 4.6: Water liquid-vapor expansion tube with phase transition at $t = 3.2$ ms. A comparison between the results of the seven-equation model (lines) and the six-equation model (symbols). The computations used 5000 cells. For the seven-equation model: The CPU time is 18.838 hours with 763,550 time steps. For the six-equation model: The CPU time is 9.447 hours with 764,150 time steps.

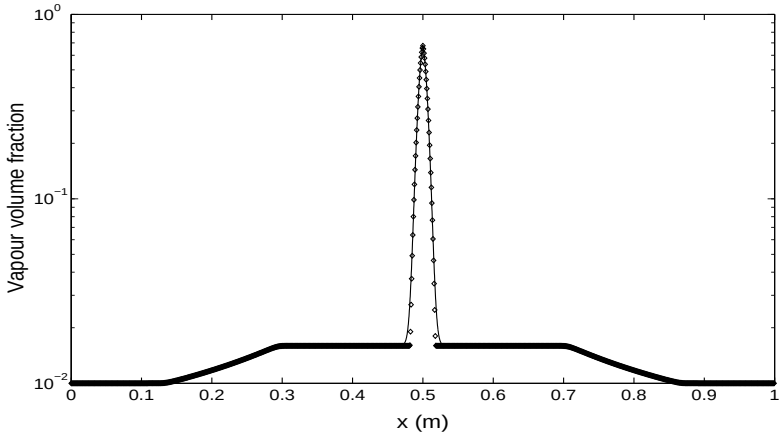

Figure 4.7: Water liquid-vapor expansion tube with phase transition at $t = 3.2$ ms, the vapor volume fraction profile on a logarithmic scale. By using the seven-equation model (lines) and six-equation model (symbols).

The vapor volume fraction profile is shown on a logarithmic scale, Figure 4.7 to highlight the four expansion waves of the solution and for the sake of comparsion, see Subsection 3.8.3.

In addition, if we consider the solution at later time, when $t = 59$ ms as in Figure 4.8, the results of the seven-equation and the six-equation models are also completely coinciding.

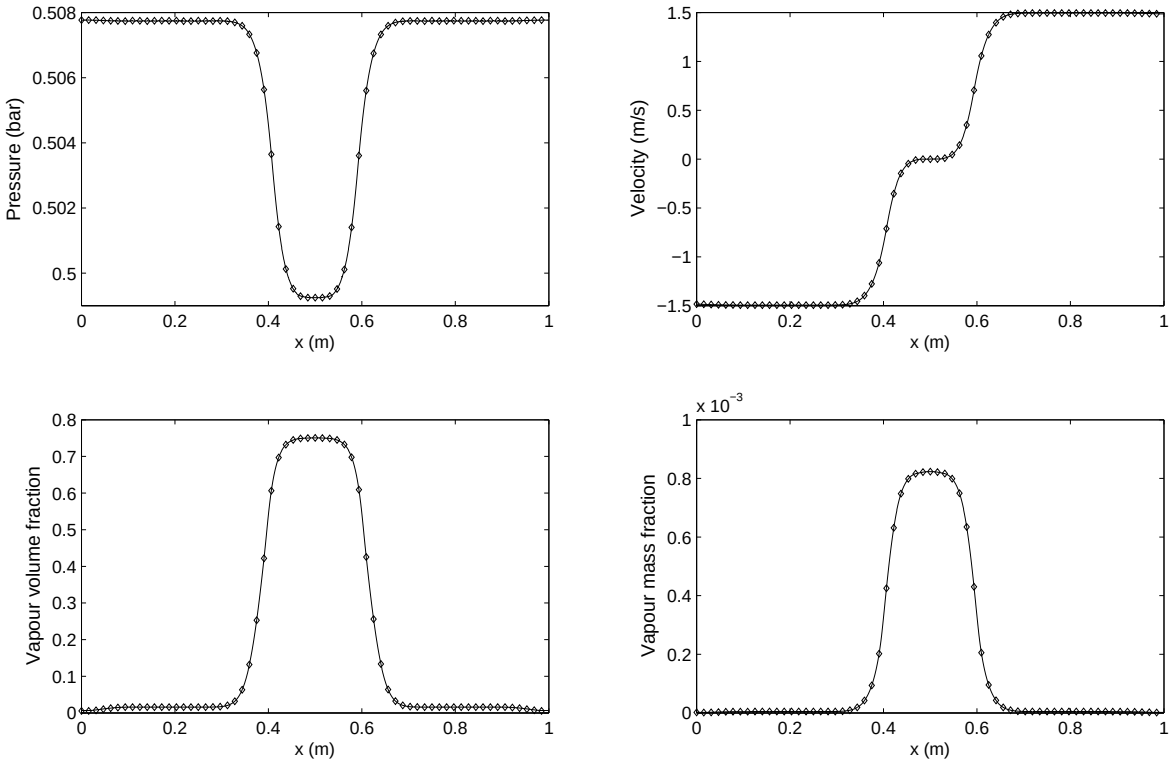

Figure 4.8: Water liquid-vapor expansion tube with phase transition at time $t = 59$ ms, by using the seven-equation model (lines) and six-equation model (symbols). The two slow evaporation waves are visible. The computations were done with 3200 cells. For the seven-equation model: The CPU time is 116.078 hours with 8,217,444 time steps. For the six-equation model: The CPU time is 99.406 hours with 8,217,444 time steps.

4.7.3 Two-phase expansion tube with strong rarefaction effects

Again consider the previous example, which is given in Subsection 3.8.3. The same initial state is used here except the initial velocity will be increased, which means an increase in the rarefaction effects.

Figure 4.9 shows the results at time $t = 1.5$ ms with an initial velocity -100 m/s on the left and 100 m/s on the right. The results of the six-equation model are completely coinciding with the results of the seven-equation model.

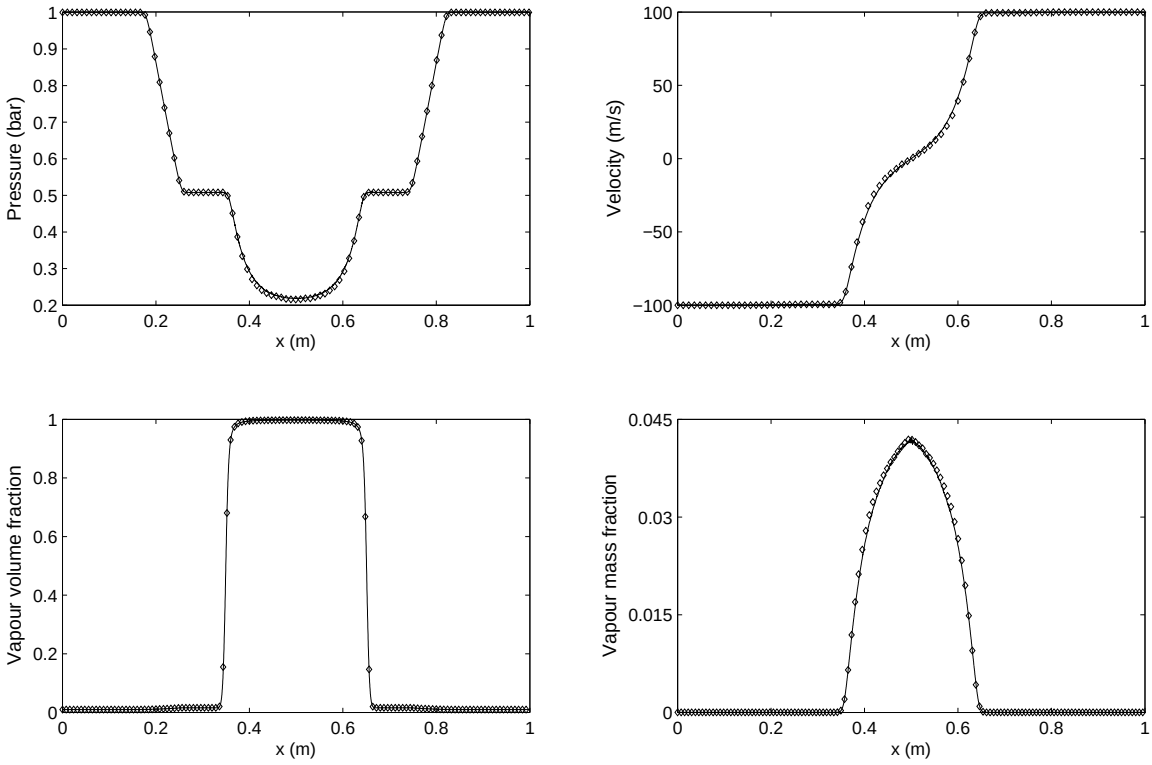

Figure 4.9: Water liquid-vapor expansion tube with phase transition and strong rarefaction effects (initial $|u| = 100$ m/s) at time $t = 1.5$ ms. By using the seven-equation model (lines) and six-equation model (symbols). The computations are done with 5000 cells. For the seven-equation model: The CPU time is 8.537 hours with 449,836 time steps. For the six-equation model: The CPU time is 5.700 hours with 381,778 time steps.

When the rarefaction effects become stronger we observe some difficulties. If the same conditions are maintained except that the velocity is increased ($\gtrsim 200$m/s), we see that there are some differences between the results of both models. To consider such a difficulty also for the sake of comparsion with the results of [126], we take the velocity -500 m/s on the left and 500 m/s on the right. The results are shown in Figure 4.10 at time $t = 0.58$ ms. There are some differences in the profiles of the pressure and the vapor mass fraction. Moreover there are some oscillations in the curve of the vapor mass fraction. We think that the differences in the results of both models may be related to the approximation of the non-conservative terms and to the fact that in seven-equation model an approximation is used in the velocity relaxation procedure. This may cause some deviation as the difference between the initial velocities is increased.

Under the grid refinement, the differences between the pressure profiles are decreased. They disappear with a very fine grid, as is shown in Figure 4.11. But the difference between the vapor mass fraction profiles remains, moreover the oscillations are more pronounced.

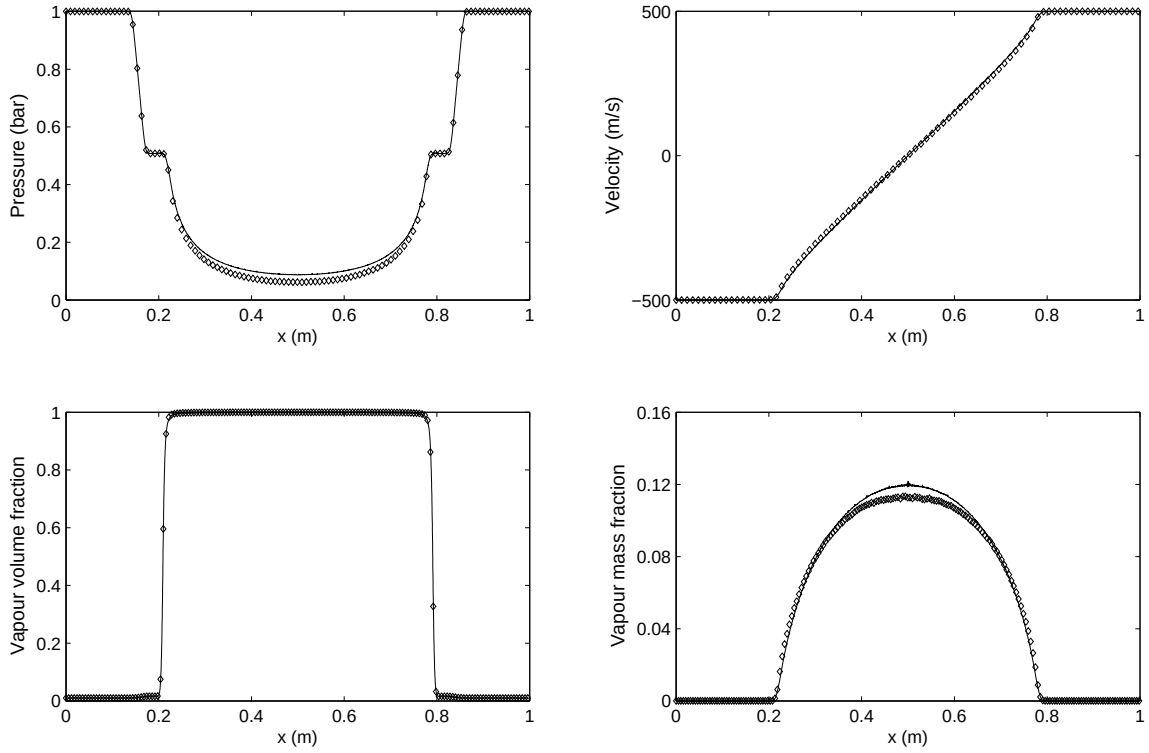

Figure 4.10: Water liquid-vapor expansion tube with phase transition and strong rarefaction effects (initial $|u| = 500$ m/s) at time $t = 0.58$ ms, by using the seven-equation model (lines) and six-equation model (symbols). The computations used 5000 cells. For the seven-equation model: The CPU time is 4.947 hours with 218,710 time steps. For the six-equation model: The CPU time is 3.372 hours with 186,601 time steps.

To understand why the oscillations increase with grid refinement, we consider all variables that are related to the vapor mass fraction $Y_1 = \dfrac{\alpha_1\rho_1}{\rho}$. We see that as the number of the cells increases the mixture density decreases to a value very close to zero with small oscillations. Also the difference between the mixture density of the two models is reduced. But since the mixture density with low values lies in the denominator of the relation of Y_1, both of the differences and the oscillations in the curves of the vapor mass fraction will be more significant.

# of Figure	4.5	4.6 & 4.7	4.8	4.9	4.10	4.11
The ratio	0.495	0.501	0.856	0.668	0.682	0.761

Table 4.2: The ratio of the CPU time for the six-equation model to the seven-equation model.

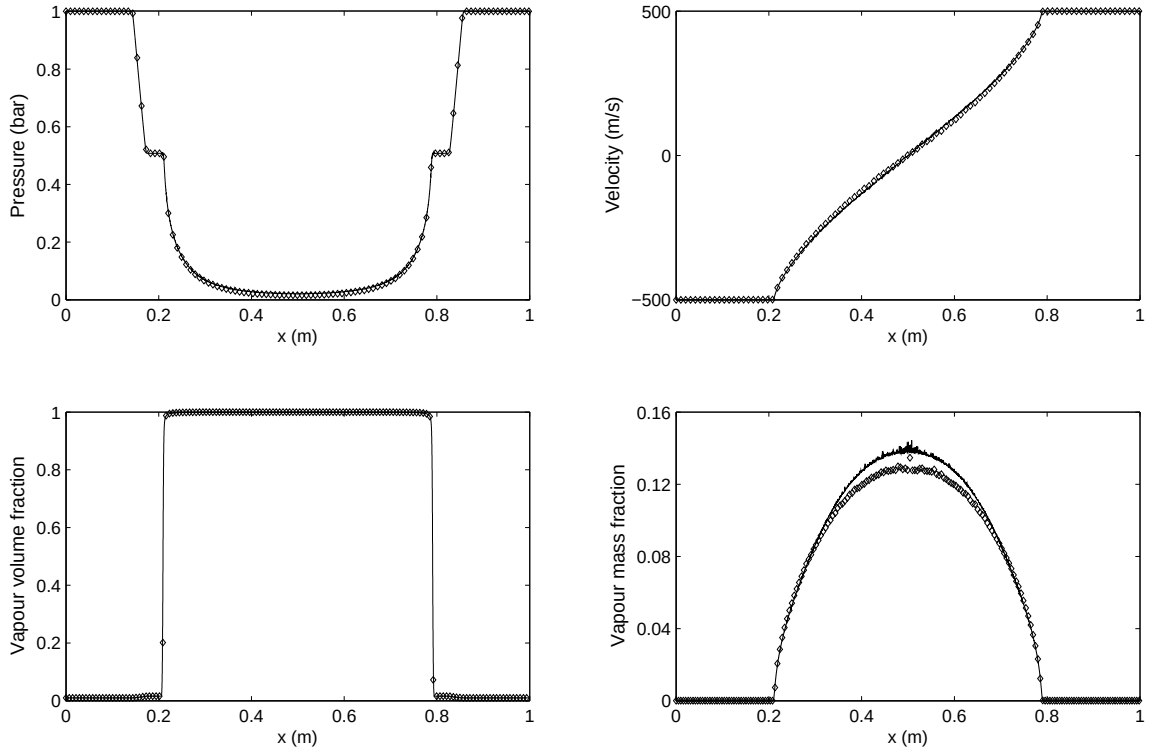

Figure 4.11: Water liquid-vapor expansion tube with phase transition and strong rarefaction effects (initial $|u| = 500$ m/s) at time $t = 0.58$ ms. By using the seven-equation model (lines) and six-equation model (symbols). The computations are done with 25,000 cells. For the seven-equation model: The CPU time is 112.393 hours with 1,090,545 time steps. For the six-equation model: The CPU time is 85.481 hours with 934,593 time steps.

Again in the expansion tube results it is noted that the required CPU time for the six-equation model is smaller than the CPU time that is required for the seven-equation model, in average it is about 66%, see Table 4.2.

In all cases the results of both models coincide except when the difference between the initial velocities increase to a certain value, after that value is reached we observe a small deviation in the results of both models, also some oscillations appear. This problem is partially reduced under grid refinement.

As a result we think that since both models give the same results and also both of them may face similar problems under extreme initial conditions. We think that the six-equation model is to be preferred for practical applications since it is less expensive. Moreover it is easier to modify this model to the multiphase case. Thus this model is adopted in the next chapter to investigate a laser-induced cavitation bubble, where a three phase flow will be considered.

For deeper understanding to the differences between the results of models we address the following remark.

Remark 4.2. From previous results of Saurel et al. [127] and Petitpas et al. [106, 108], it is noted that both the five-equation and six-equation models do not converge to a correct solution in mixtures under strong shocks. This is due to the deviation between the local thermodynamic states and the mixture Hugoniot curve in the numerical diffusion zone. This leads to a wrong numerical shock speed and wrong jumps. Unfortunately, this problem cannot be solved by grid refinement. To deal with this problem specific methods are proposed to correct the thermodynamic paths in the shock layer. The most general method is the one proposed in Petitpas et al. [108].

We found that this problem also exists in the results of the seven-equation model. Indeed, the deviation from the correct solution is less in the seven-equation results than in the six-equation results. Hereafter, we consider the same test example in [106, 108, 127] to show this phenomena numerically. The heat and mass transfer are excluded.

Consider a 1 m tube that consists of two chambers separated by an interface at $x = 0.6$ m. A mixture of epoxy and spinel fills both champers with initial densities $\rho_{epoxy} = 1185$ kg/m^3 and $\rho_{spinel} = 3622$ kg/m^3. The initial volume fractions in both champers are taken as $\alpha_{epoxy} = 0.5954$, $\alpha_{spinel} = 1 - \alpha_{epoxy}$. Both material are assumed to obey a SG-EOS (3.2a). The parameters are given in Table 4.3.

The initial pressure in the right chamber is the atmospheric pressure, while the pressure in the left chamber is equal to 1×10^{10} Pa. The results are shown in Figure 4.12 at time $t = 80\ \mu s$. The results of the seven-equation and six-equation models are coinciding with the exact solution. Here the exact solution is obtained by using the exact Riemann solution of the five-equation model that was proposed by Petitpas et al. [106].

If the initial left pressure is increased to be 2×10^{11} Pa we can see a problem of convergence for both models regardless of the number of cells. This is shown in Figure 4.13 at time $t = 30\ \mu s$, where 1000 cells were used. No change in the results under grid refinement, see Figure 4.14 where 5000 cells were used.

Therefore, under strong shocks in mixtures the seven-equation, six-equation and five-equation models may give wrong shock speeds and wrong jumps. As a result one has to be careful with extreme initial conditions in mixtures.

	γ	$\pi(Pa)$	$q(J/kg)$
Epoxy	2.43	5.3×10^9	0
Spinel	1.62	141×10^9	0

Table 4.3: EOS parameters for epoxy and spinel.

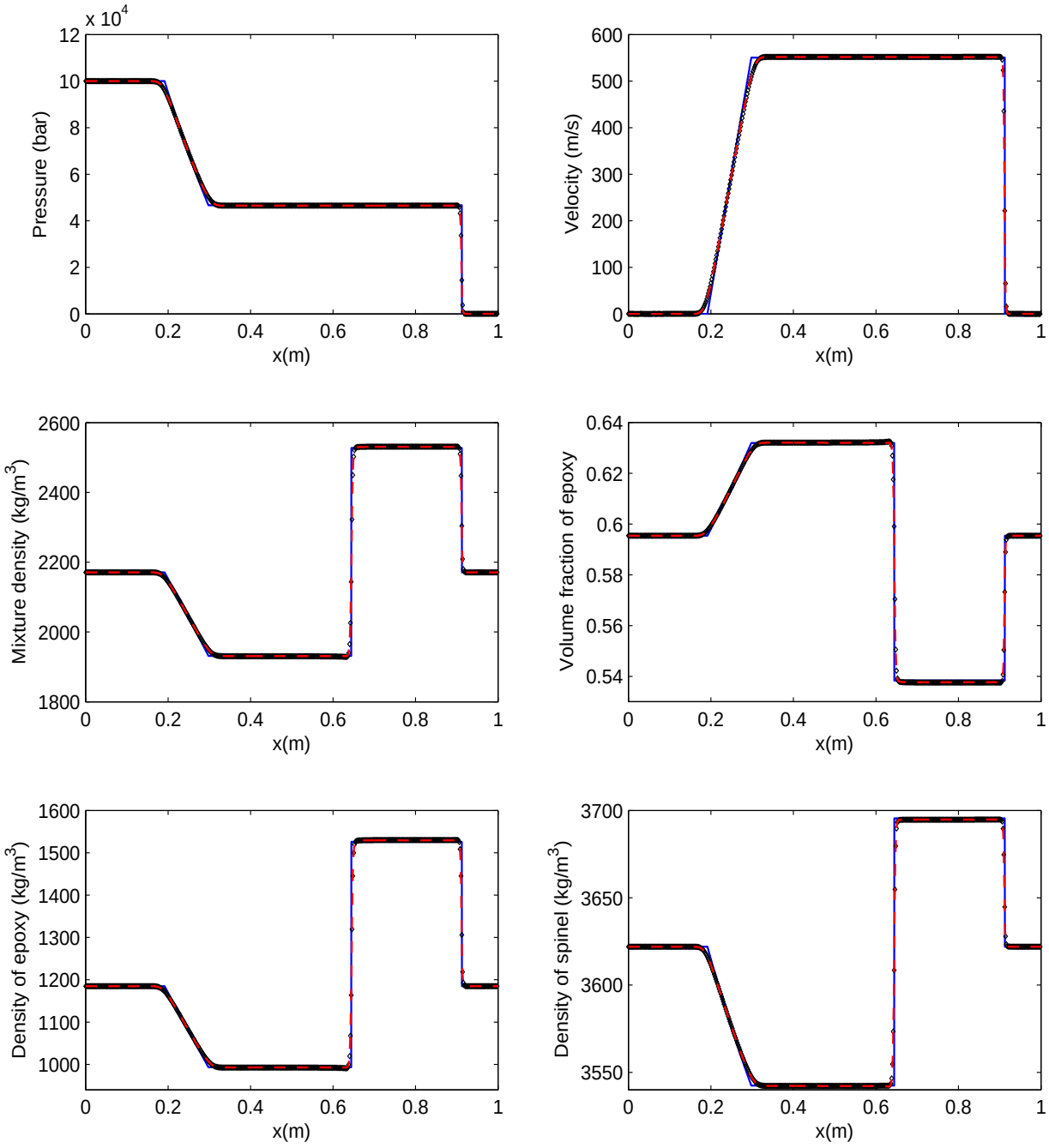

Figure 4.12: Epoxy-spinel shock tube with initial pressure ratio 10^5. The results of the seven-equation model (dashed lines) and the results of the six-equation model (symbols) are compared with the exact solution (solid lines). A 1000 cell mesh is used with CFL=0.6.

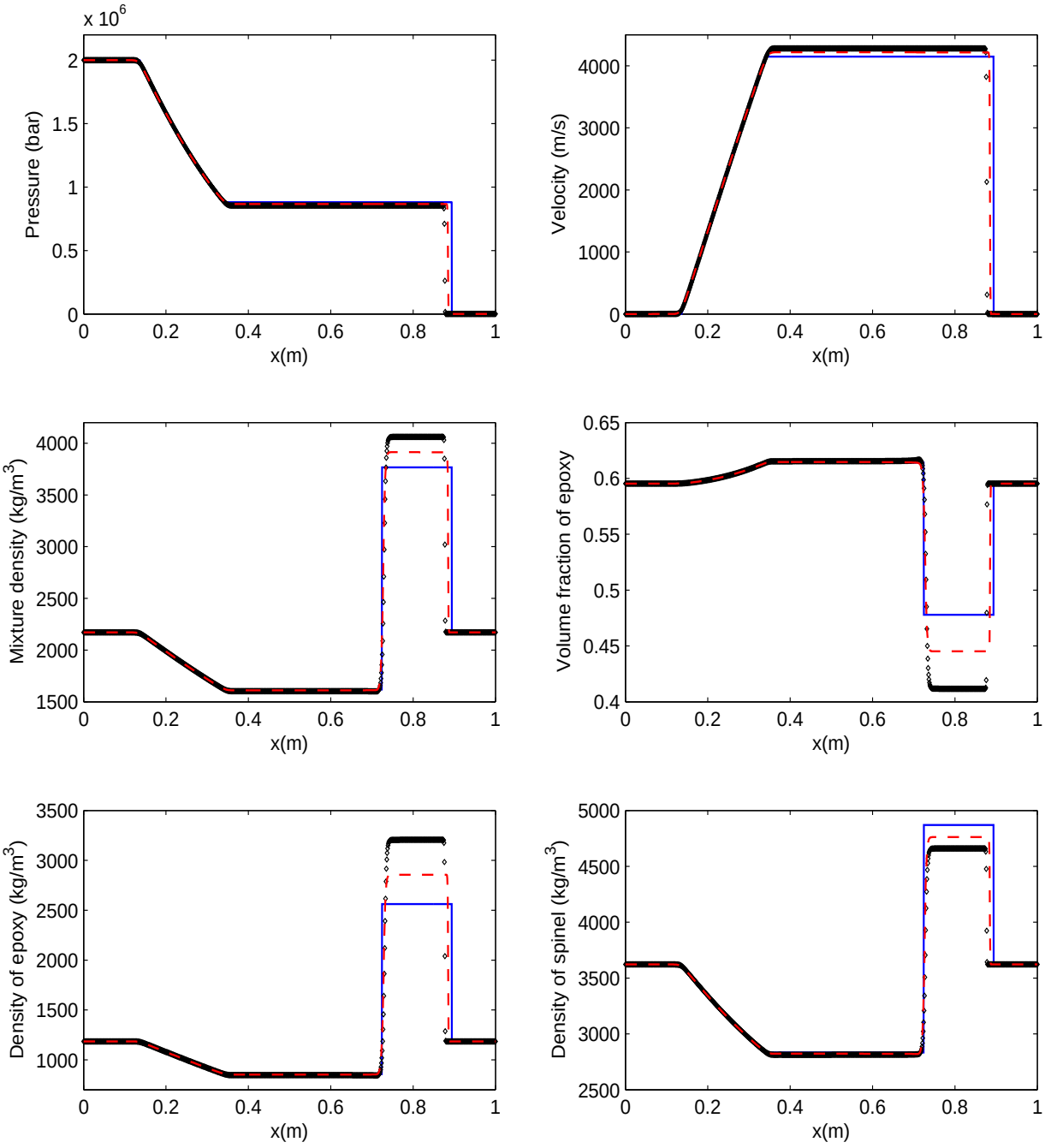

Figure 4.13: Epoxy-spinel shock tube with initial pressure ratio 2×10^6. The results of the seven-equation model (dashed lines) and the results of the six-equation model (symbols) are compared with the exact solution (solid lines). A 1000 cell mesh is used with CFL=0.6.

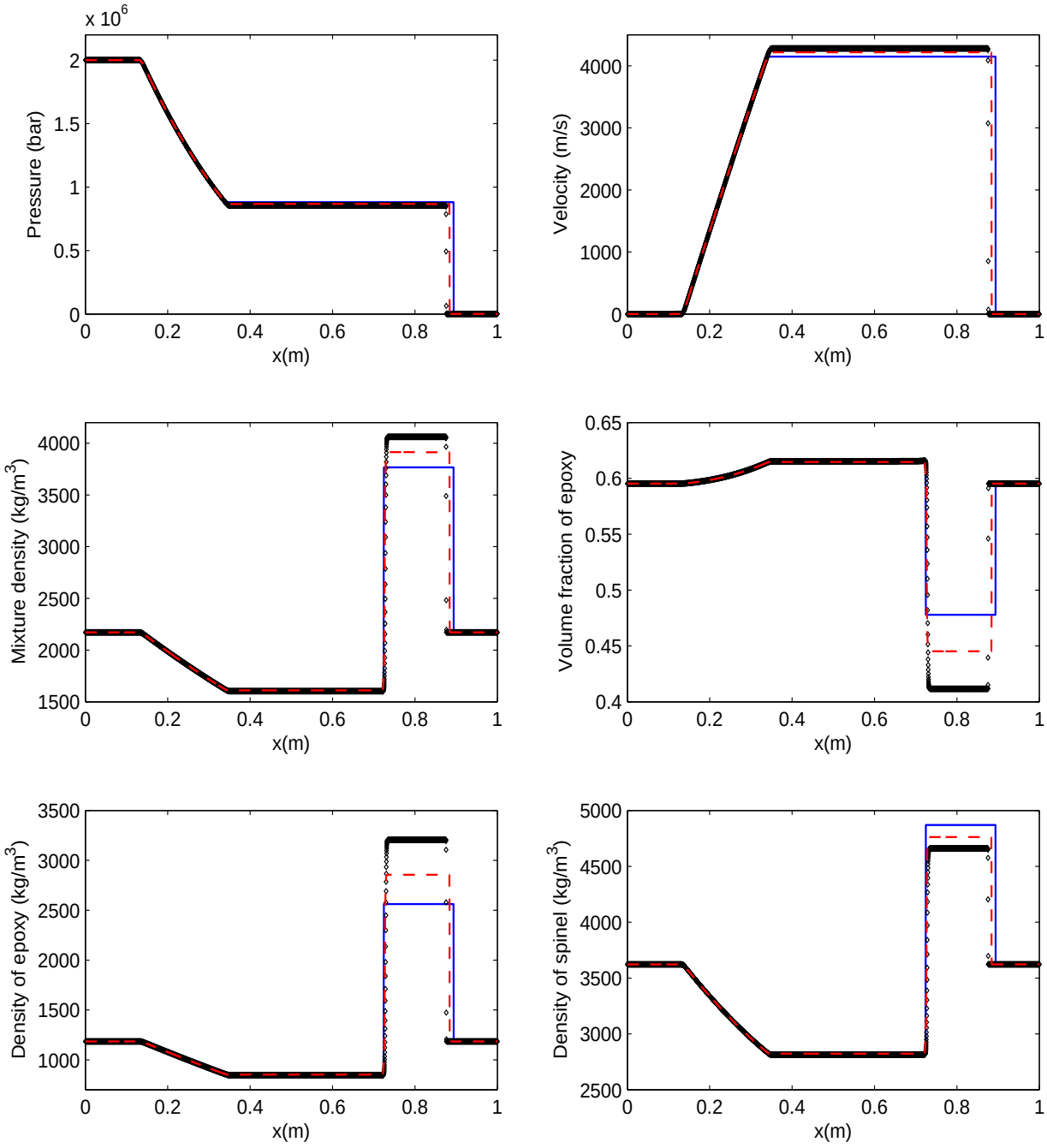

Figure 4.14: Epoxy-spinel shock tube with initial pressure ratio 2×10^6. The results of the seven-equation model (dashed lines) and the results of the six-equation model (symbols) are compared with the exact solution (solid lines). A 5000 cell mesh is used with CFL=0.6.

Chapter 5

Modeling and Simulation of a Laser-Induced Cavitation Bubble

5.1 Introduction

This chapter is concerned with the numerical investigation of the collapse and rebound of a laser-induced cavitation bubble in liquid water. Mainly we consider the effects of phase transition and the existence of a non-condensable gas on the dynamics of the collapsing bubble.

In this section we introduce an overview of the problem and previous work. Then we give an introduction to the work in this chapter.

5.1.1 Overview of the problem

Cavitation is defined as the formation of vapor bubbles in a liquid due to the reduction of the pressure. The bubbles then collapse when they entered a region of higher pressure. The collapse of a cavitation bubble causes high pressure and high temperature, this increases the noise of the system and may cause a material damage, cavitation erosion. This phenomenon may have destructive effects and it occurs in many engineering applications of hydrodynamics like pumps, piping systems and ship propellers, see Philipp and Lauterborn [109]. Therefore, a special attention is devoted in the literature to study the mechanism of cavitation erosion [18, 64, 109, 163]. On the other hand, the cavitation can be controlled to be used in several applications, for example cavitation erosion is used to clean solid surfaces, see e.g. Song et al. [140].

The dynamics of collapsing bubbles was studied first by Rayleigh [115] assuming that the surrounding liquid is incompressible and inviscid. Later the basic Rayleigh equation was modified by authors to include the effects of viscosity and surface tension. The resulting equation after several modifications is known as Rayleigh-Plesset equation, see e.g. Brennen [17], Franc and Michel [43].

A further modification was considered assuming the surrounding liquid as slightly compressible, see Trilling [152], Keller and Kolodner [67] as well as Gilmore [48].

Hickling and Plesset [55] presented some numerical solutions to describe the bubble collapse and rebound by taking into account the liquid compressibility. They used the Gilmore model [48] for a Mach number smaller than 0.1 and the Lagrangian form of the Euler equations for higher values of Mach number. The results of Hickling and Plesset show the formation of pressure waves during the rebound of the bubble.

Later several numerical algorithms were modified and several effects during the cavitation were studied like heat transfer, evaporation, condensation and the existence of a non-condensable gas inside the bubble, see [44, 65, 68, 76, 97, 98, 111–113, 139, 147, 160], in the book of Franc and Michel [43] you find a good review for the development of the models.

In fact, most of the above models are not suitable for periods of high Mach number flow, where the compressibility of the liquid plays an important role, especially at the end of the collapse. Indeed, a shock wave is emitted in the liquid at the final stage of the collapse [5, 130]. This phenomenon is confirmed by experiments, where some measurements for the strength of this shock wave were reported [5, 77]. This makes consideration the compressibility of the surrounding water of great importance especially for a strong bubble collapse. But assuming compressibility introduces severe difficulties in the numerical simulations.

Another shortcoming of the old models is the frequent assumption of the homogeneity inside the bubble. This assumption is not the general case, also there are no enough justifications for this assumption especially in the case of violent collapse. Moreover numerical investigations show that the state inside the bubble does not stay homogeneous during the collapse, see Müller et al. [94, 95].

In recent models the full Euler equations were used to describe each fluid. For instance, Akhatov et al. [5] introduced two models to describe the collapse and rebound of a laser-induced cavitation bubble. One model for the low Mach number period which assumes an incompressible surrounding liquid, and the other model for the high Mach number period which consists of the Euler equations for each phase. The second model assumes compressibility for both the vapor and the liquid phases and provides a detailed description for the behavior of both phases. Moreover, the effects of heat transfer, mass transfer and the existence of a non-condensable gas were studied. The Hertz-Knudsen-Langmuir model for the evaporation and condensation was used. Regarding the model for the high Mach number period, the heat and mass transfer were modeled separately. Thus some coupling method was required to take into account these effects in the model. Even though this is not a trivial it was unfortunately not detailed in [5]. This makes it difficult to compare their work with any other approach. In addition, the non-condensable gas was inserted in the energy equation through higher order terms. This adds extra difficulties to the

solution of the model. For this some simplifications were used in [5].

Müller et al. [94] investigated the problem of the laser-induced cavitation bubble by using recent models and numerical methods for compressible two-phase flows, but without heat and mass transfer. Indeed, Müller et al. [94] presented numerical investigations using two different methods: The Saurel and Abgrall approach [120] and the real ghost fluid method of Wang et al. [155].

In both Akhatov et al. [5] as well as Müller et al. [94] some experimental issues were discussed and comparisons with experimental results were made.

5.1.2 Current work

Both the seven-equation and the six-equation model that were considered in the previous chapters are able to take into account the compressibility of the liquid outside the bubble as well as of the vapor inside the bubble. In addition these models were tested successfully for the addition of the heat and mass transfer. Thus by using these models we are able to circumvent most of the shortcomings of the previous models.

From our study of both models in Chapter 4 we found that they almost give the same results with few differences under extreme initial conditions in mixtures. But the six-equation model is less expensive and is easier to be modified for multiphase flows. Thus this model is adopted in this chapter.

It is expected that the bubble, besides the water vapor, contains a small mass of a non-condensable gas. This may be due to the plasma recombination during the bubble creation [5]. The effect of the existence of a non-condensable gas on the dynamics of the bubble was considered by Akhatov et al. [5] and Dreyer et al. [40]. Akhatov et al. [5] showed that a small amount of non-condensable gas inside the bubble greatly influences its dynamics. The authors of [40] proposed that the rebound of the bubble after the collapse is possible only if it contains a non-condensable gas.

In this chapter, we consider both cases for the bubble, i.e. vapor bubble if it contains vapor only and gas-vapor bubble if it contains vapor and a non-condensable gas. The vapor bubble is modeled by the six-equation model. The non-condensable gas is modeled as a third phase. Thus the whole model consists of nine equations. In this situation, as in Petitpas et al. [107], the heat and mass transfer is considered only at the interface between the liquid and its vapor. But if the interface separates the liquid and the non-condensable gas the pressure relaxation is only used.

From previous computations by different models, it is known that the temperature inside the bubble exceeds the critical point through the collapsing process. So the temperature range is very wide, i.e. it starts from the room temperature and exceeds the critical temperature. This wide range should be considered in the choice of the equations of state.

Here, we use the stiffened gas equations of state (SG-EOS). We propose our own estimations for the parameters of these SG-EOS for the liquid water and its vapor.

To test our results we use experimental data for the evolution of the bubble radius. These data were achieved by the group of Prof. Lauterborn in Göttingen, see Akhatov et al. [5] and Müller et al. [94]. In the experiment a strong laser pulse is focused into liquid water. This generates a cavitation bubble, which expands to a maximum radius. Then it collapses to a non-zero minimum radius and then the bubble rebounds with a significant damping. The liquid temperature is kept fairly constant at room temperature during the experiment. Images of the bubble were taken during the experiment by using a high speed camera. These images were used to sketch the radius-time curve. For the details of the experiments see [5, 94].

Here we mainly adopt the experimental results that are shown in [94]. Where in this experiment the cuvette size is $50\times50\times50$ mm^3, the maximum radius $R_{max} = 747\ \mu\text{m}\pm0.5\%$, the minimum radius $R_{min} < 12\ \mu$m and the time from the maximum expansion of the bubble to the first collapse is $70.7\mu s$. The surrounding water is kept at the atmospheric pressure with fairly constant temperature $20\,^{\circ}$C .

In this work the computations start from the point of the maximal radius. But still the initial state inside the bubble is unknown. In fact there is no means until now to measure the physical quantities inside the bubble. Thus we have an incomplete group of experimental data.

Some authors introduced certain possibilities for the initial data inside the bubble. Hickling and Plesset [55] tested several initial pressures in the range $10^{-1} - 10^{-4}$ bar. Akhatov et al. [5] assumed the same liquid temperature inside the bubble with the corresponding saturation pressure for the initial pressure. In Müller et al. [94] the initial data were deduced from the experimental data by fitting of the computed bubble radius by the Keller-Miksis model [68] to the measured data. Other possibility for the initial data was taken by Dreyer et al. [40].

In this chapter we test several initial conditions. These tests include the assumption of the saturation state inside the bubble, several tests with different pressures and one temperature, and several tests with one pressure and several temperatures. The aim of these tests is to try to understand the effect of the initial conditions on the evolution of the bubble radius.

This chapter is organized as follows: Section 5.2 is concerned with the mathematical models. Two models are described. In particular, the modified six-equation model is rewritten in spherical coordinates assuming rotational symmetry. It is used to model the vapor bubble in liquid water. Then the nine-equation model is introduced for the gas-vapor bubble. In addition, the location of the interface in the presence of non-condensable gas is explained. Section 5.3 is devoted to the equations of state, previous criteria in the

literature are recalled and our new criterion is introduced. In Section 5.4 the numerical method is given briefly. Finally, Section 5.5 shows the numerical results and the discussion of the results. A comparison with experimental data is also shown.

5.2 Mathematical Model

The six-equation model without heat and mass transfer for two-phase flows is given as, see Subsection 2.4.2

$$\frac{\partial \alpha_1}{\partial t} + \mathbf{u} \cdot \nabla \alpha_1 = \mu(p_1 - p_2), \tag{5.1a}$$

$$\frac{\partial \alpha_1 \rho_1}{\partial t} + \nabla \cdot (\alpha_1 \rho_1 \mathbf{u}) = 0, \tag{5.1b}$$

$$\frac{\partial \alpha_2 \rho_2}{\partial t} + \nabla \cdot (\alpha_2 \rho_2 \mathbf{u}) = 0, \tag{5.1c}$$

$$\frac{\partial \rho \mathbf{u}}{\partial t} + \nabla \cdot (\rho \mathbf{u}\mathbf{u}) + \nabla(\alpha_1 p_1 + \alpha_2 p_2) = 0, \tag{5.1d}$$

$$\frac{\partial \alpha_1 \rho_1 e_1}{\partial t} + \nabla \cdot (\alpha_1 \rho_1 e_1 \mathbf{u}) + \alpha_1 p_1 \nabla \cdot \mathbf{u} = \mu p_I (p_2 - p_1), \tag{5.1e}$$

$$\frac{\partial \alpha_2 \rho_2 e_2}{\partial t} + \nabla \cdot (\alpha_2 \rho_2 e_2 \mathbf{u}) + \alpha_2 p_2 \nabla \cdot \mathbf{u} = -\mu p_I (p_2 - p_1). \tag{5.1f}$$

This system is augmented by a redundant mixture energy equation which reads

$$\frac{\partial (\rho e + \frac{1}{2}\rho \mathbf{u}^2)}{\partial t} + \nabla \cdot ((\rho e + \frac{1}{2}\rho \mathbf{u}^2 + \alpha_1 p_1 + \alpha_2 p_2)\mathbf{u}) = 0, \tag{5.2}$$

where $\rho = \alpha_1 \rho_1 + \alpha_2 \rho_2$ and $\rho e = \alpha_1 \rho_1 e_1 + \alpha_2 \rho_2 e_2$.

The interfacial pressure p_I is assumed as in (2.46), i.e.

$$p_I = \frac{Z_2 p_1 + Z_1 p_2}{Z_1 + Z_2}, \tag{5.3}$$

where the acoustic impedance Z_k, $k = 1, 2$, is defined by (2.48).

By the choice (5.3) for the interfacial pressure the model (5.1) satisfies the second law of thermodynamics, see Subsection 4.2.

5.2.1 Vapor bubble model

If the bubble contains vapor only a two-phase flow model is used. One phase is the water vapor and the other phase is the liquid water. The bubble is assumed to be perfectly spherical. Thus we consider the model (5.1) in spherical coordinates. Also we assume rotational symmetry. Moreover, the modified form of the model including the heat and

mass transfer is used, see Subsection 4.5. Thus the full model for the vapor bubble is written as

$$\frac{\partial \alpha_1}{\partial t} + u\frac{\partial \alpha_1}{\partial r} = \mu(p_1 - p_2) + \frac{1}{\kappa}Q + \frac{1}{\varrho}\dot{m}, \tag{5.4a}$$

$$\frac{\partial \alpha_1\rho_1}{\partial t} + \frac{\partial(\alpha_1\rho_1 u)}{\partial r} = \dot{m} - \frac{2}{r}\alpha_1\rho_1 u, \tag{5.4b}$$

$$\frac{\partial \alpha_2\rho_2}{\partial t} + \frac{\partial(\alpha_2\rho_2 u)}{\partial r} = -\dot{m} - \frac{2}{r}\alpha_2\rho_2 u, \tag{5.4c}$$

$$\frac{\partial \rho u}{\partial t} + \frac{\partial(\rho u^2 + \alpha_1 p_1 + \alpha_2 p_2)}{\partial r} = -\frac{2}{r}\rho u^2, \tag{5.4d}$$

$$\frac{\partial \alpha_1\rho_1 e_1}{\partial t} + \frac{\partial \alpha_1\rho_1 e_1 u}{\partial r} + \alpha_1 p_1\frac{\partial u}{\partial r} = \mu p_I(p_2 - p_1) + Q + e_i\dot{m} - \frac{2}{r}\alpha_1\rho_1 e_1 u - \frac{2}{r}\alpha_1 p_1 u, \tag{5.4e}$$

$$\frac{\partial \alpha_2\rho_2 e_2}{\partial t} + \frac{\partial \alpha_2\rho_2 e_2 u}{\partial r} + \alpha_2 p_2\frac{\partial u}{\partial r} = -\mu p_I(p_2 - p_1) - Q - e_i\dot{m} - \frac{2}{r}\alpha_2\rho_2 e_2 u - \frac{2}{r}\alpha_2 p_2 u, \tag{5.4f}$$

$$\frac{\partial(\rho e + \frac{1}{2}\rho u^2)}{\partial t} + \frac{\partial u(\rho e + \frac{1}{2}\rho u^2 + \alpha_1 p_1 + \alpha_2 p_2)}{\partial r} = - \frac{2}{r}(\rho e + \frac{1}{2}\rho u^2 + \alpha_1 p_1 + \alpha_2 p_2)u, \tag{5.4g}$$

where

$$Q = \theta(T_2 - T_1),$$
$$\dot{m} = \nu(g_2 - g_1).$$

Here u is the *radial velocity*. The variables κ, ϱ and e_i are given in (3.36), (3.54a) and (3.54b) respectively. Note that the seventh equation of the model (5.4) is the redundant equation for the mixture of the energy.

The source terms in the model (5.4) are classified into four groups as follows

$$\mathbf{S} = \mathbf{S}_P + \mathbf{S}_Q + \mathbf{S}_m + \mathbf{S}_r, \tag{5.5}$$

where $\mathbf{S}_P$, $\mathbf{S}_Q$ and $\mathbf{S}_m$ are associated with the pressure, temperature and Gibbs free energy relaxation terms respectively and $\mathbf{S}_r$ represents the geometrical terms that come from the spherical coordinates in radial direction. These source vectors are given as

$$\mathbf{S}_P = (\mu(p_1 - p_2), 0, 0, 0, \mu p_I(p_2 - p_1), -\mu p_I(p_2 - p_1), 0)^T$$
$$\mathbf{S}_Q = \left(\frac{Q}{\kappa}, 0, 0, 0, Q, -Q, 0\right)^T,$$
$$\mathbf{S}_m = \left(\frac{\dot{m}}{\varrho}, \dot{m}, -\dot{m}, 0, e_i\dot{m}, -e_i\dot{m}, 0\right)^T,$$

$$\mathbf{S}_r = -\frac{2}{r}(0, \alpha_1\rho_1 u, \alpha_2\rho_2 u, \rho u^2, (\alpha_1\rho_1 e_1 + \alpha_1 p_1)u, (\alpha_2\rho_2 e_2 + \alpha_2 p_2)u, \\ (\rho e + \frac{1}{2}\rho u^2 + \alpha_1 p_1 + \alpha_2 p_2)u)^T. \tag{5.6}$$

The relaxation parameters μ, θ and ν are assumed to be infinite, i.e. all relaxation procedures are instantaneous.

For numerical reasons, we allow the presence of a negligibly small amount of vapor outside the bubble, i.e. in the surrounding liquid, and a small amount of liquid inside the bubble, typically these values are $\varepsilon = 10^{-6}$. It is expected that these small values have no significant effects. Indeed, by using pressure relaxation in the whole domain we keep a single value for the pressure. In addition, we use the temperature relaxation in the whole domain, so we have a single temperature. This seems to be better for the resolution of the physical variables. In fact, we observed just a small change in the results if we use the temperature relaxation at the interface only.

The mass transfer is considered only at the interface, which is located by using the volume fraction of one of the phases, i.e. the interface corresponds to the following range of the volume fraction

$$\bar{\varepsilon} \leq \alpha_1 \leq 1 - \bar{\varepsilon},$$

The value of $\bar{\varepsilon}$ is taken greater enough than the value of ε to ensure that the phase transition occurs only in the interfacial zone, this is explained in Section 3.4.

5.2.2 Gas-vapor bubble model

The above model consists of two phases only. To consider the effect of a non-condensable gas inside the bubble a third phase is used.

Initially the six-equation model (5.1) is derived from the full non-equilibrium model (2.43) by the asymptotic limit of zero velocity relaxation time. Thus the six-equation model has a single velocity. To derive a multiphase model with a single velocity we proceed in the same manner, i.e. we start from the full non-equilibrium model for multiphase flows.

The full non-equilibrium model for multiphase flows of Saurel-Abgrall type [120] without heat and mass transfer is written as

$$\begin{cases} \dfrac{\partial \alpha_k}{\partial t} + \mathbf{u}_I \cdot \nabla \alpha_k = \mu(p_k - \hat{p}), \\ \dfrac{\partial \alpha_k \rho_k}{\partial t} + \nabla \cdot (\alpha_k \rho_k \mathbf{u}_k) = 0, \\ \dfrac{\partial \alpha_k \rho_k \mathbf{u}_k}{\partial t} + \nabla \cdot (\alpha_k \rho_k \mathbf{u}_k \mathbf{u}_k) + \nabla(\alpha_k p_k) = p_I \nabla \alpha_k + \lambda(\mathbf{u}_k - \hat{\mathbf{u}}), \\ \dfrac{\partial \alpha_k \rho_k E_k}{\partial t} + \nabla \cdot (\alpha_k(\rho_k E_k + p_k)\mathbf{u}_k) = p_I \mathbf{u}_I \cdot \nabla \alpha_k - \mu p_I(p_k - \hat{p}) + \lambda \mathbf{u}_I \cdot (\mathbf{u}_k - \hat{\mathbf{u}}), \end{cases} \tag{5.7}$$

where $\mathbf{u}_I$ is the interfacial velocity and $E_k = e_k + \dfrac{\mathbf{u}_k^2}{2}$ is the total specific energy for phase k. Here $k = 1, 2, ..., N$, where N is the number of phases.

The summation of all relaxation terms for the pressure respectively the velocity is zero. Thus the mixture values $\hat{\mathbf{u}}$ and $\hat{p}$ are given as

$$\hat{\mathbf{u}} = \frac{\sum_{k=1}^{N} \mathbf{u}_k}{N},$$

$$\hat{p} = \frac{\sum_{k=1}^{N} p_k}{N}.$$

Modeling the relaxation terms for the velocity and the pressure in the above way means that we assume that all velocities of different fluids have the same relaxation rate, also all pressures have the same relaxation rate. These terms can be modeled in different ways, for example see Hérard [54]. However, the above modeling is enough for our problem because we are interested in one velocity and one pressure in the whole domain of the flow.

To derive a single velocity model we apply the method of Chen et al. [22]. This method was used in Section 4.6 to derive the six-equation model of a single velocity from the full non-equilibrium seven-equation model by assuming stiff velocity relaxation.

Assume stiff velocity relaxation for the model (5.7), i.e.

$$\lambda = \frac{1}{\epsilon} \quad \text{where} \quad \epsilon \to 0^+.$$

Then following the method of Chen et al. [22], we get the following reduced model

$$\begin{cases} \dfrac{\partial \alpha_k}{\partial t} + \mathbf{u} \cdot \nabla \alpha_k = \mu(p_k - \hat{p}), \\ \dfrac{\partial \alpha_k \rho_k}{\partial t} + \nabla \cdot (\alpha_k \rho_k \mathbf{u}) = 0, \\ \dfrac{\partial \rho \mathbf{u}}{\partial t} + \nabla \cdot (\rho \mathbf{u}\mathbf{u}) + \nabla p = 0, \\ \dfrac{\partial \alpha_k \rho_k e_k}{\partial t} + \nabla \cdot (\alpha_k \rho_k e_k \mathbf{u}) + \alpha_k p_k \nabla \cdot \mathbf{u} = -\mu p_I (p_k - \hat{p}), \end{cases} \tag{5.8}$$

where $\rho = \sum_{k=1}^{N} \alpha_k \rho_k$ and $p = \sum_{k=1}^{N} \alpha_k p_k$.

A model with three phases is enough to investigate the bubble containing vapor and a non-condensable gas with surrounding liquid water. Thus the model (5.8) for three phases in spherical coordinates assuming rotational symmetry is written as

$$\begin{cases} \dfrac{\partial \alpha_1}{\partial t} + u\dfrac{\partial \alpha_1}{\partial r} = \mu(p_1 - \hat{p}), \\ \dfrac{\partial \alpha_2}{\partial t} + u\dfrac{\partial \alpha_2}{\partial r} = \mu(p_2 - \hat{p}), \\ \dfrac{\partial \alpha_k\rho_k}{\partial t} + \dfrac{\partial (\alpha_k\rho_k u)}{\partial r} = -\dfrac{2}{r}\alpha_k\rho_k u, \\ \dfrac{\partial \rho u}{\partial t} + \dfrac{\partial (\rho u^2 + p)}{\partial r} = -\dfrac{2}{r}\rho u^2, \\ \dfrac{\partial \alpha_k\rho_k e_k}{\partial t} + \dfrac{\partial \alpha_k\rho_k e_k u}{\partial r} + \alpha_k p_k \dfrac{\partial u}{\partial r} = -\mu p_I(p_k - \hat{p}) - \dfrac{2}{r}\alpha_k\rho_k e_k u - \dfrac{2}{r}\alpha_k p_k u, \\ \dfrac{\partial (\rho e + \frac{1}{2}\rho u^2)}{\partial t} + \dfrac{\partial u(\rho e + \frac{1}{2}\rho u^2 + p)}{\partial r} = -\dfrac{2}{r}(\rho e + \frac{1}{2}\rho u^2 + p)u, \end{cases} \tag{5.9}$$

where $k = 1, 2, 3$, and $\rho e = \sum_{k=1}^{3} \alpha_k \rho_k e_k$.

Here u is the radial velocity. The volume fractions for the three phases are connected by the constraint condition, $\alpha_1 + \alpha_2 + \alpha_3 = 1$.

Note that the model (5.9) consists of nine equations augmented with a redundant mixture energy equation.

The interfacial pressure in this model is taken as a generalization of the relation (5.3), i.e.

$$p_I = \frac{\sum_{k=1}^{3} \frac{p_k}{Z_k}}{\sum_{k=1}^{3} \frac{1}{Z_k}}.$$

The model of nine equations in (5.9) is a non-strictly hyperbolic model with eigenvalues u seven fold, $u - c$ and $u + c$, with

$$c^2 = \sum_{k=1}^{3} Y_k c_k^2,$$

where $Y_k = \dfrac{\alpha_k\rho_k}{\rho}$, and c_k is given by (2.49). For more information about the mathematical properties of this model see Appendix A.

After the pressure relaxation at each time step the heat and mass transfer are included through the temperature and the Gibbs free energy relaxations. Following Petitpas et al. [107] the heat and mass transfer are considered only if the interface separates between the liquid and its vapor. When dealing with the interface between the liquid and the non-condensable gas the parameters of the temperature and Gibbs free energy relaxations are set to zero. Thus, the heat and mass transfers for the model (5.9) are included exactly as done in the previous section between the liquid and its vapor.

The interface between the liquid and vapor is located as in Petitpas et al. [107] by using the volume fractions of both the vapor and liquid. Assume α_1 and α_2 to be the volume fractions of vapor and liquid respectively. Then the interface is located by

$$\bar{\varepsilon} \leq \alpha_1 \leq (1 - \bar{\varepsilon}) \quad \& \quad \bar{\varepsilon} \leq \alpha_2 \leq (1 - \bar{\varepsilon}).$$

Note that in this case the bubble is identified by the summation of the vapor volume fraction and the non-condensable gas volume fraction.

The heat and mass transfer change the pressure of the vapor and liquid. But both stay in equilibrium. To keep one pressure in the system at each time step we also set the pressure of the non-condensable gas to the new pressure. This effect modifies the internal energy of the non-condensable gas. In fact, this is some approximation. This has no bad consequences since the non-condensable gas is added in small propotions at collapse. However, the treatment with the non-condensable gas requires more investigations.

5.3 Equations of state (EOS)

As discussed in Subsection 3.2.1, to overcome the problem of negative squares of sound speed in numerical computations, each fluid obeys its own EOS as a pure substance, also these EOS should satisfy certain convexity constraints [89, 107, 126].

The stiffened gas EOS (SG-EOS) is mostly used by authors for its simplicity [9, 23, 75, 120, 126]. This EOS contains the main properties of the pure fluids, i.e. attractive and repulsive molecular effects [80, 126]. Moreover the SG-EOS satisfies the convexity constraints for stability that were discussed by Menikoff and Plohr [89].

The SG-EOS for the internal energy as a function of the pressure and the density is written as, see Le Metayer et al. [80], Barberon and Helluy [13, 14]

$$e(p, \rho) = \frac{p + \gamma\pi}{\rho(\gamma - 1)} + q, \tag{5.10}$$

where the parameters γ, π and q are characteristic constants of the thermodynamic behavior of the fluid. The expression (5.10) initially was introduced without the parameter q, see Harlo and Amsden [53].

Following [80], expressions for the temperature and the entropy were deduced by using relation (5.10) with the Maxwell relations. Thus the SG-EOS for each phase reads

$$e(p,v) = \frac{p+\gamma\pi}{(\gamma-1)}v + q, \tag{5.11a}$$

$$h(T) = C_p T + q, \tag{5.11b}$$

$$T(p,v) = \frac{p+\pi}{C_v(\gamma-1)}v, \tag{5.11c}$$

$$s(p,T) = C_v \ln \frac{T^\gamma}{(p+\pi)^{(\gamma-1)}} + q', \tag{5.11d}$$

$$g(p,T) = (\gamma C_v - q')T - C_v T \ln \frac{T^\gamma}{(p+\pi)^{(\gamma-1)}} + q, \tag{5.11e}$$

where recall that $v = \dfrac{1}{\rho}$ is the specific volume, h the specific enthalpy, T the temperature, s the specific entropy, g the Gibbs free energy, C_v the specific heat capacity at constant volume, C_p the specific heat capacity at constant pressure, and q' is a characteristic constant.

The parameters of the SG-EOS are determined by using a reference curve. In the literature two types of curves are used: The Hugoniot curve and the saturation curve. Using the saturation curves is more recent and was introduced for a liquid and its vapor in view of phase transition.

Using the Hugoniot curve as a reference is the classical way used by authors for two-phase flow models to determine the parameters that appear in the internal energy equation (5.11a), see Cochi et al. [25], Saurel and Abgrall [121]. In their approach the parameter q is set to zero. The parameters γ and π are determined by using experimental data linking the shock speed to the particle speed. Indeed, the experimental data used by [25, 121] show that the relation between the shock speed and the particle speed is almost linear, it is expressed as

$$u_s = c_0 + a u_p, \tag{5.12}$$

where u_s is the shock speed, u_p the particle speed, a is a dimensionless constant and c_0 is the sound speed in the material at rest. From the empirical relation (5.12) one can estimate the sound speed c_0.

A theoretical relation between the shock speed and the particle speed is derived from the Rankine-Hugoniot conditions of the Euler equations, it is given as

$$u_s = \sqrt{c_0^2 + (\frac{\gamma+1}{4}u_p)^2} + \frac{\gamma+1}{4}u_p \tag{5.13}$$

Then the parameter γ is chosen to give the closest agreement between the experimental data and the theoretical curve. After that, the parameter π is determined by using the

expression of the sound speed (2.49). In context of the SG-EOS the sound speed is given as

$$c = \sqrt{\frac{\gamma(p+\pi)}{\rho}}. \tag{5.14}$$

From this expression and by using some reference state $\pi = \frac{\rho_0 c_0^2}{\gamma} - p_0$. For all details see [25, 121].

In the literature we find different choices for the values of γ and π that were achieved in this way. This is due to the range of experimental data that were considered. For example, in [25] the parameters were taken as $\gamma = 5.5$ and $\pi = 4.921 \times 10^8$. In [121] the parameters were taken as $\gamma = 4.4$ and $\pi = 6.0 \times 10^8$.

Using the saturation curve as a reference seems to be more relevant to the phase transition. This idea was introduced by Barberon and Helluy [13, 14]. Then it was modified by Le Metayer et al. [80]. The main idea of this method is the following: Linking the two pure fluid EOS under thermodynamic equilibrium must be able to reproduce the liquid-vapor phase diagram. Therefore, the various parameters of the pure EOS are linked to each other to fulfill some constraints to recover the phase diagram [80].

The method of Le Metayer et al. [80] is summarized as:

- Choose two reference states, for example in [80] the chosen temperature range is $298 - 473\ K$. Then all experimental data that correspond to each temperature are taken from the saturation tables.
- From the linearity of the relation between the enthalpy and the temperature both C_p (the slope) and q (reference energy at a given state) are determined, see (5.11b).
- Use the experimental curve $p = p_{sat}(T)$ in (5.11c), thus the specific volume is expressed in terms of temperature. Using the two known states with some manipulation the parameter π is determined, then C_v is also determined.
- Find γ by $\gamma = C_p/C_v$. Note that C_p is determined from the second step.
- At thermodynamic equilibrium the Gibbs free energies are equal, i.e. $g_l = g_g$. By this equality with the definition (5.11e) we have

$$(\gamma_l C_{vl} - q_l')T - C_{vl}T \ln \frac{T^{\gamma_l}}{(p+\pi_l)^{(\gamma_l - 1)}} + q_l = (\gamma_g C_{vg} - q_g')T - C_{vg}T \ln \frac{T^{\gamma_g}}{(p+\pi_g)^{(\gamma_g - 1)}} + q_g. \tag{5.15}$$

  This equation is nonlinear and can be solved to find the saturation temperature in terms of the saturation pressure. But still the entropy constants q_g' and q_l' are unknown. The authors of [80] chose to set the parameter $q_l' = 0$ and chose the parameter q_g' that provides the best fit between the theoretical and experimental saturation curves.

Phase	γ	$\pi(Pa)$	$C_v(J/kg/K)$	$C_p(J/kg/K)$	$q(J/kg)$	$q'(J/kg/K)$
vapor	1.43	0	1.04×10^3	1.487×10^3	2030×10^3	-23×10^3
liquid	2.35	10^9	1.816×10^3	4.267×10^3	-1167×10^3	0

Table 5.1: EOS parameters for vapor and liquid water, Le Metayer et al. [80].

All parameters that are determined by the above method are given in Table 5.1 for the temperature range $298 - 473$ K.

The group of parameters given by Table 5.1, provides a good agreement between the theoretical and experimental curves for the saturation curve and the enthalpies in the specified range of temperature, see [80]. Outside of this range the accuracy decreases. This is due to the fact that the saturation curves are nonlinear or may be considered as quasi-linear, while the SG-EOS provides a linear approximation in the (p, v)-plane. The above method mainly depends on the linearity of the relation between the enthalpy and temperature, but this linearity holds in limited ranges only. In fact near the critical point the nonlinear feature appears strongly. Moreover, the choice of the entropy constants q'_k may lead to negative values for the entropy.

In the problem under consideration i.e. bubble collapse, the range of the temperature is very wide. It starts from the room temperature and exceeds the critical point. Thus choosing appropriate parameters for EOS is not an easy task. Moreover, including the heat and mass transfer requires more attention. In fact, finding EOS that cover very wide ranges of properties and provide the required stability for the solution of the hyperbolic system is a big issue and this involves us with the complexity of determining the EOS.

In this work we adopt the SG-EOS (5.11). We use our own method for the determination of the parameters. In this method we keep the main aim of the previous method, that the various parameters of each EOS are linked to each other to recover the saturation curve.

Since the range of the temperature is very wide it is impossible to obtain good agreements between the theoretical and the experimental curves by one group of parameters. Instead of that we aim to keep the physical properties of the quantities besides reasonable agreements with the tendency of the relations between the various quantities.

Now, we show the determination of the parameters for the water vapor then we show that for the liquid water.

5.3.1 Determination of the SG-EOS for the water vapor

For gases it is typical to set $\pi_g = 0$. For example, if we follow the method of Le Metayer et al. [80] for some short ranges of temperatures we find that π_g is either negative or has

small values. Thus we choose $\pi_g = 0$.

Using $\pi_g = 0$, it is easy to see from (5.11a) and (5.11c) that

$$e_g(T) = C_{vg}T + q_g. \tag{5.16}$$

This is a linear equation. In the literature we find several values that can be taken for the specific heat at constant volume for the water vapor, more precisely they are in the range $(1.04 - 1.4) \times 10^3$ J/kg/K, see [80, 141]. The choice depends on the range of the temperature. In our case we choose $C_{vg} = 1.2 \times 10^3$ J/kg/K.

Then we choose q_g which gives a good fitting for the experimental relation between e_g and T. For the experimental data we use the saturation tables, see [99, 141]. We found that the choice of $q_g = 1995 \times 10^3$ J/kg provides a good fitting for the experimental data, see Figure 5.1. Here we did not use any mathematical method to find the best line. In fact we are not interested in the best line since the nonlinearity effect has a smaller range. Instead of that we choose our line in order to be close to the experimental curve in the wide range of linearity.

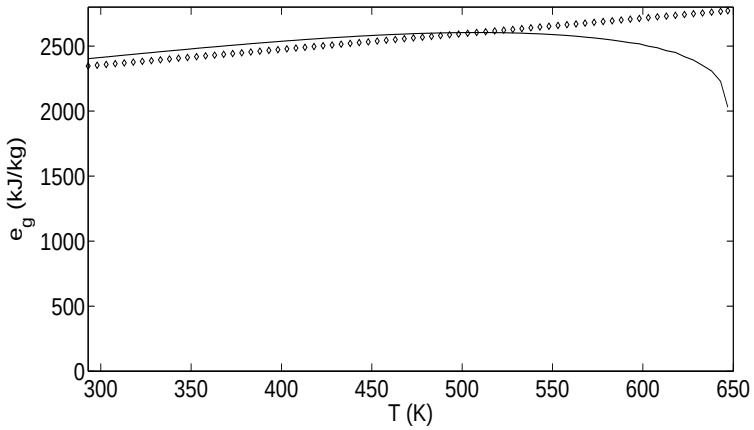

Figure 5.1: Saturation internal energy for the water vapor. Experimental curves are shown in lines and the SG-EOS approximation with symbols.

The relation (5.11c) can be reformulated as

$$v_g(T) = \frac{(\gamma_g - 1)C_{vg}T}{p_{sat}(T)}. \tag{5.17}$$

Then we choose the value of γ_g which provides a good fit between the theoretical and experimental curves of v_g versus T. Indeed, the value of $\gamma_g = 1.327$ provides such a good fitting, see Figure 5.2.

Still the parameter q'_g is unknown. We will postpone this after the presentation of the liquid water parameters.

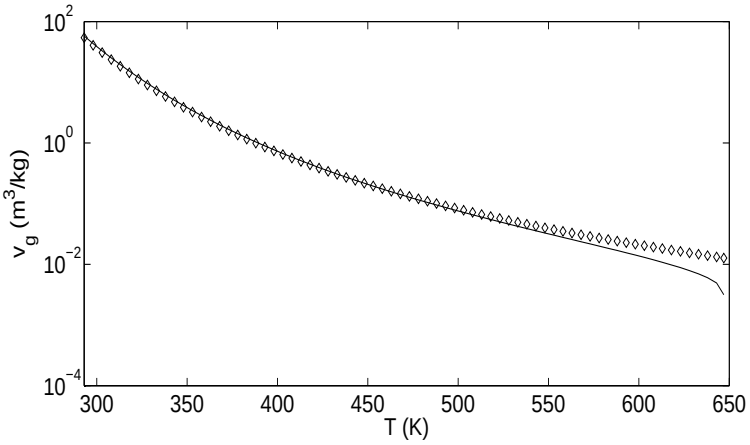

Figure 5.2: Saturation specific volume for the water vapor. Experimental curves are shown in lines and the SG-EOS approximation with symbols.

5.3.2 Determination of the SG-EOS for the liquid water

For the liquid water the situation is more complicated and the nonlinear feature for the internal energy is stronger. From the thermodynamic approximations it is known that the internal energy and the specific volume for the compressed water can be approximated by the saturated values, while the enthalpy of the compressed water is approximated by the saturated enthalpy by adding a correction, see e.g. Moran and Shapiro [91]. Moreover, the internal energy appears explicitly in the models. Thus we use the saturated values for the internal energy e and specific volume v in our criteria.

We start from the idea that the internal energy e is a convex function of the specific volume v. The relation between e and v is non linear, but the SG-EOS (5.11a) provides a linear approximation in the (p, v)-plane. Here, we choose two states from the saturation tables: The first state is the initial temperature of the liquid, i.e. the room temperature. The second state is chosen to be a little bit less than the critical temperature since near the critical temperature the quantities change dramatically. Indeed, we choose the first temperature $T_1 = 293$ K and the second temperature $T_2 = 623$ K. Note that the critical temperature is $T_{cr} = 647$ K.

The experimental data corresponding to T_1 and T_2 are, see [99, 141]:

$$\left|\begin{array}{l|l|l} p_{sat}(T_1) = 2339 \text{ Pa} & e_l(T_1) = 83.94 \times 10^3 \text{ J/kg} & v_l(T_1) = 0.001002 \text{ m}^3/\text{kg} \\ p_{sat}(T_2) = 16.514 \times 10^6 \text{ Pa} & e_l(T_2) = 1641.81 \times 10^3 \text{ J/kg} & v_l(T_2) = 0.00174 \text{ m}^3/\text{kg} \end{array}\right|$$

Substitute each group of the experimental data into the relation (5.11a). We obtain two equations

$$83.94 \times 10^3 = (0.001002)\frac{2339 + \gamma_l \pi_l}{\gamma_l - 1} + q_l, \tag{5.18}$$

$$1641.81 \times 10^3 = (0.00174)\frac{16.514 \times 10^6 + \gamma_l \pi_l}{\gamma_l - 1} + q_l. \tag{5.19}$$

Equations (5.18) and (5.19) are two equations of three variables, so a third equation is required. For the third equation we use the expression of the sound speed (5.14). The sound speed in the liquid water is 1482 m/s at $T_1 = 293$ K. Thus we get the following equation

$$(1482)^2 = 0.001002\gamma_l(2339 + \pi_l). \tag{5.20}$$

We have three equations with three unknowns. Solving the equations (5.18)-(5.20), we obtain

$$\gamma_l = 2.057, \qquad \pi_l = 1.066 \times 10^9, \qquad q_l = -1.994674 \times 10^6.$$

To determine C_{vl} we use the temperature expression (5.11c) with one of the known states. In fact this will produce a big error. Indeed the expression (5.11c) itself is an approximation derived initially from a linear approximation in terms of v, see Le Metayer et al. [80]. But it is expected in the bubble collapse that the water will stay at the initial temperature during the whole process. Thus we choose to use the initial state to find C_{vl} to reduce the error. Substituting the experimental data related to T_1 in (5.11c) we have $C_{vl} = 3.449 \times 10^3$ J/kg/K.

From (5.11a) and (5.11c) we can write the internal energy in terms of v and T, i.e.

$$e_l(T, v) = C_{vl}T + \pi_l v + q_l. \tag{5.21}$$

Also we can write the internal energy in terms of T and p as

$$e_l(T, p) = \frac{p + \gamma_l \pi}{p + \pi} C_{vl}T + q_l,$$

or

$$e_l(T) = \frac{p_{sat}(T) + \gamma_l \pi_l}{p_{sat}(T) + \pi_l} C_{vl}T + q_l. \tag{5.22}$$

To see the experimental curves versus the theoretical ones, we use the relation (5.21) and draw the internal energy versus the temperature. For v we use the values that are given in the saturation tables, see the left graph of Figure 5.3. Then we use the relation (5.22) and draw the internal energy versus the temperature, see the right graph of Figure 5.3.

In fact the relation (5.21) shows a reasonable agreement between the theoretical and experimental curves. But in this case the values of specific volume are taken directly from the tables. This indicates that the equation (5.21) provides a reliable description for the relation between the internal energy with T and v. But if the specific volume is written in terms of the saturation temperature, i.e. the internal energy is a function of temperature, then we see that the agreement between the experimental and theoretical curves is bad.

This is due to the choice of the temperature expression (5.11c). In other words, there is a relatively big error in the relation between T and v. To reduce the effect of this error we give more attention to the initial state since it is expected that the water outside the bubble will keep the initial temperature throughout all of the process of collapse as is explained above. However, we think that the expression (5.11c) for the temperature should be improved to give more realistic values.

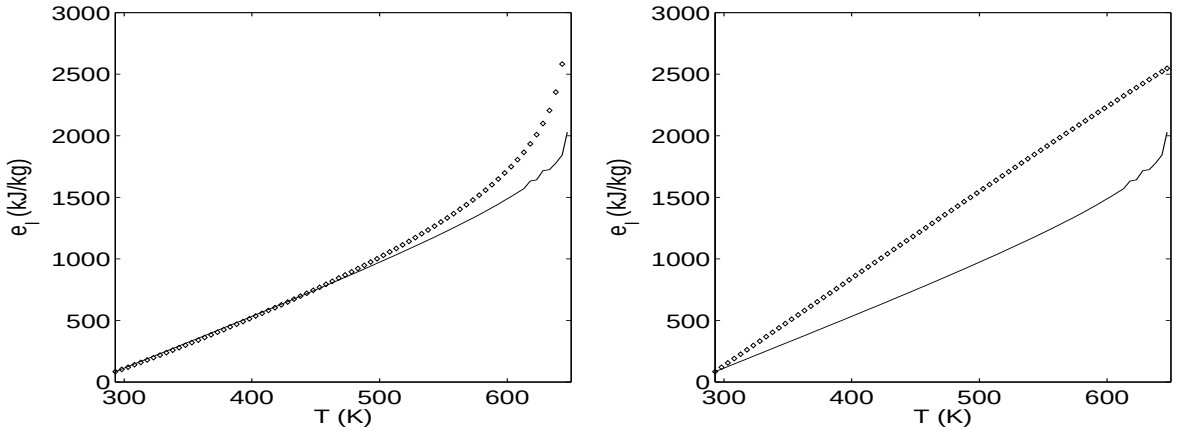

Figure 5.3: Saturation internal energy for the liquid water. Experimental curves are shown in lines and the SG-EOS approximation with symbols.

5.3.3 Determination of the entropy constants

To determine the entropy constants q_l' and q_g' the same idea of Le Metayer et al. [80] is used, i.e. at thermodynamic equilibrium the Gibbs free energies are equal, see equation (5.15). In our case we did not set any of the parameters to zero to avoid negative values for the entropy. Instead of that we take q_l' to satisfy the initial value of the entropy of the liquid. Then we choose q_g' in order to obtain a good fitting for the saturation curve.

The entropy of the liquid at $T_1 = 293$ K is $s_{l1} = 0.296$ kJ/kg/K. Using these data in (5.11d) we find $q_l' = 35.78$ kJ/kg/K.

We can obtain a good agreement to the experimental saturation curve in the range $293 - 500$ K if we choose $q_g' = 2.41$ kJ/kg/K, see Figure 5.4. Out of this range of temperature the agreement is bad. If the expected range of the temperature within specified range then this choice is enough, but if the temperature can exceed 500 K an improvement is required.

In fact to obtain a good agreement to the experimental saturation curve with one choice of q_g' in the whole range is impossible. Instead of that we choose more than one value to

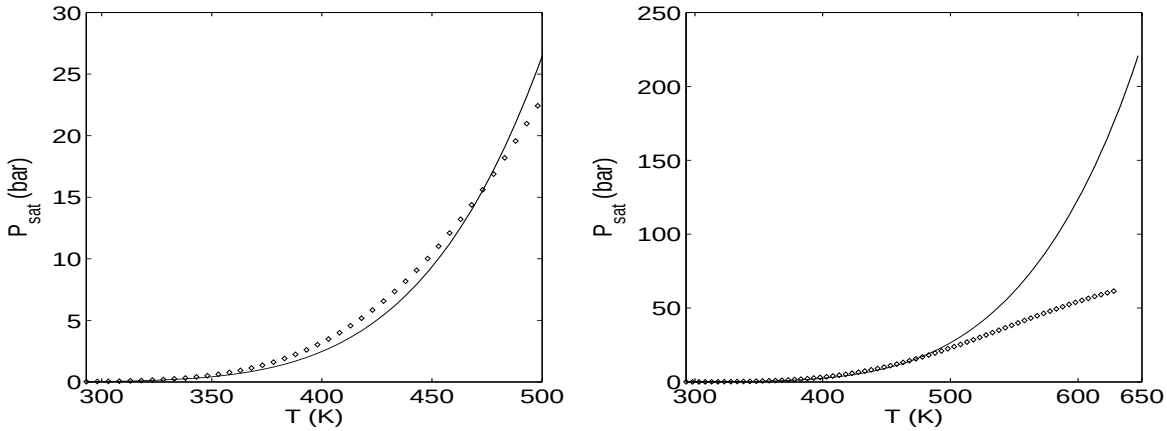

Figure 5.4: Saturation curve of the water. Experimental curves are shown in lines and the SG-EOS approximation with symbols.

q'_g depending on the temperature range. For example, choose $q'_l = 35.64$ kJ/kg/K and

$$q'_g = \begin{cases} 2.41, & T < 573 \\ 2.51, & 573 \leq T \leq 593 \\ 2.57, & 593 \leq T \leq 613 \\ 2.61, & T > 613 \end{cases} \tag{5.23}$$

where the unit of T is K and the unit of q'_g is kJ/kg/K. By these values the saturation curve is recovered for a wide range of temperature with a reasonable accuracy, see Figure 5.5.

In the computations of test problems in this chapter we saw that if the phase transition is included the interfacial temperature increases as the time evolves. After about 550 K the change of the temperature becomes very fast, then the bubble collapses. Thus, the several values of q'_g in (5.23) are used just for very short intervals of time with respect to the total time of the evolution. Thus for most time the computations are made with $q'_g = 2.41$ kJ/kg/K.

In Summary the parameters of the SG-EOS by this method are given in Table 5.2.

Phase	γ	$\pi(Pa)$	$C_v(J/kg/K)$	$q(J/kg)$	$q'(J/kg/K)$
vapor	1.327	0	1.2×10^3	1995×10^3	2.41×10^3
liquid	2.057	1.066×10^9	3.449×10^3	-1994.674×10^3	35.78×10^3

Table 5.2: EOS parameters for vapor and liquid water by the present method.

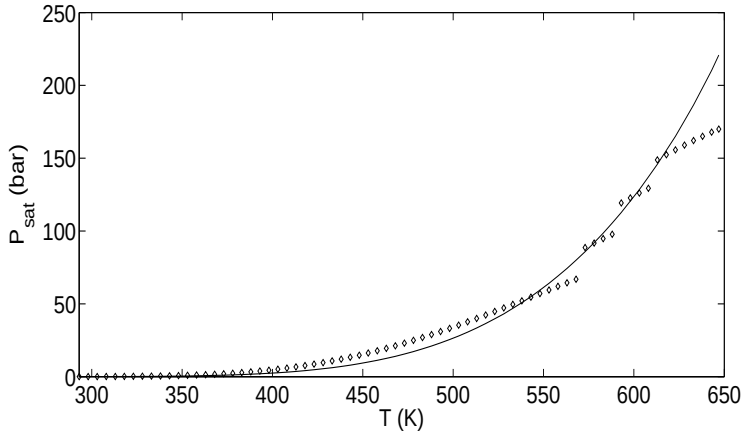

Figure 5.5: Saturation curve of the water. Experimental curves are shown in lines and the SG-EOS approximation with symbols.

5.4 Numerical method

The system (5.4) is solved by the numerical method that was introduced in Section 4.7. The only difference is that including the discretization of the geometrical terms (5.6). The discretization of these terms is considered in the hyperbolic step as the average between the left and right states of the cell. Indeed, the equations of the system (5.4) that are written in a conservative form are discretized as

$$\mathbf{u}_j^{n+1} = \mathbf{u}_j^n - \frac{\Delta t}{\Delta r}[\mathbf{f}(\mathbf{u}^*(\mathbf{u}_j^n, \mathbf{u}_{j+1}^n)) - \mathbf{f}(\mathbf{u}^*(\mathbf{u}_{j-1}^n, \mathbf{u}_j^n))] + \Delta t \mathbf{S}_{rj}^n,$$

where

$$\mathbf{u} = (\alpha_1\rho_1,\ \alpha_2\rho_2,\ \rho u,\ \rho e + \frac{1}{2}\rho u^2)^T,$$

$$\mathbf{f(u)} = (\alpha_1\rho_1 u,\ \alpha_2\rho_2 u,\ \rho u^2 + \alpha_1 p_1 + \alpha_2 p_2,\ u(\rho e + \frac{1}{2}\rho u^2 + \alpha_1 p_1 + \alpha_2 p_2))^T.$$

The numerical approximation $\mathbf{S}_{rj}^n$ of the geometrical source vector (5.6) is evaluated as the average between the left and right states $\mathbf{u}_j^n, \mathbf{u}_{j+1}^n$.

The volume fraction equation and the internal energy equations are discretized as

$$\alpha_{1j}^{n+1} = \alpha_{1j}^n - \frac{\Delta t}{\Delta r}((u\alpha_1)_{j+\frac{1}{2}}^* - (u\alpha_1)_{j-\frac{1}{2}}^* - \alpha_{1j}^n(u_{j+\frac{1}{2}}^* - u_{j-\frac{1}{2}}^*)),$$

$$(\alpha\rho e)_{kj}^{n+1} = (\alpha\rho e)_{kj}^n - \frac{\Delta t}{\Delta r}((\alpha\rho eu)_{k,j+\frac{1}{2}}^* - (\alpha\rho eu)_{k,j-\frac{1}{2}}^* + (\alpha p)_{kj}^n(u_{j+\frac{1}{2}}^* - u_{j-\frac{1}{2}}^*)) - \frac{2}{r_j}(\alpha\rho eu + \alpha pu)_{kj}^n.$$

The geometrical term $\frac{2}{r_j}(\alpha\rho eu + \alpha pu)_{kj}^n$ is taken as the average between the left and right states.

The same numerical procedure is easily extended to the system (5.9). The HLLC-type Riemann solver that was given in Subsection 4.4.3 and the pressure relaxation that was given in Subsection 4.4.4 are both extended directly for the system (5.9).

5.5 Numerical Results

In this section, we provide numerical computations for the dynamics of a laser-induced bubble. The results are shown by the six-equation model (5.4) for the two-phase flow if the bubble contains vapor only. While if the bubble contains a percentage of non-condensable gas also, then the three-phase model of nine equations (5.9) is used.

In all computations the CFL number is fixed to 0.6 and a uniform grid is used. The first Gibbs free energy relaxation procedure that was introduced in Subsection 3.6.3 is used when the mass transfer is included.

For validation we use the experimental radius-time curve that appears in Müller et al. [94]. Thus for all computations, unless mentioned, the initial conditions are taken as follows: The radius of the bubble $R_{max} = 0.75$ mm. The surrounding water has a pressure $p_l = 1$ bar and temperature $T_l = 293$ K.

Since the initial state inside the bubble is unknown, we choose several possibilities to provide a description for the dynamics of the collapsing bubble with different initial conditions. These tests include:

- The assumption of saturation state at temperature $T_v = 293$ K, i.e. the initial pressure is the saturation pressure $p_v = 2339$ Pa.
- Several tests with one temperature and different pressures.
- Several tests with one pressure and different temperatures.

The computational domain is taken to be suitably large compared to the bubble size to avoid the boundary effects. In our computations the domain is chosen to be the interval $[0, 99]$ mm. The left boundary conditions, i.e. at the center of the bubble, are the symmetric conditions. For the right boundary conditions, i.e. at the far wall of the domain, there are two choices in the literature. Müller et al. [94] assumed a reflected velocity at the far field wall. In Dreyer et al. [40] the velocity at the far wall is set to be zero. In our computations both choices are tested, there is no significant effect on the results. This may be due to the large size of the computational domain.

Since the grid is uniform and the computational domain is very large compared to the bubble radius, we choose to refer to the number of cells by N_I. Where N_I represents the number of cells inside the bubble from its center to its wall at the initial state, i.e. the number of cells that cover the maximum radius of the bubble at the initial state. In Table 5.3, the values of N_I are shown with the corresponding numbers of the cells in the whole domain.

N_I	250	500	750	1000
# of cells	33,000	66,000	99,000	132,000

Table 5.3: The concept of N_I.

For numerical reasons, we allow the presence of a small volume fraction of the liquid water inside the bubble and a small volume fraction of vapor outside the bubble, typically these small values are taken 10^{-6}.

5.5.1 Tests for vapor bubble

This subsection deals with the case that the bubble contains vapor only. Assume that the initial state inside the bubble is the saturation state, i.e. $T_v = 293$ K and $p_v = 2339$ Pa. The results without mass transfer are shown in Figure 5.6. If the mass transfer is included the results are shown in Figure 5.7.

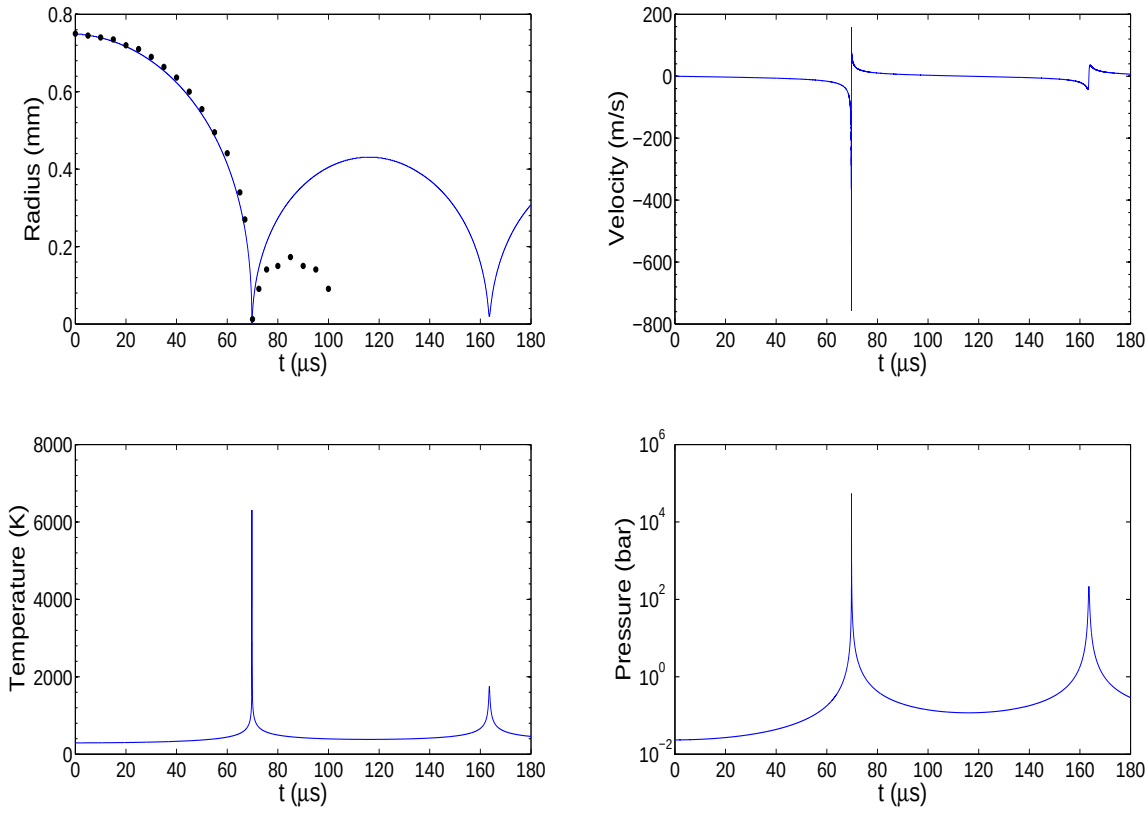

Figure 5.6: The collapse and rebound of the vapor bubble without mass transfer. The computed radius is compared with the experimental data (dots). The pressure and temperature are taken at the center of the bubble while the velocity at the interface. $N_I = 500$ cells, $T_v = 293$ K and $p_v = 2339$ Pa.

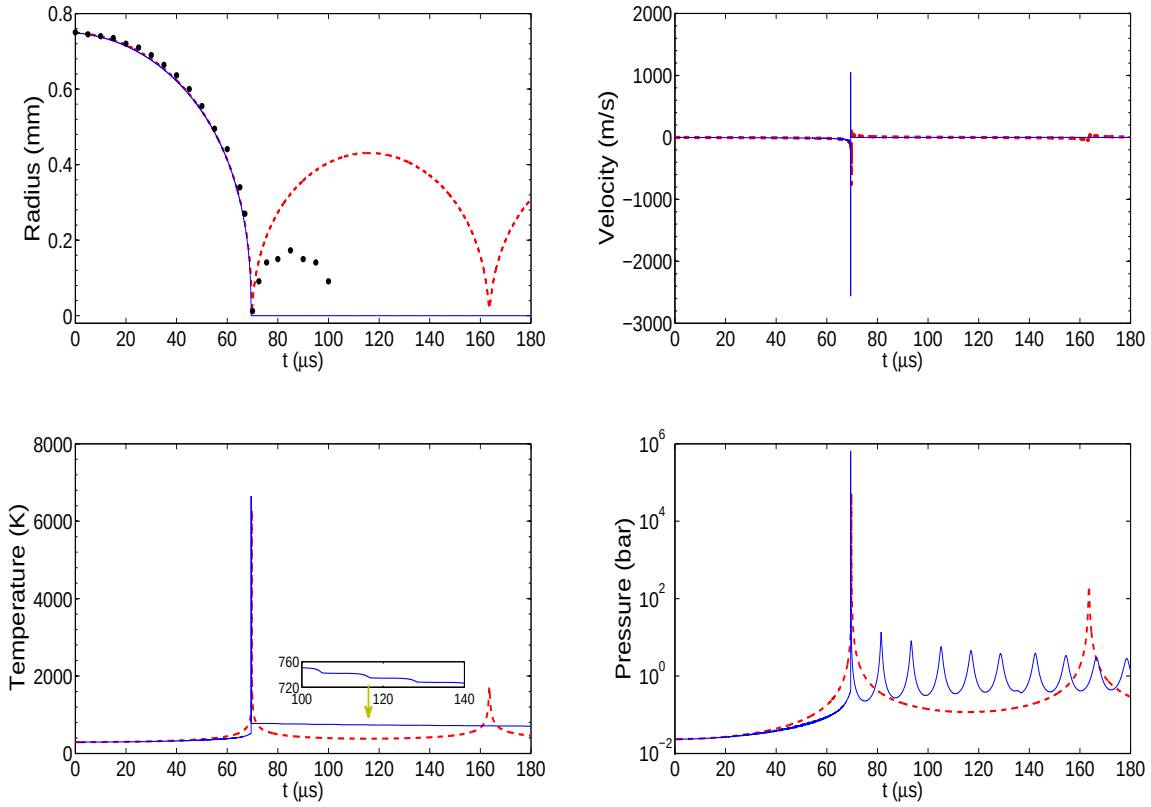

Figure 5.7: The collapsing vapor bubble results with mass transfer (solid line) compared to those without mass transfer (dashed line). The computed radii are compared with the experimental data (dots). The pressure and temperature are taken at the center of the bubble while the velocity at the interface. $N_I = 500$ cells, $T_v = 293$ K and $p_v = 2339$ Pa.

Following Akhatov et al. [5] and Dreyer et al. [40], the mass transfer is activated from the beginning of the evolution until the critical state is exceeded, the critical temperature of the water is $T_{cr} = 647$ K. If the interfacial temperature of the bubble exceeds the critical temperature the mass transfer is stopped. This is due to the fact that there is no difference between the phases at the bubble interface beyond the critical state. Then the mass transfer is activated again after the collapse when the temperature falls below the critical temperature.

In the computations, we observe that in the case with no mass transfer the temperature inside the bubble after reaching 1500 K increases rapidly and then the collapse occurs. The temperature reaches almost immediately a very high value (> 6000 K). If the phase transition is included the temperature after reaching 515 K increases rapidly and then the collapse occurs. The temperature again becomes greater than 6000 K.

It is clear from Figure 5.7 that there is no rebound if the phase transition is included. This occurs since most of the vapor mass leaves the bubble and there is no mechanism for a rebound. In real experiments this behavior is not observed. Always there is a rebound of the bubble. This motivates us to consider a percentage of non-condensable gas inside the bubble besides the water vapor. This will be investigated numerically in Subsection 5.5.2.

The radius-time curves before the collapsing point are coinciding and in an excellent agreement with the experimental data, see the radius graph in Figure 5.7. The collapse occurs slightly earlier if the mass transfer is included. Indeed, in this case the collapse occurs at time $t = 69.431\ \mu s$, while if the mass transfer is excluded the collapse occurs at time $t = 69.743\ \mu s$. Both values for the collapsing time are very close to the experimental value $t = 70.7\ \mu s$.

In the computations, before the instant of the collapse, we observe that the temperature and the pressure inside the bubble when the phase transition is included is less than the corresponding values if the phase transition is not considered, see Figures 5.7 and 5.8. In Figure 5.8 the temperature and the pressure are shown before the collapse point. We think this behavior is physically correct, since a part of the energy inside the bubble is consumed by the phase transition process.

At the collapse time, both the pressure and the temperature at the center of the bubble almost jump to very high values. These values are higher in the case of mass transfer than the case without mass transfer. This indicates that the collapse is more violent if the mass transfer is included and the bubble vanishes. In fact we cannot say more about how the physics of this behavior is. Moreover, there seems to be no way to check such comparisons experimentally.

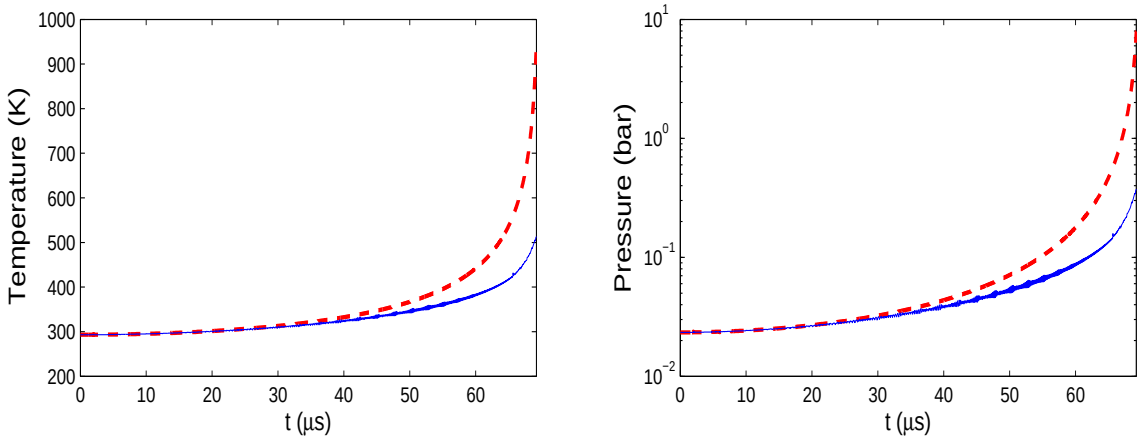

Figure 5.8: The center temperature and pressure of the bubble before the collapse instant. The Results with mass transfer (solid line) compared to those without mass transfer (dashed line). The graphs here are some zoom of the temperature and pressure graphs in Figure 5.7.

In the case of phase transition after the collapse the bubble vanishes, so it is expected that after a certain time the pressure and the temperature in all of the domain will be like the values of the liquid water. From the pressure profile we see after the collapse point that there are some oscillations around the value of atmospheric pressure. From the temperature profile we see that the temperature remains quite high. In fact even though the bubble vanishes there still is a certain small remaining vapor concentration. This is shown in Figure 5.9. The left side graphs are shown for a very small domain while the right graphs are shown for the distance equal to the initial maximum radius. It is clear from the figure that there still is some concentration of vapor at the bubble center. Moreover, the oscillations of the pressure in Figure 5.7 have decreasing amplitudes in time, also the temperature decreases with time but very slowly.

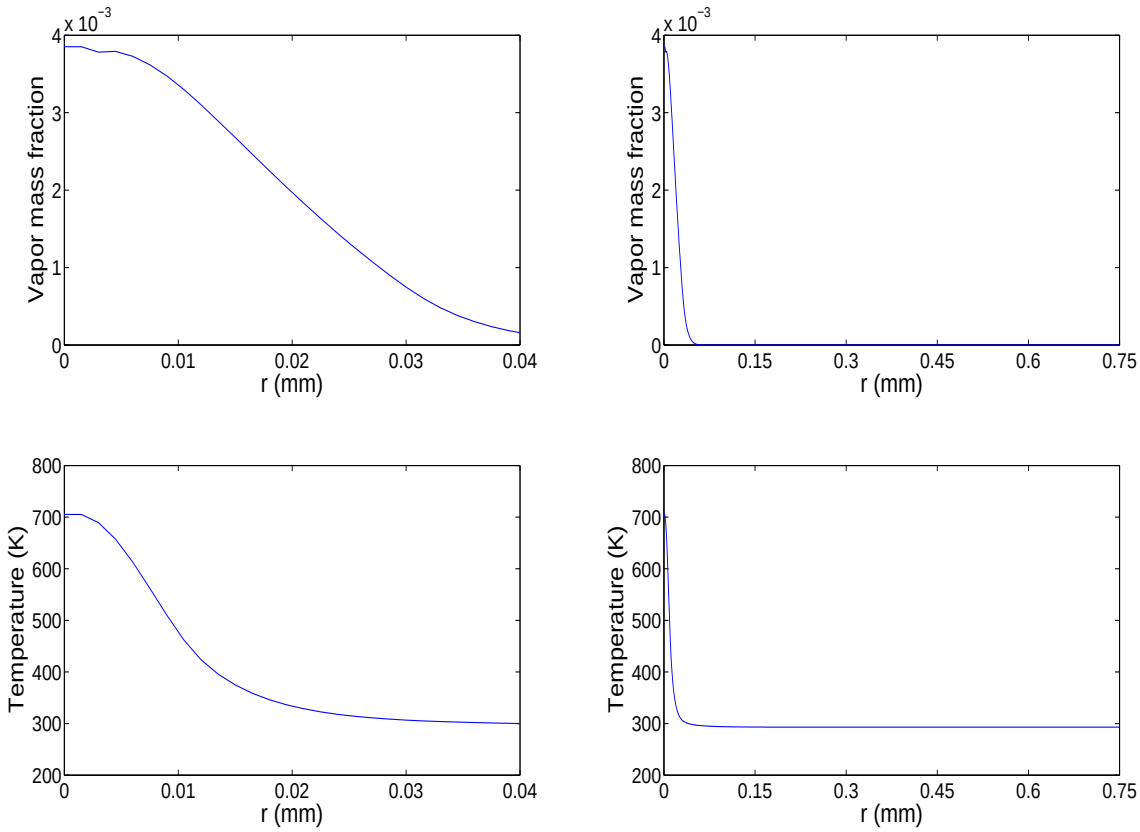

Figure 5.9: The vapor mass fraction and temperature versus radial direction if the phase transition is included at time $t = 180\ \mu s$. With $N_I = 500$ cells, $T_v = 293$ K and $p_v = 2339$ Pa.

We repeat the same problem with a different number of cells, without mass transfer as shown in Figures 5.10 and 5.12 as well as with mass transfer as in Figure 5.13. A common feature is that before the instant of the collapse all curves are almost coinciding. In addition there is an excellent agreement with the experimental data.

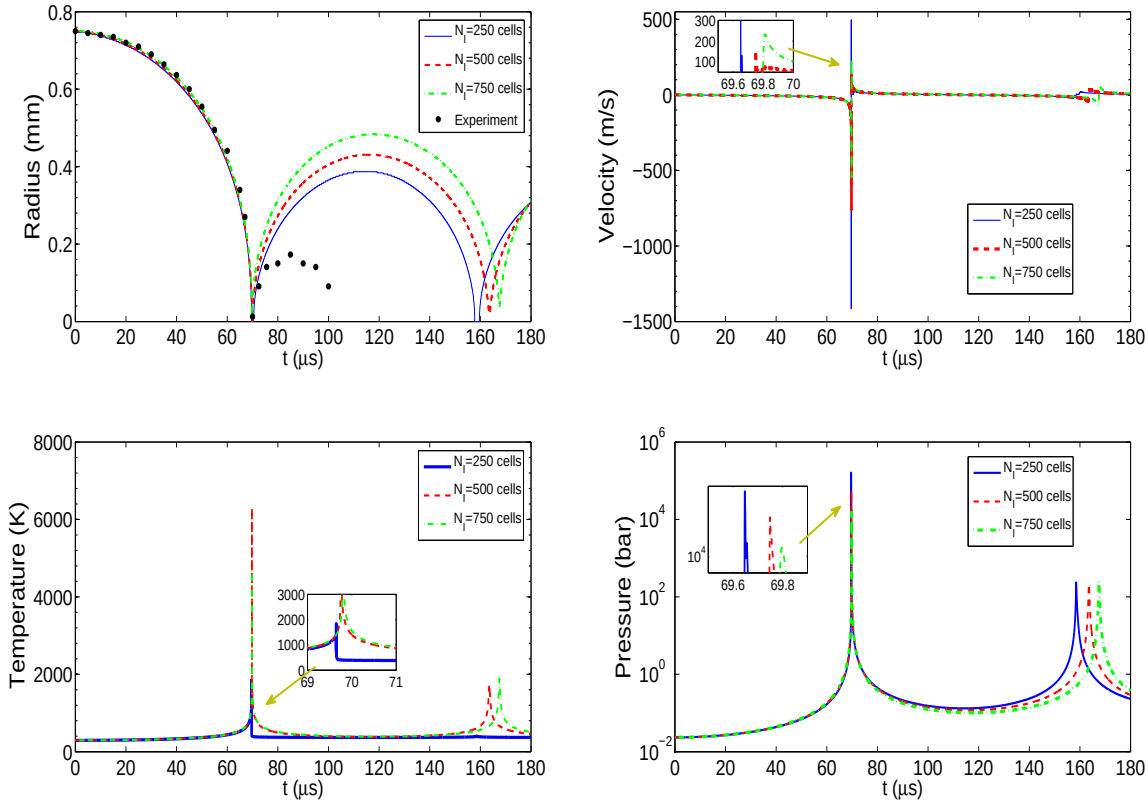

Figure 5.10: Vapor bubble without mass transfer, comparison using several grids. The computed radii are compared with the experimental data (dots). The pressure and temperature are taken at the center of the bubble while the velocity at the interface. Initial values $T_v = 293$ K and $p_v = 2339$ Pa.

Figure 5.10 shows that there is a significant difference between the curves for a different number of cells after the collapse point. To understand the reasons we draw the volume fraction profiles at different instants of time, see Figure 5.11. It is clear that the interface diffusion is less if the number of cells is higher. Long before the time of collapse the diffusion in the curves is very small, thus the radius curves coincide, see graph (a), the results are shown at time $t = 50\ \mu s$. Around the time of collapse the curves start to diffuse. See graphs (b) and (c), where the diffusion now became more serious. Graphs (d) and (e) show the results after the collapse but still very close to the collapsing time. There is a big diffusion across the interface especially for $N_I = 250$ cells. The diffusion will be reduced again as the time evolves as in graph (f), but now the curves remain clearly distinct from each other. This produces the differences in the radii curves. Hence, we conclude that the diffusion of the curves increase around the collapse point. In addition, the pressure and temperature relaxations reduce some amount of the vapor inside the bubble, this is higher if the interface is more diffusive. Thus passing through the collapse point the diffusion has a significant effect which will continue to be observed after the collapse. So it is important to reduce the diffusion as much possible.

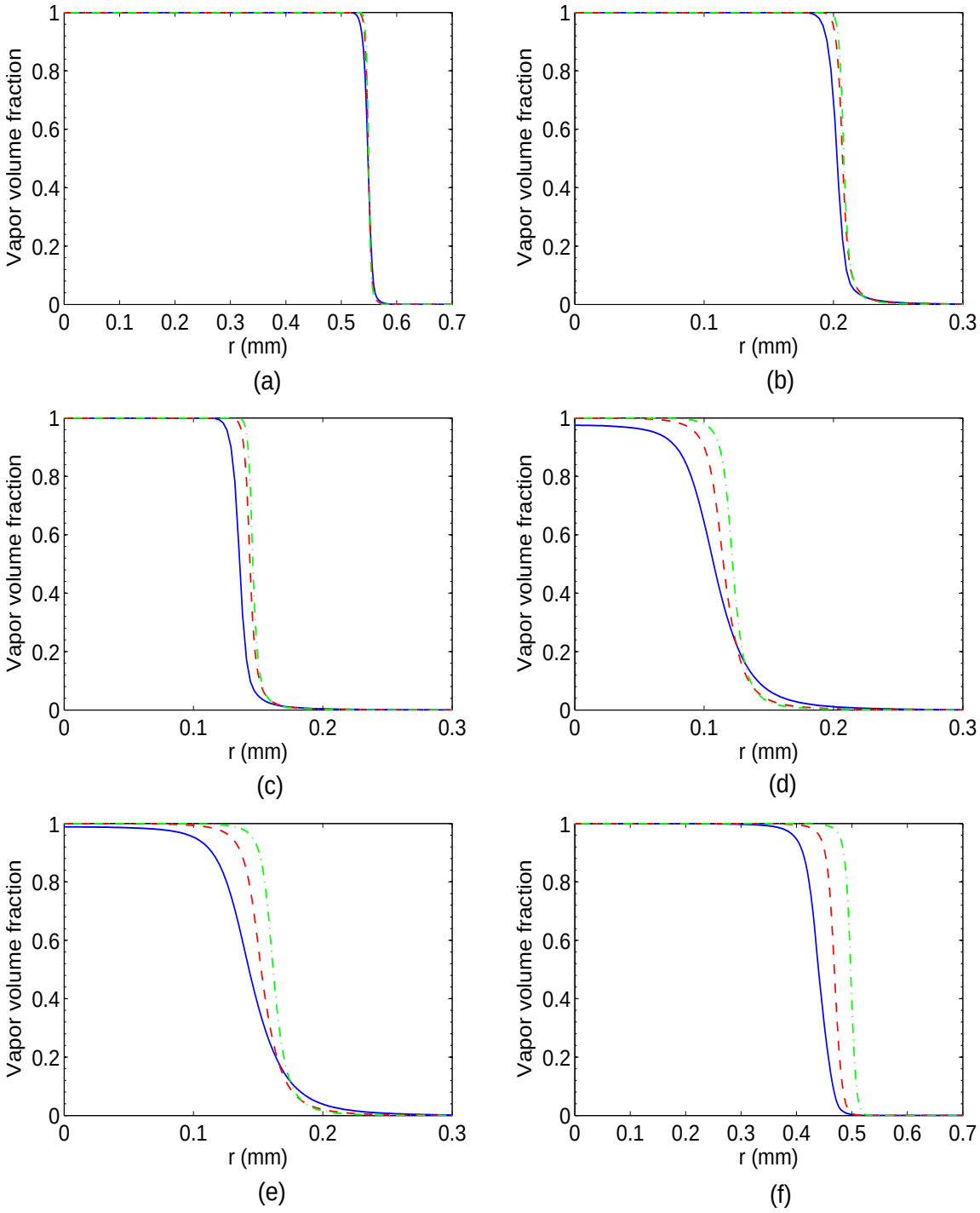

Figure 5.11: Vapor volume fraction profiles of the results in Figure 5.10, they are shown at times (a) $t = 50\ \mu s$ (b) $t = 68\ \mu s$ (c) $t = 69\ \mu s$ (d) $t = 71\ \mu s$ (e) $t = 72\ \mu s$ (f) $t = 120\ \mu s$. The computations are made with $N_I = 250$ cells (solid line), $N_I = 500$ cells (dashed line), and $N_I = 750$ cells (dashed-dotted line).

In the temperature profiles of Figure 5.10 one cannot conclude anything about the effect of the number of cells on the direction of the maximal temperature at the collapse time. This may come from the big diffusion for $N_I = 250$ cells.

We repeated the results with a higher number of cells as in Figure 5.12. In this figure we see that all curves behave in similar manner if the number of cells is increased.

In the case of phase transition as in Figure 5.13, it is clear that the bubble vanishes in all cases. There are noticeable differences in other values as the number of cells is increased. This is effected by the diffusion of the interface, where in the case of $N_I = 250$ cells the bubble vanishes before the others and the concentration of the mass fraction after the collapse times is lower.

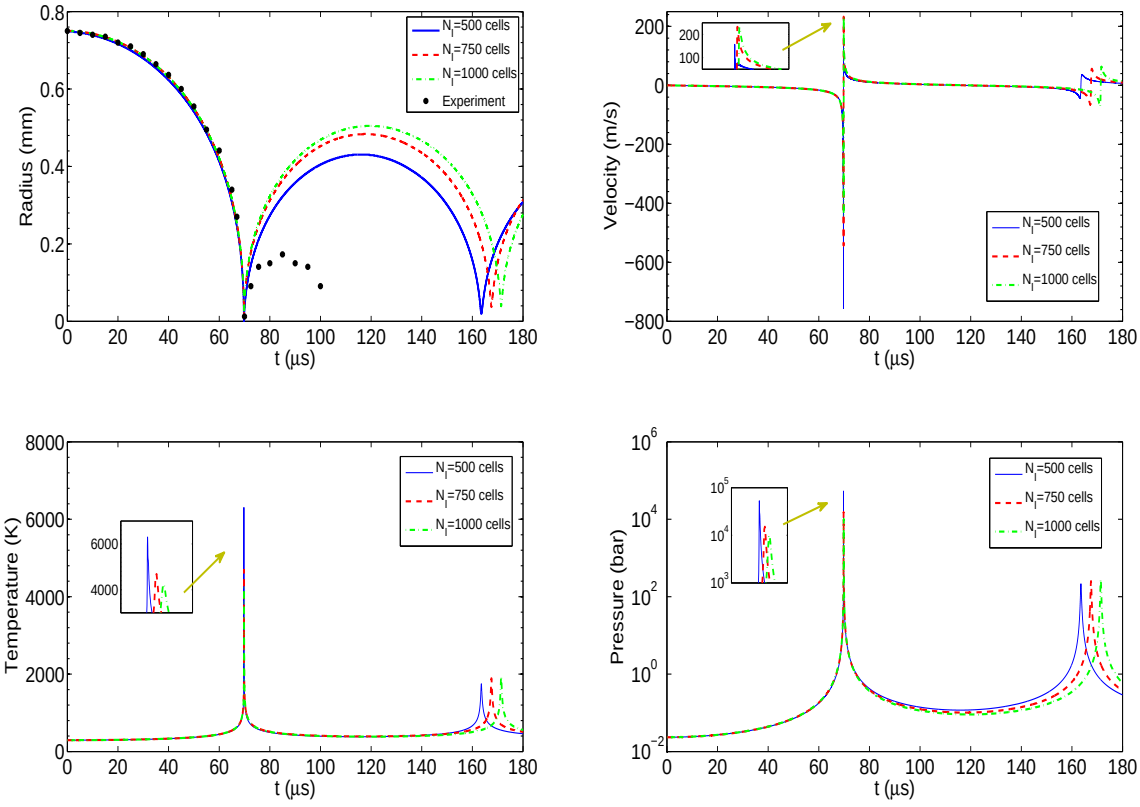

Figure 5.12: Vapor bubble without mass transfer, comparison at several grids. The computed radii are compared with the experimental data (dots). The pressure and temperature are taken at the center of the bubble while the velocity at the interface. Initial values $T_v = 293$ K and $p_v = 2339$ Pa.

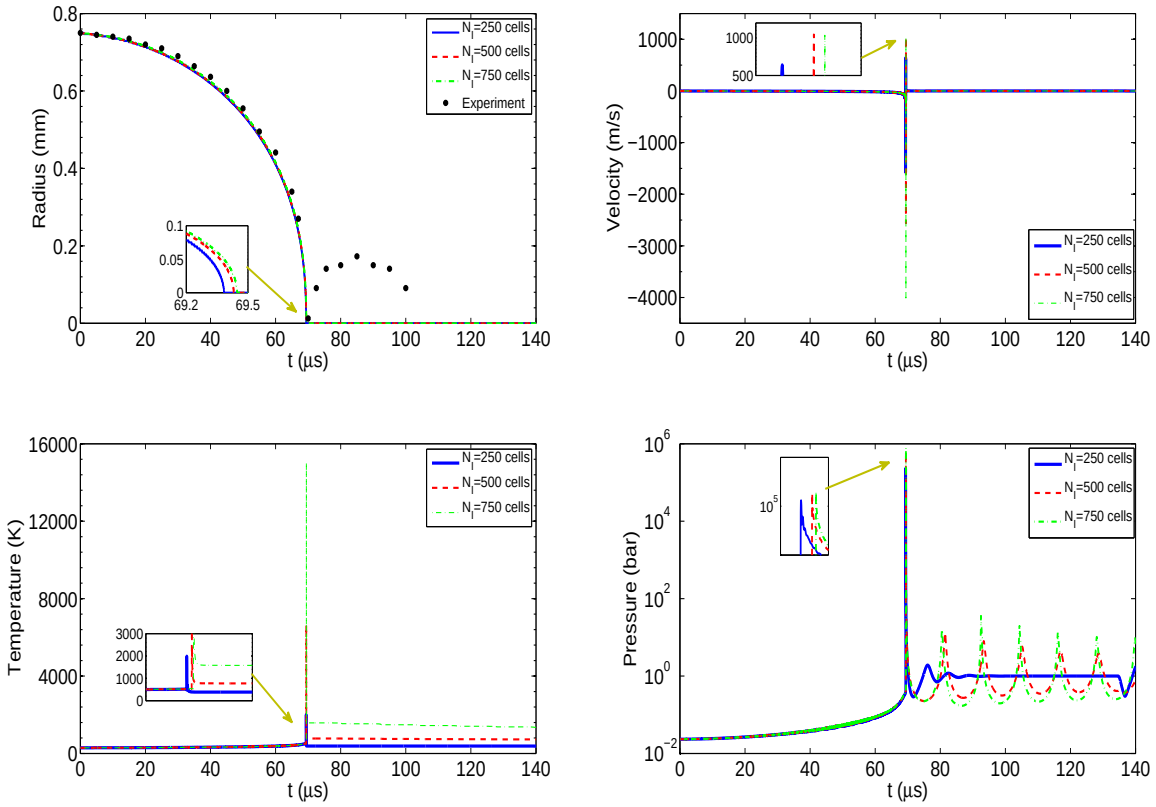

Figure 5.13: Vapor bubble with mass transfer, comparison at several grids. The computed radii are compared with the experimental data (dots). The pressure and temperature are taken at the center of the bubble while the velocity at the interface. Initial values $T_v = 293$ K and $p_v = 2339$ Pa.

However, in both cases, i.e. with or without phase transition the diffusion of the interface has bad consequences on the results after the collapse point. A similar problem was also discussed in Müller et al. [94] for the Saurel and Abgrall model [120], i.e. the seven-equation model.

In next tests to reduce the effects of diffusion we use a relatively high number of cells, we use $N_I = 500$ cells. In fact using high number of cells is expensive. Thus the issue of diffusion requires more investigation.

Let us now study the effects of the initial values of the temperature and the pressure inside the bubble on its dynamics.

First, we keep the temperature inside the bubble constant at $T_v = 293$ K and change the values of the pressure. The results for the case without mass transfer are shown in Figure 5.14. We see the following features in the results for the lower initial pressure:

- The collapse occurs earlier.
- The rebound is faster and more damped.
- The values of pressure, temperature and velocity are higher at the collapse instant.

If the phase transition is included the results are shown in Figure 5.15. For lower pressure the collapse occurs earlier with a higher temperature. The velocities and pressures are almost the same.

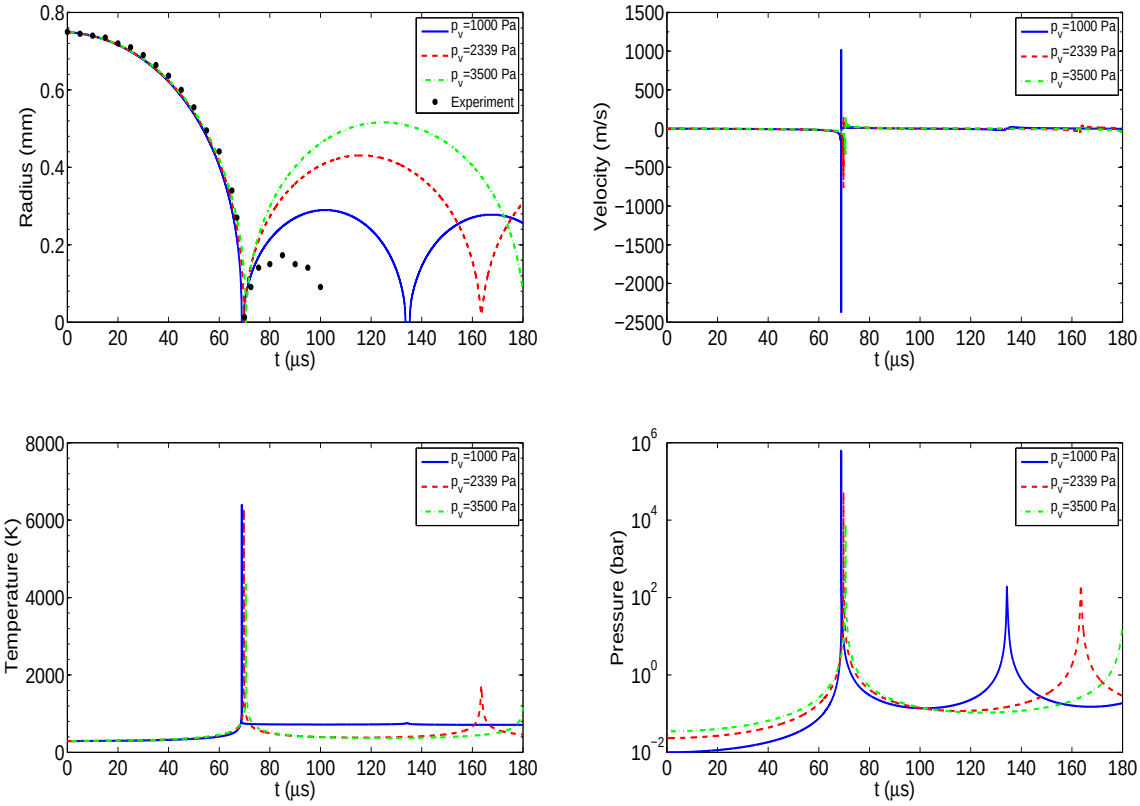

Figure 5.14: Vapor bubble without mass transfer, comparison between different initial bubble pressures at $T_v = 293$ K. The computed radii are compared with the experimental data (dots). The pressure and temperature are taken at the center of the bubble while the velocity at the interface. The computations are made with $N_I = 500$ cells.

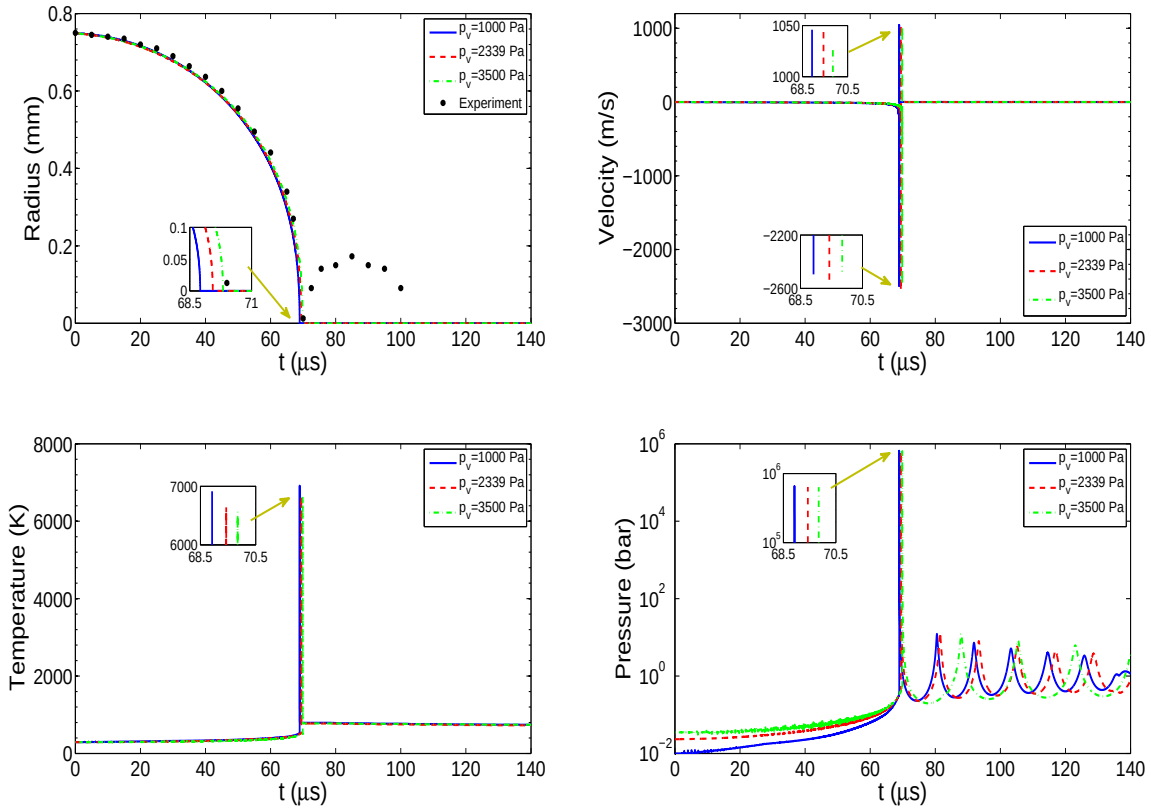

Figure 5.15: Vapor bubble with mass transfer, comparison between different initial bubble pressures at $T_v = 293$ K. The computed radii are compared with the experimental data (dots). The pressure and temperature are taken at the center of the bubble while the velocity at the interface. The computations are made with $N_I = 500$ cells.

Second, we keep the initial pressure inside the bubble constant at $p_v = 2339$ Pa and change the temperature. The results are shown in Figure 5.16 with no mass transfer and in Figure 5.17 if the mass transfer is included. The differences between the curves in both figures are small. In both cases, it is noted that for the higher initial temperature the collapse is a little bit faster and the temperature at the center of the bubble after the collapse is higher.

Whatever the initial state inside the bubble we can conclude the following results for the collapsing of the vapor bubble:

- There is no rebound of the bubble after the collapse if the mass transfer is included.
- In all cases at the collapse time the pressure and temperature at the bubble center

jump to very high values. The high pressure shows the importance of considering compressibility for the surrounding water.

- Before the collapse time the curves for the radius of the bubble in all cases are coinciding. In addition, in this period there is a perfect agreement with the experimental data.
- The pressure and temperature inside the bubble before the collapse time when the mass transfer is included are less than those values with no mass transfer. This is due to the loss of energy by the phase transition process.
- In the cases of no mass transfer it is noted that the first collapse is much more violent than the second one.

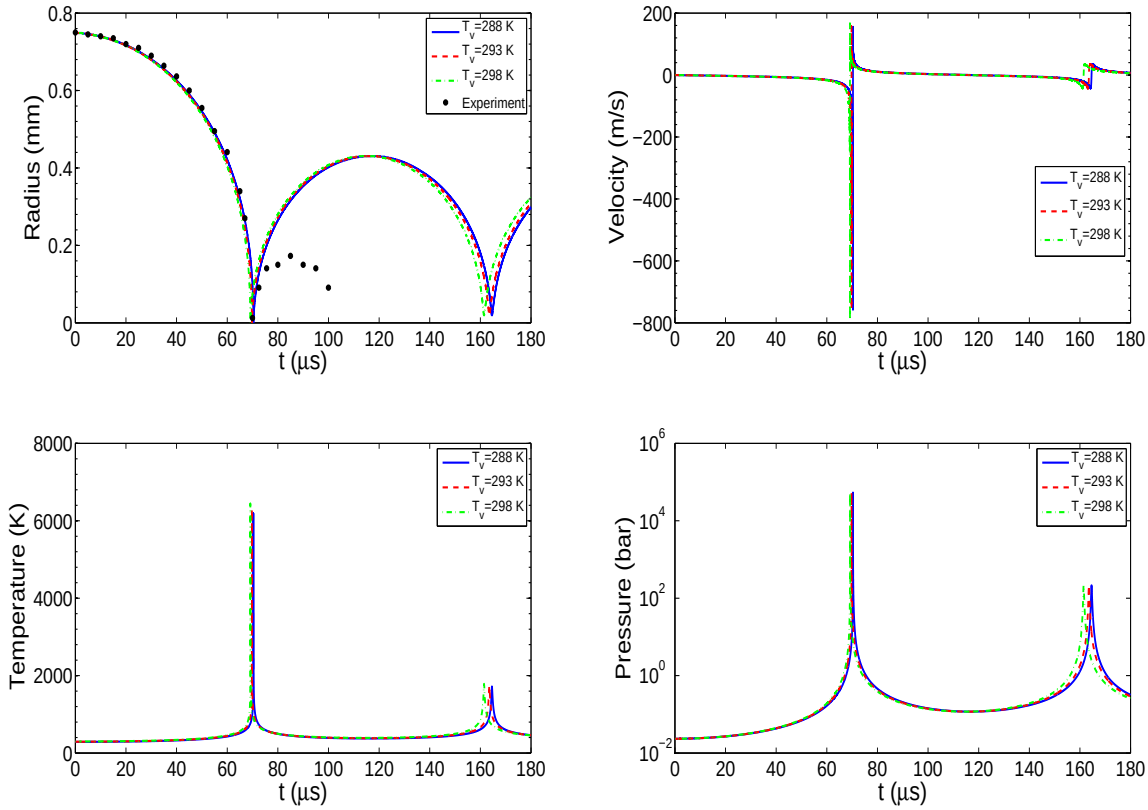

Figure 5.16: Vapor bubble without mass transfer, comparison between different initial bubble temperatures at $p_v = 2339$ Pa. The computed radii are compared with the experimental data (dots). The pressure and temperature are taken at the center of the bubble while the velocity at the interface. The computations are made with $N_I = 500$ cells.

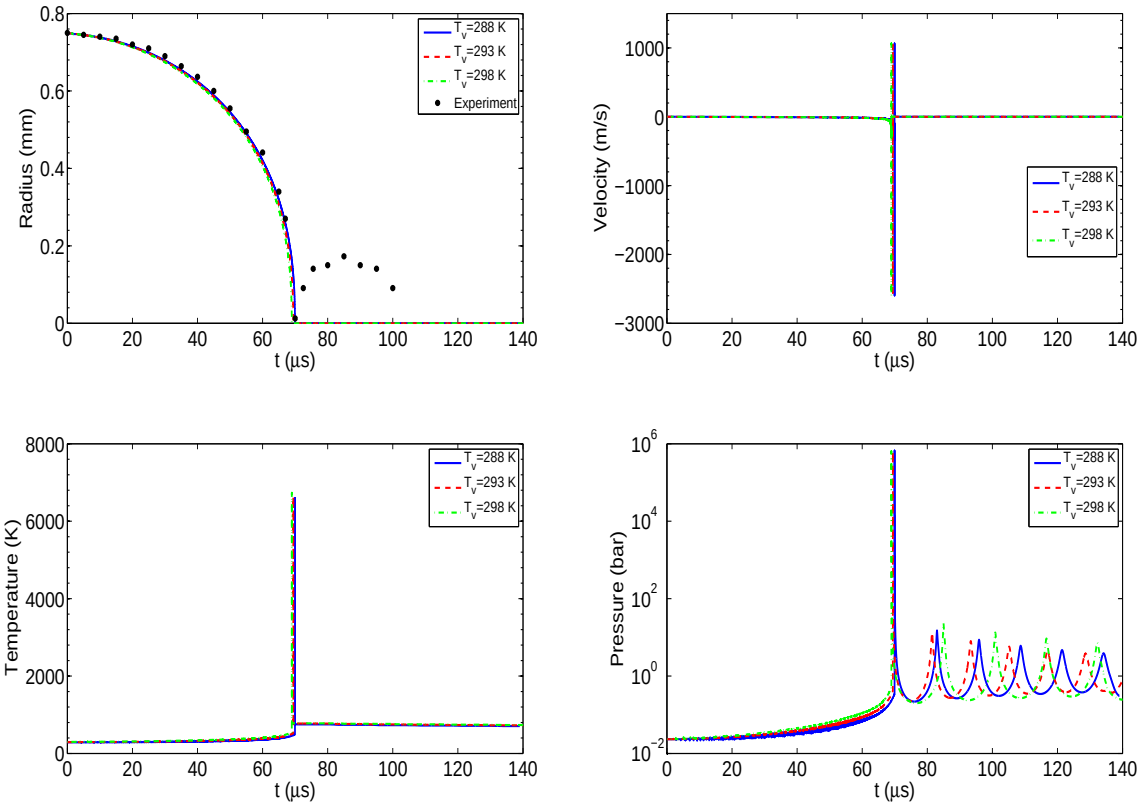

Figure 5.17: Vapor bubble with mass transfer, comparison between different initial bubble temperatures at $p_v = 2339$ Pa. The computed radii are compared with the experimental data (dots). The pressure and temperature are taken at the center of the bubble while the velocity at the interface. The computations are made with $N_I = 500$ cells.

5.5.2 Tests for gas-vapor bubble

In the tests of this subsection, besides the vapor inside the bubble we assume a percentage of non-condensable gas. The existence of such gas is justified physically, but its specific nature is not really known. As our aim is just to consider the general effect of the existence of such gas we use several assumptions. Following Dreyer et al. [40], Hydrogen H_2 and Oxygen O_2 are most probably present since they are the components of water and may be produced by the plasma due to the laser beam. Here we deal with both gases, i.e. Hydrogen or Oxygen.

We assume that the non-condensable gas obeys the SG-EOS, i.e. it obeys equations (5.11). For both Hydrogen and Oxygen we assume $\gamma = 1.4$, $\pi = 0$ and $q = 0$. For Hydrogen we use $C_v = 10.1$ kJ/kg/K. For Oxygen we take $C_v = 0.662$ kJ/kg/K.

Consider a saturation state inside the bubble at temperature $T = 293$ K, i.e. the pressure is $p = 2339$ Pa. Then, assume an initial 1% of Hydrogen mass inside the bubble. Always, for numerical reasons, we assume a small volume fraction of non-condensable gas outside the bubble, i.e. in the liquid water, typically 10^{-6}. The results with mass transfer are shown in Figure 5.18 for vapor and gas-vapor bubbles.

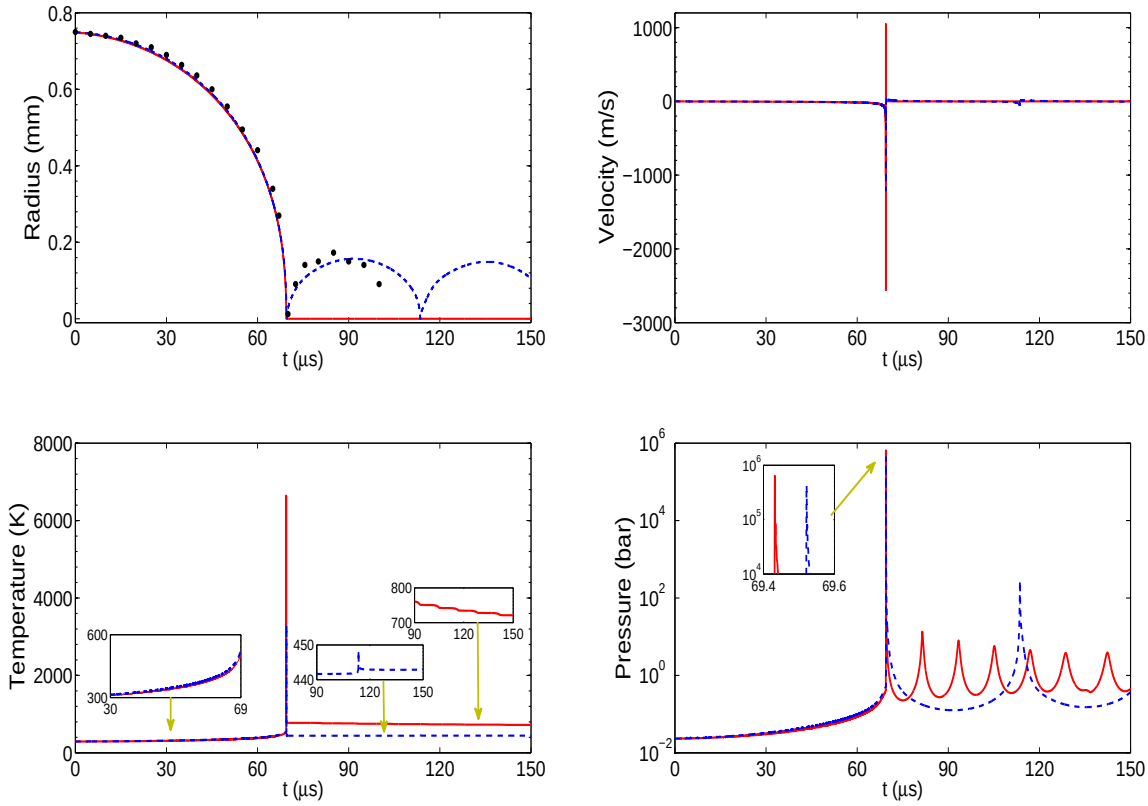

Figure 5.18: Bubble results with mass transfer, comparison between the results of vapor bubble (solid line) with gas-vapor bubble (dashed line). The computed radii are compared with the experimental data (dots). The pressure and temperature are taken at the center of the bubble while the velocity at the interface. Computations are made with $N_I = 500$ cells, initial state inside the bubble: $T = 293$ K and $p = 2339$ Pa. The non-condensable gas is Hydrogen with a mass fraction of 1%.

The main feature of the results is that: *The bubble rebounds again after the collapse if it contains a non-condensable gas, whereas the bubble dies if it contains vapor only.* In fact, in the literature there are two different considerations of this experiment and the issue of rebound. For example, the numerical results of Akhatov et al. [5] show that the existence of non-condensable gas has a strong influence on the dynamics of the bubble. But in their

results the rebound occurs even if the bubble contains vapor only. A different consideration was proposed by Dreyer et al. [40]. It depends on some fundamental thermodynamic properties. Due to these the rebound of the bubble after the first collapse is possible only if there is a non-condensable gas inside the bubble. Our computational results confirm the ideas of Dreyer et al. [40]. However, this point requires more investigations.

It is clear from Figure 5.18 that the maximal values of temperature, pressure and velocity are reduced for the gas-vapor bubble. Moreover, the temperature and pressure inside the bubble before the instant of collapse are smaller in the results of vapor bubble than those of gas-vapor bubble. Again we think this is physical since the action of the phase transition is stronger in the vapor bubble than in the gas-vapor bubble.

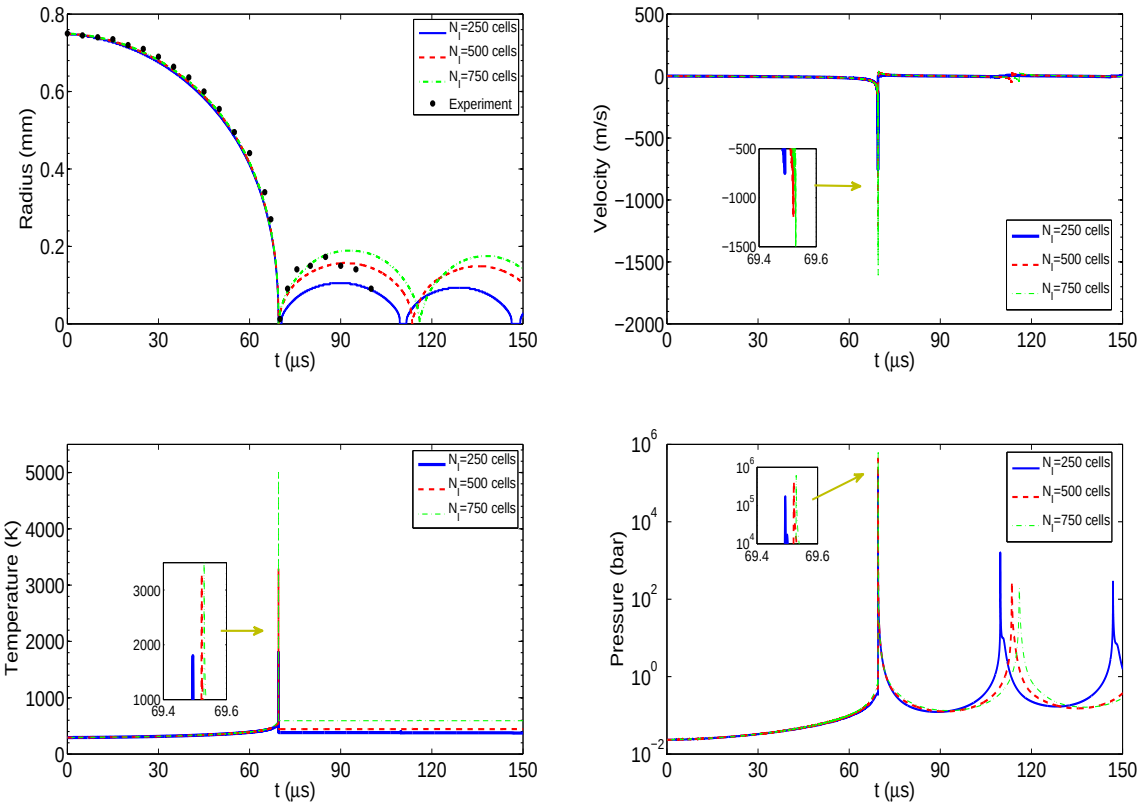

Figure 5.19: Gas-vapor bubble with mass transfer, comparison at different grids. The computed radii are compared with the experimental data (dots). The pressure and temperature are taken at the center of the bubble while the velocity at the interface. Initial state inside the bubble: $T = 293$ K and $p = 2339$ Pa. The non-condensable gas is Hydrogen with a mass fraction of 1%.

Figure 5.19 shows the results for a gas-vapor bubble using a different number of computational cells. The same previous conditions with a mass fraction of 1% of Hydrogen are used. We see in all cases that the bubble rebounds after the collapse. The differences in the curves are due to the diffusion of the interface especially through passing the collapse point, see the discussion in the previous subsection.

For more validation consider the gas-vapor bubble with the same initial state except that instead of Hydrogen we assume Oxygen with a mass fraction of 2.2%. The results are shown in Figure 5.20. To achieve this percentage we set the initial value of the volume fraction of the Oxygen to be 0.015. For the previous case of Hydrogen to get 1% of mass fraction we set the initial volume fraction to 0.1. These values depend on the values of heat capacity C_v since we keep the temperature constant.

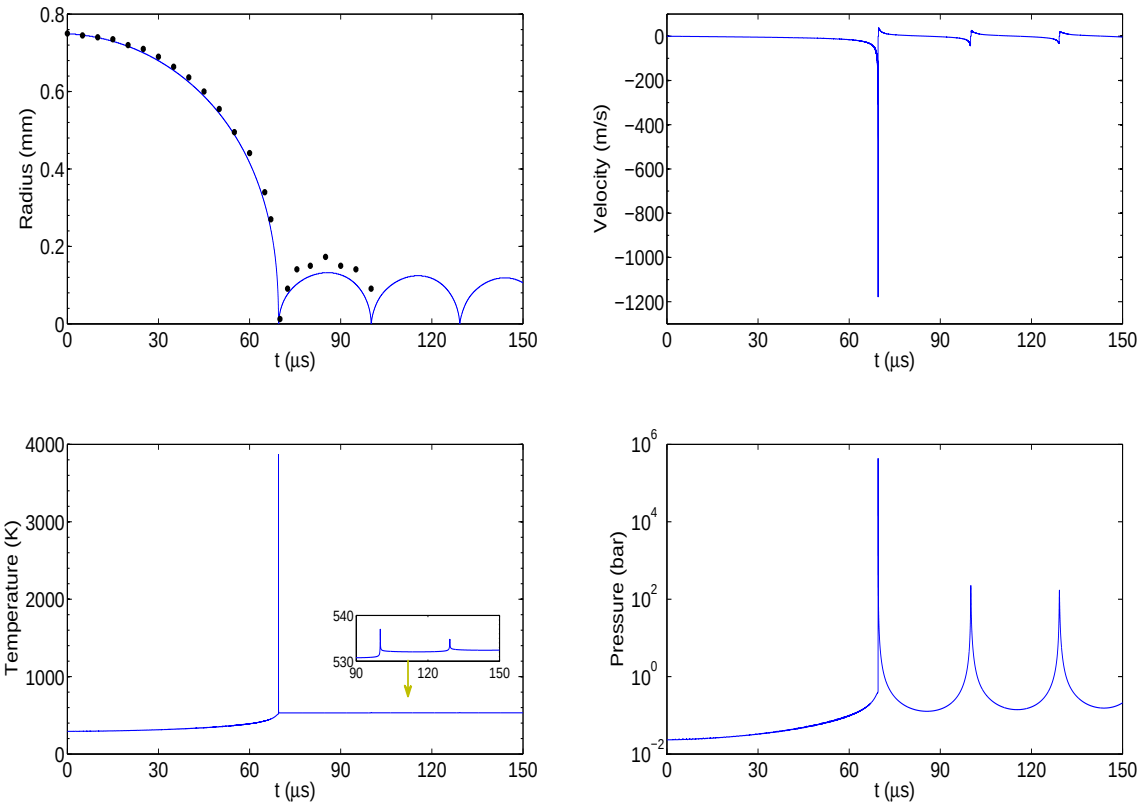

Figure 5.20: Gas-vapor bubble with mass transfer, the non-condensable gas is Oxygen with a mass fraction of 2.2%. The computed radii are compared with the experimental data (dots). The pressure and temperature are taken at the center of the bubble while the velocity at the interface. Computations are made with $N_I = 500$ cells, initial state inside the bubble: $T = 293$ K and $p = 2339$ Pa.

Consider the same gas-vapor problem with Oxygen as a non-condensable gas with different percentages. This is shown in Figure 5.21. For the lower value of volume fraction we note that the maximum radius after the collapse is smaller and the center temperature is higher.

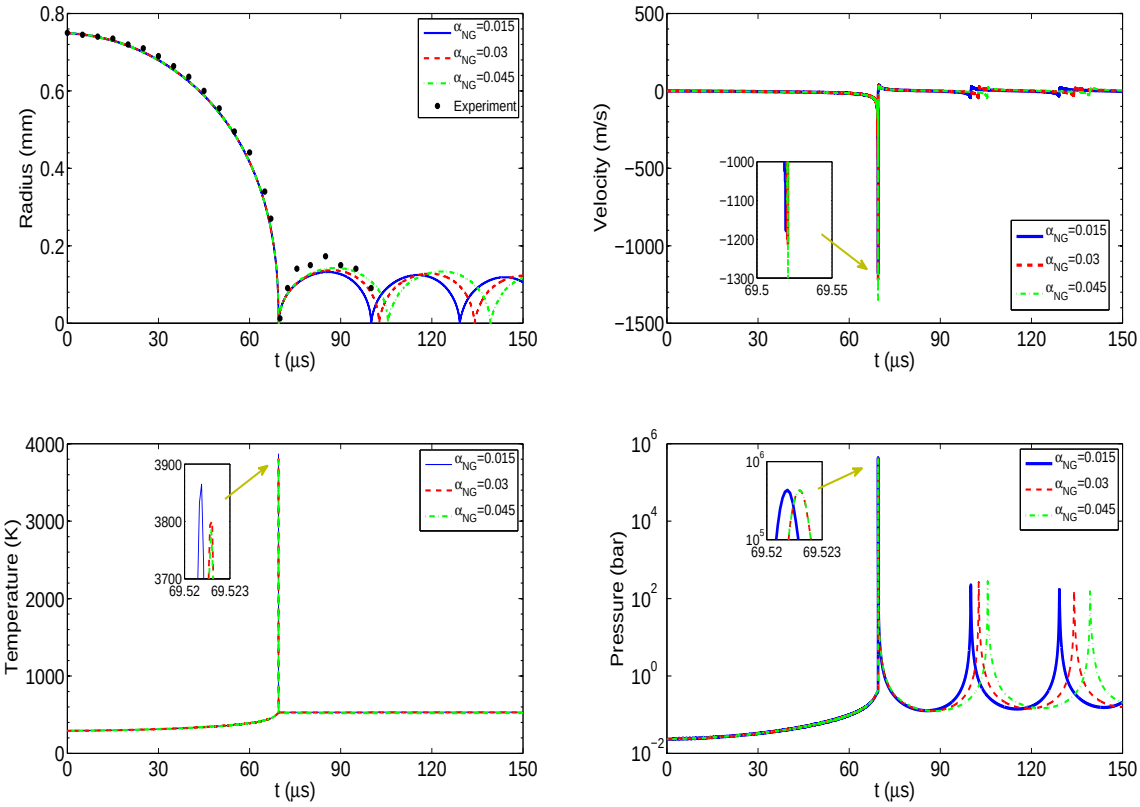

Figure 5.21: Gas-vapor bubble with mass transfer, the non-condensable gas is Oxygen with different percentages. The computed radii are compared with the experimental data (dots). The pressure and temperature are taken at the center of the bubble while the velocity at the interface. Computations are made with $N_I = 500$ cells, initial state inside the bubble: $T = 293$ K and $p = 2339$ Pa. Note that NG stands for non-condensable gas.

In Figures 5.22 and 5.23 the solution of the problem is shown for different assumptions for the non-condensable gas, i.e. different values of the specific heat C_v. In Figure 5.22 the results are shown with an assumption of a 2% mass fraction for all gases. For Figure 5.23 the volume fraction is taken to be 0.045 for all gases. The results in Figure 5.23 are very close. Thus the equal initial volume fractions for different non-condensable gases give results not so far from each other.

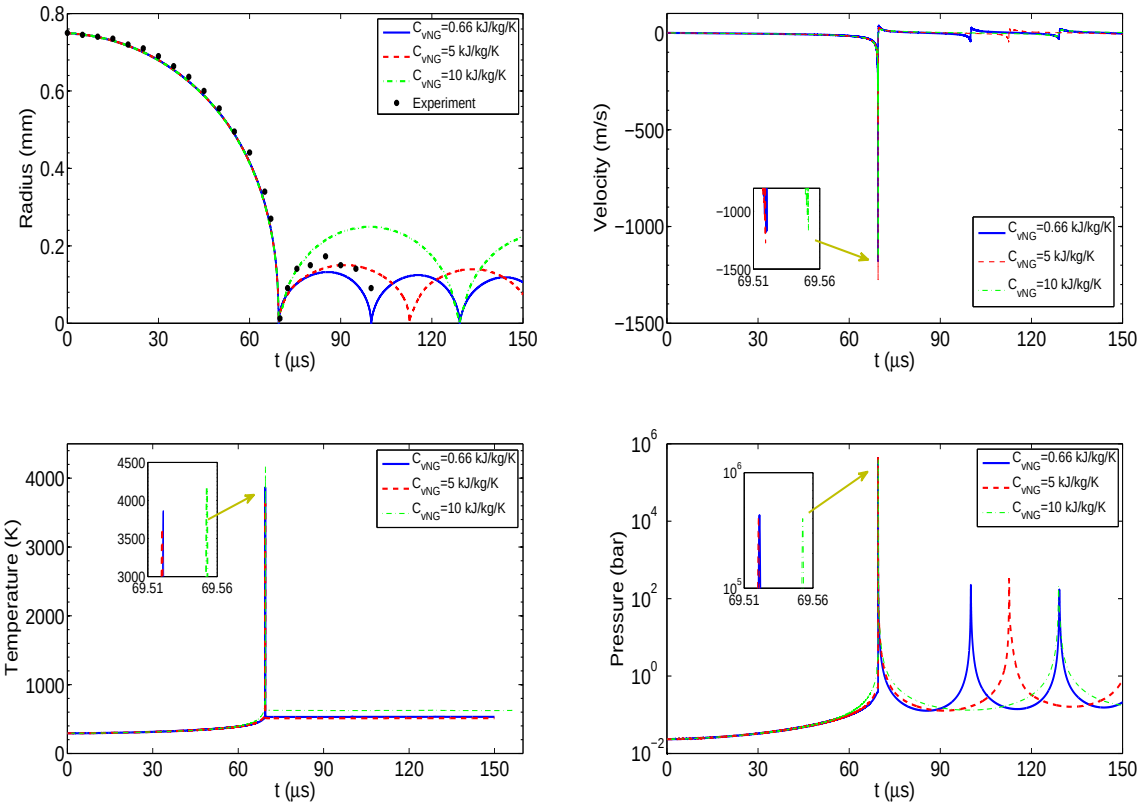

Figure 5.22: Gas-vapor bubble with mass transfer, different gases with percent 2% in mass. The computed radii are compared with the experimental data (dots). The pressure and temperature are taken at the center of the bubble while the velocity at the interface. Computations are made with $N_I = 500$ cells, initial state inside the bubble: $T = 293$ K and $p = 2339$ Pa.

In addition, we see during the computations that an assumption of a too small percentage for the non-condensable gas is insignificant for the rebound.

We conclude the following results for the collapse of the gas-vapor bubble:

- The existence of sufficient amount of non-condensable gas is essential for the rebound after the collapse if the mass transfer is included.
- The behavior of the rebound depends on the percentage of the non-condensable gas and on the nature of the gas.

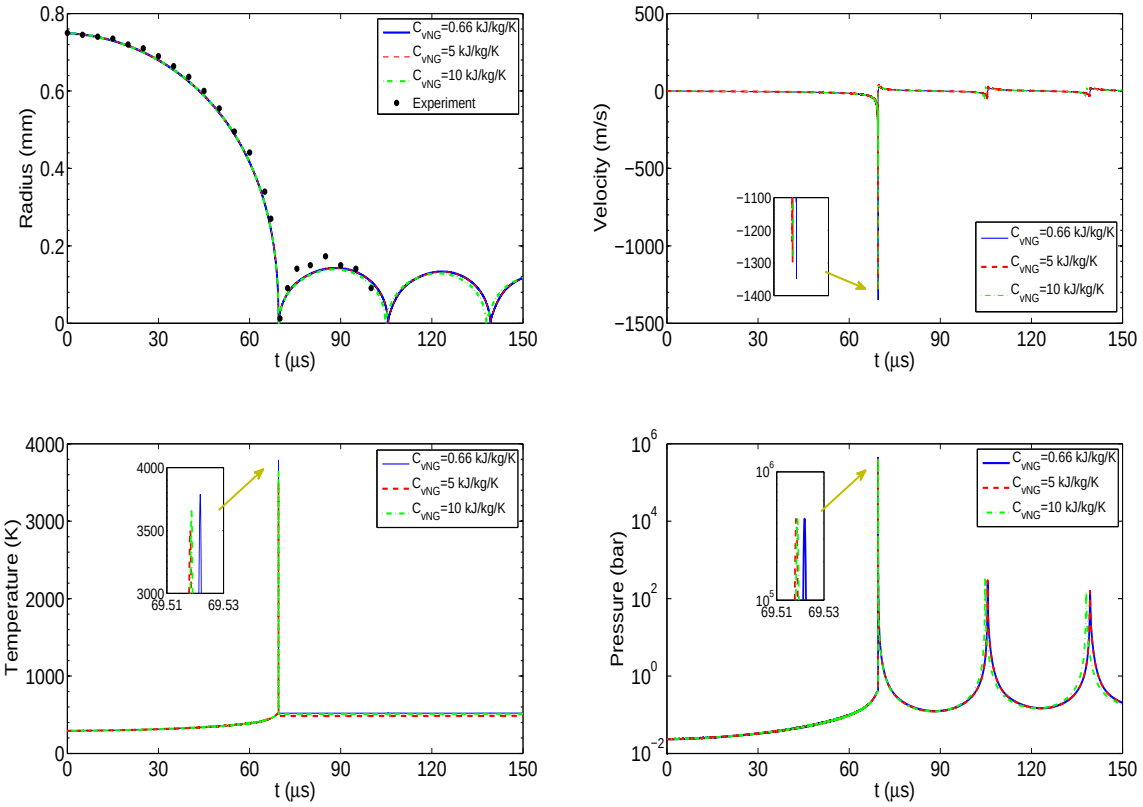

Figure 5.23: Gas-vapor bubble with mass transfer, different gases with initial volume fraction 0.045. The computed radii are compared with the experimental data (dots). The pressure and temperature are taken at the center of the bubble while the velocity at the interface. Computations are made with $N_I = 500$ cells, initial state inside the bubble: $T = 293$ K and $p = 2339$ Pa.

For more validation we compute the maximum radius after the first collapse for several values of initial radius of the bubble. Then we compare these values with experimental data of Akhatov et al. [5]. For this test the initial temperature is assumed to be $T = 296$ K inside and outside the bubble with pressure inside the bubble $p = 2339$ Pa. For the non-condensable gas we assume $C_v = 5$ kJ/kg/K with 1.5% mass fraction. We choose this assumption for the heat capacity to be in the middle between the values of Hydrogen and Oxygen. The results are shown in Figure 5.24. It is clear that the computed results have the same tendency as the experimental ones. In Figure 5.25 detailed results for different initial radii are shown.

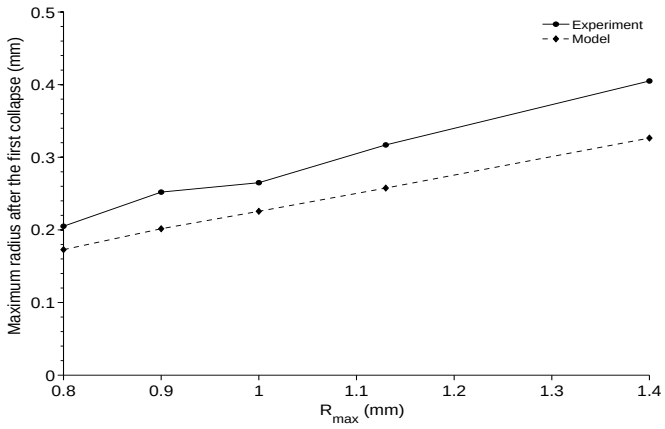

Figure 5.24: The maximum radius after the first collapse versus the initial bubble radius. Computations are made with a uniform grid, $\Delta r = 1.6 \times 10^{-6}$.

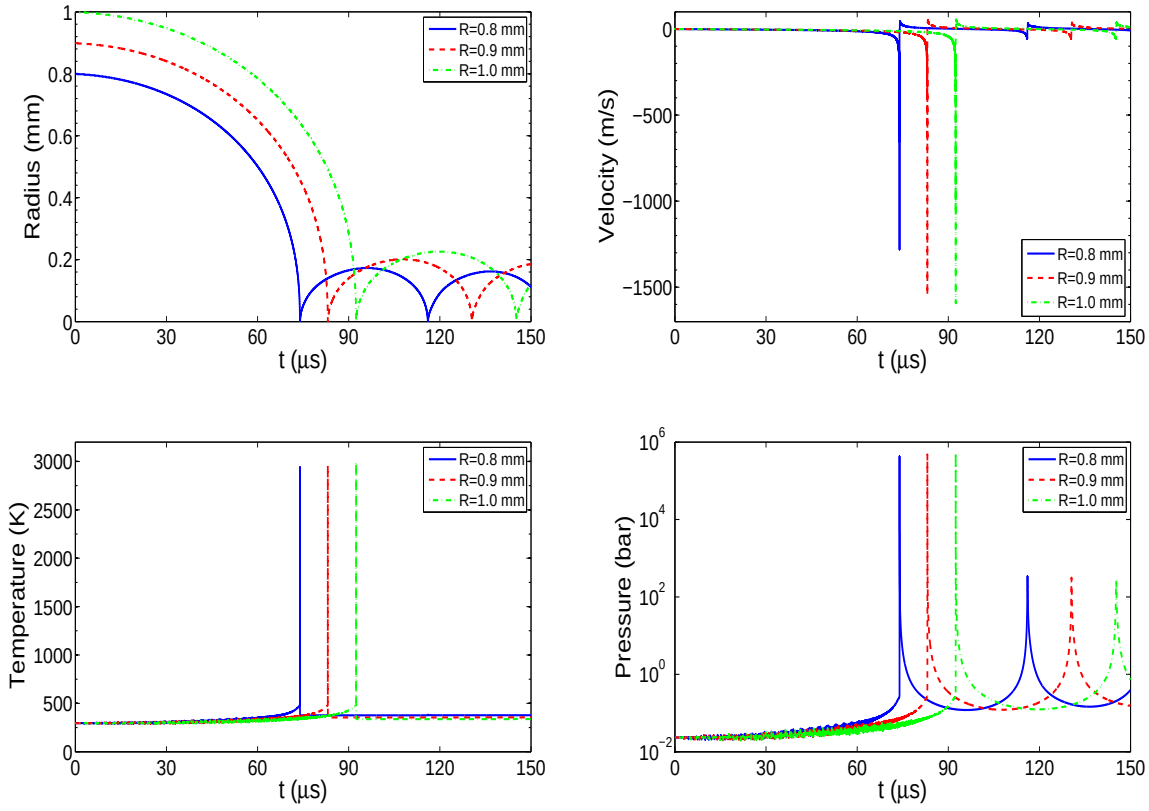

Figure 5.25: Gas-vapor bubble with mass transfer, different initial radii. The pressure and temperature are taken at the center of the bubble while the velocity at the interface. Computations are made with a uniform grid, $\Delta r = 1.6 \times 10^{-6}$, initial state inside the bubble: $T = 296$ K and $p = 2339$ Pa.

Chapter 6

Outlook

In this thesis, we modified the seven-equation model for two-phase flows to include the heat and mass transfer through relaxation effects. Based on the second law of thermodynamics and on the assumption that each property relaxes in a time that is considerably different from the other characteristic times, we were able to model the effect of heat and mass transfer by using temperature and Gibbs free energy relaxations. Some similarities between our new relaxation terms and the relaxation terms of Saurel et al. [126] were discussed in Subsections 3.5.1 and 3.6.1.

The same ideas and assumptions were also applied to model the heat and mass transfer for the six-equation model with a single velocity, which is obtained from the seven equation-model in the limit of zero velocity relaxation time. Alternatively, the six-equation model including the heat and mass transfer was derived directly from the modified seven-equation model by using the reduction criteria of Chen et al. [22] assuming stiff velocity relaxation.

By these modifications we obtained hierarchical models in which the relaxation steps are performed in the following order: first mechanical relaxations, then temperature relaxation and at last Gibbs free energy relaxation. During the temperature relaxation the pressure stays in equilibrium and during the Gibbs free energy relaxation both the pressure and temperature stay in equilibrium.

A Godunov-type method was used to solve the hyperbolic part of each model, while new numerical relaxation procedures were proposed for the temperature and Gibbs free energy relaxations. These procedures are used at each time step directly after the mechanical relaxation procedures.

We tested the new models on the test problems of Saurel et al. [126] for metastable liquids. We were able to see the extra expansion waves in our results which correspond to the evaporation fronts. Our results are similar to the results of [126] with a few differences.

Computed front speeds of the evaporation waves in a dodecane shock tube at different initial temperatures are compared with experimental ones of Simões-Moreira and Shepherd

[136]. A good agreement is achieved.

A comparison between the results of the seven-equation and the six-equation models was made. In general, both models almost give the same results, but the six-equation model is less expensive than the seven-equation model and easier to be extended to multiphase flows.

Due to the relaxation processes stiffness may be encountered during the numerical computations. This requires a smaller time step than is needed for the hydrodynamic system. In particular, if the stiffness comes from the Gibbs free energy relaxation procedure it is possible to use a limitation on the source terms which can be used to find reduced time steps. Then a successive point integration is used to cover the complete hydrodynamic time step. Otherwise small CFL numbers would used and this consumes more computation time. In fact, this point still requires further efforts. For future work, the efficiency of the numerical method must be improved by using some adaptive discretizations. This will be particularly important when the method is applied to two or three dimensional problems.

We observed that in mixtures under a high difference in the initial velocities there is a small deviation between the results of the seven-equation and six-equation models. This is reduced under grid refinement. We think this deviation is related to the approximation of the non-conservative terms and to some approximation used in velocity relaxation for the seven-equation model. However, to build a specific understanding for this point still more investigations are required. In fact, an extensive convergence study for both models would be very useful for this comparison and further insight into the models. This is a challenging issue for future work.

After the comparison between the results of both models in metastable liquids, we adopted the six-equation model to investigate the problem of a laser-induced cavitation bubble in liquid water. This choice was due to the fact that the six-equation model is less expensive and it is easily extended to multiphase flows. In fact, the problem of a laser-induced cavitation bubble is difficult in itself and still requires more investigations. In this work we considered the most important physical effects on the dynamics of the collapsing bubble, these effects are: the compressibility, heat transfer, mass transfer and the existence of a non-condensable gas inside the bubble.

If the bubble contains vapor only we used our modified six-equation model. This model was extended to include a non-condensable gas as a third phase, i.e. we obtained a nine-equation model. The heat and mass transfer are considered only at the interfaces separating the liquid and its vapor, whereas for the interfaces between the non-condensable gas and liquid a pressure equilibrium is imposed.

For the collapsing bubble in liquid water, we proposed new estimates for the parameters of the stiffened gas equations of state for the vapor and liquid. These new values are

able to take into account a wide range of temperature. In addition, they are linked to each other in a way to recover the saturation curve.

The main result from the computations of the collapsing bubble is that if the mass transfer is included then the rebound of the bubble after the collapse is only possible when a non-condensable gas presents inside the bubble. This result confirms the ideas of Dreyer et al. [40] that based on some thermodynamics considerations.

The computations show a high pressure and temperature at the center of the bubble at the collapse point. In addition, using mass transfer reduces the pressure and temperature inside the bubble before the collapse time. This behavior is due to the consumption of energy in the mass transfer process.

The diffusive interface may have bad effects on the results of collapsing bubble. This diffusion increases around the collapse point which has strong effects on the results after the collapse point. To avoid this problem in the computations we used a higher number of cells. For future work some adaptive discretization should be used to improve the capturing of the interface. Also, we plan to study the coupling between our approach here with the ideas of sharp interface modeling just around the collapse point. By this coupling we expect to collect the benefits of considering the phase transition as well as avoiding the problem of diffusion through the collapse.

Appendix A

Mathematical properties of the three-phase model

In order to investigate the mathematical properties of the model (5.9), without the redundent equation, we rewrite its hyperbolic part in terms of primitive variables as

$$\frac{\partial \mathbf{W}}{\partial t} + \mathbf{A}\frac{\partial \mathbf{W}}{\partial x} = 0,$$

where

$$\mathbf{W} = (\alpha_1, \alpha_2, \rho_1, \rho_2, \rho_3, u, p_1, p_2, p_3).$$

The matrix $\mathbf{A}$ is given as

$$\mathbf{A} = \begin{bmatrix} u & 0 & 0 & 0 & 0 & 0 & 0 & 0 & 0 \\ 0 & u & 0 & 0 & 0 & 0 & 0 & 0 & 0 \\ 0 & 0 & u & 0 & 0 & \rho_1 & 0 & 0 & 0 \\ 0 & 0 & 0 & u & 0 & \rho_2 & 0 & 0 & 0 \\ 0 & 0 & 0 & 0 & u & \rho_3 & 0 & 0 & 0 \\ \frac{p_1 - p_3}{\rho} & \frac{p_2 - p_3}{\rho} & 0 & 0 & 0 & u & \frac{\alpha_1}{\rho} & \frac{\alpha_2}{\rho} & \frac{1-\alpha_1-\alpha_2}{\rho} \\ 0 & 0 & 0 & 0 & 0 & \rho_1 c_1^2 & u & 0 & 0 \\ 0 & 0 & 0 & 0 & 0 & \rho_2 c_2^2 & 0 & u & 0 \\ 0 & 0 & 0 & 0 & 0 & \rho_3 c_3^2 & 0 & 0 & u \end{bmatrix}.$$

The matrix $\mathbf{A}$ has real eigenvalues that are given by the following expressions

$$\begin{aligned} &\lambda_1 = \lambda_2 = ... = \lambda_7 = u, \\ &\lambda_8 = u + c, \\ &\lambda_9 = u - c. \end{aligned}$$

Here c is the mixture sound speed for the model and is expressed as

$$c^2 = \frac{\alpha_1\rho_1}{\rho}c_1^2 + \frac{\alpha_2\rho_2}{\rho}c_2^2 + \frac{\alpha_3\rho_3}{\rho}c_3^2.$$

The sound speeds c_k, $k = 1, 2$, are defined by (2.49).

The corresponding right eigenvectors are

$$\mathbf{r}_1 = \begin{bmatrix} 0 \\ 0 \\ 0 \\ 0 \\ 0 \\ 0 \\ -\frac{\alpha_3}{\alpha_1} \\ 0 \\ 1 \end{bmatrix}, \quad \mathbf{r}_2 = \begin{bmatrix} 0 \\ 0 \\ 0 \\ 0 \\ 0 \\ 0 \\ -\frac{\alpha_2}{\alpha_1} \\ 1 \\ 0 \end{bmatrix}, \quad \mathbf{r}_3 = \begin{bmatrix} 0 \\ 0 \\ 0 \\ 0 \\ 1 \\ 0 \\ 0 \\ 0 \\ 0 \end{bmatrix}, \quad \mathbf{r}_4 = \begin{bmatrix} 0 \\ 0 \\ 0 \\ 1 \\ 0 \\ 0 \\ 0 \\ 0 \\ 0 \end{bmatrix}, \quad \mathbf{r}_5 = \begin{bmatrix} 0 \\ 0 \\ 1 \\ 0 \\ 0 \\ 0 \\ 0 \\ 0 \\ 0 \end{bmatrix},$$

$$\mathbf{r}_6 = \begin{bmatrix} 0 \\ 1 \\ 0 \\ 0 \\ 0 \\ 0 \\ \frac{p_3 - p_2}{\alpha_1} \\ 0 \\ 0 \end{bmatrix}, \quad \mathbf{r}_7 = \begin{bmatrix} 1 \\ 0 \\ 0 \\ 0 \\ 0 \\ 0 \\ \frac{p_3 - p_1}{\alpha_1} \\ 0 \\ 0 \end{bmatrix}, \quad \mathbf{r}_8 = \begin{bmatrix} 0 \\ 0 \\ 1 \\ \rho_2/\rho_1 \\ \rho_3/\rho_1 \\ c/\rho_1 \\ c_1^2 \\ \rho_2 c_2^2/\rho_1 \\ \rho_3 c_3^2/\rho_1 \end{bmatrix}, \quad \mathbf{r}_9 = \begin{bmatrix} 0 \\ 0 \\ 1 \\ \rho_2/\rho_1 \\ \rho_3/\rho_1 \\ -c/\rho_1 \\ c_1^2 \\ \rho_2 c_2^2/\rho_1 \\ \rho_3 c_3^2/\rho_1 \end{bmatrix},$$

Thus, the system (5.9) is non strictly hyperbolic.

Bibliography

[1] R. Abgrall. How to prevent pressure oscillations in multicomponent flow calculations: A quasi conservative approach. *J. Comput. Phys.*, 125(1):150–160, 1996.

[2] R. Abgrall and S. Karni. A comment on the computation of non-conservative products. *J. Comput. Phys.*, 229(8):2759–2763, 2010.

[3] R. Abgrall and V. Perrier. Asymptotic expansion of a multiscale numerical scheme for compressible multiphase flow. *SIAM Multiscale Model. Simul.*, 5(1):84–115, 2006.

[4] R. Abgrall and R. Saurel. Discrete equations for physical and numerical compressible multiphase mixtures. *J. Comput. Phys.*, 186(2):361–396, 2003.

[5] I. Akhatov, O. Lindau, A. Topolnikov, R. Mettin, N. Vakhitova, and W. Lauterborn. Collapse and rebound of a laser-induced cavitation bubble. *Phys. Fluids*, 13:2805–2819, 2003.

[6] G. Allaire, S. Clerc, and S. Kokh. A five-equation model for the simulation of interfaces between compressible fluids. *J. Comput. Phys.*, 181:577–616, 2002.

[7] N. Andrianov. CONSTRUCT: A collection of MATLAB routines for constructing the exact solution to the Riemann problem for the Baer-Nunziato model of two-phase flows. Available at:
http://www-ian.math.uni-magdeburg.de/home/andriano/CONSTRUCT.

[8] N. Andrianov. *Analytical and numerical investigation of two-phase flows.* PhD thesis, Otto-von-Guericke University, 2003.

[9] N. Andrianov, R. Saurel, and G. Warnecke. A simple method for compressible multiphase mixtures and interfaces. *Int. J. Numer. Meth. Fluids*, 41:109–131, 2003.

[10] N. Andrianov and G. Warnecke. The Riemann problem for the Baer-Nunziato two-phase flow model. *J. Comput. Phys.*, 195:434–464, 2004.

[11] R. Aris. *Vectors, Tensors, and the Basic Equations of Fluid Mechanics.* Dover Publications, 1962.

[12] M. Baer and J. Nunziato. A two-phase mixture theory for the deflagration-to-detonation transition (DDT) in reactive granular materials. *Int. J. Multiphase Flows*, 12:861–889, 1986.

[13] T. Barberon and P. Helluy. Finite volume simulations of cavitating flows. In Finite volumes for complex applications, III (Porquerolles, 2002), 441-448 . Lab. Anal. Topol. Probab. CNRS, Marseille, 2002.

[14] T. Barberon and P. Helluy. Finite volume simulation of cavitating flows. *Computers & Fluids*, 34:832–858, 2005.

[15] R. A. Berry. Notes on well-posed, ensemble averaged conservation equations for multiphase, multi-component, and multi-material flows. Technical Report INL/EXT-05-00516, Idaho National Laboratory (INL), 2005.

[16] Z. Bilicki, R. Kwidzinski, and S. A. Mohammadein. An estimation of a relaxation time of heat and mass exchange in the liquid-vapour bubble flow. *Int. J. Heat Mass Transfer*, 39(4):753759, 1996.

[17] C. E. Brennen. *Cavitation and Bubble Dynamics*. Oxford University Press, 1995.

[18] E. A. Brujan, G. S. Keen, A. Vogel, and J. R. Blake. The final stage of the collapse of a cavitation bubble close to a rigid boundary. *Phys. fluids*, 14:85–92, 2002.

[19] C. Castro and E. Toro. A Riemann solver and upwind methods for a two-phase flow model in nonconservative form. *Int. J. Numer. Meth. Fluids*, 50:275–307, 2006.

[20] M. Castro, J. Gallardo, and C. Parés. High order finite volume schemes based on reconstruction of states for solving hyperbolic systems with nonconservative products. Applications to shallow water systems. *Math. Comp.*, 75:1103–1134, 2006.

[21] M. J. Castro, P. G. LeFloch, M. L. Muñoz, and C. Parés. Why many theories of shock waves are necessary: Convergence error in formally path-consistent schemes. *J. Comput. Phys.*, 227:8107–8129, 2008.

[22] G. Chen, C. Levermore, and T. Liu. Hyperbolic conservation laws with stiff relaxation terms and entropy. *Comm. Pure. Appl. Math.*, 47:787–830, 1994.

[23] A. Chinnayya, E. Daniel, and R. Saurel. Modelling detonation waves in heterogeneous energetic materials. *J. Comput. Phys.*, 196(2):490–538, 2004.

[24] J. P. Cocchi and R. Saurel. A Riemann problem based method for the resolution of compressible multimaterial flows. *J. Comput. Phys.*, 137:265–298, 1997.

[25] J. P. Cocchi, R. Saurel, and J. C. Loraud. Treatment of interface problems with Godunov-type schemes. *Shock Waves*, 5:347–357, 1996.

[26] F. Coquel, T. Gallouët, J. Hérard, and N. Seguin. Closure laws for a two-fluid two-pressure model. *C. R. Acad. Sci. Paris, Ser. I*, 332:927–932, 2002.

[27] G. Crasta and P. LeFloch. A class of nonconservative and non strictly hyperbolic systems. *Comm. Pure Appl. Anal.*, 1:513–530, 2002.

[28] C. M. Dafermos. The entropy rate admissible criterion for solutions of hyperbolic conservation laws. *J. Diff. Equations*, 14:202–212, 1973.

[29] C. M. Dafermos. *Hyperbolic conservation laws in continuum physics*. Springer, Berlin, 2000.

[30] G. Dal Maso, P. LeFloch, , and F. Murat. Definition and weak stability of nonconservative products. *J. Math. Pures Appl.*, 74:483–548, 1995.

[31] S. F. Davis. Simplified second-order Godunov-type methods. *SIAM J. Sci. Statist. Comput.*, 9:445–473, 1998.

[32] V. Deledicque and M. V. Papalexandris. An exact Riemann solver for compressible two-phase flow models containing non-conservative products. *J. Comput. Phys.*, 222:217–245, 2007.

[33] V. Deledicque and M. V. Papalexandris. A conservative approximation to compressible two-phase flow models in the stiff mechanical relaxation limit. *J. Comput. Phys.*, 227(21):9241–9270, 2008.

[34] J. Donea1, A. Huerta, J.-P. Ponthot, and A. Rodríguez-Ferran. Arbitrary Lagrangian-Eulerian Methods. In E. Stein, R. de Borst, and T. J. Hughes, editors, *Encyclopedia of Computational Mechanics*, chapter 14. John Wiley & Sons, 2004.

[35] D. Drew. Average field equations for two-phase media. *Stud. Appl. Math.*, 2:133–166, 1971.

[36] D. Drew. Mathematical modeling of two-phase flow. *Ann. Rev. Fluid Mech.*, 15:261–291, 1983.

[37] D. A. Drew and R. T. Lahey. Analytical modeling of multiphase flow. in particulate two-phase flow. In M. C. Roco, editor, *Particulate Two-Phase Flow*, pages 509–566. Butterworth-Heinemann, Boston, 1993.

[38] D. A. Drew and S. L. Passman. *Theory of multicomponent fluids*. Springer, 1998.

[39] W. Dreyer. On jump conditions at phase boundaries for ordered and disordered phases. Technical report, WIAS Preprint No. 869, 2003.

[40] W. Dreyer, F. Duderstadt, M. Hantke, and G. Warnecke. On phase change of a vapor bubble in liquid water. Technical report, WIAS Preprint No. 1424, 2009.

[41] M. Dumbser, A. Hidalgo, M. Castro, C. Parés, and E. Toro. FORCE schemes on unstructured meshes II: Non-conservative hyperbolic systems. *Comput. Methods Appl. Mech. Engrg.*, 199:625–647, 2010.

[42] P. Embid and M. Baer. Mathematical analysis of a two-phase continuum mixture theory. *Continuum Mech. Thermodyn.*, 4:279–312, 1992.

[43] J. P. Franc and J. M. Michel. *Fundamentals of Cavitation*. Springer Science and Business Media, Inc., 2005.

[44] S. Fujikawa and T. Akamatsu. Effects of the non-equilibrium condensation of vapor on the pressure wave produced by the collapse of a bubble in a liquid. *J. Fluid. Mech.*, 97:481–512, 1980.

[45] T. Gallouët, J. M. Hérard, and N. Seguin. Numerical modelling of two-phase flows using the two-fluid two-pressure approach. *Math. Mod. and Meth. in Applied Sciences*, 14(5):663–700, 2004.

[46] T. Gallouët and J. M. Masella. Un schéma de Godunov approaché. *Comptes Rendus Académie des Sciences Paris Série I*, 323:77–84, 1996.

[47] T. Gallouët and R. Saurel. *Modéles et méthodes numériques pour les écoulements fluides*. cours de DEA, Centre de Mathématiques et d'Informatique, Université de Provence, 1998.

[48] F. R. Gilmore. The growth or collapse of a spherical bubble in a viscous compressible liquid. Technical Report 26-4, Hydrodynamics Laboratory, California Institute of Technology, Pasadena, California, 1952.

[49] E. Godlewski and P.-A. Raviart. *Numerical approximation of hyperbolic systems of conservation laws*. Springer, New York, 1996.

[50] K. A. Gonthier and J. M. Powers. A high-resolution numerical method for a two-phase model of deflagration to detonation transition. *J. Comput. Phys.*, 163:376–433, 2000.

[51] H. Guillard and M. Labois. Numerical modeling of compressible two-phase flows. European Conference on Computational Fluid Dynamics ECCOMAS CFD, P. Wesseling and E. Onate and J. Priaux (Eds), 2006.

[52] V. Guinot. *Godunov-type Schemes: An introduction for engineers*. Elsevier, 2003.

[53] F. Harlow and A. Amsden. *Fluid Dynamics*. Los Alamos Scientific Laboratory Monograph, LA-4700, second edition, 1971.

[54] J. M. Hérard. An hyperbolic three phase flow model. *CRAS Paris, I-342*, 10:779–784, 2006.

[55] R. Hickling and M. Plesset. Collapse and rebound of a spherical bubble in water. *Phys. Fluids*, 7:7–14, 1964.

[56] C. Hirt and B. Nichols. Volume of Fluid (VOF) method for the dynamics of free boundaries. *J. Comput. Phys.*, 39:201–225, 1981.

[57] C. W. Hirt, A. A. Amsden, and J. L. Cook. An arbitrary Lagrangian-Eulerian computing method for all flow speeds. *J. Comp. Phys.*, 14:227–253, 1974.

[58] L. Hörmander. *The analysis of linear partial differential operators I.* Springer-Verlag, second edition, 1990.

[59] T. Hou and P. LeFloch. Why non-conservative schemes converge to the wrong solution: Error analysis. *Math. Comput.*, 62:497–530, 1994.

[60] H. H. Hu, N. A. Patankarb, and M. Y. Zhua. Direct numerical simulations of fluid-solid systems using the arbitrary Lagrangian-Eulerian technique. *J. Comput. Phys.*, 169:427–462, 2001.

[61] M. Ishii and T. Hibiki. *Thermo fluid dynamics of two-phase flow.* Springer Science + Business Media, 2006.

[62] M. Ishii and K. Mishima. Two-fluid model and hydrodynamic constitutive relations. *Nucl. Engng Des.*, 82:107–126, 1984.

[63] M. Ishii and N. Zuber. Drag coefficient and relative velocity in bubbly, droplet or particulate flows. *AIChE J.*, 25:843–855, 1979.

[64] J. C. Isselin, A. P. Alloncle, and M. Autric. On laser induced single bubble near a solid boundary: Contribution to the understanding of erosion phenomena. *J. Appl. Phys.*, 84(10):5766–5771, 1998.

[65] V. Kamath and A. Prosperetti. Numerical integration methods in gas bubble dynamics. *J. Acoust. Soc. Am.*, 85:1538–1548, 1989.

[66] A. Kapila, R. Menikoff, J. Bdzil, S. Son, and D. Stewart. Two-phase modelling of DDT in granular materials: Reduced equations. *Phys. Fluid*, 13:3002–3024, 2001.

[67] J. B. Keller and I. I. Kolodner. Damping of underwater explosion bubble oscillations. *J. Appl. Phys.*, 27:1152–1161, 1956.

[68] J. B. Keller and M. Miksis. Bubble oscillations of large amplitude. *J. Acoust. Soc. Am.*, 68:628–633, 1980.

[69] C. Kleinstreuer. *Engineering Fluid Dynamics- An Interdisciplinary Systems Approach.* Cambridge University Press, 1997.

[70] D. Kröner. *Numerical schemes for conservation laws.* John Wiley and Sons, Chichester, 1997.

[71] A. Kumbaro, V. Seignole, and J. Ghidaglia. Flux schemes for the two-fluid model of the TRIO-U code. AMIF/ESF Workshop, Computing Methods for Two-Phase Flows, 12-14 January, Aussois, France, 2000.

[72] M. Labois. *Modélisation des déséquilibres mécaniques pour les écoulements diphasiques: approches par relaxation et par modèle réduit.* PhD thesis, Université de Provence - Aix-Marseille I, 2008.

[73] M. Labois, H. Guillard, and M. Grandotto. A five-equation dissipative model for the simulation of two-phase flows. pages 257–265. International Conference on Advances in Fluid Mechanics VII, The New Forest, 21-23 may 2008, WITpress, The New Forest, UK, 2008.

[74] M. H. Lallemand, A. Chinnayya, and O. Le Metayer. Pressure relaxation procedures for multiphase compressible flows. *Int. J. Numer. Meth. Fluids*, 49(1):1–56, 2005.

[75] M. H. Lallemand and R. Saurel. Pressure relaxation procedures for multiphase compressible flows. Technical Report 4038, INRIA, 2000.

[76] W. Lauterborn. Numerical investigation of nonlinear oscillations of gas bubbles in liquids. *J. Acoust. Soc. Am.*, 59(2):283–293, 1976.

[77] W. Lauterborn, T. Kurz, C. Schencke, O. Lindau, and B. Wolfrum. Laser-induced bubbles in cavitation research. In *Proceedings of the IUTAM Symposium on Free Surface Flows*. Birmingham United Kingdom, 2000.

[78] P. D. Lax. Hyperbolic of conservation laws II. *Comm. Pure Appl. Math.*, 10:537–566, 1957.

[79] P. D. Lax. *Hyperbolic systems of conservation laws and mathematical theory of shock waves*. SIAM Regional Conf. Ser. Appl. Math., Number 11, 1972.

[80] O. Le Metayer, J. Massoni, and R. Saurel. Elaborating equations of state of a liquid and its vapor for two-phase flow models (in french). *Int. J. Thermal Sci.*, 43(3):265–276, 2004.

[81] O. Le Metayer, J. Massoni, and R. Saurel. Modelling evaporation fronts with reactive Riemann solvers. *J. Comput. phys.*, 205:567–610, 2005.

[82] P. LeFloch. Shock waves for nonlinear hyperbolic systems in nonconservative form. Institute for Math. and its Appl., Minneapolis, Preprint No. 593, 1989.

[83] P. LeFloch. *Hyperbolic Systems of Conservation Laws. The theory of classical and nonclassical shock waves*. Lectures in Mathematics-ETH Zurich. Birkhauser Verlag, Basel, 2002.

[84] R. J. LeVeque. *Numerical methods for conservation laws*. Birkhauser Verlag, Basel, 1992.

[85] R. J. LeVeque. *Finite volume methods for hyperbolic problems*. Cambridge University Press, 2004.

[86] T. Liu. The entropy condition and the admissibility of shocks. *J. Math. Anal. Appl.*, 53:78–88, 1976.

[87] T. Liu. Uniqueness of weak solutions of the Cauchy problem for general 2×2 conservation laws. *J. Diff. Equations*, 20:369–388, 1976.

[88] L. Margolin. Introduction to "An arbitrary Lagrangian-Eulerian computing method for all flow speeds". *J. Comput. phys.*, 135:198–202, 1997.

[89] R. Menikoff and B. Plohr. The Riemann problem for fluid flow of real materials. *Rev. Mod. Phys.*, 61(1):75–130, 1989.

[90] G. H. Miller and E. G. Puckett. A high-order Godunov method for multiple condensed phases. *J. Comput. phys.*, 128:134–164, 1996.

[91] M. J. Moran and H. N. Shapiro. *Fundamentals of Engineering Thermodynamics*. John Wiley & sons, Inc., fourth edition, 2000.

[92] I. Müller. *Thermodynamics, Interaction of Mechanics and mathematics Series*. Pitman Advanced Publihing Program, Boston, 1985.

[93] I. Müller and W. H. Müller. *Fundamentals of Thermodynamics and Applications: With Historical Annotations and Many Citations from Avogadro to Zermelo*. Springer-Verlag Berlin Heidelberg, 2009.

[94] S. Müller, M. Bachmann, D. Kröninger, T. Kurz, and P. Helluy. Comparison and validation of compressible flow simulations of laser-induced cavitation bubbles. *Computers and Fluids*, 38:1850–1862, 2009.

[95] S. Müller, P. Helluy, and J. Ballmann. Numerical simulation of cavitation bubbles by compressible two-phase fluids. *Int. J. Fluid Mech.*, 2009. doi:10.1002/fld.2033.

[96] A. Murrone and H. Guillard. A five-equation reduced model for compressible two-phase flow problems. *J. Comput. Phys.*, 202(2):664–698, 2005.

[97] R. I. Nigmatulin, I. S. Akhatov, N. K. Vakhitova, and R. T. Lahey. On the forced oscillations of a small gas bubble in a spherical liquid filled flask. *J. Fluid Mech.*, 414:47–73, 2000.

[98] R. I. Nigmatulin and N. S. Khabeev. Heat exchange between a gas bubble and a liquid. *rdquo Izv. Akad. Nauk SSSR, Mekh. Zhidk. Gaza*, 5, 1974.

[99] R. Oldendourg. *Properties of water and steam in SI-units*. Springer, 1989.

[100] E. Olsson and G. Kreiss. A conservative level set method for two-phase flow. *J. Comput. Phys.*, 210:225–246, 2005.

[101] S. Osher and R. Fedkiw. Level set methods: An overview and some recent results. *J. Comput. Phys.*, 169(2):463–502, 2001.

[102] S. Osher and J. Sethian. Fronts propagating with curvature dependent speed: Algorithms based on the Hamilton-Jacobi formulation. *J. Comput. Phys.*, 79:12–49, 1988.

[103] C. Parés. Numerical methods for nonconservative hyperbolic systems: A theoretical framework. *SIAM J. Numer. Anal.*, 44:300–321, 2006.

[104] S. L. Passman, J. W. Nunziato, and E. K. Walsh. A theory of multiphase mixture. In C. Truesdell, editor, *Rational Thermodynamics*, pages 286–325. McGraw-Hill, New York, 1984.

[105] G. Perigaud and R. Saurel. A compressible flow model with capillary effects. *J. Comput. Phys.*, 209:139–178, 2005.

[106] F. Petitpas, E. Franquet, R. Saurel, and O. Le Metayer. A relaxation-projection method for compressible flows. Part II: Artificial heat exchanges for multiphase shocks. *J. Comput. Phys.*, 225(2):2214–2248, 2007.

[107] F. Petitpas, J. Massoni, R. Saurel, E. Lapebie, and L. Munier. Diffuse interface models for high speed cavitating underwater systems. *Int. J. Multiphase Flows*, 35(8):747–759, 2009.

[108] F. Petitpas, R. Saurel, E. Franquet, and A. Chinnayya. Modelling detonation waves in condensed materials: Multiphase CJ conditions and multidimensional computations. *Shock waves*, 19:377–401, 2009.

[109] A. Philipp and W. Lauterborn. Cavitation erosion by single laser-produced bubbles. *J. Fluid. Mech*, 361:75–116, 1998.

[110] J. Pilliod and E. Puckett. Second-order accurate Volume-of-Fluid algorithms for tracking material interfaces. *J. Comput. Phys.*, 199:465–502, 2004.

[111] M. S. Plesset and A. Prosperetti. Bubble dynamics and cavitation. *Annu. Rev. Fluid Mech.*, 9:145–185, 1977.

[112] A. Prosperetti, L. A. Crum, and K. W. Commander. Nonlinear bubble dynamics. *J. Acoust. Soc. Am.*, 83:502–514, 1988.

[113] A. Prosperetti and A. Lezzi. Bubble dynamics in a compressible liquid. Part 1. First order theory. *J. Fluid Mech.*, 168:457–478, 1986.

[114] L. Qiang, F. Jian-hu, C. Ti-min, and H. Chun-bo. Difference scheme for two-phase flow. *Appl. Math. Mech.*, 25(5):536–545, 2004.

[115] L. Rayleigh. On the pressure developed in a liquid during the collapse of a spherical cavity. *Phil. Mag.*, 34:94–98, 1917.

[116] W. Rider and D. Kothe. Reconstructing volume tracking. *J. Comput. Phys.*, 141:112–152, 1998.

[117] P. L. Roe. Approximate Riemann solvers, parameter vectors, and difference schemes. *J. Comput. Phys.*, 43:357–372, 1981.

[118] L. Sainsaulieu. Finite volume approximation of two-phase fluid flows based on an approximate Roe-type Riemann solver. *J. Comput. Phys.*, 121:1–28, 1995.

[119] R. Saurel. Interfaces, detonation waves, cavitation and the multiphase Godunov method. In E. F. Toro, editor, *Godunov Methods: Theory and Applications*, pages 785–807. Kluwer Academic/ Plenum Publishers, 2001.

[120] R. Saurel and R. Abgrall. A multiphase Godunov method for compressbile multifluid and multiphase flows. *J. Comput. Phys.*, 150(2):425–467, 1999.

[121] R. Saurel and R. Abgrall. A simple method for compressible multifluid flows. *SIAM J. Sci. Comput.*, 21:1115–1145, 1999.

[122] R. Saurel, E. Franquet, E. Daniel, and O. Le Metayer. A relaxation-projection method for compressible flows. Part I: The numerical equation of state for the Euler equations. *J. Comput. Phys.*, 223(2):822–845, 2007.

[123] R. Saurel, S. Gavrilyuk, and F. Renaud. A multiphase model with internal degree of freedom, application to shock-bubble interaction. *J. Fluid. Mech.*, 495:283–321, 2003.

[124] R. Saurel and O. Le Metayer. A multiphase model for interfaces, shocks, detonation waves and cavitation. *J. Fluid Mech.*, 431:239–271, 2001.

[125] R. Saurel, O. Le Metayer, J. Massoni, and S. Gavrilyuk. Shock jump relations for multiphase mixtures with stiff mechanical properties. *Shock waves*, 16:209–232, 2007.

[126] R. Saurel, F. Petitpas, and R. Abgrall. Modelling phase transition in metastable liquids: Application to cavitating and flashing flows. *J. Fluid. Mech.*, 607:313–350, 2008.

[127] R. Saurel, F. Petitpas, and R. A. Berry. Simple and efficient relaxation methods for interfaces separating compressible fluids, cavitating flows and shocks in multiphase mixtures. *J. Comput. Phys.*, 228(5):1678–1712, 2009.

[128] R. Scardovelli and S. Zaleski. Direct numerical simulation of free-surface and interfacial flow. *Annu. Rev. Fluid Mech.*, 31:567–603, 1999.

[129] D. Scheffler and J. Zukas. Practical aspects of numerical simulations of dynamic events: Material interfaces. *Int. J. Impact Eng.*, 24(8):821–842, 2000.

[130] G. H. Schnerr, I. H. Sezal, and S. J. Schmidt. Numerical investigation of three-dimensional cloud cavitation with special emphasis on collapse induced shock dynamics. *Phys. Fluids*, 20(4):040703, 2008.

[131] D. Schwendeman, C. Wahle, and A. Kapila. The Riemann problem and a high-resolution Godunov method for a model of compressible two-phase flow. *J. Comput. Phys.*, 212:490–526, 2006.

[132] D. Serre. *Systems of conservation laws.* Cambridge University Press, Cambridge, 1999.

[133] J. A. Sethian. *Level Set Methods: Evolving Interfaces in Geometry, Fluid. Mechanics, Computer Vision and Material Science*. Cambridge University Press, 1996.

[134] K.-M. Shyue. An efficient shock-capturing algorithm for compressible multicomponent problems. *J. Comp. Phys.*, 142:208–242, 1998.

[135] J. R. Simões-Moreira. *Adiabatic evaporation waves*. PhD thesis, Rensselaer Polytechnic Institute, 1994.

[136] J. R. Simões-Moreira and J. E. Shepherd. Evaporation waves in superheated dodecane. *J. Fluid Mech.*, 382:63–86, 1999.

[137] J. Slattery, L. Sagis, and E. S. Oh. *Interfacial Transport Phenomena*. Springer Science and Business Media, second edition, 2007.

[138] J. Smoller. *Shock waves and reaction-diffusion equations*. Springer, New York, 1983.

[139] S. Sochard, A. Wilhem, and H. Delmas. Modeling of free radical production in a collapsing gas-vapour bubble. *Ultrason. Sonochem*, 4:77–84, 1997.

[140] W. D. Song, M. H. Hong, B. Lukyanchuk, and T. C. Chong. Laser-induced cavitation bubbles for cleaning of solid surfaces. *J. Appl. Phys.*, 95(6):2952–2956, 2004.

[141] R. Sonntag and C. Borgnakke. *Introduction to engineering thermodynamics*. John Wiley and Sons, Inc., 2001.

[142] S. L. Soo. *Multiphase fluid dynamics*. Science Press and Gower Technical, 1990.

[143] H. Stewart and B. Wendroff. Two-phase flow: Models and methods. *J. Comput. Phys.*, 56:363–409, 1984.

[144] G. Strang. On the construction and comparison of difference schemes. *SIAM J. Num. Anal.*, 5:506–517, 1968.

[145] I. Tiselj and S. Petelin. Modeling of two-phase flow with second-order accurate scheme. *J. Comput. Phys.*, 136:503–521, 1997.

[146] S. Tokareva and E. Toro. HLLC-type Riemann solver for the Baer-Nunziato equations of compressible two-phase flow. *J. Comput. Phys.*, 229(10):3573–3604, 2010.

[147] Y. Tomita and A. Shima. On the behavior of a spherical bubble and the impulse pressure in a viscous compressible liquid. *Bull. JSME*, 20:1453–1460, 1977.

[148] E. F. Toro. *Riemann Solvers and Numerical Methods for Fluid Dynamics*. Springer, Berlin, 1999.

[149] I. Toro. Riemann-problem-based techniques for computing reactive two-phase flows. In *the third International conference on numerical combustion*, volume 351 of *Lecture Notes in Physics*, pages 472–481. Springer-Verlag, 1989.

[150] I. Toumi. A weak formulation of Roe's approximate Riemann solver. *J. Comput. Phys.*, 102:360–373, 1992.

[151] I. Toumi and P. Raymond. Upwind numerical scheme for two-fluid two-phase model. In *the 14th International Conference on Numerical Methods in Fluid Dynamics*, volume 453 of *Lecture Notes in Physics*, pages 299–306. Springer-Verlag, 1995.

[152] L. Trilling. The collapse and rebound of a gas bubble. *J. Appl. Phys.*, 23:14–17, 1952.

[153] G. Tryggvason, B. Bunner, A. Esmaeeli, D. Juric, N. Al-Rawahi, W. Tauber, J. Han, S. Nas, and Y. J. Jan. A front-tracking method for the computations of multiphase flow. *J. Comput. Phys.*, 169:708–759, 2001.

[154] S. Unverdi and G. Tryggvason. A front tracking method for viscous incompressible flows. *J. Comput. Phys.*, 100:25–37, 1992.

[155] C. W. Wang, T. G. Liu, and B. C. Khoo. A real-ghost fluid method for the simulation of multi-medium compressible flow. *SIAM J. Sci. Computing*, 28:278–302, 2006.

[156] G. Warnecke. *Analytische Methoden in der Theorie der Erhaltungsgleichungen.* TEUBNER-TEXTE zur Mathematik Band 138, B.G. Teubner, Stuttgart-Leipzig, 1999.

[157] S. Whitaker. *The method of volume averaging.* Kluwer Academic Publishers, 1999.

[158] A. Wood. *A textbook of sound.* G. Bell & Sons Ltd., London, 1930.

[159] M. Wörner. A compact introduction to the numerical modeling of multiphase flows. Technical report, Wissenschaftliche Berichte, FZKA 6932, 2003.

[160] K. Yasui. Effects of thermal conduction on bubble dynamics near the sonoluminescence threshold. *J. Acoust. Soc. Amer.*, 98(5):2772–2782, 1995.

[161] A. Zein, M. Hantke, and G. Warnecke. On the modeling and simulation of a laser-induced cavitation bubble. Submitted, 2010.

[162] A. Zein, M. Hantke, and G. Warnecke. Modeling phase transition for compressible two-phase flows applied to metastable liquids. *J. Comput. Phys.*, 229(8):2964–2998, 2010.

[163] R. Zhao, Z. c. Liang, R. q. Xu, J. Lu, and X. w Ni. Dynamics of laser-induced cavitation bubble near solid boundary. *Jpn. J. Appl. Phys.*, 47(7):5482–5485, 2008.